

**UNIVERSITY of
STIRLING**



**Scotland's Pockmarks: understanding their formation
and relationship to buried carbon in fjordic systems**

Allan Audsley

A thesis presented for the degree of Doctor of Philosophy

Biological & Environmental Sciences
School of Natural Science
University of Stirling

December 2021

Supervisors:

Dr. Tom Bradwell

Prof. John Howe

Prof John Baxter

Statement of originality

I hereby confirm that the research contained in this thesis is original, has been completed by the author and all the work contained herein has not been submitted for any other degree. All published material has been duly acknowledged and cited.

A handwritten signature in black ink that reads "Allan Audsley". The signature is written in a cursive style with a large, sweeping initial 'A'.

Allan Audsley

Date: 23/12/2021

“I think our maps contributed to a revolution in geological thinking, which in some ways compares to the Copernican revolution. Scientists and the general public got their first relatively realistic image of a vast part of the planet that they could never see.”

- Marie Tharp

“The sea is everything. It covers seven tenths of the terrestrial globe. Its breath is pure and healthy. It is an immense desert, where man is never lonely, for he feels life stirring on all sides. The sea is only the embodiment of a supernatural and wonderful existence. It is nothing but love and emotion; it is the Living Infinite.”

- Jules Verne, Twenty Thousand Leagues Under the Sea

Acknowledgments

I would first like to thank the numerous funding bodies that helped to make this project a reality. This includes the Marine Alliance for Science and Technology for Scotland, University of Stirling, Nature Scot, Scottish Government, Scottish Blue Carbon Forum, Scottish Alliance for Geosciences Environment and Society, and the Edinburgh Geological Society. Without their support this research would not have been possible, and many unforgettable experiences would not have happened.

I would also like to express my gratitude to my supervisors, Dr. Tom Bradwell, Prof. John Howe and Prof. John Baxter for all their support throughout the last four years. I would like to give a special thanks to Dr. Tom Bradwell for being my main point of support throughout this project. Without his supervision, guidance and friendship this project would not be what it is today.

A big thanks to all the support from staff at the University of Stirling, namely Lynn Macgregor for always helping with administrative help, Ronnie Balfour for all the logistical help and Scott Jackson for all my IT support and Lorna English and Ian Washbourne for advising my sediment analysis. A further thanks to all the crew on MRV. Scotia and colleagues at Marine Scotland for organising an unforgettable research cruise that took me all around Scottish waters collecting amazing data. Thanks to all the laughs, it never felt like work. Another thanks to the team at the British Ocean Sediment Core Research Facility for all the advice and work analysing my sediment cores, their expertise is second to none.

I will always be grateful to all the friends I made in Stirling and elsewhere. It was great to know that we were all in this together and grabbing a drink was always a welcomed distraction. Even during the lockdowns of COVID-19, the organized virtual pub quizzes and games showed the strength of our community.

I would also like to thank my supporting family and old friends that have had to put up with extended periods of little to no contact from me during stressful times. They know more than most the challenges faced and words can't describe my thanks to them for being there.

A final and important thanks goes to my lovely partner Lucy Nevard. Experiencing this journey with her has provided an enormous amount of emotional support and I can't wait to spend our weekends together again.

Abstract

Pockmarks are concave seabed depressions formed by the venting of sub-seabed fluids into the water column. These fluids can contain greenhouse gases such as methane and carbon dioxide, formed by the microbial breakdown of organic carbon, thus creating a strong link between pockmarks and the marine carbon cycle. Pockmarks have been reported from the offshore waters around the UK, but until now no detailed study has been conducted on pockmarks in Scottish waters. It is important to understand the processes that lead to pockmark formation in order to assess their activity status and morphological evolution. Twelve study areas around western Scotland were selected, where pockmarks are observed, with three primary research aims: (i) to map the location and morphological characteristics of pockmarks; (ii) to map the distribution of sub-seabed gas and its spatial association with pockmarks; (iii) to characterise the physical and geochemical sediment stratigraphy from inside and outside pockmarks. Using statistical GIS methods, pockmark morphologies and distributions have been mapped and used to construct a classification system. The physical and geochemical stratigraphy of five sediment cores have also been analysed at a mm-scale resolution. 1015 previously unreported pockmarks have been mapped around western Scotland and separated into three distinct classes: common, elongated and deep; from which pockmark activity status can be inferred. This research has found that localised pockmark hot-spots are probably associated with areas of higher organic carbon within fjordic and extra-fjordic environments; these are not currently included in national carbon inventories. Finally, the geochemical analysis has shown that a shallowing of the redox zone inferred from Mn/ Fe ratio may provide a useful proxy for recent pockmark activity. These results will aid the assessment of pockmarks when considering geohazards and promote future research on the importance of pockmarks supporting vulnerable marine biotopes.

Table of Contents

Statement of originality.....	2
Acknowledgments	4
Abstract.....	5
Table of Contents.....	6
List of Figures	9
List of Tables.....	13
Chapter 1: The formation and development of pockmarks	14
1.1 How gas is formed and stored within sub-seabed sediments.....	14
1.2 Evidence of sub-seabed gas from geophysical surveys.....	18
1.3 Pockmark formation.....	21
1.4 Variation in pockmark morphology and distribution	23
1.5 Importance of understanding fluid flow and pockmark formation	26
1.6 Links between pockmarks and blue carbon.....	28
1.7 Project rationale.....	29
Chapter 2: Study areas	31
2.1 Loch Linnhe, Firth of Lorn, Loch Melfort and Loch Spelve	34
2.2 Inner Sea of Hebrides, Arisaig Bay and Loch Slapin.....	35
2.3 Summer Isles, Loch Broom and Little Loch Broom	35
2.4 Stornoway Bay and the North Minch	36
2.5 North Sea and the Scanner/ Scotia Pockmarks SAC	37
Chapter 3: Morphology and distribution of pockmarks around western Scotland.	39
3.1 Introduction.....	39
3.2 Methods.....	44
3.3 Results.....	49
3.4 Discussion	62
3.4.1 Pockmark morphology.....	62
3.4.2 Pockmarks classification	66
3.5 Conclusions	68
Chapter 4: The distribution of gas bearing sediments around Western Scotland	70
4.1 Introduction.....	70

4.2	Materials and methods	73
4.2.1	Sub-seabed geophysical data acquisition	73
4.2.2	Inverse distance weighting	80
4.2.3	Hot-spot analysis	81
4.3	Results.....	82
4.3.1	Loch Linnhe	82
4.3.2	Stornoway Bay	88
4.3.3	Loch Broom	96
4.3.4	Inner Sea of Hebrides and Arisaig Bay	99
4.4	Discussion	104
4.4.1	Hot-spot analysis and gas distribution in the study areas	104
4.4.2	Gas migration and pockmark activity.....	112
4.4.3	Geohazard assessment.....	118
4.5	Conclusions	118
Chapter 5: How Pockmarks affect the physical and chemical properties of marine sediments.....		
		120
5.1	Introduction	120
5.2	Materials and methods	122
5.2.1	Core collection.....	122
5.2.2	Core X-radiography	126
5.2.3	Multi Sensor Core Logger – Standard	126
5.2.4	Multi Sensor Core Logger – Core Imaging System	126
5.2.5	Multi Sensor Core Logger – XYZ.....	127
5.2.6	Manual core logging	127
5.2.7	ITRAX – XRF Core Scanner.....	128
5.2.8	Particle size analysis	128
5.2.9	Organic carbon and nitrogen analysis	129
5.3	Results.....	129
5.3.1	GC006	130
5.3.2	GC008	134

5.3.3	GC021	138
5.3.4	GC023	142
5.3.5	GC027	146
5.4	Discussion	150
5.4.1	East of Eigg pockmark.....	150
5.4.2	Stornoway Bay pockmarks.....	153
5.4.3	Scotia pockmark.....	155
5.5	Conclusions	158
Chapter 6: Discussion		159
6.1	Introduction	159
6.2	Formation and distribution of pockmarks around western Scotland	159
6.2.1	Distribution of pockmarks and its implications to their formation and organic carbon research.....	159
6.2.2	Distribution of free gas in sub-seabed sediments.....	163
6.2.3	The use of morphological characteristics for interpreting pockmark formation and activity status.	165
6.2.4	Pockmark activity status inferred from physical and chemical stratigraphy of sub-seabed sediments.....	167
6.3	Active venting of the Scotia Pockmark	168
6.4	Implications of pockmark formation	170
6.4.1	Geohazard.....	170
6.4.2	Biological communities	172
6.5	Future Research.....	175
6.6	Summary and Conclusions.....	176
References.....		178
Appendix A.....		201

List of Figures

Figure 1.1. A record of some of the global locations that pockmarks can be found.....	16
Figure 1.2. Types of bubbles within marine sediments adapted from Anderson et al. (1998).....	17
Figure 1.3. Evidence of gas associated acoustic facies.....	20
Figure 1.4. Formation model for pockmarks taken from (Hovland & Judd 1988).....	21
Figure 1.5. Adapted from Böttner et al. (2019) showing the uncommonly large Class 1 pockmarks and the much more common, small Class 2 pockmarks which cover much of the seabed.	25
Figure 1.6. Variations of pockmark morphologies (from Chen et al., (2015)).	26
Figure 2.1 Study locations across western Scotland. Inset map shows the region that is designated as a Special Area of Conservation (SAC)..	32
Figure 2.2 Maps showing the bedrock geology (including faults) in the main study areas of western Scotland.....	33
Figure 2.3. Maps showing the seabed sediment type, based on the Folk classification system.....	34
Figure 2.4. Regions of the Scottish seabed with either Marine Protected Area (MPA) or Special Area of Conservation (SAC) protection status..	38
Figure 3.1. Examples of crater-like depressions or pockmarks in the different chosen study areas of Western Scotland.	43
Figure 3.2. Study regions around western Scotland.	44
Figure 3.3. Schematic showing the workflow for pockmark delineation using the BGS seabed mapping toolbox in ArcGIS 10.6 followed by statistical analysis performed in R.	45
Figure 3.4. Example of pockmark delineation within the Firth of Lorn study area.....	47
Figure 3.5. Water depths of each pockmark delineated and associated study region (colour coded)..	50
Figure 3.6 Vertical relief (pockmark depth) as a function of the Area of pockmarks across western Scotland.	51
Figure 3.7. Vertical relief as a function of Area of pockmarks within each study region..	52
Figure 3.8. Morphological characteristics of pockmarks.	53
Figure 3.9. Elongation as a function of Area of pockmarks within each study region.	54
Figure 3.10. Elongation as a function of Area of all pockmarks mapped	55
Figure 3.11. Morphological characteristics of pockmarks within each study region.....	56
Figure 3.12. Clustering of pockmarks based on Vertical relief as a function of Area.....	57

Figure 3.13. Clustering of pockmarks based on Vertical relief as a function of Elongation.....	58
Figure 3.14. Identified classes of pockmarks based on the results of the Elongation as a function of vertical relief partition plot.....	59
Figure 3.15 Map of study regions and pockmark classes.....	61
Figure 3.16. Vertical relief (pockmark depth) as a function of the Area of pockmarks across western Scotland, showing the different possible trends visually observed.....	65
Figure 4.1. Maps of Loch Linnhe.....	75
Figure 4.2 Bathymetry and location of seismic lines, pockmarks and BGS borehole 78/4 in Stornoway Bay.....	76
Figure 4.3 Seismic lines from Stornoway Bay separated by instrument type.....	77
Figure 4.4. Maps of Loch Broom.....	78
Figure 4.5. Bathymetry and location of geophysical survey lines and pockmarks in the Inner Sea of Hebrides and Arisaig Bay.....	79
Figure 4.6. Geophysical survey lines from the Inner Sea of Hebrides separated by instrument type.....	80
Figure 4.7. Hot-spot analysis using the Getis-ord G_i^* statistic of pockmarks within Loch Linnhe along with an inset map showing main basins.....	83
Figure 4.8. Seismic analysis of selected lines that contains evidence of gas/fluid accumulation in the form of acoustic turbidity (LLSF2b), pockmarks and pull downs.....	85
Figure 4.9. Seismic analysis of selected lines that contained pockmarks.....	86
Figure 4.10. Seismic analysis of selected lines that contain pull-down reflectors.....	87
Figure 4.11. Seismic analysis of selected lines that contained a pockmark and nearby pull-down reflectors.....	87
Figure 4.12. Primary study region of Loch Linnhe that includes the boomer seismic survey.....	88
Figure 4.13. Hot-spot analysis using the Getis-ord G_i^* statistic of pockmarks in Stornoway Bay.....	89
Figure 4.14. Seismic analysis of Seismic line 1985/7 in Stornoway Bay.....	92
Figure 4.15. Seismic analysis of seismic lines 1985/5 in Stornoway Bay.....	93
Figure 4.16. Seismic analysis of seismic line 1977/2. Line A shows the sparker seismic profile.....	94
Figure 4.17. Seismic analysis of seismic lines 1973/22 and 1968/34.....	95
Figure 4.18. Distribution of gas identified from all pinger seismic lines available in Stornoway Bay.....	96
Figure 4.19. Seismic analysis of Boomer seismic lines 2012/53 and 2012/8.....	97
Figure 4.20. Seismic analysis of Boomer seismic lines 2012/49, 2012/50 and 2012/7.....	98

Figure 4.21. Depth to gas front analysis of the Inner Loch Broom study region.	99
Figure 4.22 Hot-spot analysis using the Getis-ord G_i^* statistic of pockmarks within the Inner Seab of Hebrides and Arisaig Bay.....	100
Figure 4.23. Position of a transit sonar survey from 1971 within the Inner Sea of Hebrides.....	101
Figure 4.24. Seismic Analysis of sparker seismic lines 1968/27+ (A) and 1970/M29 (B).	102
Figure 4.25. Seismic analysis of geophysical surveys using a pinger seismic system..	103
Figure 4.26 Distribution of gas identified from pinger seismic lines in the Inner Sea of Hebrides and Arisaig Bay.....	104
Figure 4.27. Presence of sub-seabed gas identified from zones of acoustic turbidity alongside areas of pockmark hot-spots in Loch Linnhe	105
Figure 4.28. Presence of sub-seabed gas identified from zones of acoustic turbidity alongside areas of pockmark hot-spots in Stornoway Bay	107
Figure 4.29. Presence of sub-seabed gas identified from zones of acoustic turbidity alongside areas of pockmark hot-spots in the Inner Sea of Hebrides.....	110
Figure 5.1. Map showing the location of selected cores used in this study and the course taken by the MRV. Scotia on cruise SA1019S.....	124
Figure 5.2 Maps showing the coring locations within key pockmarks.....	125
Figure 5.3. Acoustic flare emanating from Scotia Pockmark, North Sea surveyed on 29/7/19 using a EK60 echosounder.....	125
Figure 5.4 Gas fractures observed within sediment cores from Western Scotland.	131
Figure 5.5 GC006 core log.....	132
Figure 5.6. GC006; p-wave velocity and resistivity data from MSCL-S..	133
Figure 5.7. GC006: physical and chemical properties derived MSCL-XYZ and ITRAX respectively..	133
Figure 5.8 GC008 core log.....	136
Figure 5.9. GC008: p-wave velocity and resistivity.	137
Figure 5.10. GC008: physical and chemical properties derived MSCL-XYZ and ITRAX respectively.	137
Figure 5.11 GC021 core log.....	140
Figure 5.12. GC021 particle size plot.....	141
Figure 5.13. GC021: physical and chemical properties derived MSCL-XYZ and ITRAX respectively..	141
Figure 5.14 GC023 core log.....	144
Figure 5.15 Particle size plot for core GC023.	145

Figure 5.16 GC023: physical and chemical properties derived MSCL-XYZ and ITRAX respectively..	145
Figure 5.17. GC027 core log.....	148
Figure 5.18. GC027 particle size plot.....	149
Figure 5.19. GC027: physical and chemical properties derived MSCL-XYZ and ITRAX respectively..	149
Figure 5.20. Interpretation of cores GC021 and GC023 from east of Eigg.....	152
Figure 5.21. Interpretation of cores GC006 and GC008 from Stornoway Bay.....	155
Figure 5.22. Interpretation of core GC027 from Scotia Pockmark, N. Sea.....	158
Figure 6.1 Pockmark hotspots in fjordic and extra-fjordic regions..	160
Figure 6.2. Conceptual model of acoustic facies associated with gas..	164
Figure 6.3 Classes of pockmarks around western Scotland..	166
Figure 6.4 Echograms showing gas flares released from seafloor.	170
Figure 6.5(a) Spawning and nursery grounds for Nephrops (Coull et al. 1998) and Nephrops burrows identified from Underwater Television (UWTV) surveys. (b) Suitable habitats for Nephrops identified from ICES Functional Units, Vessel Monitoring System (VMS) and distribution of muddy sediment. (c) Nephrops burrows identified from UWTV and trawling intensity derived from VMS data.....	174

List of Tables

Table 3.1. Number of Pockmarks mapped within each study area.....	49
Table 3.2. Number of pockmarks mapped within each study region and the percentage within each class.....	60
Table 4.1. Estimated Carbon stocks of study regions or nearby locations where not available, adapted from Smeaton et al. (2016)	73
Table 4.2. Geophysical surveys and relevant metadata where data was available for each study site.....	74
Table 4.3. Seismic Facies of Loch Linnhe and their interpretations adapted from McIntyre 2012.....	84
Table 4.4. Seismic facies present in Stornoway Bay from Sparker and Pinger profiles. These facies are described according to their appearance and distribution characteristics.....	90
Table 4.5. Interpretation of seismic facies observed in seismic profiles from Stornoway Bay. The interpretation and lithological character of the facies is adapted from the interpretation of BGS borehole 78/4, Stornoway Bay (Graham et al 1990).	91
Table 5.1. Cores collected during the SA1019S onboard the MRV Scotia. Table also records the analysis conducted for each core.....	123

Chapter 1: The formation and development of pockmarks

Pockmarks were first discovered offshore Nova Scotia, on the seabed of the Scotian shelf (King & Maclean 1970). Although the term conjures images of a medieval plague (Hovland & Judd 1988), it most fittingly describes their overall appearance on the ocean floor. They were first defined as “*cone-shaped depressions*” found in large numbers and ranging from 15 – 45 m wide and 5 – 10 m deep (King & Maclean 1970). Since the 1970s pockmarks have been discovered during numerous oil and gas surveys, most notably on the seafloor in the Norwegian Sea and North Sea (Van Weering *et al.* 1973; Hovland & Judd 1988). They have since been found worldwide (Figure 1.1), especially in shallow shelf seas and large lakes (García-García *et al.* 1999; Hovland *et al.* 2002; Rogers *et al.* 2006; Wessels *et al.* 2010; Bussmann *et al.* 2011), sparking immense interest into their formation and role of subsurface fluid flow (Hovland *et al.* 2002, 2010; Roy *et al.* 2014; Smith *et al.* 2014; Velayatham *et al.* 2018; Coughlan *et al.* 2021). When pockmarks were first discovered, their method of formation was hypothesized as erosional; whereby escaping water or gas remove sediment, putting it into suspension where it is then carried by currents (King & Maclean 1970). Gas venting was favoured as the main pockmark forming process (Josenhans *et al.* 1978), however little evidence could be gathered to confirm this for many years. It was not until 1983, in the North Sea that proof of gas seepage was found at an actively venting of a pockmark (Hovland & Sommerville 1985; Hovland *et al.* 1987). Pockmarks now represent an incredibly important gateway to understand the distribution and migration strategy of fluids and free gas within the Earth’s crust and sub-seabed sediments. Tryon *et al.* (2001) state that “*Subsurface fluid flow is a key area of Earth science research, because fluids effect almost every physical chemical, mechanic and thermal property of the upper crust*”. Furthermore, an understanding on pockmark formation will further research into gas-hydrates (Solheim & Elverhøi 1993), deep-sea biology (Webb *et al.* 2009b), and contributions of methane to the marine carbon cycle (Judd 2003).

1.1 How gas is formed and stored within sub-seabed sediments

Gas within the marine environment can be defined based on its origin. Gas can be formed in the marine environments through three main processes:

1. Biogenic gas can be created within the first few hundred metres of sub-seabed sediment. It involves the breakdown of organic material by bacteria (Parkes *et al.* 1990). The process normally requires closely packed sediment to insure anaerobic

conditions. The anaerobic decomposition of organic matter is a competitive multi-step process involving different groups of bacteria. As such, in marine sediments much of the organic matter is involved in methanogenesis, producing carbon rich gases such as methane and carbon-dioxide. However, this only occurs below the sulphate-reduction zone as sulphate reducing bacteria out-compete the methanogenic bacteria. With enough organic matter, methane concentrations can become high enough to form gas bubbles (Albert *et al.* 1998; Martens *et al.* 1998).

2. Thermogenic gas is created deeper within the earth, typically at depths of 1000 metres or more. As with biogenic gas, organic matter is deposited on the seafloor and buried with fine-grained sediments. Through increased burial over time the pressure and temperature increases leading to the diagenetically formed (mature) source rocks containing hydrocarbons (Floodgate & Judd 1992). Gas formed in this way can migrate to shallow regions mostly by diffusion in pore waters, lighter hydrocarbons, such as methane, are expected to be the most mobile (Krooss *et al.* 1992).
3. Abiogenic gas is released into the ocean from deep within the Earth's crust through hydrothermal vents and volcanic fissures. It is possibly remnants of primordial material that first formed when the Earth was developing (Gold & Soter 1982).

Methane is the most common hydrocarbon gas, normally found within sediments which are anoxic (Judd *et al.* 1997; Fleischer *et al.* 2001a). Many gases flowing within shallow sub-seabed sediments can be actively venting into the ocean and cause various chemical reactions in the water column (O'Hara *et al.* 1995). Venting of gas is caused by the buoyancy of gas bubbles, which would naturally tend to migrate upwards to the sediment/water interface (King & Maclean 1970; Hovland *et al.* 1984). Globally, marine gas is considered to be 72 to 99% methane (Tizzard 2008) despite major microbial obstacles such as the sulphate methane transition zone, which consumes methane gas and produces carbon dioxide (Hinrichs & Boetius 2002). Methane is a potent greenhouse gas, roughly thirty times more effective as a heat-trapping gas than carbon-dioxide (Yvon-Durocher *et al.* 2014). Fluid-flow features, such as pockmarks and hydrothermal vents, have been found in every ocean in the world (Judd 2003) (Figure 1.1). Due to the geographical distribution of pockmarks and the potency of methane as a powerful greenhouse gas it is important to consider seabed gas escape as a potentially important contributor to the global carbon budget (Judd *et al.* 1997; Fleischer *et al.* 2001b; Krämer *et al.* 2017).

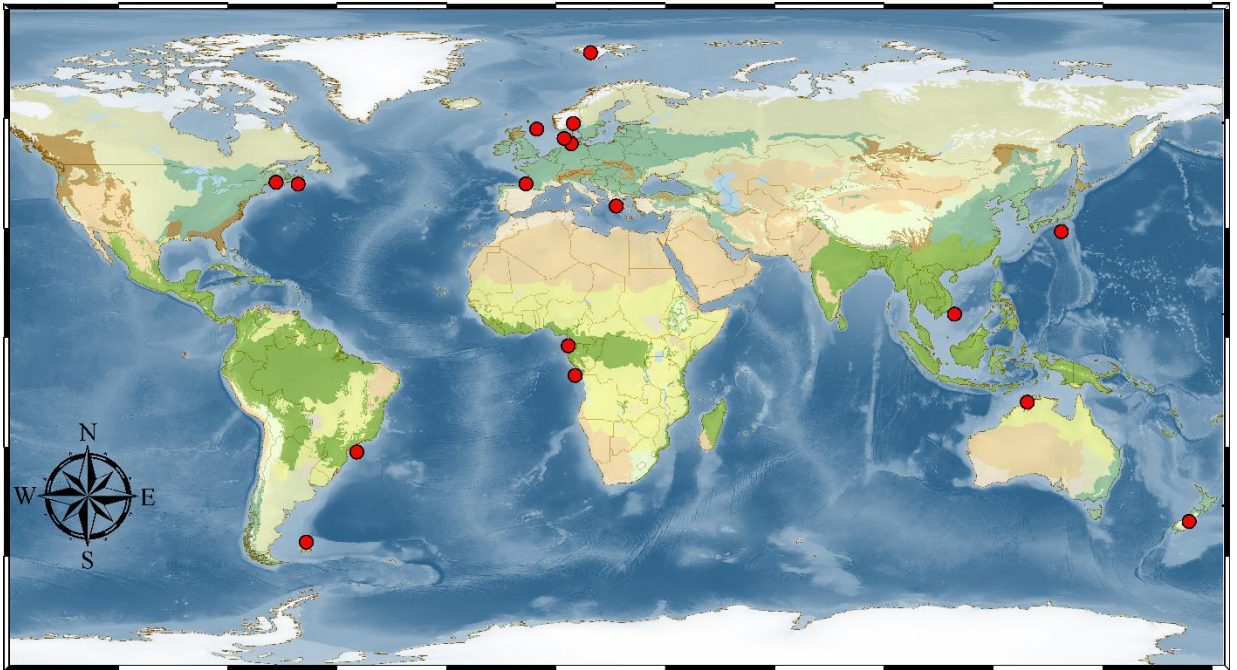


Figure 1.1. A record of some of the global locations that pockmarks can be found, these have been reported on in literature. The geographic regions where pockmarks have been reported have been taken from Judd and Hovland (2007).

As gas is formed within the sediment its buoyancy would suggest a vertical migration through overlying sediment layers. However, as these sediments can have a range of shear strengths and cohesion, it is important to understand the migration pathways of fluid flow through sub-seabed sediment. It has been remarked by Cevatoglu *et al.* (2015) that an advanced model describing the physical character of sediments alongside an improved understanding of how gas occupies and moves within pore spaces is needed to improve quantifications of gas volume and fluid flow dynamics.

One of the first models developed showing how gas occupies sediment, presents three different types of unsaturated (partly gaseous) sediments (Wheeler 1988). These sediment types are solely differentiated on their degree of saturation, with type one showing a primarily gas filled sediment and type three showing only discrete bubbles within an overall water filled matrix. One major assumption of the Wheeler (1988) model is that in order for gas to move it must pass in and out of dissolution with the surrounding pore water. Gas can exchange from one bubble to another, but can only do so when dissolved and is dependent on bubble pressure and fluid concentration gradients. The model also requires assumptions on sediment physical properties to be made in order to estimate elastic/shear strength qualities (Wheeler 1989); it assumed that the material can be modelled as either elastic and plastic dependant on which sediment property is of

interest. The model evolved somewhat, whereby a critical radius of bubble defines the ability of gas to migrate or become confined (stored) in place (Wheeler 1990). Building on the Wheeler (1988) models Anderson *et al.* (1998) propose a different physical model describing three different ways in which gas can occupy areas within sediments (Figure 1.2). These examples are based on X-ray Computed Tomography (CT) scans showing bubble characteristics within pressurised cores retrieved from Eckernforde Bay (Abegg & Anderson 1997; Anderson *et al.* 1998). These results showed that gas can be found in near spherical forms alongside oblate spheroids (coin-shaped) gas bubbles, that form in a vertical orientation, sizes of bubbles have been found to be up to 2.5cm in diameter.

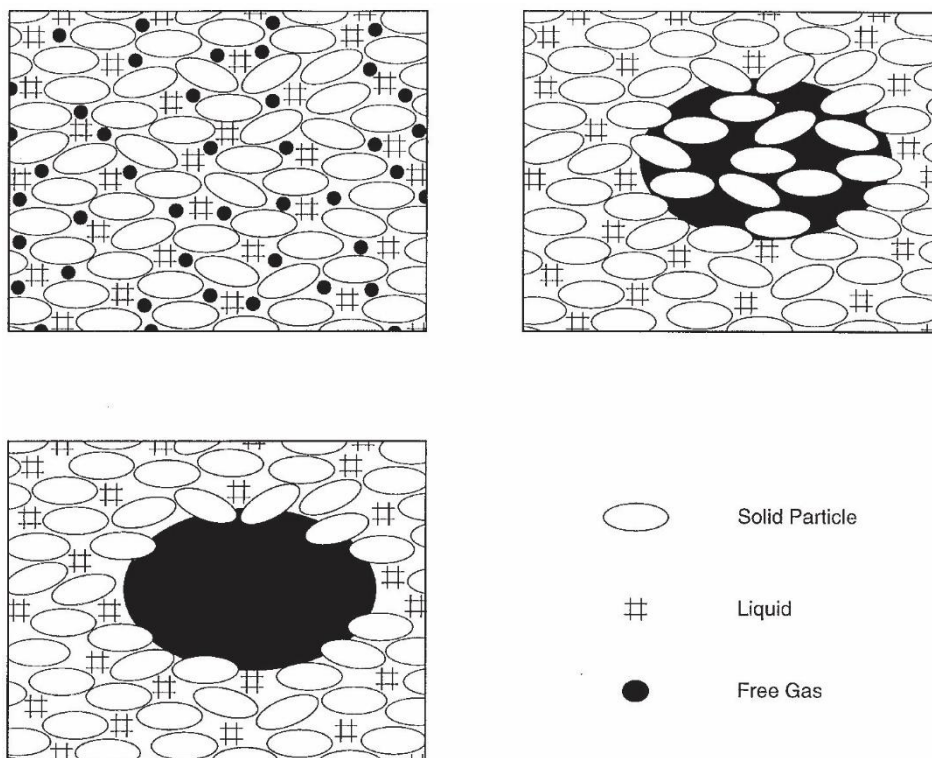


Figure 1.2. Types of bubbles within marine sediments adapted from Anderson et al. (1998). (Top-left) Interstitial bubbles. (Top-right) Reservoir bubbles. (Bottom-left) sediment-displacing bubbles.

Gas formation and gas residence in sediments is important, but it is equally important to understand gas mobility in sediments. Wheeler (1988) adapted his work from a concept of a stationary bubble to one that can vertically migrate within the sediment (Wheeler 1990). Here a spherical bubble with a critical radius can move vertically by deformation of the surrounding fine-grained media or through fissures and minute zones of weakness. The critical radius is essential as a required buoyancy has to be achieved to overcome

the cohesive strength of the sediment. Studies have shown that the shape of the bubble can alter the critical radius value; as pressure within oblate spheroids changes depending on location within the bubble (Wheeler 1990).

The Quantifying and Monitoring Potential Ecosystem Impacts of Geological Carbon Storage (QICS) project was the first controlled release of CO₂ beneath the seabed in Ardmucknish Bay, Western Scotland. This project provided an opportunity to observe the impact of the vertical migration of gases in seabed sediments in a region which is nearby Loch Linnhe, a study region of this PhD project. It was found that during initial gas release capillary invasion and fluidisation facilitated the movement of gas within the sediment (Blackford *et al.* 2014). Later within the experiment, and perhaps a critical factor to breach a pressure head, and allow for rapid vertical release of gas towards the seabed, the volume of injected gas controls the migration. This principle of a critical value that is reached before gas migration can occur is developed using Linear Elastic Fracture Mechanics (LEFM) theory (Johnson *et al.* 2002; Algar & Boudreau 2009, 2010; Barry *et al.* 2010). This theory describes how a material cracks under a stress. LEFM has found to reliably model the growth of gas bubbles within a visco-elastic-plastic medium, where bubble growth is calculated using a critical stress factor, and the rate of methane production (Boudreau *et al.* 2005; Barry *et al.* 2010). The critical stress factor can change in the material, where one sediment horizon can have a different stress factor than the one above or below. As a result, a higher stress factor horizon would inhibit the further buoyant rise of gas until the gas reaches the critical pressure that would continue the fracture. At these sites gas may also migrate horizontally along a layer until a weakness, such as preformed gas tubes in the sediment, which exhibit a lower critical stress factor is found. Recognition of floating free gas voids within X-rays of sediment shows that the majority of the gas leaves the sediment as gas bubbles which have migrated through established tubes within the sediment structure (Martens & Klump 1984). Therefore changes in the sediments physical characteristics can aid the understanding of how gas pressure and volume can build within a defined sediment type. This knowledge could be especially useful for understanding the formation, distribution and activity status of pockmarks and other fluid-escape features.

1.2 Evidence of sub-seabed gas from geophysical surveys

Where sub-bottom geophysical surveys of sediments exist around the world they are sometimes characterised by the presence of chaotic acoustic facies. Below these zones, any other acoustic structures are no longer visible and reflections below this gaseous

region are also entirely or partially obscured (Judd & Hovland 2007). This phenomenon was termed the “becken effect” (basin effect) by Schuller (1952) from his observations in Eckernforde Bay, Germany. This effect was later termed “acoustic turbidity” (Hovland & Judd 1988) and is also referred to as acoustic masking (Siddiquie *et al.* 1981), acoustic blanking (Yuan *et al.* 1992) and sometimes acoustic smearing (Papatheodorou *et al.* 1993). It is the most common acoustic expression of gas in sub-seabed sediments (Judd & Hovland 2007). Acoustic turbidity represents the attenuation, or intensity reduction, of energy in a sound wave. This attenuation is the result of either sonar scattering or absorption by gas bubbles, forming chaotic reflections that have no visible internal structure. Later research within Eckernforde Bay has shown that this gas identified on acoustic records was mostly methane, with concentrations ranging from 7 – 12.7 mmol/l (Abegg & Anderson 1997; Anderson *et al.* 1998). Similar, earlier work in the Irish Sea Basin, found that sediments cores retrieved from an area of acoustic turbidity have shown that methane concentrations range from $>100 \text{ nmol}^{-1}$ to $<10 \text{ nmol}^{-1}$ within the uppermost 1.6 m of seabed sediment (Jones *et al.* 1986).

Regions or zones of acoustic turbidity can take different shapes and sizes on geophysical (seismic) records. Therefore Taylor (1992) coined various descriptive terms such as acoustic curtains, acoustic blankets and plumes to differentiate between forms of acoustic turbidity that have different lateral distributions (Figure 1.3). Taylor (1992) states that the type of acoustic signature returned by gas accumulations can be related to the underlying geological controls. Baltzer *et al.* (2005) classification supports the work of Taylor (1992) by showing that acoustic turbidity, in the form of curtains, blankets plus two other facies known as white and black fringes relate to the depositional environments. These were identified by phase changes of the acoustic impedance signals (Baltzer *et al.* 2005). Judd & Hovland (2007) suggested that the terms acoustic curtain and acoustic blanket are not necessary and that only two types of gas-related acoustic turbidity, plumes and gas chimney can be reliably identified. These were taken to be the best acoustic representations of vertical migration of sub-seabed gas (Judd & Hovland 2007).

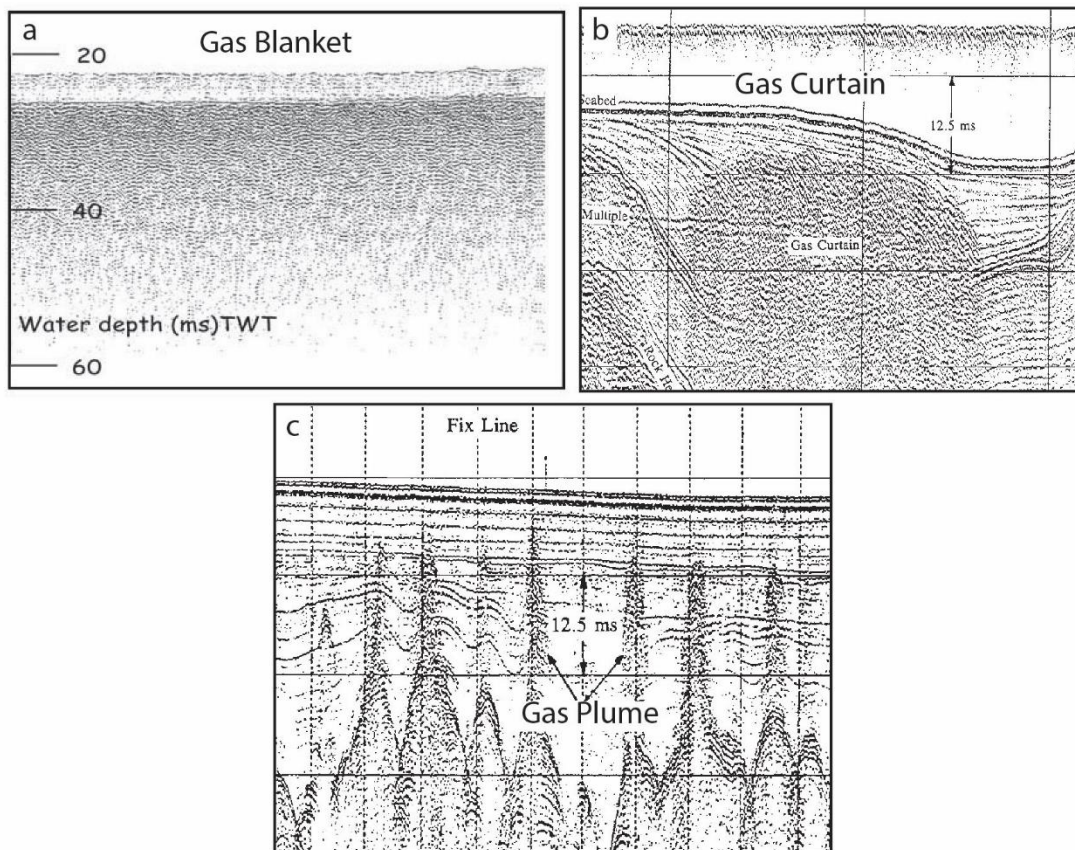


Figure 1.3. Evidence of gas associated acoustic facies. (a) Gas Blanket. (b) Gas Curtain. (c) Gas Plume. Figure adapted from Taylor (1992); Baltzer *et al.* (2005).

Gas plumes are narrow zones of acoustic turbidity with distinct lateral boundaries, typically <50 m wide, and with an apparent connection to a gas source (Taylor 1992; Baltzer *et al.* 2005; Judd *et al.* 2007). Gas plumes have been observed as having numerous high-amplitude parabolic reflectors and can also appear as an amorphous cloud of dispersed chaotic reflections (Taylor 1992; Yuan *et al.* 1992). Gas chimneys are narrow vertical zones of disturbance caused by previous focused gas migration and are characterised by a series of reflectors which dip downwards (Cevatoglu *et al.* 2015). It is noted that these terms indicate direct evidence of present/past gas migration. Much work has been conducted to detect and map the 3D structures of gas chimneys in order to understand their role in hydrocarbon migration, as they can create unfavourable conditions for seabed infrastructure and can lead to pockmark formation (Meldahl *et al.* 1999; Camargo *et al.* 2019).

1.3 Pockmark formation

The formation of a pockmark is intrinsically connected to the formation, accumulation and escape of gas/ fluids from the seabed and into the water column. Early hypothesis, broke up the process of pockmark formation into its most basic stages; these are shown in a conceptual model (Figure 1.2) (Hovland & Judd 1988). The initial stage involves the accumulation of gas to a point where the sediment pore pressure is increased (Figure 1.4A). Doming of the seabed can be observed at this stage and can be an indicator of imminent gas release. This doming may also be observed within the sub-seabed reflections in geophysical records. Small surface fractures may be observed at this stage on the flanks and around the centre of the dome (Withjack & Scheiner 1982).

As pressure continues to increase and more fractures are developed a hydraulic connection is formed which results in a sudden drop in pressure as gas can then violently escape, forming a pockmark (Figure 1.4B). As the gas rises it also expands, causing the surrounding sediments to fail by fluidisation whereby sediment and gas mix and are entrained, forming an energetic gas/sediment flare which rises into the water column (Figure 1.4C). Upwelling water helps to disperse this sediment in a process called “gasturbation” (Josenhans *et al.* 1978). At this stage bottom currents will disperse and alter the direction of the gas/sediment flare and may affect the newly formed pockmark sidewall. Erosion of this sidewall by currents would develop an elongated pockmark, whereby the direction of the currents matches with the orientation of the pockmark long axis. Even long after pockmark activity has ceased, currents can continue to modify the pockmark shape, further elongating it (Hovland 1983; Yu *et al.* 2021).

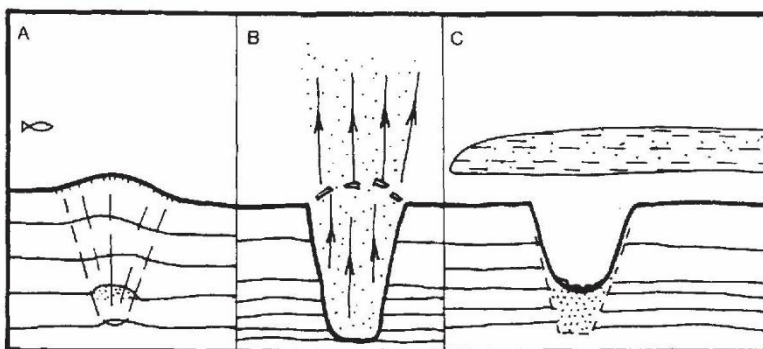


Figure 1.4. Formation model for pockmarks taken from (Hovland & Judd 1988). (A) Increase in pressure as gas forms/accumulates. (B) eruption phase. (C) post eruption phase with suspended sediment in water column.

The further activity and modification of pockmarks, post-formation, depend on the hydrographic setting and further supply of gas (Michel *et al.* 2017). Although the initial release of gas and formation of a pockmark can be violent, subsequent gas release does not have to overcome the same overburden pressure, therefore gas escape can occur at lower pressures (Hovland 1989). It is assumed that pockmarks experience repeated gas venting, though this is considered to be episodic, as gas will have to accumulate within reservoirs before having a suitable level of buoyancy and pressure to rise through the previously formed fractures (Barry *et al.* 2010). It is believed that the majority of pockmarks are dormant, the period between times of activity and the duration venting is currently unknown. To observe a pockmark actively venting is considered rare and to date no naturally forming pockmarks have been observed (Judd *et al.* 1997; Anderson *et al.* 1998; de Vries *et al.* 2007; Krämer *et al.* 2017) with the exception of human induced pockmark formation (Blackford *et al.* 2014).

After initial formation it is likely that pockmark sidewalls are over-steepened and are susceptible to slumping. Any sidewall slumping would partially infill the base of the pockmark and increase the total area of the pockmark. These (partially) infilled pockmarks can potentially block any future fluid release occurring at the centre of the pockmark (Hovland 2002; Picard *et al.* 2018). Instead, sub-seabed fluid can be redirected towards the walls of the pockmark or at new vent sites, forming on the flanks of the pockmark. These are known as complex pockmarks, characterised by two or more vent sites (Hovland *et al.* 2005; Judd & Hovland 2007).

Once a pockmark has formed the fluid pressure of the surrounding sediment is reduced. Therefore, a pockmark and the immediately surrounding area can be considered as a drainage-cell, whereby gas will preferentially migrate towards this pockmark. Within this drainage cell sub-seabed gas or other fluids will be directed through this single pockmark. Only when a suitable migration route is not available due to the sediments physical properties will an additional pockmark form. The theoretical distance around each pockmark in which another pockmark cannot form is known as the exclusion zone (Moss *et al.* 2012b). The exclusion zone is equal to half the average distance to the nearest neighbouring pockmark. It is highly probable that the density of pockmarks in a region will depend on the sediment's physical properties (e.g. thickness, density and porosity) as well as the volume of gas present (Moss *et al.* 2012b).

Overtime should a pockmark become inactive it will become infilled as sidewalls collapse, marine sedimentation and sediment redistribution occurs (Gafeira & Long 2015b). In bathymetrically shallow regions, such as continental seas, the impact of energetic storms

has been known to trigger pockmark formation and then completely remove evidence of pockmarks (Krämer *et al.* 2017).

1.4 Variation in pockmark morphology and distribution

Due to the variation in physical properties of sediments, supply of gas and pockmark activity/ venting, a wide variety of different pockmark morphologies can occur. It is believed that these variations in shape and size can be related to the activity status of pockmarks as well as the type of hydrographic and geological setting they have formed in (Gafeira *et al.* 2018; Picard *et al.* 2018).

This interest in pockmark morphology has encouraged growing research into the different forms pockmarks can take. Initially the research into pockmark morphologies was determined from 2D marine geophysical surveys. From these datasets the most common forms of pockmarks were recorded these include: unit pockmarks, normal pockmarks, elongated pockmarks, eyed pockmarks, composite pockmarks and strings of pockmarks (Hovland *et al.* 2002). However, as this is based on a 2D dataset and the terms were largely descriptive it has not been possible to capture the full range of pockmark morphologies.

A quantitative analysis of pockmark morphology was needed to develop a scientifically robust and transferable classification of pockmark forms. Advances in GIS technologies made it possible to semi-automate the mapping of pockmarks whilst simultaneously measuring a range of morphometric indices that could be best used to characterise pockmark shape. Andrews *et al.* (2010) were the first to apply such a GIS solution to an entire pockmark field in Belfast Bay, Maine. From a total of 1767 pockmarks they found that there was a positive linear relationship between pockmark depth and diameter, and that pockmarks were on average 7.6 m deep and 84.8 m in diameter. Their study represented an important step towards gathering and interpreting large datasets of pockmark morphology from entire pockmark fields rather than just from isolated regions with 2D geophysical line surveys. From approaches like this it might be possible to establish a systematic quantitative analysis of pockmark morphology worldwide.

Further large-scale pockmark mapping and characterisation was conducted across 18 study sites in the central North Sea Basin, where 4146 pockmarks were mapped (Gafeira *et al.* 2012). Through this characterisation of pockmark shape it was found that there was no relationship between pockmark depth and water depth within the North Sea Basin, however such a relationship was found within Belfast Bay, Maine (Andrews *et al.* 2010).

The work of previous researchers (Fleischer *et al.* 2001b; Judd 2003) have shown the range of settings in which pockmarks can form and highlights that a number of variables controlling pockmark formation and development are still unknown. Additionally, Gafeira *et al.* (2012) found that five pockmarks were unusually deep, including one which was nearly 18m in depth (below the surrounding seabed). These pockmarks have been known about for quite some time and named the Scotia, Scanner and Challenger pockmarks; whereby the first two exist as a complex pockmark of two individual pockmarks each (Hovland *et al.* 1984; Judd & Hovland 2007; Gafeira & Long 2015b). Böttner *et al.* (2019) developed this work by separating the pockmarks of the North Sea into two broad classes: Class 1, which are those that are generally larger and uncommon (> 6m deep >250m long and > 75m wide); and Class 2, generally those which are smaller and far more common (0.9 – 3.1m deep, 16 – 140m long and 14 – 57m wide) (Figure 1.5). The difference between these two types of pockmarks is probably due to differences in the physical properties of the sediment and the flux and/or source of fluids being released (Gafeira *et al.* 2012; Böttner *et al.* 2019). Class 1 pockmarks have formed in areas which are hydraulically connected to deeper strata through a series of fractures and vertical heterogeneities. These pockmarks in the North Sea are interpreted to have formed between 13,000 and 27,000 cal. years BP, and have been regularly active since then, probably venting a mixture of biogenic gas from Mid- to Late Pleistocene sediments and deeper thermogenic gas from deeper pre-Quaternary sources (Böttner *et al.* 2019). Whereas Class 2 pockmarks have formed solely within soft, fine-grained sediments of the Witch Ground Formation, are restricted to the surface Late Pleistocene layers, and their activity status remains unknown (Böttner *et al.* 2019). Morphological characteristics of these pockmarks reflect the physical properties of sediment and source of gas, and could be used to aid the interpretation of formation and activity status.

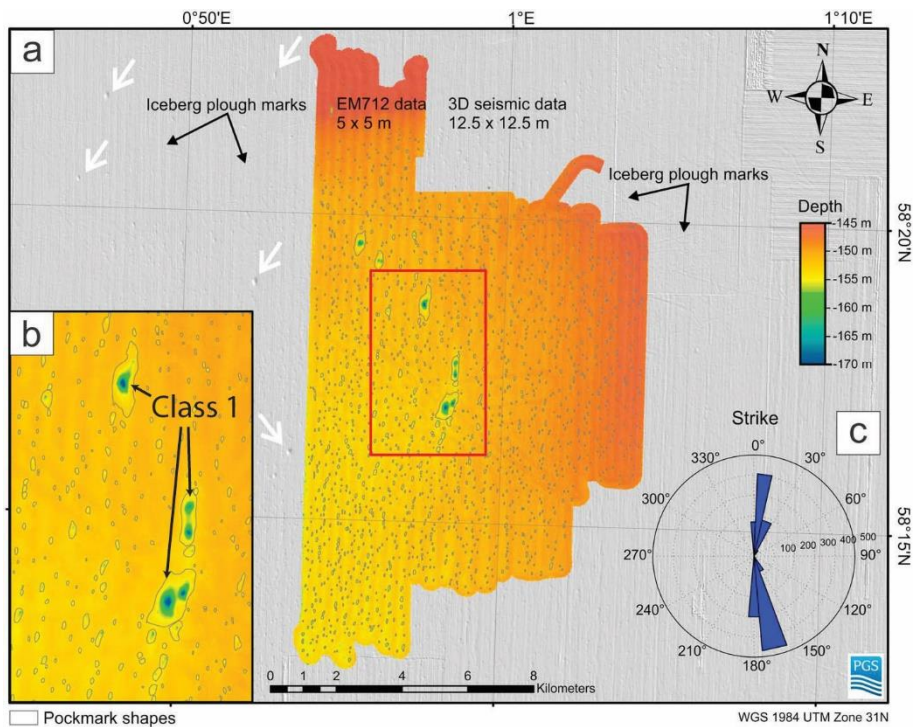


Figure 1.5. Adapted from Böttner *et al.* (2019) showing the uncommonly large Class 1 pockmarks and the much more common, small Class 2 pockmarks which cover much of the seabed.

The large variation in documented pockmark shape and size has led to an increasingly large glossary of terms to describe them. As researchers continue to observe new instances of pockmarks within previously un-surveyed regions of the ocean, new terms are used to describe them (Judd 2001; Judd & Hovland 2007; Chen *et al.* 2015). This has resulted in some terminology being introduced which often include synonyms for similar forms and complicates the literature with unnecessary jargon. For example, pockmark strings are a commonly observed feature where pockmarks have formed close to one another and in a linear or sometimes radial fashion (Hovland 1981b; Judd & Hovland 2007). These “strings” of pockmarks have also been more recently described as “chains” (Andrews *et al.* 2010; Chen *et al.* 2015) and even “trains” (Pilcher & Argent 2007; Yu *et al.* 2021) with little to no distinction between them based on size and form. In an attempt to streamline the terminology used in pockmark research a glossary was included in research by Chen *et al.* (2015), which shows the range of pockmark morphologies present on the seabed, offshore China and common terminology used to describe them. The glossary (Figure 1.6) includes the shape in plan-view of the pockmark, the size of the pockmark and the composite pattern. This was in order to capture the full range of pockmark forms present. This terminology could therefore allow an observer to classify a pockmark based on the general shape and size of a pockmark and also describe any

larger scale composite patterns which have been created. This represents the first attempt at a controlled vocabulary to describe variations in pockmark morphology. An important aspect of Chen *et al.* (2015) research is the inclusion of composite features, as these are a result of the distribution of pockmarks and could be an important geomorphological aspect to consider when interpreting formation and fluid migration pathways.

Table 1

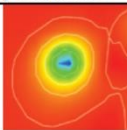
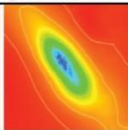
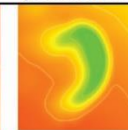
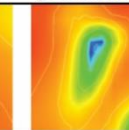
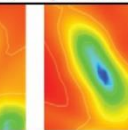
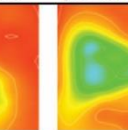
Types	Circular pockmarks	Elliptical pockmarks	Crescent pockmarks	Comet pockmarks	Elongated pockmarks	Irregular pockmarks
Plan view						

Table 2

Magnitude of size	Meters	Dozens of meters	Hundreds of meters	Kilometers
Types	Small pockmarks	(Normal) pockmarks	Giant pockmarks	Mega-pockmarks

Table 3

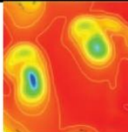
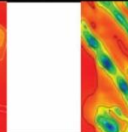
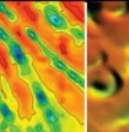
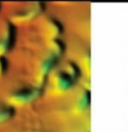
Composite pattern	Composite pockmarks	Pockmark strings	Pockmark group	
Plan view				

Figure 1.6. Variations of pockmark morphologies (from Chen *et al.*, (2015)). (Table 1) pockmark shape in plan view. (Table 2) pockmark size in diameter or width. (Table 3) pockmark composite patterns.

There is a growing consideration that the morphology of pockmarks can aid the interpretation of their formation, sub-surface fluid migration and potentially their activity status. This is due to pockmark morphology being dependant on the physical characteristics of sediment and the flux of gas to the seabed. However, morphology is also altered by the effect local hydrographic conditions such as currents and turbulence from storms. Therefore, to determine the possible formation mechanisms of pockmarks, large datasets of pockmarks are required that also investigate the sediments in which pockmarks form, particularly their chemical and physical properties. Conducting such research should theoretically allow a 3D understanding of what is happening within the sub-surface by simply observing the seabed and thus removing the need for expensive sub-bottom geophysical surveys.

1.5 Importance of understanding fluid flow and pockmark formation

Offshore activity, whether it is drilling, mining, or establishing sites for offshore renewables are all subject to natural geohazards. These “geohazards” are defined as geological

conditions which may adversely affect the installations of offshore infrastructure (Fannin 1979). Commonly listed geohazards include sediment instability, gasified sediment, seismicity, rapidly changing sediment conditions and pockmarks (Camargo *et al.* 2019). Although pockmarks are considered a geohazard on their own, many of the other geohazards are also associated with regions where pockmarks are likely to form and the process of pockmark formation. How much of a hazard each of these may pose is debated and is an important question for marine engineers when planning the development of offshore infrastructure. Pockmarks are commonly referred to as geohazards within literature (Hovland *et al.* 2002; Sun *et al.* 2017; Camargo *et al.* 2019; Coughlan *et al.* 2021). This is largely due to their formation mechanism via fluid migration, which is known to trigger large-scale sediment instability in the form of sediment slumps and slide (Sun *et al.* 2017). These could bury and/or damage marine infrastructure, particularly submarine cables (Judd 2001). Pockmarks themselves would also add stress to submarine cables should they form beneath cables; and also pose an obstacle for laying cables due to the sometimes large variations in bathymetry. However, it is still debated whether pockmarks are to be universally considered as geohazards, as there is some evidence that their presence may actually enhance seafloor stability (Riboulot *et al.* 2019). It is suggested, based on the size of pockmarks within the North Sea, that some may not have formed during a catastrophic release of gas, and that they are only intermittently active (Fannin 1979; Judd *et al.* 1997), venting low volumes of gas. Pockmarks may also become relict features whereby they are no longer active and therefore do not pose a risk (Fannin 1979; Camargo *et al.* 2019). Therefore, although many geohazards associated with pockmarks may pose a risk to offshore infrastructure, pockmarks themselves may not always be seen as a marine geohazard.

Pockmarks also provide important sites for supporting biological communities, particularly where species are able to overcome the anoxic conditions present. Several pockmarks in the UK and Norwegian sectors (Hovland & Judd 1988; Jensen 1992) of the North Sea have shown a variety of marine life within the centre of pockmarks. Most notably the Tommelitan (Hovland & Judd 1988) and Scanner Pockmark (Dando 1991; Webb *et al.* 2009b) where a greater density of flora and fauna have been recorded within pockmarks than the surrounding seabed. The presence of Methane Derived Authigenic Carbonates (MDAC) in the Scanner Pockmark have formed unique habitats for marine life which protects them from trawling activity (Dando 1991; Webb *et al.* 2009b; Gafeira & Long 2015b). The relationship between pockmarks and marine life has also been noted in other regions, such as offshore Brittany, France where it was found that pockmarks might support *Haploop* communities (Champilou *et al.* 2019). However, this finding that

pockmarks support a higher diversity and abundance of marine life is not universally accepted and is highly variable between sites, and may potentially be only relevant when MDAC or other hard substrates are present (Dando 1991).

1.6 Links between pockmarks and blue carbon

As global greenhouse gas emissions continue to rise and the effects of climate change become more severe countries have recognised the important role the ocean plays in the global carbon cycle (Nellemann *et al.* 2009). Over half of the worlds biological carbon is captured by marine organisms. the oceans are also responsible for storing and cycling 93% of the Earth's carbon dioxide, giving rise to the term "blue carbon" (Nellemann *et al.* 2009). Furthermore, it has been calculated that the top 1 m of the worlds sediments contain ~2322 Pg C, and yet only 2% are in fully protected areas (Atwood *et al.* 2020). The importance of recognising the worlds carbon inventories is to help to inform management of human activities and ensure that these carbon stores are undisturbed (Atwood *et al.* 2020; Smeaton *et al.* 2021).

The inshore and offshore waters of Scotland have been the focus of several studies aiming to create carbon store inventory (Stahl 2012a; Burrows *et al.* 2014; Smeaton *et al.* 2016). Initially this focused on marine organisms and environments such as kelp, seagrasses and salt marshes as the key sequesters of carbon (Stahl 2012a, b) and later included soft seabed sediments (Burrows *et al.* 2014; Smeaton *et al.* 2016). Scotland's fjords and firths are now recognised as globally important stores of organic carbon; naturally sequestering organic-rich material in seafloor sediment basins (Smeaton *et al.* 2017, 2020). Despite fjordic environments being recognised three decades ago as major carbon stores (Syvitski *et al.* 1987), quantifying the carbon in Scotland's fjordic, and even more so for further offshore sedimentary systems, has remained a largely neglected topic.

Pockmarks are known to form in soft muddy sediments, where large volumes of carbon rich gases have formed from the microbial decomposition of organic matter (Abegg & Anderson 1997; Judd & Hovland 2007). Studies have shown that the percentage weight of organic carbon in the surface sediments of pockmarks can range between 1.2 wt.% and 8 wt.% globally (Abegg & Anderson 1997; Kuşçu *et al.* 2005; Webb *et al.* 2009a; Wessels *et al.* 2010). In the North Sea, sediments within pockmarks have been reported to contain on average 2.8 ± 0.23 wt.% organic carbon (Webb *et al.* 2009b). The average fraction of organic carbon in recent seabed sediment samples is 2.5 wt.% globally (Siddiquie *et al.* 1981; Kuşçu *et al.* 2005). However, there is a considerable amount of spatial heterogeneity in carbon rich areas particularly in offshore sediments (Diesing *et al.*

2021; Smeaton *et al.* 2021), where small-scale variability is not considered (Seiter *et al.* 2004). This suggests that pockmarks may indicate important regions of higher carbon stocks and a need for further sampling, monitoring and protection of the seabed (Atwood *et al.* 2020; Smeaton *et al.* 2021).

It is clear that understanding the location, distribution and formation of pockmarks is important for geohazard assessments for offshore industries. But it is also important to consider that pockmarks, in some cases, can provide refuges or niches for vulnerable benthic communities and potentially indicate important regions containing high volumes of organic carbon. Therefore pockmarks need to be considered by marine spatial planners in the designation of future Marine Protected Areas (MPAs).

1.7 Project aims

Pockmarks around western Scotland have been occasionally reported in the scientific literature (Howe *et al.* 2002; Stoker *et al.* 2006; McIntyre & Howe 2010; McIntyre 2012; Gordon *et al.* 2016). However, to date no focused study has been conducted on pockmarks in Scotland inshore / territorial waters (<12nm). The overall aim of this project is to be the first comprehensive scientific research on pockmark characteristics from key sites around western Scotland – in fjordic, extra fjordic and other nearshore settings. This aim will be achieved by targeting three areas of pockmark research: (i) pockmark morphology, (ii) pockmark distribution and (iii) physical and geochemical sedimentology/stratigraphy.

The scientific aims, which are addressed in Chapters 3, 4 and 5, of this research are:

1. Chapter 3 aims to establish whether there are any morphological trends which can be used to infer activity status and build a novel morphological classification system. This will be achieved by mapping pockmarks across 12 study sites around western Scotland and identify the range of pockmark morphologies present – aiming to devise a robust and quantitative classification system.
2. Chapter 4 aims to investigate whether the distribution of pockmarks correlates with the presence and coverage of sub-seabed gas. This will be achieved by collating marine geophysical datasets and interpreting the seismic stratigraphy in order to establish the potential origin of gas in sub-seabed sediments. This will be compared to the locations of pockmarks mapped using geo-statistical techniques to establish why pockmarks form in certain geographic settings.

3. Chapter 5 of this thesis aims to investigate whether evidence of gas-venting can be inferred from the geochemical and physical stratigraphy of sediments from inside and outside selected pockmarks. This will be achieved by comparing sediments cores from inside and outside pockmarks collected during this PhD project.

By targeting these three specific research areas of interest this project seeks to provide aid the interpretation of pockmark morphology and distribution in a NW European setting and investigate potential pockmark formation and activity status in different hydrographic environments. This project will also develop mapping products which show the distribution and presence of pockmarks and their relationship with gas-rich sediments in fjordic environments of western Scotland. Pockmark activity status and their potential role as geohazards is also a key line of interest and will be addressed within each area of research. This research project aims to significantly develop and advance our understanding of pockmark formation and pockmark activity status in nearshore Scottish waters. The results of this research can be used to inform industry and marine (geological/biological) conservation planning.

Chapter 2: Study areas

The main study areas for this project are spread across the nearshore/inshore water of western Scotland. These study areas include: (i) fjords - regions defined as glacially over-deepened marine basins with restricted circulation (Howe *et al.* 2010; McIntyre & Howe 2010; Smeaton *et al.* 2017); (ii) fjord approach and glaciated bays - regions which lie outside main fjords and more open to marine influence but are usually surrounded by local headlands or islands; (iii) extra-fjordic - regions which are the most hydrodynamically exposed areas and located within the wider inlets/straits where they are influenced by stronger currents (Figure 2.1). The majority of the study areas are within the Inner Hebrides and the Minches Special Area of Conservation (SAC). Other regions also have further protection status, the Firth of Lorn, Summer Isles and Loch Broom, Inner Sea of Hebrides study areas are also designated as Marine Protected Areas (MPA). Loch Linnhe is the only study site which does not have any protection status. The SACs and MPAs have been designated largely on the basis of the marine life present, with some consideration of the geological formations and submarine landforms such as glacial lineations, glaciated channels/ troughs, and well preserved recessional moraines. The Wester Ross MPA which covers the Summer Isles, Loch Broom and Little Loch Broom considers the preservation status of pockmarks, showing that these structures are indeed important to protect (Gordon 2016).

The study areas chosen for this study include those which have reported the presence of pockmarks such as Loch Broom, Loch Linnhe and Inner Sea of Hebrides (Stoker *et al.* 2006). Others study areas were also chosen due to the known, yet unpublished presence, of pockmarks based on the recently available higher-resolution bathymetric data. As the formation of pockmarks can be due to gas formed through either thermogenic or biogenic sources it is important to consider the bedrock (Figure 2.2) and overlying Quaternary geology of the study areas. As pockmarks can normally form in regions with fine grained muddy / cohesive sediment (Judd & Hovland 2007) it is also necessary to understand the mapped distribution of seabed sediment types (Figure 2.3). The presence of faults may also be important as pockmark formation has been linked to trigger events such as earthquakes (Hasiotis *et al.* 1995). It is therefore expected that pockmarks may form in regions where major faults are present (Figure 2.2 and Figure 2.3). In the following sections the geological and bathymetric characteristics of each study area will be

described, with a particular focus on those factors which may relate to the formation of pockmarks.

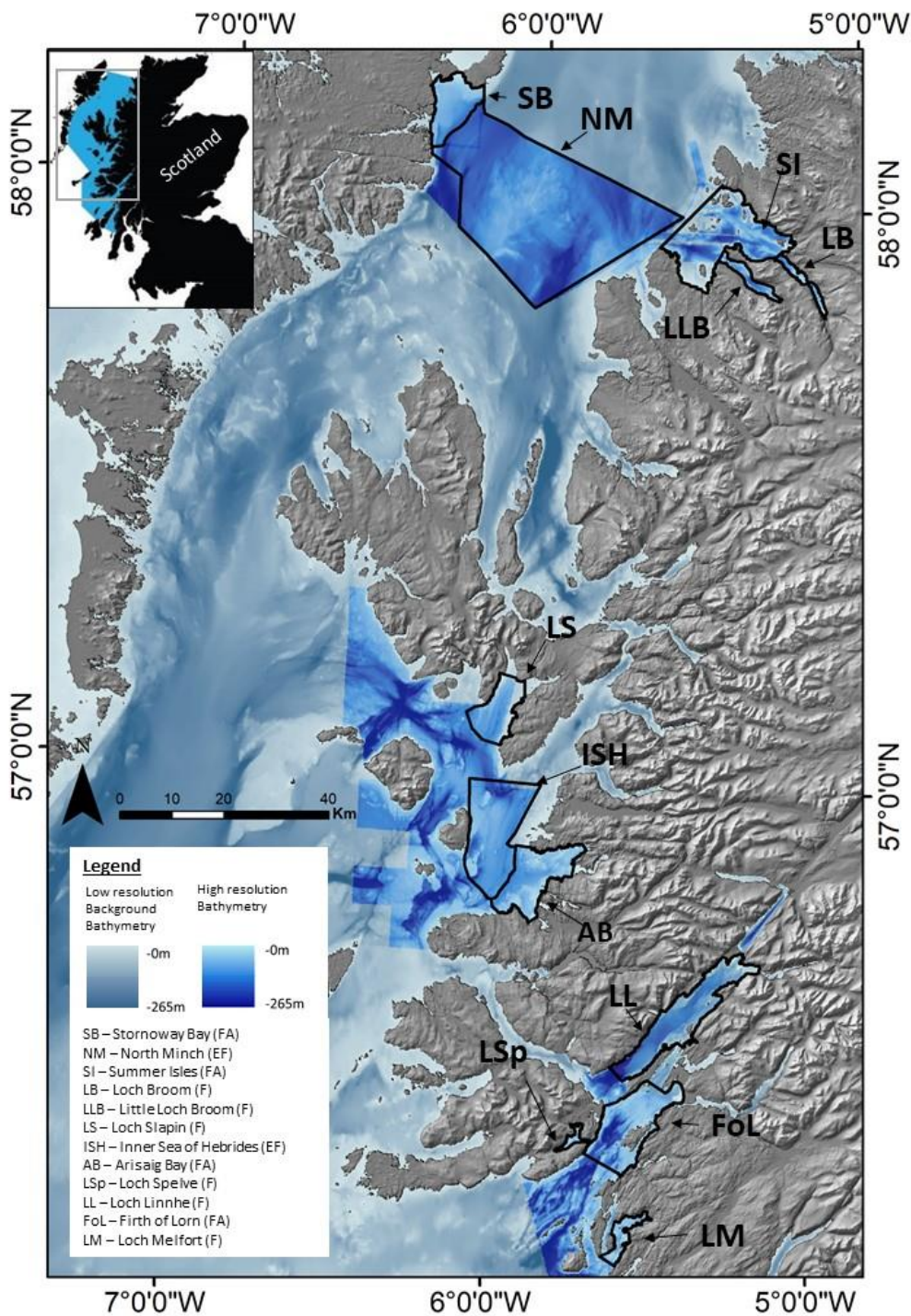


Figure 2.1 Study locations across western Scotland. Inset map shows the region that is designated as a Special Area of Conservation (SAC). Labels of study regions describe their hydrographic setting, including Fjord Adjacent (FA), Extra-fjordic (EF) and Fjordic (F) settings.

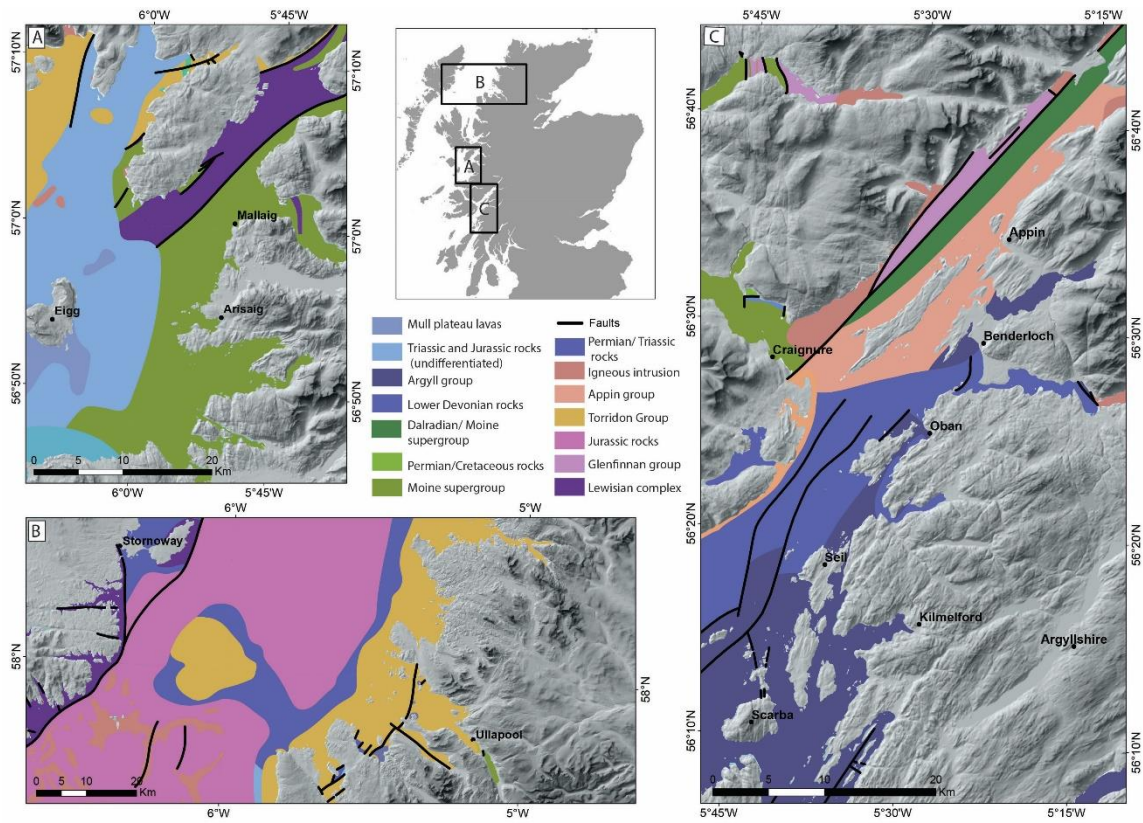


Figure 2.2 Maps showing the bedrock geology (including faults) in the main study areas of western Scotland. From the BGS Offshore GeoIndex [2021].

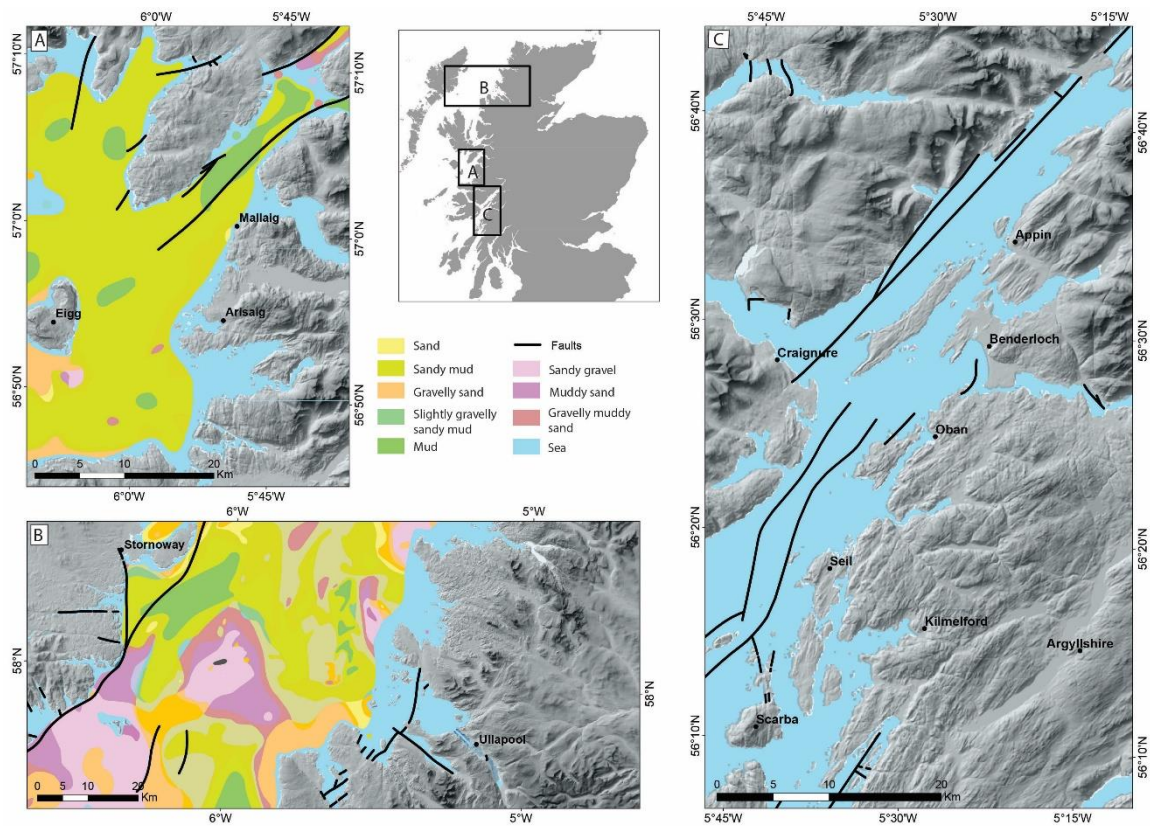


Figure 2.3. Maps showing the seabed sediment type, based on the Folk classification system. Note that no data is available for the Firth of Lorn (Map C). From the BGS Offshore GeoIndex [2021].

2.1 Loch Linnhe, Firth of Lorn, Loch Melfort and Loch Spelve

The Firth of Lorn and adjoining bathymetric regions are geologically diverse spanning a time period from the Precambrian to the Holocene (Howe *et al.* 2015). The oldest rocks, which dominate a large part of the Firth of Lorn include Dalradian slates, limestones and schists. These are overlain by the Old Red Sandstone succession which is composed of sandstones and conglomerates as well as the Lorn plateau lavas. There are also small areas of other bedrock formations which include Jurassic rocks around Mull and on the Ardnamurchan peninsula. Within Loch Linnhe the main fault system related to The Great Glen Fault (Kennedy 1946) which separates the bedrock into the Moine metamorphic series to the western side of Loch Linnhe and Dalradian metamorphic series to the eastern side of the fault complex.

The region has experienced successive glaciations throughout the Quaternary (last 2.6 Ma) (Golledge *et al.* 2009; McIntyre & Howe 2010). As a result numerous deep rock basins have been carved throughout the region. Glacial still stands and readvances have created

a patchwork of moraines on submarine bedrock and sometimes in deeper basins (Howe *et al.* 2015). The last ice mass to effect Loch Linnhe was during the Younger Dryas ~12.8 – 11.5 ka BP when a substantial tide-water glacier terminated in the vicinity of Shuna Island (Golledge *et al.* 2009; McIntyre 2012).

2.2 Inner Sea of Hebrides, Arisaig Bay and Loch Slapin

These regions are also noted as being geologically complex where numerous tectonic features related to the Moine Thrust and younger geological episodes are present (Fyfe *et al.* 1993). The main bedrock types include Precambrian Torridonian sandstone, Triassic and Jurassic rocks exposed at seabed in the two main basins, Little Minch trough and Inner Hebrides trough. Evidence of volcanic activity is also prevalent within the region, originating from the nearby Skye, Eigg, Mull and Ardnamurchan Paleogene volcanic centres (Brown *et al.* 2009). The presence of Jurassic rocks in the Inner Hebrides Basin, between Eigg and Ardnamurchan, may elude to potential thermogenic sources of gas in this region – with organic rich Liassic source rocks have been noted in some areas of the Inner Hebrides Basin (Hesselbo & Coe 2000; Hesselbo *et al.* 2010).

The effect of glaciation in the study area is clearly observed on the bathymetry where the seabed has been shaped by a South flowing ice stream (Howe *et al.* 2012) part of Hebrides Ice Stream or the Barra-Donegal Fan Ice Stream (Howe *et al.* 2012; Dove *et al.* 2015); a southern equivalent to The Minch Ice Stream (Bradwell *et al.* 2007, 2021) during times of ice sheet glaciation. The Quaternary sequences within the region mostly consists of the Jura Formation. This Formation is interpreted as glaciomarine to marine sediments deposited between 13.5 ka BP and 16.5 ka BP (Davies *et al.* 1984; Fyfe *et al.* 1993). The Jura Formation has been subdivided into four members on seismo-stratigraphic grounds; from oldest to youngest: Muck (glaciomarine), Rum (mainly marine), Arisaig (marine) and Sleat (modern) (Howe *et al.* 2012; Arosio *et al.* 2018).

2.3 Summer Isles, Loch Broom and Little Loch Broom

Like most of the seaboard of western Scotland, the areas around the Summer Isles has been heavily glaciated. The Summer Isles contain ten islands and separated by a large number of skerries, representing the top of streamlined bedrock features. Feeding into the Summer Isles are two narrow sea lochs; Loch Broom and Little Loch Broom. These troughs or fjords were eroded and sculpted by the passage of warm based highly erosive glaciers which fed into the main paleo-ice stream flow through The Minch (Stoker *et al.*

2006). The bedrock of the region is characterised by Precambrian Torridonian sandstone, overlain by Moine supergroup rocks to the East of the Moine Thrust. It has been suggested that the orientation of the sea lochs are controlled by NW trending faults; a known fault runs along the length of Little Loch Broom (Stoker & Bradwell 2009).

Deglacial sediments found below seabed in these fjords began to be deposited ~14 ka BP when the glacial ice mass retreated from the Summer Isles and into the sea lochs (Stoker & Bradwell 2009). Tidewater glacier advance and retreat deposited what is referred to as the Assynt Glacigenic Formation and Annat Bay Formations (Stoker *et al.* 2009). The uppermost formation present in Loch Broom is the Summer Isles Formation, consisting of marine sediments of varying grade deposited during the Holocene, after 8 ka BP. Other relevant geomorphological features within the Lochs are large debris lobes and slumps which indicate periods of instability, possible due to earthquake activity triggered by rapid deglaciation between 15 and 14 ka BP (Stoker & Bradwell 2009; Stoker *et al.* 2009). This neotectonic activity has been associated with rare fluid release within the fjord and localised sinking of the seabed (Stoker & Bradwell 2009).

2.4 Stornoway Bay and the North Minch

There is less bedrock geology diversity within these study areas. The majority of the bedrock is recorded as undifferentiated Jurassic sandstones and limestones across the majority of the Minch, although exposure of the bedrock is very rare owing to the considerable thickness of Quaternary and Holocene sediments. The exception to this is the central Minch where a large outcrop of Torridonian sandstone, known as the East Shiant Bank, lies partially exposed at the seabed. In Stornoway Bay, parallel to the coast of Lewis the bedrock changes to red Permian and Triassic sandstones before abruptly coming in contact with Lewisian Gneiss complex close to the shore. The presence of Jurassic rocks has long been considered as a source for potential hydrocarbons in the North Minch (Graham *et al.* 1990; Morton 1993). A prominent major fault runs parallel to the coast of Lewis, within Stornoway Bay (Imber *et al.* 2002). The presence of this fault alongside deeper Jurassic source rocks allows a potential thermogenic source of gas and migration pathways in the vicinity of Stornoway bay.

The glacial history of this region is dominated by the presence of the Minch palaeo ice-stream (Bradwell & Stoker 2015). Interpreted from a range of streamlined bedforms present on land and seabed, the ice-stream drained the northwest sector of the Scottish ice sheet during the last glacial stage. This ice-stream is responsible for the deeper N-S trending buried troughs/basins within the Minch, and the sculpted, streamlines

bathymetric form of Stornoway Bay. Further from shore glacial sediments lineations and drumlins are observed on and around the Torridonian bedrock of East Shiant Bank (Bradwell *et al.* 2007). The post-glacial sediments within the region are variable in thickness probably due to the strong currents within the Minch. In Stornoway Bay, the seabed borehole 78/4 (Graham *et al.* 1990) displays seven units which reflect the main environmental changes. These results combined with cosmogenic and optically stimulated luminescence dates from boulders and deltaic deposits from the Northeast coast of Lewis provide a minimum age of deglaciation in the Minch, ca. 20-18 ka BP, with ice-free conditions by 16 ka BP or even earlier (Bradwell *et al.* 2021).

2.5 North Sea and the Scanner/ Scotia Pockmarks SAC

The North Sea, specifically the region known as the Witch Ground Basin (Figure 2.1) has been a sediment depocenter during the Late Jurassic and Early Cretaceous periods and again throughout the Quaternary period (King & Maclean 1970, Böttner *et al.* 2019). The stratigraphy of the Witch Ground Basin is composed of clays interbedded with sandstone and limestone during the Paleogene and Neogene sequences (Judd *et al.* 1994). The Quaternary sequence of sediments (~600m) include evidence of subglacial, glaciomarine and marine conditions, especially within the early Pleistocene of the Aberdeen Formation (Hovland & Sommerville 1985, Evans *et al.* 2021). The Coal Pit formation deposited during Marine Isotope Stage 3 – 6 consists of glacial till and hard dark to light grey, pebbly sands, sandy mud and mud (Davies *et al.* 2011). The Swatchway Formation is characteristic of glaciomarine conditions where pebbles are rare amongst sandy clays (Stoker & Long 1984). The uppermost part of the Witch Ground Formation is of Holocene age where sedimentation has ceased since the last 8 ka (Judd *et al.* 1994).

The presence of shallow gas has been of key interest in the North Sea since the 1970s for the development of the oil and gas industries (King & Maclean 1970). As such hundreds of pockmarks have been discovered and studied (Gafeira *et al.* 2012). The origin of the gas which has formed these pockmarks has been attributed to both biogenic and thermogenic sources (Judd *et al.* 1994). Several studies have also focused on analysing the variation of pockmark morphology (Böttner *et al.* 2019). An important finding has been that there exists a class of pockmarks which are atypically large (Gafeira *et al.* 2012, Böttner *et al.* 2019). These include the Scanner, Scotia, Challenger and Breemar pockmarks (Hovland & Sommerville 1985). The Scanner and Scotia pockmark (Figure 2.4) have also been designated as a special area of conservation due to the presence of

methane derived authigenic carbonate. These structures made by leaking gas provide suitable protection and heterogenous substrate for a diverse range of marine life.

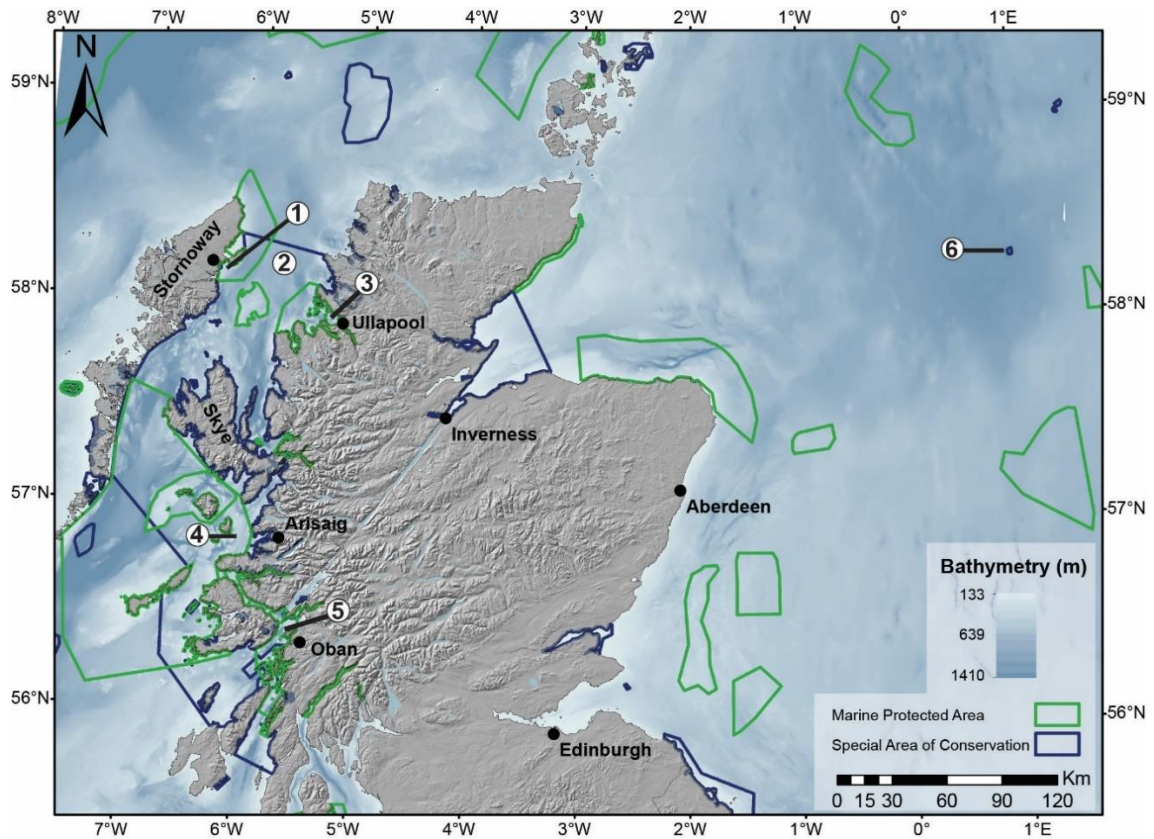


Figure 2.4. Regions of the Scottish seabed with either Marine Protected Area (MPA) or Special Area of Conservation (SAC) protection status. (1) North East Lewis MPA and Inner Hebrides and the Minches SAC. (2) Inner Hebrides and the Minches SAC. (3) Wester Ross MPA. (4) Sea of Hebrides MPA and Inner Hebrides and the Minches SAC. (5) Loch Sunart to the Sound of Jura MPA and Inner Hebrides and the Minches SAC. (6) Scanner Pockmarks SAC. Figure contains Joint Nature Conservation Committee data © copyright and database right (2020). Contains NatureScot data © copyright and database right (2020). Contains UK Hydrographic Office data © copyright and database right (2020).

Chapter 3: Morphology and distribution of pockmarks around western Scotland.

N.B. An earlier version of this chapter has been published in Audsley, A., Bradwell, T., Howe, J.A. & Baxter, J.M. 2019. Distribution and classification of pockmarks on the seabed around western Scotland. Journal of Maps, 15, 807–817. The main focus of this paper was to report the methodology used to build a classification model for pockmarks. This chapter covers this and also includes extra graphical plots on pockmark morphological trends not shown in the published version. Furthermore this chapter expands on the interpretation of how pockmark morphology can be used to gain an understanding of pockmark activity status and the local hydrographic conditions.

3.1 Introduction

Pockmarks are classically described as crater-like seabed depressions, but can vary greatly in shape and size (Park *et al.* 1979; Hovland & Sommerville 1985; Andresen *et al.* 2021). They are typically formed by the focused migration and venting of carbon-rich fluids, commonly methane, from the sub-seabed sediment into the water column (Judd & Hovland 2007). It is widely held that the presence of pockmarks at the seabed reflects the presence or former presence of gas-rich sub-surface sediments (King & Maclean 1970). Determining the age and activity status of pockmarks can be challenging, however there is growing agreement that their distribution, density and morphology could be useful indicators of the gas-storage potential of the sediments beneath (Hovland *et al.* 2010; Krämer *et al.* 2017; Andresen *et al.* 2021). Pockmark morphology can also provide insights into their formation as no observations of a pockmark forming exist (Joseph 2017). Chen *et al.* (2015) created a speculative formation model through morphological analysis, for crescent pockmarks forming in strings. Although the model required seismic data in order to provide suitable evidence in support of the interpretations, this type of work provides a useful insight into the formation of this type of pockmark. Chen *et al.* (2015) suggest that in the future, researchers may only need to observe morphological traits in order to provide a suitable formation model.

Pockmarks usually form in large fields consisting of hundreds to thousands of individual features. As such, there is a need for semi-automated techniques that reduces the time spent on mapping and measuring morphological parameters. Such a digital toolset was developed and successfully used to map large pockmark fields in Canada (Andrews *et al.* 2010) and the North Sea (Gafeira *et al.* 2012). The published results using this toolset

offer support for the use of morphology as a proxy for sub-seabed conditions and fluid-migration resulting in pockmark formation (Gafeira et al., 2018). For example, it has been interpreted that the number of pockmarks within the Witch Ground Basin are controlled by the thickness of soft, late glacial sediments (Gafeira et al. 2012). In turn the density of pockmarks within this region can be used to predict the variations in sediment thickness. However, it has been shown in the Barents Sea that the density of pockmarks seem independent of sediment thickness, although the authors do report a correlation between the size of pockmarks and the thickness of fine-grained sediments within the region (Rise et al. 2014). Therefore, the use of pockmarks as proxies may only be relevant to regional settings due to the complexity and variation in pockmark morphology. There is potential for pockmark morphology to act as a proxy for regional sub-seabed conditions and fluid-migration, however these not only require a mapping toolset but a descriptive classification system that allows for the recognition of similar pockmark types.

The challenge in creating a classification system for pockmarks is that they exhibit large variation in shape and size. The first published set of commonly observed forms of pockmarks includes *unit pockmarks*, *normal pockmarks*, *elongated pockmarks*, *eyed pockmarks*, *composite pockmarks* and *pockmark strings* (Hovland et al. 2002). These six classes are loosely defined by qualitative observations of pockmark shape and size, and sometimes refer to the length of the major axis when separating unit, normal and elongate pockmarks. Further definitions of pockmark types have been suggested in the literature, sometimes using terms for pockmark formations which are synonyms for other previously named forms. Such terms include *pockmark chains* (Iglesias et al. 2010), which are very similar to pockmark strings and used interchangeably; *mega* and *giant pockmarks* which are determined by the area or length of the pockmarks (Chen et al. 2015). A consequence of having a terminology which includes numerous definitions with similarities between such definitions is that the objective of understanding the relationship between pockmark morphology and sub-seabed conditions becomes obscured. An additional complexity is that *normal pockmarks* consist of two sub-types; *regular* and *asymmetric* (Hovland et al. 2002). Which in turn can include, *circular*, *elliptical*, *crescent* and *comet pockmarks* (Chen et al. 2015). The issue is that all these definitions only consider the shape and size of a pockmark based on the plan view of the feature, none include a depth measurement of the pockmark. This variable is frequently used in combination with area and can aid interpretation of pockmark activity status / history (Gafeira et al. 2018). To develop a robust classification system, each recognised pockmark form must be statistically distinguishable and their potential size ranges must be included. Furthermore, a controlled

vocabulary needs to be established to avoid unnecessary jargon which can confuse interpretation even more.

In some cases, the presence of submarine structures made by leaking gases can be relevant for designation as a Special Area of Conservation (SAC), such as the European Union designated Scanner pockmark SAC in the North Sea (Gafeira & Long 2015b; JNCC 2018) (Figure 2.4). Pockmarks have been discovered in many locations on ocean floors worldwide and at a range of depths from >1000 m in the abyssal ocean (Pilcher & Argent 2007; Panieri *et al.* 2017) to much shallower settings on the continental shelf (<100 m), providing evidence of their wide bathymetric range. In European waters, gas/fluid- escape related pockmarks have been identified from high-resolution bathymetry and geophysical data in all the shelf seas: in the Mediterranean (Marinaro *et al.* 2006), Black Sea (Papatheodorou *et al.* 1993; Çifj *et al.* 2003), Baltic (Whiticar & Werner 1981), Barents Sea (Hovland & Judd 1988; Solheim & Elverhøi 1993), North Sea Basins (Judd & Hovland 2007; Gafeira & Long 2015a, b; Krämer *et al.* 2017) and the Irish Sea (Reilly *et al.* 2012; Szpak *et al.* 2012; Coughlan *et al.* 2021). So far, no inventory or detailed studies have been conducted of pockmarks in Scottish fjords or the adjacent inshore waters and shelf seas west of the UK. Not only can such data be used to promote the establishment of further MPAs but it can also help to inform industry regarding the development of offshore infrastructure. The presence of gas-release features are considered as a significant geo-hazard to offshore developments (Best *et al.* 2006), therefore a detailed inventory of mapped pockmarks, and their activity status would be extremely valuable to the development of sustainable and safe marine infrastructure.

Over the past fifteen years, the inshore (territorial) waters of western Scotland (<12 nautical miles from shore) have been surveyed using a range of different hydro-acoustic multibeam (swath) echo-sounder (MBES) systems, chiefly as part of the Civil Hydrography Programme (CHP) of the UK Hydrographic Office (UKHO), under the auspices of the UK Maritime and Coastguard Agency (MCA). The resulting high-resolution bathymetric datasets provide substantial coverage of the seafloor around Western Scotland with a horizontal (grid) resolution of 1–10 m and a vertical resolution of generally <0.5 m (Figure 3.1). A range of seabed gas-release and instability-related features have been identified from MBES imagery in the fjords and coastal waters of West Scotland, often coupled with other sub- seabed acoustic data (Stoker *et al.* 2006; Stoker & Bradwell 2009; Hillman *et al.* 2015; Arosio *et al.* 2018). The pockmarks previously mapped, from the fjords of Western Scotland, are thought to be a testament to the large volume of organic material deposited within these nearshore semi-enclosed basins before, during

and immediately after ice-sheet deglaciation (Stoker *et al.* 2006; Smeaton *et al.* 2016, 2017).

Numerous crater-like depressions have been observed on bathymetric surveys used from the water around Western Scotland (Figure 3.1). This study aims to produce the first widespread mapping of crater-like depressions, hereby interpreted as pockmarks across western Scotland. This work builds upon previously reported observations of pockmarks, within Scottish inshore settings (Stoker & Bradwell 2009; Howe *et al.* 2010) and importantly produce a quality-controlled geodatabase which can be accessed by stakeholders to advance the assessment and development of offshore infrastructure and the spatial planning of MPAs.

To advance the current pockmark classification schemes, this chapter also aims to develop a novel, statistically robust classification methodology. In doing so, it is hoped that a foundation for pockmark classification can be established and developed in future studies. The aim of the new classification system is to include a limited but clearly defined set of pockmark types which include commonly measure variables of pockmark shape and size.

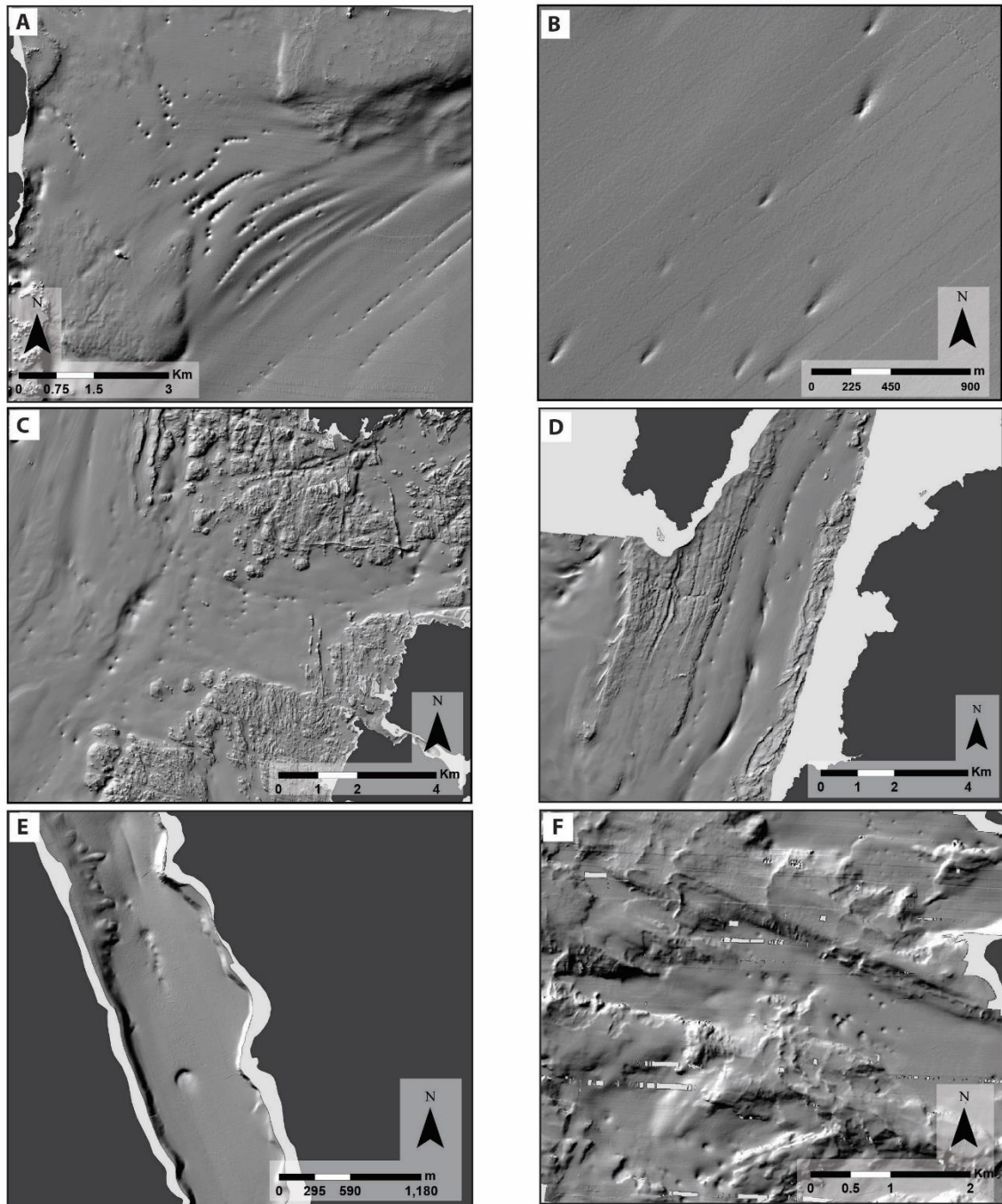


Figure 3.1. Examples of crater-like depressions or pockmarks in the different chosen study areas of Western Scotland. (A) Stornoway Bay. (B) North Minch. (C) Arisaig Bay. (D) Loch Slapin. (E) Loch Broom. (F) Summer Isles. Contains public sector information, licence v3.0, from UK Hydrographic Office.

3.2 Methods

This study uses twelve high resolution MBES hydrographic datasets from inshore waters of western Scotland which were collected between 2005 and 2015 by the UKHO (Figure 3.2). The surveys were conducted to the International Hydrographic Organisation order 1a specification (IHO 2020) using several research vessels and echosounder models. Multibeam data was processed using CARIS HIPS and SIPS software and gridded at a variety of resolutions from 2 m to 12 m.

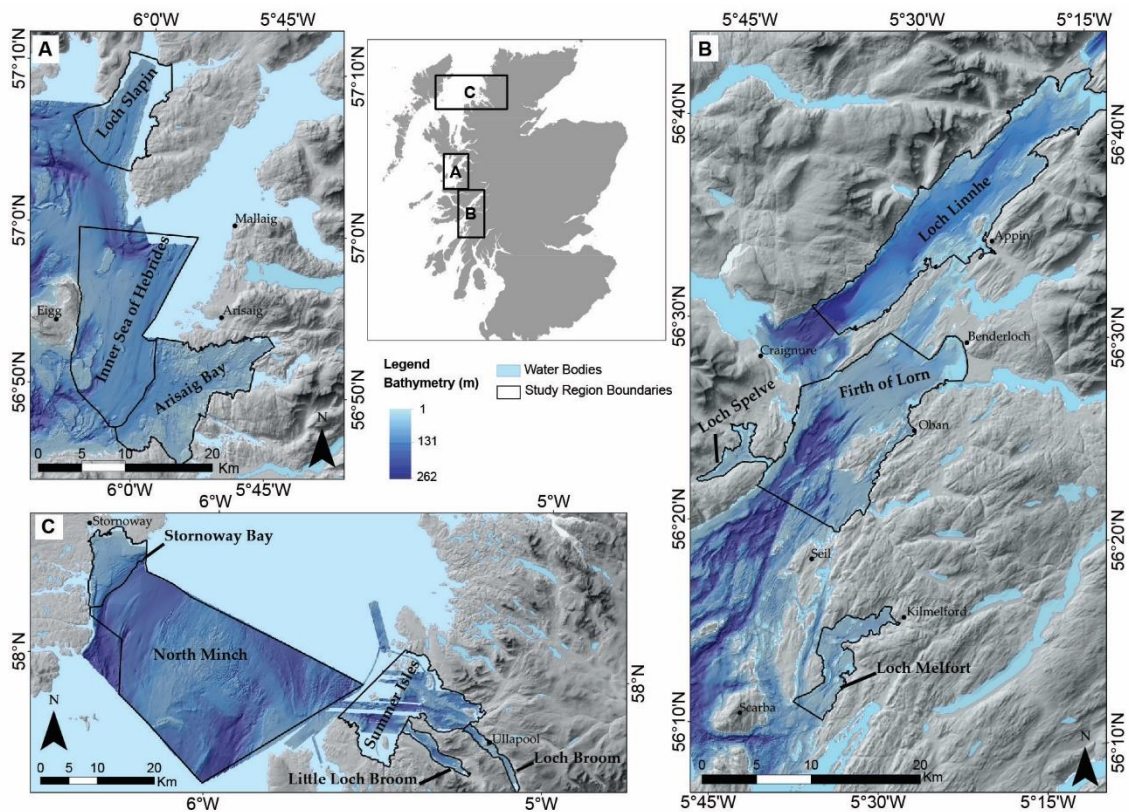


Figure 3.2. Study regions around western Scotland. Map contains the boundaries of named study regions used within this research. Figure contains UK Hydrographic Office data © copyright and database right (2020). UKHO survey numbers: Stornoway Bay HI1255, North Minch HI1352, Summer Isles HI1300, Inner Sea of Hebrides and Arisaig Bay HI1257, Loch Slapin HI1299, Loch Linnhe HI1373, Firth of Lorn / Loch Spelve / Loch Melfort HI1354. Loch Broom survey code – 2020-191660.

These MBES datasets were imported and analysed within ArcGIS 10.4 and seabed mapping was conducted using the BGS Seabed Mapping Toolbox (Gafeira *et al.* 2012). The toolbox allows for the user to set their own limits to the geospatial analysis to map specific features of the seabed. For this study the tool was set to identify confined depressions (Figure 3.1) within each study site using a bespoke methodology (Figure 3.3).

This workflow involved three main stages: (i) raster preparation, (ii) feature delineation and (iii) statistical classification.

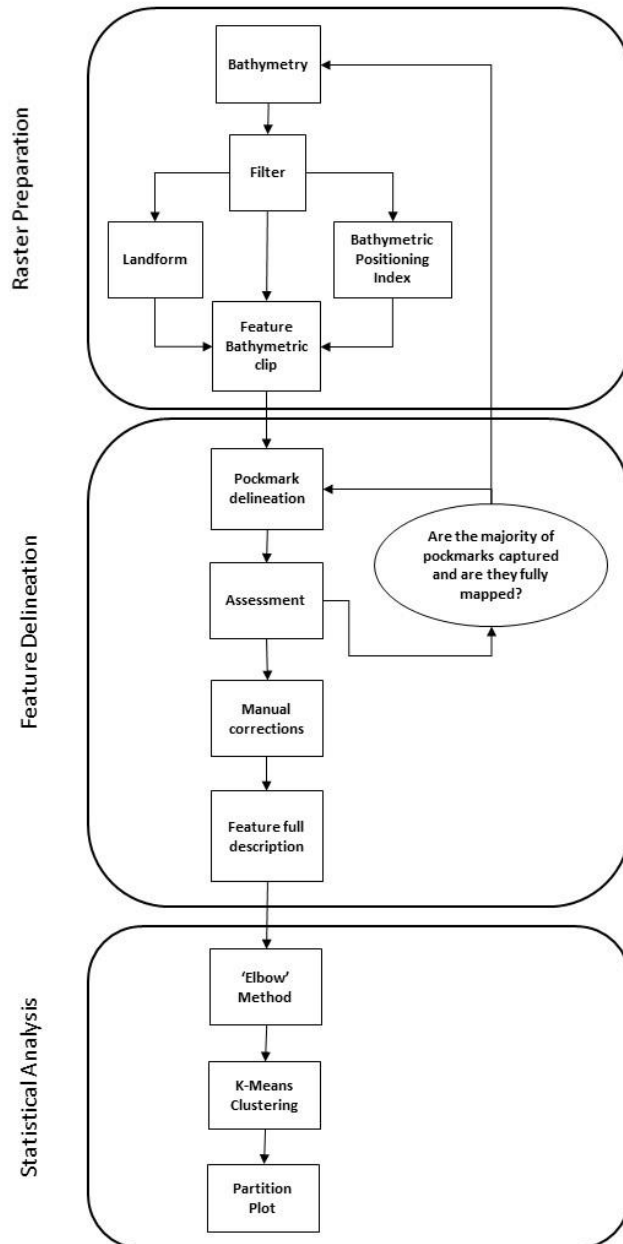


Figure 3.3. Schematic showing the workflow for pockmark delineation using the BGS seabed mapping toolbox in ArcGIS 10.6 followed by statistical analysis performed in R.

The first stage of preparing the raster was necessary as it is challenging to isolate features based on the original MBES datasets, that is if the bathymetry of the region is anything other than flat with few features/ artifacts. Regions that did include artifacts, resulting from data collection, were smoothed using the ArcGIS 'Filter tool'. This was used conservatively and with low thresholds as to not manipulate the bathymetry and adversely

affect the characteristics of the features of interest. The 'Filter-based Clip' tool within the BGS toolbox allowed for the isolation of the main regions of interest; those which contained confined depressions. By clipping the raster, it is possible to reduce the processing/mapping time and remove the effect large basins and artifacts have on the mapping process. From this point it is possible to select several methods that transform the raster into a derived terrain. Although this process changes the units of the raster surface it highlights various bathymetric characteristics and aids desired feature recognition. The 'Landform' tool within the 'Geomorphometry and Gradient Metrics' toolbox (Evans *et al.* 2014) proved the most useful. This process highlights regions of concavity/ convexity based on Bolstad and Lillesand, (1992). The 'Benthic Terrain Modeller' can also be used at fine and broad scales to create a Bathymetric Position Index (BPI) which is derived from the original bathymetry (Walbridge *et al.* 2018). The new BPI layer defines the location of specific features and regions in relation to other features and regions within the same area, in this case we are interested in changes of depth. BPI is a commonly used tool for geoscientists for this type of landform research (Gafeira *et al.* 2018; Walbridge *et al.* 2018) although it does require testing several settings to achieve the desired results. At this stage any number of methods can be used to simplify the raster and highlight the features of interest in order to aid mapping. In general, several of these methods were used in each study site, requiring testing at each study site in order to achieve the best result using the seabed mapping toolbox. It was found that the landform derived surface and a fine/broad scale BPI surface provided a suitable raster that highlighted regions of confined depressions, allowing for a more accurate delineation in most study regions. However, due to the featureless bathymetry of the North Minch it was possible to achieve accurate delineation using the multibeam bathymetry raster itself.

The second stage of analysis used the 'Feature Delineation Bathy' or the 'Feature Delineation BPI' tool within the seabed mapping toolbox, depending on what prior raster modification methods were used previously. The tool is fundamentally based on hydrological principles in that a "sink" is recognised where no cells surrounding the feature are lower. The "fill" tool is the basis of feature delineation as it first fills all "sinks" within a region to the "overflow" point. In the case of pockmarks, this is the level of the seabed. This newly "filled" raster is then subtracted from the original. The delineation tools require several limits to be set to target a specific feature of interest. These limits include: cut-off vertical relief, minimum vertical relief, minimum width, minimum width / length ratio and buffer distance (Gafeira *et al.* 2012, 2018). The cut-off vertical relief is the contour line that will be used to delineate the pockmark. The minimum vertical relief, width and width / length ratio set the limits for which features will be delineated. The buffer distance allows

for an additional area to be included and compensates for the cut-off vertical relief being based on the internal contour of the feature, this value is estimated according to how much the feature is outside the cut-off contour. For this stage it was also found that several passes of the tool, using varying values for the limits, were required to capture the majority of features and delineate them accurately. It is common for features of interest to be missed during the delineation process or they might return inaccurate delineations. In the case of this study, since there were only a few hundred features of interest within each study region, it was possible to visually assess the accuracy of the mapping. At this stage the user can also manually delineate the feature of interests that may not have been picked out during the mapping process. The toolbox then calculates a range of morphological characteristics, recording them in an attribute table. It also creates a polygon shapefile representing the feature of interest, and two point shapefiles indicating the geometrical centre and deepest point of the feature (Figure 3.4). Morphological characteristics within the attribute table of each feature include: the depth of the pockmark depression itself also known as vertical relief; elongation, calculated as width / length ratio; minimum water depth, which is the depth of the water column to the 'fill' level. We use these key attributes to describe the morphology of the features. Additional characteristics are also calculated including the profile indicator which calculates a value that defines the shape of the cross-sectional bathymetric profile. In the case of pockmarks this can either be V-shaped or U-shaped, expressed as values between 0 – 1 respectively. The slope angle is also recorded; however, this is taken from a raster which has been calculated using the "slope" tool within ArcGIS spatial analyst toolbox.

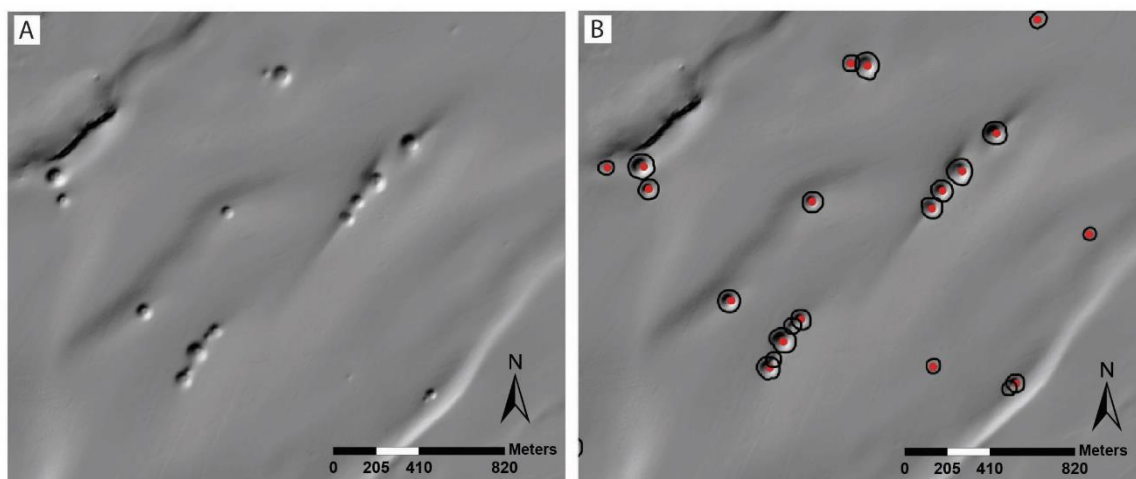


Figure 3.4. Example of pockmark delineation within the Firth of Lorn study area. (A) Bathymetry showing conical shaped depressions interpreted as pockmarks. (B) Pockmarks have been delineated (black polygon) and a point shapefile (red point) created indicating the deepest point of the pockmark.

The morphological classification of pockmarks was conducted using a statistical k-means clustering algorithm (MacQueen 1967; Wagstaff *et al.* 2001) within the software R. For this study three main morphological variables were chosen to investigate clustering as these are the most common characteristics that refer to the size of pockmarks (Gafeira *et al.* 2012, 2018; Schattner *et al.* 2016; de Mahiques *et al.* 2017), these were: (i) area, (ii) vertical relief and (iii) elongation. Elongation was calculated by the seabed mapping toolbox as width divided by length. To help visualize these results the following amendment to the calculation was performed: $\text{elongation} = 1 - (\text{width}/\text{length})$. In doing this the viewer can read values which approach 1 as more elongated. The k-means clustering algorithm requires a set number of clusters which were determined using the 'elbow' method (MacQueen 1967; Wagstaff *et al.* 2001). This method examines the ratio of the between sum-of-squares and total sum-of-squares for the dataset when we add 1-10 clusters. The point at which the gradient of the line changes the most (the 'elbow') indicates the number of clusters that are most likely present. Each additional cluster added after this point explains less of the variation within the dataset. Once a number of clusters has been chosen it is used within the k-means clustering algorithm to separate the dataset into one of three clusters. This is determined by the algorithm placing a random centroid for each cluster. As more observations are added the centroid is recalculated as the mean value of the observation within that cluster. Each cluster therefore contains all the observations that are more similar to each other than to members of another cluster. Each observation is then allocated to the cluster to which it belongs according to the k-means clustering algorithm. It is then possible to assess the amount of error using a quadratic function partition plot to separate the clusters. If observations cannot be separated into distinct clusters by this equation, then an application error rate is returned. Therefore, the ability for this quadratic function to explain the clusters is assessed and a low application error rate is desired. This process used the 'partimat' package within R.

3.3 Results

In total, 1015 pockmarks have been mapped across the twelve study regions (Table 3.1). Stornoway Bay has the highest number of pockmarks at 191, whilst Loch Spelve has only 13 pockmarks recorded. When the size of the study region is taken into account Stornoway Bay has the highest density of pockmarks recorded, with 2.21 pockmarks/ km² whilst North Minch has the lowest density 0.2 pockmarks/km².

Table 3.1. Number of Pockmarks mapped within each study area.

Region	Area (km ²)	No. of Pockmarks	Pockmark/km ²
Stornoway Bay	86.4	191	2.21
North Minch	876.8	178	0.2
Summer Isles	232.1	70	0.3
Loch Broom	18.1	23	1.27
Little Loch Broom	24.1	18	0.75
Loch Slapin	82.1	41	0.5
Inner Sea of Hebrides	205.1	66	0.52
Arisaig Bay	125.8	85	0.68
Loch Linnhe	168.3	169	1
Firth of Lorn	161.2	123	0.76
Loch Spelve	9.8	13	1.33
Loch Melfort	28.3	38	1.34
All Regions	2018.1	1015	0.5

It was found that the highest number of pockmarks are in water depths of 35m, with two additional peaks at 70m and 115m water depth (Figure 3.5A). Across almost all study regions the median water depth where pockmarks have formed is less than 75m, except for Summer Isles with a median depth of 80m and North Minch where most pockmarks form deeper than 100m and up to a maximum of 150m (Figure 3.5B).

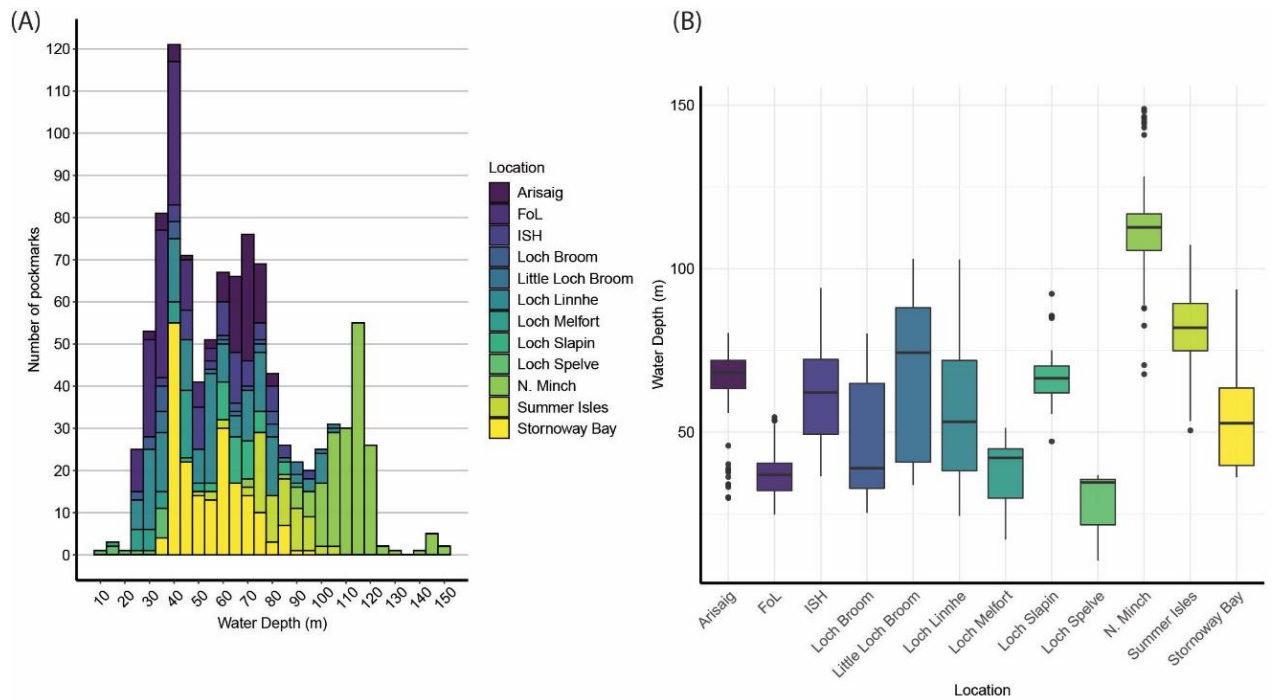


Figure 3.5. Water depths of each pockmark delineated and associated study region (colour coded). (A) Histogram showing number of pockmarks delineated and the water depth range they are found in. (B) box plots showing the range of water depths found where pockmarks are delineated in each study region. Boxplots show the median, interquartile range (IQR), maximum ($Q3 + 1.5 \times IQR$) and minimum ($Q1 - 1.5 \times IQR$) values and outliers which are $\geq 3 \times IQR$ above and below the first and third quartile.

When vertical relief is presented as a function of area across all study regions, it is observed that there are some discrete trends where it appears that the two variables share a relationship (Figure 3.6A). This is further explored in the scatterplots which show the strength of the observed correlations (Figure 3.7). The low p-value within each study region shows that this relationship is not due to random chance and that there is a strong statistical significance of the observed dataset. Therefore, it is accepted that there is a positive relationship between pockmark vertical relief and pockmark area. The Pearson's r correlation coefficient of the Arisaig pockmarks has the strongest relationship between vertical relief and area. The weakest correlation is found within Loch Linnhe and North Minch. Across all study regions the correlation is positive showing that with an increase in vertical relief there is a relative increase in area. It was only found that a relatively small increase in area with deeper pockmarks is observed within certain areas such as Firth of Lorn and Loch Linnhe compared with regions such as the North Minch. Regions such as Stornoway Bay and Arisaig form their own trend, which show that with an increase in vertical relief there is an approximately equal increase in area.

Western Scotland is not the only region where pockmarks have formed. It has been well documented that pockmarks form further offshore in the North Sea Basin. Two atypically large pockmarks are found within this region: the Scanner pockmark and Scotia Pockmark, both of which are complexes of two separate pockmarks. West scanner pockmark has a much greater area than any other pockmark recorded across western Scotland and the North Sea Basin. When these pockmarks are presented alongside the pockmarks mapped within this study the data become strongly skewed (Figure 3.6B). Nonetheless the observed trends are still visible, and they even highlight the difference between the pockmarks forming around western Scotland compared to the atypically large pockmarks of the North Sea.

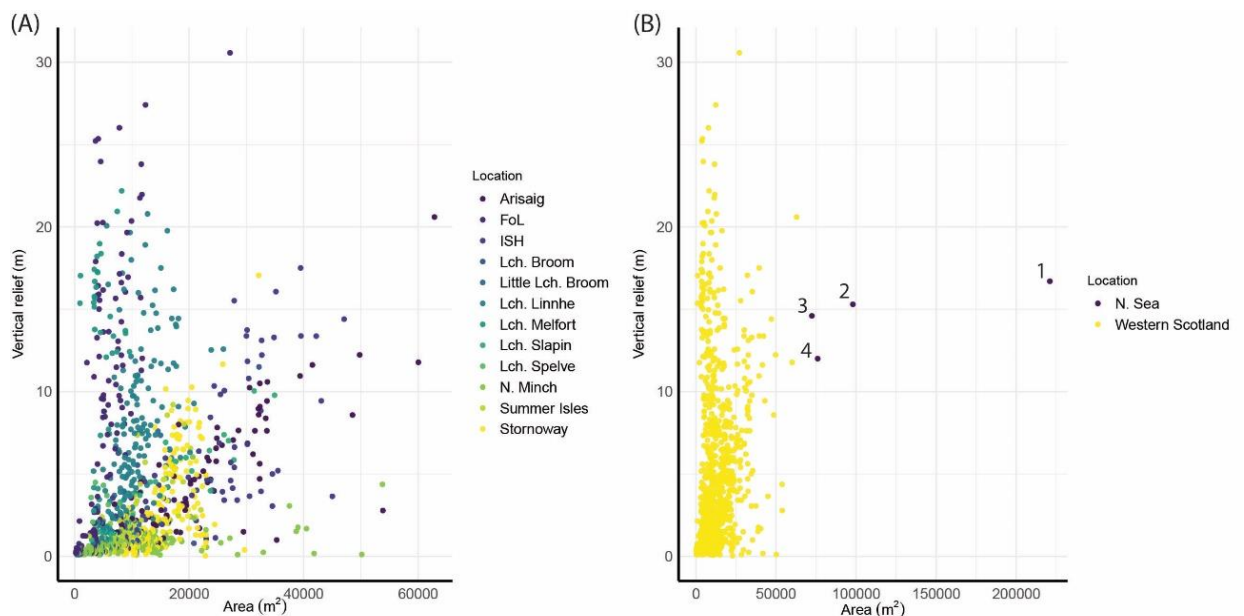


Figure 3.6 Vertical relief (pockmark depth) as a function of the Area of pockmarks across western Scotland. (A) Results of pockmarks mapped within study regions (colour coded). (B) Results of pockmarks delineated across study sites of western Scotland and those of atypically large pockmarks of the North Sea (1) West Scanner, (2) East Scanner, (3) South Scotia, (4) North Scotia

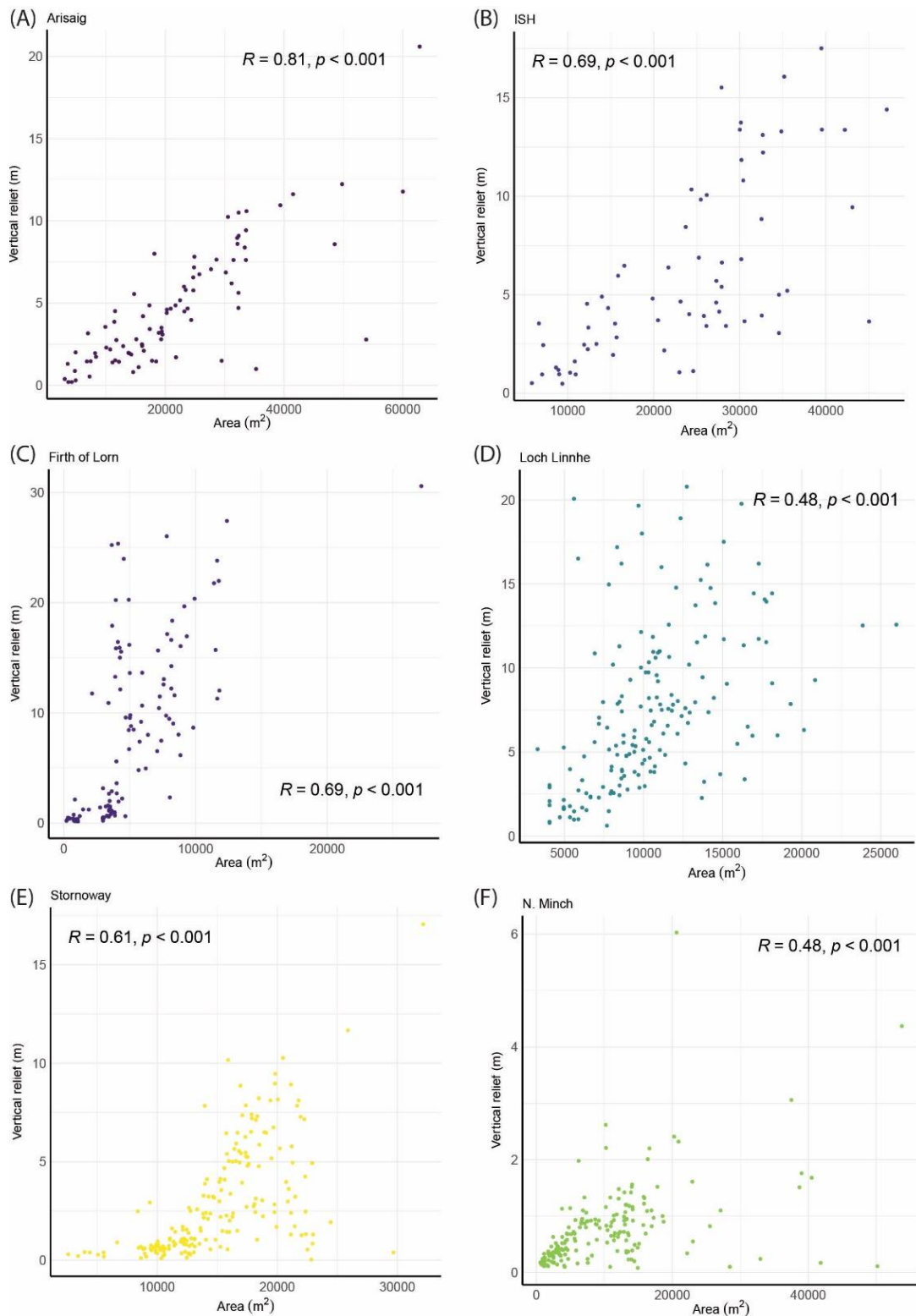


Figure 3.7. Vertical relief as a function of Area of pockmarks within each study region. Strength of the correlation (Pearsons *r*-values; *p*-values) are also shown. (A) Arisaig Bay, (B) Inner Sea of Hebrides, (C) Firth of Lorn, (D) Loch Linnhe, (E) Stornoway Bay, (F) North Minch.

Another relationship that should be investigated is that of elongation and vertical relief. It would be expected that with an increase in elongation there would also be an increase in pockmark area. No clear trends are seen within the scatter plot of pockmark elongation vs pockmark vertical relief. The most elongated pockmarks, with values ≥ 0.6 , are found in the North Minch, Inner Sea of Hebrides and a single pockmark outlier in Arisaig Bay (Figure 3.8). In all regions, circular pockmarks (values ≤ 0.2) are most common, with the median elongation value for the majority of regions ≤ 0.2 . Most pockmarks within the study region of Western Scotland are circular in plan-view.

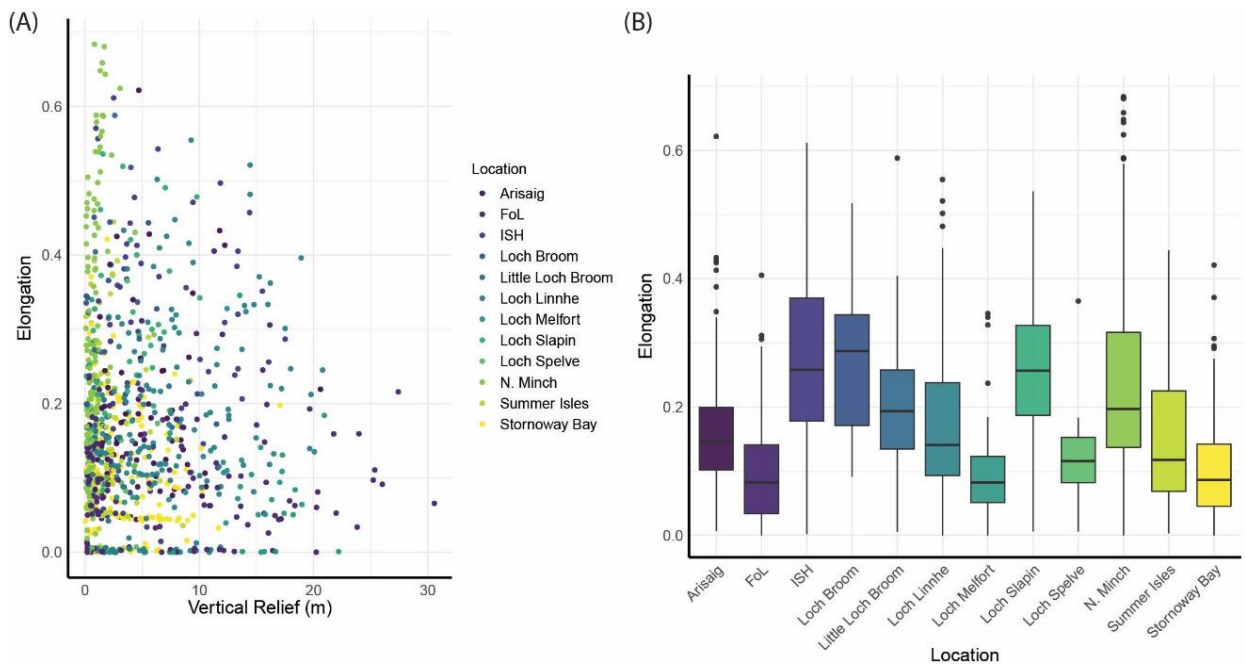


Figure 3.8. Morphological characteristics of pockmarks. (A) Elongation as a function of Vertical Relief of pockmarks within each study region (colour coded). (B) Boxplot showing the elongation values of pockmarks within each study region.

To test the relationship between elongation and area the strength of the correlation was investigated (Figure 3.9, Figure 3.10). In the regions of Inner Sea of Hebrides and Firth of Lorn the p-value is greater than the 0.05 significance level and therefore we cannot accept that these two variables are related in these regions. In all other regions we can accept that elongation is related to area. Typically, as pockmark elongation increases there is a relative increase in pockmark area. However, due to the strength of the correlations and multi-modality of the datasets this relationship is not strong and does not hold in all case. It must also be noted that an increase in area does not always imply an increase in elongation; many pockmarks can show an increase in area whilst remaining circular.

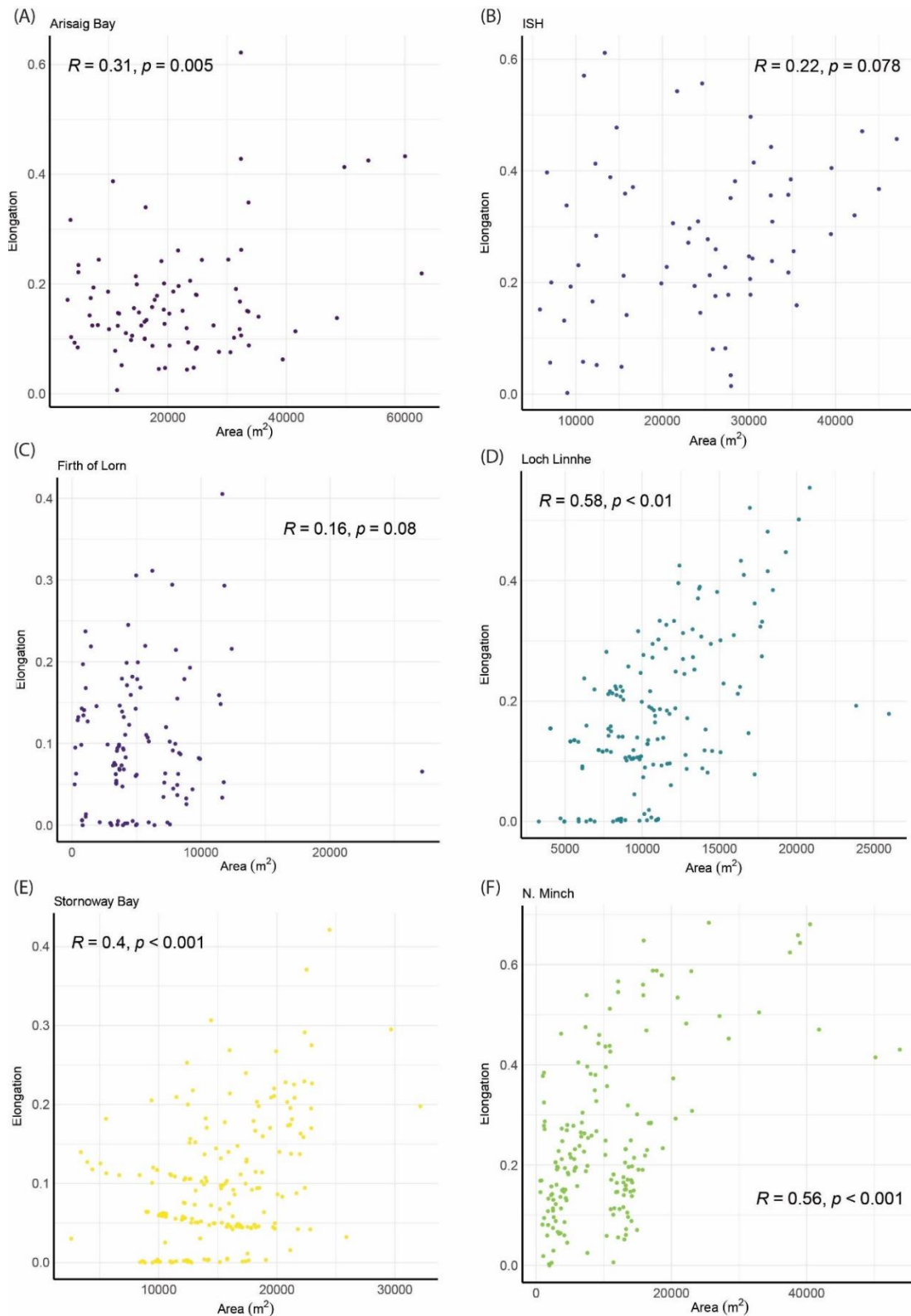


Figure 3.9. Elongation as a function of Area of pockmarks within each study region. Strength of the correlation (Pearson's r value; p -values) also shown. (A) Arisaig Bay, (B) Inner Sea of Hebrides, (C) Firth of Lorn, (D) Loch Linnhe, (E) Stornoway Bay, (F) North Minch.

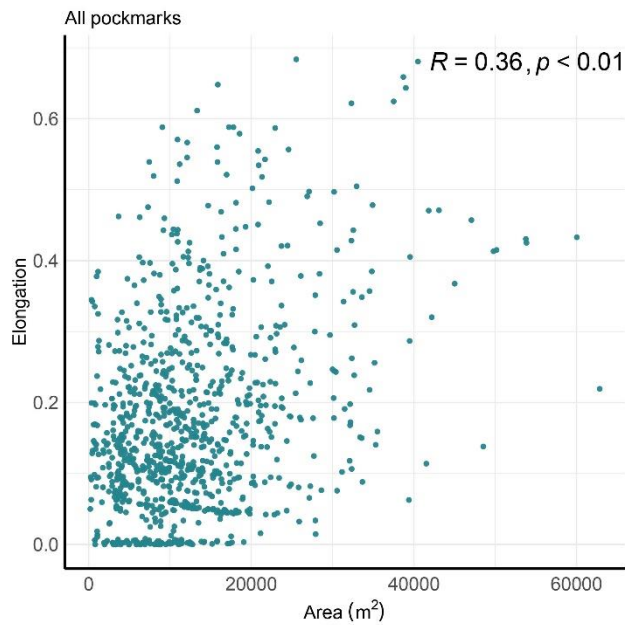


Figure 3.10. Elongation as a function of Area of all pockmarks mapped. Strength of the correlation (Pearson's r value; p -values) also shown.

Another set of morphological characteristics that were investigated is the profile indicator and maximum slope angle (Figure 3.11). The median profile indicator value is between 0.4-0.6 across all study regions, showing that the majority of pockmark profiles are neither V-shaped nor U-shaped but fall somewhere between the two end members. Firth of Lorn contains pockmarks which have the highest and lowest profile indicator values, where V-shaped and U-shaped pockmarks are present. Firth of Lorn is also the region where pockmarks are found to have the highest maximum slope angle, greater than 40°. In general, the median maximum slope angle is below 10° with the exception of Loch Melfort and Loch Linnhe which are >10°.

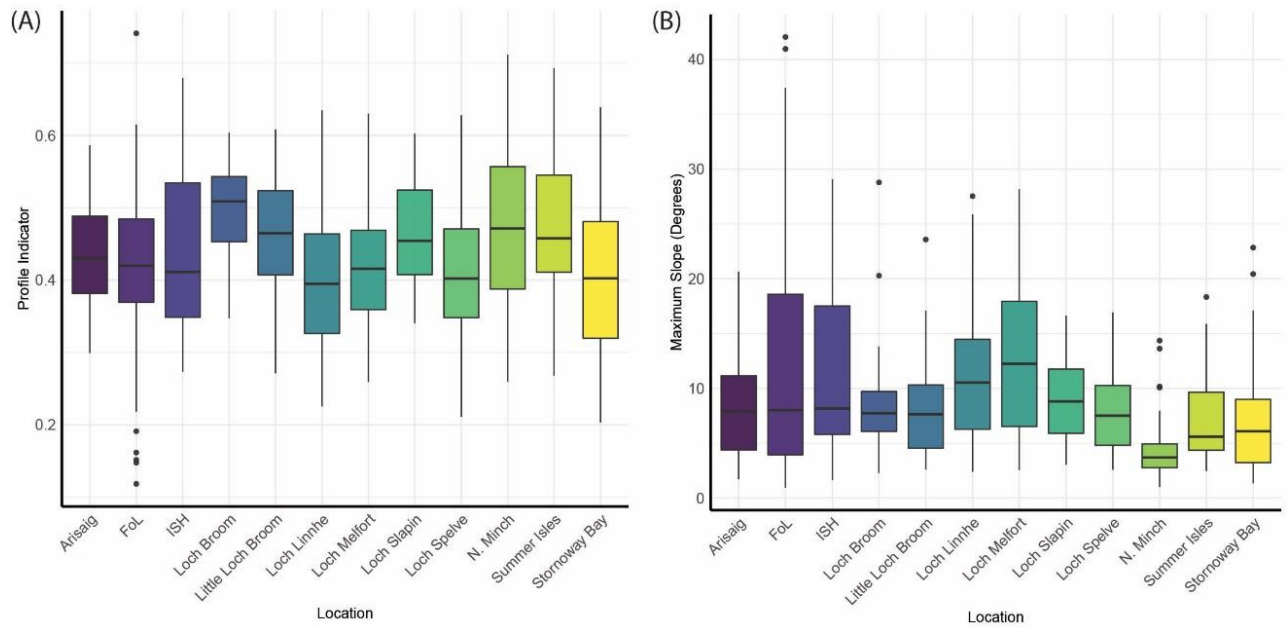


Figure 3.11. Morphological characteristics of pockmarks within each study region. (A) Boxplots showing the profile indicator values of pockmarks. (B) Boxplot showing the maximum slope angle for pockmarks.

Due to the relationship identified between pockmark vertical relief and pockmark area, a cluster analysis was performed to investigate whether pockmarks are naturally forming preferential shapes and sizes. The results of the elbow plot (Figure 3.12A) show that three clusters are likely to be present within the entire dataset. When the k-means clustering algorithm is set to 3, a low application error rate of 0.045 is returned from the partition plot (Figure 3.12B). This low error rating is due to observations which have been assigned to a cluster not being distinguishable from another cluster in the dataset by a quadratic function. It was also found that when setting the clustering algorithm three classes performed most efficiently, with the lowest application error rate. Therefore the ‘elbow’ method described here is a reliable method to inform the user on the expected number of classes/clusters present in a dataset. Setting the number of clusters to less than or greater than 3 resulted in higher application error rates.

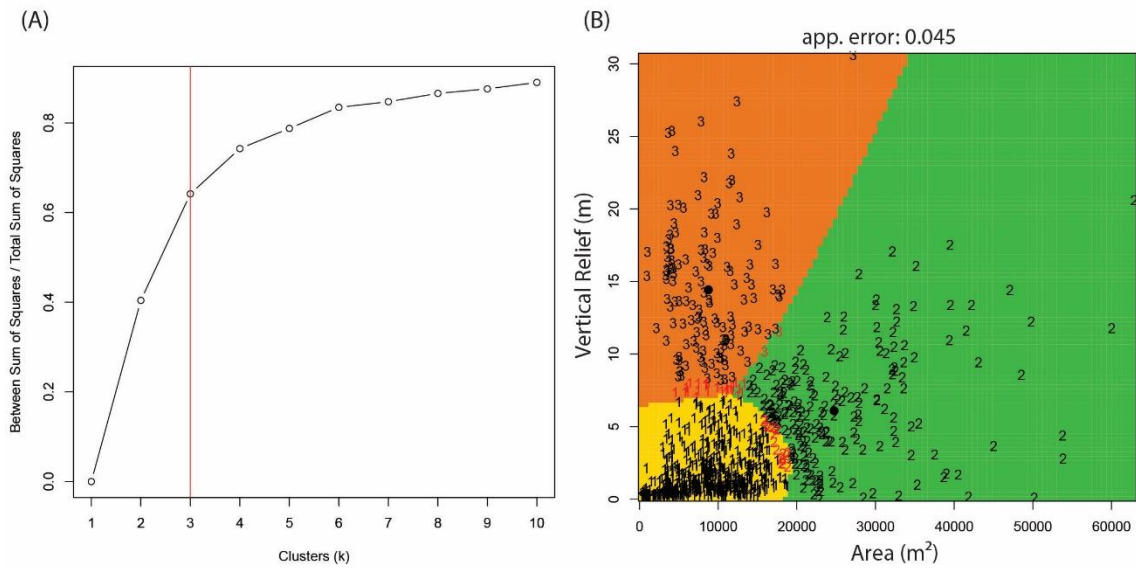


Figure 3.12. Clustering of pockmarks based on Vertical relief as a function of Area. (A) Elbow plot showing the variance within the data as a function of number of clusters, here we can see a change in the angle of the line at $k=3$ clusters. (B) Partition plot, where pockmarks have been separated into three classes, an application error rate represents the pockmarks which do not separate into the clusters they have been designated (numbers in red).

The identified relationship between elongation and area makes it also necessary to explore possible clustering between elongation and vertical relief. Elongation is a useful variable to describe the morphology of a pockmark. The elbow plot also shows three probable clusters within this dataset (Figure 3.13). The partition plot shows a lower application error rate of 0.022, compared to that of vertical relief vs area (Figure 3.13). This classification can therefore be separated into three classes with greater accuracy.

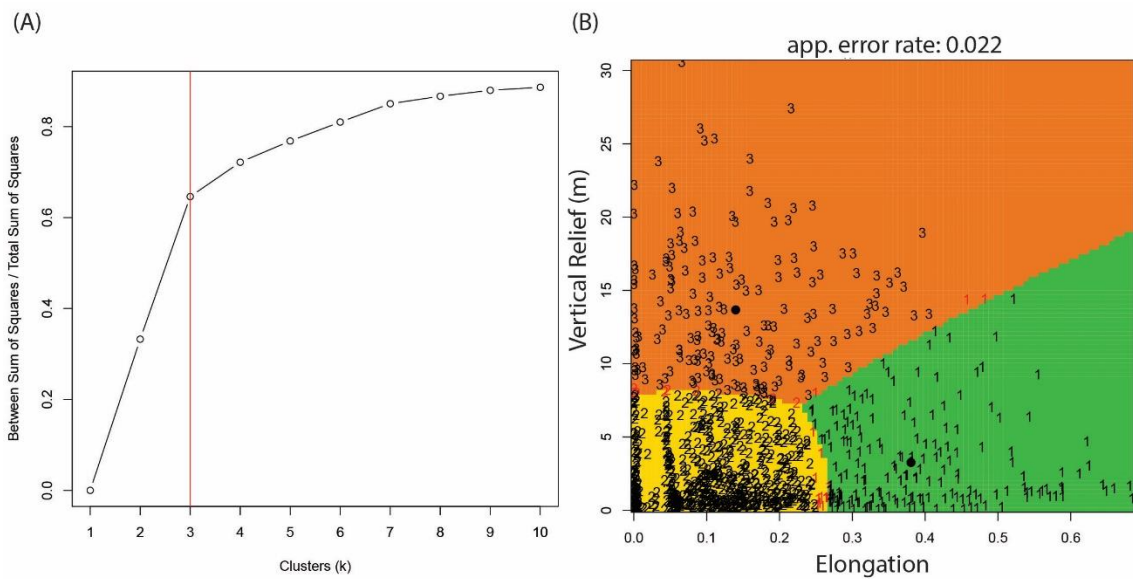


Figure 3.13. Clustering of pockmarks based on Vertical relief as a function of Elongation. (A) Elbow plot showing the variance within the data as a function of number of clusters, here we can see a change in the angle of the line at $k=3$ clusters. (B) Partition plot, where pockmarks have been separated into three classes, an application error rate represents the pockmarks which do not separate into the clusters they have been designated (numbers in red).

Due to the lower error application rate for the cluster analysis, vertical relief vs elongation was chosen to separate the dataset and map their distribution. The morphological characteristics shown in Figure 3.14 help to create descriptive terms to represent the clusters. These include *elongated* for cluster 1, *common* for cluster 2 and *deep* for cluster 3. Class 2 is classed as common (rather than regular) due to this form having the greatest number of observations (Table 3.2). The second most common form across all study regions are the elongated forms, found mainly within Loch Broom, Loch Slapin and North Minch. the highest percentage of deep pockmarks are found within Loch Melfort, Firth of Lorn and Loch Linnhe.

This analysis has only considered the inclusion of vertical relief, pockmark area and pockmark elongation as these morphometrics can capture the three dimensional characteristics of pockmarks. Initially other variables were also considered, however these produced results with a high application error rates. It was found that these less robust and not as useful for distinguishing different pockmark classes. As such these were not included in further analysis and discussion concentrates on the three variables mentioned: vertical relief, pockmark area, pockmark elongation. The same conclusion was made for setting the number of clusters to be less than or greater than three. This also produced

results with a higher application error rate and supports the use of the 'elbow plot' for determining the number of clusters present within a dataset.

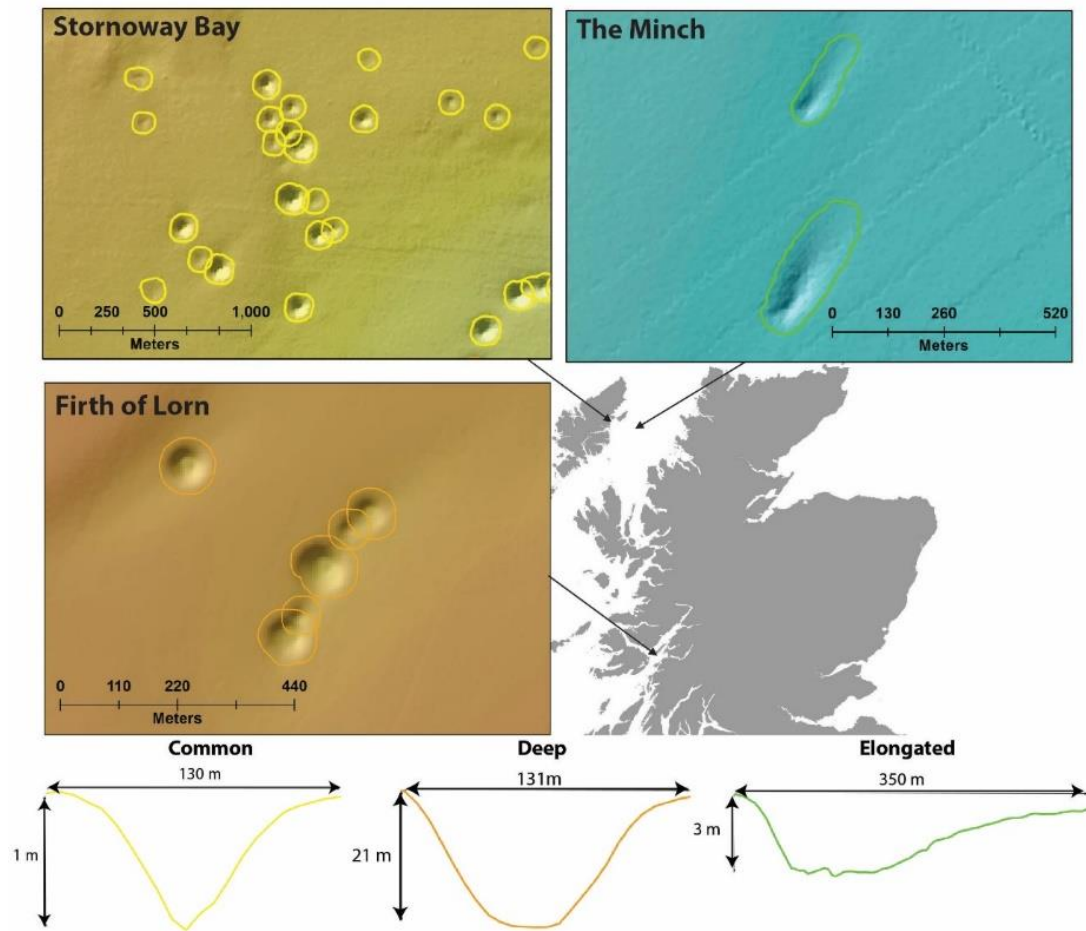
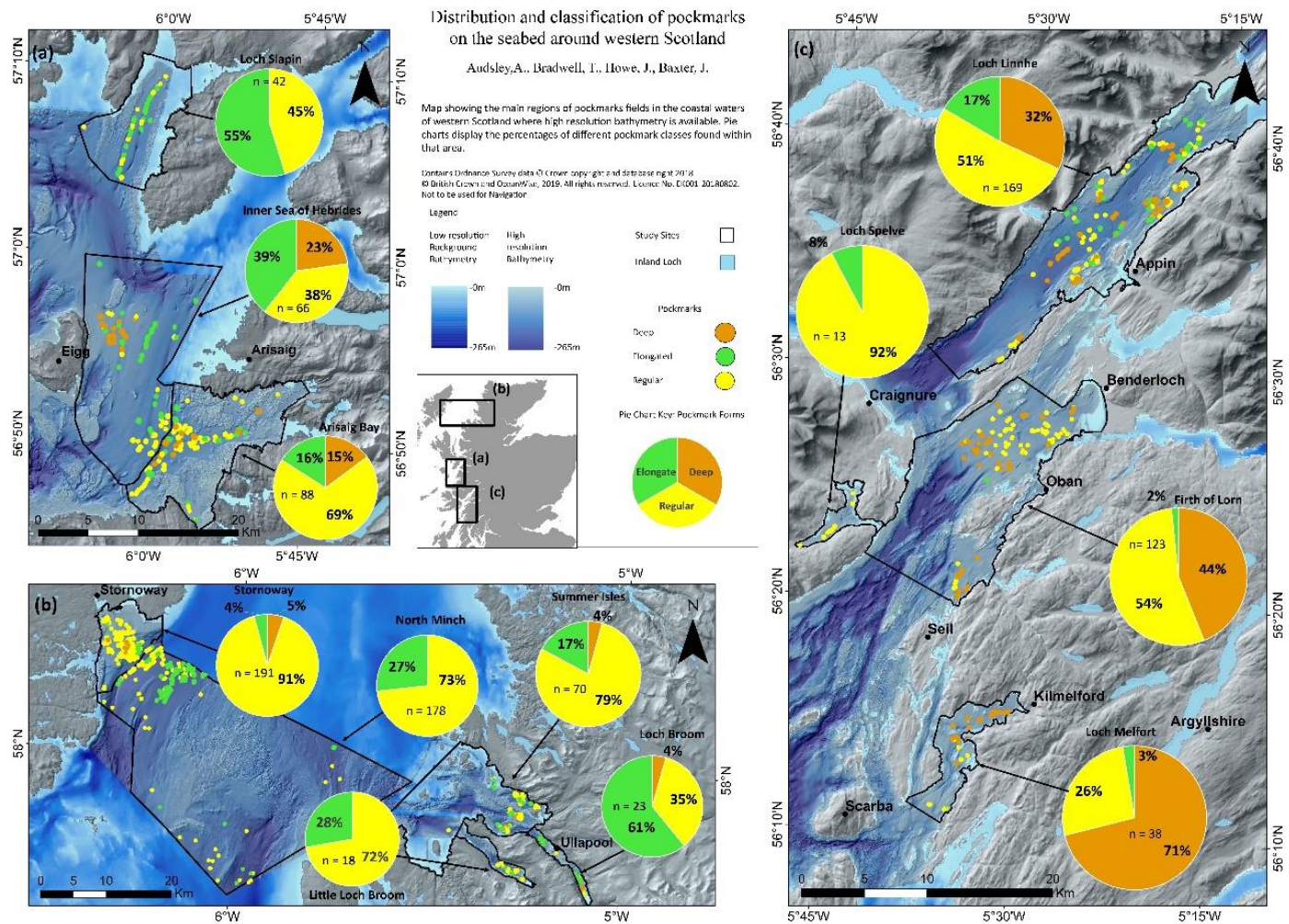


Figure 3.14. Identified classes of pockmarks based on the results of the Elongation as a function of vertical relief partition plot. (Yellow) Example of “common” pockmarks present within Stornoway Bay. (Green) Example of “elongated” pockmarks present within the North Minch. (Orange) Example of “deep” pockmarks present within the Firth of Lorn. Figure also shows examples of the profiles for each pockmark class.

Table 3.2. Number of pockmarks mapped within each study region and the percentage within each class.

Region	Area (km ²)	No. of Pockmarks	Pockmark/ km ²	Common (%)	Elongate (%)	Deep (%)
Stornoway Bay	86.4	191	2.21	90.6	4.2	5.2
North Minch	876.8	178	0.2	63.5	36.5	0.0
Summer Isles	232.1	70	0.3	78.6	17.1	4.3
Loch Broom	18.1	23	1.27	34.8	60.9	4.3
Little Loch Broom	24.1	18	0.75	72.2	27.8	0.0
Loch Slapin	82.1	41	0.5	46.3	53.7	0.0
Inner Sea of Hebrides	205.1	66	0.52	37.9	39.4	22.7
Arisaig Bay	125.8	85	0.68	71.8	14.1	14.1
Loch Linnhe	168.3	169	1	51.5	16.6	32.0
Firth of Lorn	161.2	123	0.76	54.5	1.6	43.9
Loch Spelve	9.8	13	1.33	92.3	7.7	0.0
Loch Melfort	28.3	38	1.34	26.3	2.6	71.1
All Regions	2018.1	1015	0.5	63.3	19.3	17.3



Legend:

- Low resolution Bathymetry: -0m to -265m
- High resolution Bathymetry: -0m to >265m
- Study Sites: Inland Loch, Pockmarks (Deep, Elongate, Regular)
- Pie Chart Key: Pockmark Forms (Elongate, Deep, Regular)

Figure 3.15 Map of study regions and pockmark classes. Pie charts show the proportion of each pockmark class and number of pockmarks present within each study region (Audsley et al. 2019)

3.4 Discussion

A total of 1015 crater-like depressions interpreted as pockmarks, have been mapped within twelve fjordic and extra-fjordic study areas around western Scotland between 56.1°N and 58°N (Figure 3.15). This study provides the first detailed mapping of pockmarks and their morphological characteristics. However, owing to increasing access to bathymetric datasets many more pockmarks are likely to be identified within the inshore waters of western Scotland in the future.

3.4.1 Pockmark morphology

The position and morphology of pockmarks have been mapped across 12 study sites of western Scotland using the BGS Seabed Mapping Toolbox. The methodology followed in this study has been previously conducted in several studies with the intention of mapping pockmarks (Gafeira *et al.* 2012, 2018; Roelofse *et al.* 2019). It has been found that this method is more effective than manual mapping in terms of user subjectivity and speed (Gafeira *et al.* 2018). This toolbox has also been tested against other mapping strategies, such as pixel-based applications or object-based classification where it was found that BGS approach is not only a simpler alternative but also provides a full characterisation of morphological attributes alongside a delineation of the pockmark. No studies have been published on the successful application of pixel-based or object-based classification approaches for pockmarks even though these are becoming popular in other areas of seabed mapping (Diesing *et al.* 2014; Diesing & Thorsnes 2018). These approaches are complex and require multiple user inputs; and are less effective at distinguishing and mapping pockmarks. Although similar approaches to the BGS toolbox have been developed for use in other studies (Picard *et al.* 2018), it was decided that the BGS toolbox would be used to delineate the pockmarks of this study due to it being thoroughly tested and specifically designed to delineate and characterise pockmarks.

Water depths within the study regions range between 10 – 260 m, where the deepest areas are found in basins carved out during successive glaciations. Analysis into the water depths in which pockmarks occur (Figure 3.5) show that most have formed between 10 – 120 m, even in areas where deeper waters exist. It is only in the North Minch where pockmarks can be found in deeper water than this (120 – 150 m), although the number of pockmarks recorded are much lower at this depth range. Between 150 – 260 m no pockmarks were observed in any of the study areas. It is interpreted that this is likely due to a reduced supply of organic-rich material in the over-deepened basins further from shore. This organic-rich sediment is required for the formation of biogenic gas and the

subsequent formation of a pockmark (Park *et al.* 1979; Brothers *et al.* 2012). Between 0 – 120 m water depth there does not seem to be a clear depth control on pockmark formation, as pockmarks can be found at any depth within this range in each of the different study regions.

The profile indicator value indicates the shape of the pockmark's cross-sectional profile, where high values indicate U-shaped and low values are V-shaped forms. This can be useful to interpret the formation history or the morphological composition of pockmarks; those that are complex whereby they are composed of several vent sites versus those with a single vent site as would be the case with V-shaped profiles. The results from Western Scotland pockmarks show that the median of most study regions fall between 0.4 – 0.6. Therefore, most pockmarks are between V-shaped or U-shaped in profile. Within the Firth of Lorn study region the profile indicators are the highest and lowest compared to every other study region. It is interpreted that the profile indicator not only provides a picture on the cross-sectional shape of the pockmark but can give an indication to the activity status and development history of the pockmark since formation.

It is expected that when a pockmark forms via a single focused vent site it allows gas to escape and send sediment in suspension, creating a symmetrical, V-shaped pockmark. Depending on the slope angle of this new pockmark and the period of inactivity this profile will become more U-shaped as slope collapse and sedimentation widens and flattens the pockmark floor and reduce the slope angle of its walls. This U-shaped profile will become more pronounced as further sedimentation occurs and/or new vent sites open, creating a wider pockmark (increased area) and potentially a W-shaped profile. Not that, at this stage that a W-shaped profile cannot be defined with a profile indicator value. With this interpretation in mind, it is possible to state that the majority of pockmarks have either been inactive for an extended period of time or multiple vent sites have opened which would be indicated by pockmarks with an above-average area. It is also possible that within the Firth of Lorn where the most V-shaped pockmarks are recorded, has experienced the most recent pockmark activity/ formation. It is suggested that when considering the profile indicator of an entire dataset, this will give an indication of the range of pockmark shapes and sizes and thus could provide a general description of the potential gas venting status of the region. To gain a better interpretation of activity status, specific pockmarks would need to be targeted to examine the relationship between the profile indicator, area and vertical relief. The elongation ratio can also be used to determine whether currents are affecting sedimentation patterns within the region.

The relationship between vertical relief (or depth) and pockmark area is typically used to describe morphology (Gafeira *et al.* 2018). The deepest pockmarks mapped within the North Sea Basin, in UK licence Block 15/25 (Gafeira *et al.* 2018), are known to be regularly active (Hovland *et al.* 1984; Hovland & Sommerville 1985; Dando 1991). Pockmark area has been shown to correlate well with vertical relief (Figure 3.7). A pockmarks area can increase when slope collapse occurs, leading to a decrease in vertical relief. Area can also increase when additional vent sites form within or adjacent to an existing pockmark. Therefore, the relationship between vertical relief and area could be a useful characteristic to investigate the activity status of pockmarks. Despite this relationship and its usefulness to interpret pockmark development, depth has not previously been used as a metric to define pockmark type (Hovland *et al.*, 2002). Definitions of pockmark types are solely based on the plan view of the pockmark with an occasional reference to area and/or length of the major axis.

This study has found that three trends occur within the scatter plot of vertical relief vs area. The correlation plots (Figure 3.8) support that these two variables share a relationship, and these trends may reflect pockmarks which share similar formation and/or activity status. These trends can be generally described as: (3) those which have a greater vertical relief: area ratio; (2) those which have a lower vertical relief: area ratio; and (1) those which fall in between these two previous trends.. These three trends are interpreted as follows: (3) those which share a high vertical relief: area ratio have probably formed recently and consist of a single vent or have experienced regular venting at single site; (2) pockmarks with a low vertical relief: area ratio are interpreted to have been inactive for a prolonged period of time and probably undergone subsequent side wall collapse. This results in an increased area and infilling of the pockmark. It is also possible that multiple vent sites exist which have experienced minor activity resulting in low vertical relief values but increased area. (1) the final group lying between these two endmembers represent pockmarks which experience periodic venting that increases/maintains vertical relief; or pockmarks which are inactive and are becoming slowly buried by sedimentation and/or sidewall collapse.

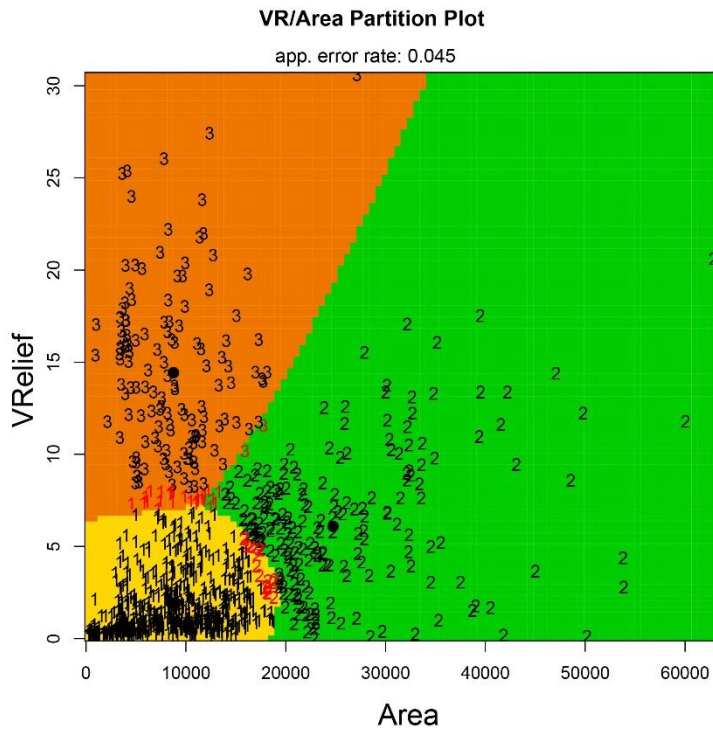


Figure 3.16. Vertical relief (pockmark depth) as a function of the Area of pockmarks across western Scotland, showing the different possible trends visually observed. (3) High vertical relief: area ratio. (1) medium vertical relief: area ratio. (2) Low vertical relief: area ratio.

Pockmark elongation is another characteristic that can be used to describe pockmark morphology as it relates to the impact of local hydrographic conditions. Directional displacement of sediment can indicate the direction of local bottom currents over time (Andrews *et al.* 2010; Picard *et al.* 2018). The results from pockmarks around western Scotland show that elongation values range between 0 – 0.7. The most elongated pockmarks are present within the North Minch and Inner Sea of Hebrides study regions. These are the most extra-fjordic regions (furthest offshore) and are therefore the most exposed to the effect of bottom currents. Study regions which are located within fjord approaches, , such as Loch Linnhe and Loch Slapin, but are not as hydrographically restricted as fjords also contain pockmarks which are significantly more elongated than other pockmarks in other regions. This is due to the effect of bottom currents which circulate water and preferentially redistribute sediment in these settings. Pockmarks within Loch Broom, Loch Melfort and Loch Spelve show very few elongated forms. This is likely due to weaker bottom currents in these narrow, more hydrographically restricted fjords/ sea lochs.

One aspect of pockmark morphology which is not captured by the morphometrics discussed so far are the broadscale distribution patterns and trends. An example of this are the large pockmark strings/chains present in Stornoway Bay (Figure 3.2a). These pockmarks have formed in close vicinity of one another, and in places currents have scoured and elongated them causing them to appear as curvilinear troughs. Several of these strings are observed in the Stornoway Bay following a similar NE-SW orientation. The interpretation is that these pockmarks are likely following a weakness within the Quaternary seabed sediment possibly the result of neotectonic faulting in the region (Graham *et al.* 1990). It is unclear from this study whether these faults have guided pockmark string formation within Stornoway Bay. Similar strings/chains of pockmarks were first recorded within the Norwegian trench (Hovland 1981b) and can form linear or radial patterns often originating from a larger 'parental' pockmark. These are not due to random chance but have formed due to weaknesses in the sediment column e.g. fissures, flexures and microfractures (Hovland 1981a).

3.4.2 *Pockmarks classification*

There is currently a wide, unhelpful, variety of descriptive terms used to classify pockmarks based on their morphological character e.g. unit pockmarks, normal (including regular/circular and asymmetric) pockmarks, elongated pockmarks, eyed pockmarks, crescent pockmarks and strings of pockmarks and complex/ composite pockmarks (Hovland *et al.* 2002). Uncommon descriptive terms also used include: giant/mega-pockmarks (Pilcher & Argent 2007; Chen *et al.* 2015; Luo *et al.* 2015) crescent pockmarks elliptical and comet pockmarks (Chen *et al.* 2015). However, none of these classifications of pockmark morphology are based on statistically distinct pockmark forms or cluster analysis, and are instead purely qualitative descriptions of morphology. As a result of this few examples are given on the range of values of a particular morphological variable e.g. how large in area does a pockmark have to be in order for it to be considered a common or giant pockmark? Chen *et al.* (2015) made the first attempt at providing these ranges, however these have not been statistically verified and are instead a subjective system based on the researcher's knowledge and understanding of the pockmark variations presented in literature. The issue is that pockmarks can form a wide range of shapes and sizes and when a dataset becomes larger more pockmarks are observed in different times of their activity status/ history and therefore a continuum of pockmark development is captured. This makes the objective of separating pockmark datasets into classes very difficult. It is clear though that the current definitions of pockmark types are left lacking.

This chapter has focused on three morphometrics to achieve such a statistically based classification system, these include vertical relief, area and elongation. Vertical relief and area are two variables that have been used to describe the morphology of a pockmark (Gafeira *et al.* 2012, 2018; de Mahiques *et al.* 2017). These do not consider elongation of a pockmark and therefore a separate classification system based on vertical relief and elongation is also used within this study. The combination of morphometric variables can be used as a powerful way not only to interpret the activity status/ development history of a pockmark but also the hydrographic setting.

The first classification system used to define pockmark forms was based on their vertical relief and area values. The dataset was separated into three clusters with an error rate of 0.045. Following this system, one of the clusters were able to separate those pockmarks which are deeper and therefore classed as deep pockmarks. The other classes likely incorporated several pockmark forms that are mentioned within literature including normal pockmarks, and elongated pockmarks (Hovland *et al.* 2002). The only pockmark form to be identified that can aid interpretation of activity status are those assigned to the “*deep*” class. Therefore, at a minimum, pockmark classification strategies should include a depth component in order to aid interpretation and assessment of activity status.

The second classification system substituted area for elongation values of pockmarks in order to differentiate this particular class. As with the first classification system it also used vertical relief in order to differentiate those pockmarks previously classed as deep. This produced three clusters with an error rate of 0.022. These include the cluster classified as “*deep*” identified within the first classification attempt. It now also includes an elongated class, which is already defined within literature and a commonly observed pockmark type (Hovland *et al.* 2002). The final cluster identified is classed as “*common*”, this type likely includes regular and unit pockmarks which are referred to in literature. However, they must be circular in shape (low elongation value) to be included within this class. This classification attempt is more successful in separating the dataset into clusters and is also more useful in providing a series of descriptive classes which can aid the interpretation of pockmark development relevant to their activity status and alteration by hydrographic conditions.

Due to the wide variety of pockmark shape and size a myriad of terms have been developed in order to describe their form (Hovland *et al.* 2002; Pilcher & Argent 2007; Chen *et al.* 2015; Luo *et al.* 2015). This has created an unnecessary jargon which confuses the research and further complicates when comparisons are made to interpret possible pockmark activity status and development history. It is suggested by the results

of this project that it is possible to separate pockmark types based on their morphological characteristics using a statistically robust methodology. Such a classification system produces results which can set the size and shape limits which pockmark classes can take before being considered a different form. It allows for the quick and easy assessment of which types of pockmarks are present based on shape and size parameters. From this it would then be possible to establish a controlled vocabulary to describe pockmark types defined by their morphometrics. This project has focused on the use of vertical relief (depth of the pockmark), pockmark area and/or pockmark elongation. Furthermore, should a conceptual model which shows the development of various pockmark types be developed it would be possible for interpretations to be made on the potential activity status and development history of a pockmark. Such conceptual models can be found throughout literature (Hovland & Judd 1988; Cathles *et al.* 2010; Brothers *et al.* 2012; Moss *et al.* 2012a, b; Luo *et al.* 2015) however, these have mostly focused on the initial formation and do not refer to the diverse morphologies pockmarks can take.

During the planning stage of developing offshore infrastructure such as within the oil and gas and renewables industries, pockmarks are considered as a geohazard due to the potential catastrophic release of gas during formation (Hovland *et al.* 2002; Orange *et al.* 2005; Camargo *et al.* 2019). By identifying fields of pockmarks which have likely been inactive for a prolonged period based on their morphology, may allude to the region no longer containing large volumes of pressurized gas. Pockmarks may have instead helped to stabilise the seabed (Riboulot *et al.* 2019) and allow for marine infrastructure to be developed despite pockmarks being present. It has been suggested that pockmarks also support marine communities by redistributing nutrients such as organic carbon. Evidence of such has been reported from pockmarks offshore Brittany which are supporting *Haploopsis* communities (Champilou *et al.* 2019) which have been recently protected under the OSPAR Convention of threatened and declining species and habitats. By establishing a standardised glossary of pockmark types and using an interpretive conceptual model which highlights their activity status/ development would prove to be of great use to marine industries and designation of future marine protected areas.

3.5 Conclusions

- 1015 pockmarks have been mapped in 12 study sites across western Scotland.
- A robust statistical classification system has been developed to identify distinct pockmark forms. Such a classification system could be used in global studies to aid the definition of pockmark forms and develop a standardised glossary.

- 3 different forms of pockmarks have been found to be present across western Scotland. These are defined as Deep, Elongated and Common.
- Pockmarks classed as Deep are expected to have been recently or regularly active since formation and should be targeted in future studies focusing on pockmark activity periods and volumes of expelled fluids.

Chapter 4: The distribution of gas bearing sediments around Western Scotland

N.B. Parts of this chapter have been published in Audsley, A., Bradwell, T., Howe, J. & Baxter, J. 2021. Spatial Relationships between Pockmarks and Sub-Seabed Gas in Fjordic Settings: Evidence from Loch Linnhe, West Scotland. Geosciences, 11. which focused on the results from Loch Linnhe. Further results and discussion are presented here which are currently unpublished. This includes the analysis and discussion of datasets from Stornoway Bay, Loch Broom and the Inner Sea of Hebrides.

4.1 Introduction

Gas within marine/aquatic sediments was first recognised within seismic records by Schuller (1952), who recorded the presence of the “becken effekt” (basin effect). This effect was later termed “acoustic turbidity” and is the most common acoustic expression of gas within sub-seabed sediments (Abegg & Anderson 1997; Judd & Hovland 2007). Confusingly it is also termed acoustic masking, acoustic blanking and smears, from here on the term acoustic turbidity is used as it is commonly used within the literature (Judd & Hovland 2007). Acoustic turbidity represents the attenuation of energy, through the intensity reduction of a sound wave, either through the scattering or absorption by gas bubbles to form chaotic reflections that have no discernible internal structure (Baltzer *et al.* 2005; Judd & Hovland 2007). Sediment cores taken from within an area of acoustic turbidity in the Irish Sea Basin confirmed that this is the result of gas presence (Jones *et al.* 1986). The concentration of methane was high within this Irish Sea zone of acoustic turbidity with concentrations ranging from $>100 \text{ nmol}^{-1}$ to $<10 \text{ nmol}^{-1}$ within the uppermost 1.6 m of seabed sediment. Any other acoustic structures present in the acoustic turbidity are no longer visible and reflections below this gaseous region are also entirely or partially obscured (Judd & Hovland 2007).

On seismic records, regions of acoustic turbidity can take different shapes and sizes. Therefore Taylor (1992) coined the descriptive terms such as acoustic curtains, acoustic blankets and plumes to help to differentiate between forms of acoustically turbid regions that have different lateral distributions. Taylor describes these three forms from geophysical datasets collected from the UK nearshore regions using uniboomer and pinger records, he states that the type of acoustic signature can be related to underlying geological controls. Baltzer *et al.* (2005) support this assertion and shows that acoustic

turbidity, in the form of curtains and blankets plus two other facies, white and black fringes related to the depositional environments. These acoustic expressions are represented by phase changes of the acoustic signatures. It has been suggested by Judd & Hovland (2007) that the terms curtain and blanking are not necessary and that only two types of gas-related acoustic turbidity can be reliably identified, therefore there is still debate on whether or not numerous definitions of similar acoustic signatures are necessary.

Further acoustic evidence of sub-seabed gas includes gas chimneys and plumes. Gas plumes are narrow zones of acoustic turbidity with distinct lateral boundaries, typically <50 m wide, and with an apparent connection to a gas source (Taylor 1992; Baltzer *et al.* 2005; Judd *et al.* 2007). They have been observed as having numerous high-amplitude parabolic reflectors and can also appear as an amorphous cloud. Gas chimneys are narrow vertical zones of disturbance caused by gas migration. Some workers support the use of terms that describe the vertical migration of gas such as plume and chimney, as these indicate direct evidence of gas migration. Much work has been conducted to detect and map the 3D structures of gas chimneys in order to understand their role in hydrocarbon migration, as they can create unfavourable conditions for seabed infrastructure and lead to pockmark formation (Meldahl *et al.* 1999).

The term “geohazard” refers to geological features or conditions that may pose a danger to offshore infrastructure installed on or in the seabed. These include: slope instability, open and buried channels, gasified sediment, active sand wave fields, extensive bare rock exposure and deeply weathered rock profiles, pockmarks, iceberg scour marks, seismicity and rapid and unpredictable changes in soil properties (McQuillin & Fannin 1979). However the degree to which each of these hazards pose a threat to installations is variable to the type of installation. In the case of gasified sediment the impact of such a hazard has been observed on numerous occasions during gas blow-outs from the offshore oil and gas industry; including the Deep water Horizon disaster (Valentine *et al.* 2010) and a still active blow-out crater within the North Sea at well 22/4b (Leifer & Judd 2015; Wiggins *et al.* 2015). It has also been hypothesized that the sudden release of gas can pose a risk to ships. It is speculated that a trawler found at the centre of a pockmark within the Witch Ground, North Sea was victim to such a hazard (Marchant 2000) along with another ship in the centre of a pockmark within the Skagerrak seep (Dando 1991). Furthermore, the rapid dissociation of methane hydrates leading to the release of gas is one hypothesis for the mysteries of the Bermuda triangle (Joseph 2017).

Identifying pockmarks and shallow sub-seabed gas is an essential part of determining the potential hazards posed to offshore infrastructure (Orange *et al.* 2005; Camargo *et al.*

2019). However, the degree to which pockmarks are considered a geohazard is still debated (Riboulot *et al.* 2019). This is largely due to the formation of pockmarks being dependent on gas pressure, which can vary greatly. As such, a detailed understanding of pockmark formation and seabed fluid flow in certain offshore settings is still lacking. Pockmarks that have experienced long-term venting have been observed in the North Sea, where methane-derived authigenic carbonates (MDAC) have formed and been exposed on the seabed (Hovland *et al.* 1985; Gafeira & Long 2015b; Böttner *et al.* 2019). MDAC is considered an important geological structure worthy of marine protection status, typically within special areas of conservation (SAC). There is general agreement that pockmarks are indicators of hazardous seabed settings including tectonic/seismic activity (Hasiotis *et al.* 1995; Hovland *et al.* 2002), areas of potential gas hydrate and also potential seabed slumps and slides (Hovland *et al.* 2002). Pockmarks can also indicate the presence of deep hydrocarbon accumulations in offshore basins (McQuillin & Fannin 1979). However, little work to date has explored the importance of pockmarks as geohazards in nearshore settings.

Seabed pockmarks are relatively widespread across the continental shelf around Scotland, occurring mainly in the North Sea sector, discovered during oil and gas surveys (Hovland *et al.* 1984; Hovland & Sommerville 1985; Böttner *et al.* 2019). More recently, pockmarks have also been discovered further inshore within the fjords and fjord approaches of western Scotland (Stoker *et al.* 2006; Audsley *et al.* 2019), similar in size and bathymetric setting to those identified in the western fjords of Arctic Svalbard (Howe *et al.* 2003; Roy *et al.* 2019). These fjordic environments are shown to be effective stores of organic carbon (Table 4.1) (Smeaton *et al.* 2017, 2020). However, the presence of pockmarks indicate that these stores are not permanent and that gases, such as methane, can seep into the water column back into the marine carbon cycle (Judd & Hovland 2007; Krämer *et al.* 2017). Some studies have shown that this gas can also enter the atmosphere (Krämer *et al.* 2017; Lohrberg *et al.* 2020), although this is dependent on water depth and local hydrographic/meteorological factors (McGinnis *et al.* 2006). It is thought that pockmarks in Scotland's fjords are formed by the release of shallow biogenic gas, whereas those further offshore in the North Sea sector are related to deeper-seated thermogenic gas accumulations (Hovland & Sommerville 1985). This is supported by research into the carbon signature of fjordic and offshore/shelf sediments, where the majority of organic carbon is stored within fjordic systems; however, localised hot-spots of organic and inorganic carbon can also be found in sediments on the wider continental shelf (Smeaton *et al.* 2021).

Table 4.1. Estimated Carbon stocks of study regions or nearby locations where not available, adapted from Smeaton *et al.* (2016)

Fjord	Organic Carbon (Mt)			Inorganic Carbon (Mt)		
	Mean	Min	Max	Mean	Min	Max
Loch Linnhe	38.96	36.97	42.87	20.42	18.34	23.11
Loch Broom	2.41	1.47	3.35	2.69	1.81	3.57
Stornoway	0.27	0.25	0.29	0.34	0.26	0.57
Loch Ailort	0.72	0.68	0.76	0.76	0.71	0.9

Regional mapping of pockmarks in Scottish west-coast waters, as part of the PhD project, has suggested a link between pockmark morphology, hydrographic setting and the activity history of pockmarks (Audsley *et al.* 2019). Previous PhD research investigating the glacial history of the wider region also found some geophysical evidence of sub-seabed gas in Loch Linnhe (a classic Scottish fjord) (Greene 1995; McIntyre 2012). However, neither of these studies fully explored the relationship between sub-seabed gas and the presence of pockmarks at the seabed. In this chapter, the three-dimensional spatial relationships between sub-seabed gas presence and pockmark formation are explored in each study area. This chapter aims to answer the following questions:

1. How widespread and how deep is the (near-surface) sub-seabed gas stored in Scotland's fjordic sediments?
2. What can the distribution of sub-seabed gas tell us about pockmark formation and possible trigger mechanisms in Scotland's fjords?
3. Can we infer pockmark age relationships or activity status based on present-day gas presence or absence?

4.2 Materials and methods

4.2.1 Sub-seabed geophysical data acquisition

The geophysical data from a variety of legacy seismic surveys conducted around Western Scotland is available via the British Geological Survey (BGS) Offshore GeoIndex (<https://www.bgs.ac.uk/map-viewers/geoindex-offshore> (accessed on 29/01/19)). This archive includes line and point shapefiles showing the path of the survey and points indicating the position of 'fixes' at a variety of resolutions. The quality of the metadata records of each survey varies; there are presented in Table 4.2. Additionally the printed seismic records for Loch Linnhe were provided by the Scottish Association for Marine

Science. These records were also analysed by McIntyre (2012) whilst investigating the Quaternary successions, however no analysis or interpretation was made during this study on the presence of sub-seabed gas or the presence of pockmarks. The distribution of seismic lines within each study site are presented in Figures 4.1 – 4.6.

Table 4.2. Geophysical surveys and relevant metadata where data was available for each study site.

Study Area	Survey year	Survey equipment	Two-Way Travel Time interval (msec)	Shot point interval (m)
Loch Linnhe	2010	AA300 Surface-tow boomer	20	140
Stornoway Bay	1968	1000-joule Sparker	Unknown	1500
	1973	Sparker	Unknown	2560
	1977	Sparker	Unknown	1300
		Pinger	Unknown	1300
1985	Sparker	100	1800	
	Pinger	25	1800	
Loch Broom	2012	Boomer	50	80
Inner Sea of Hebrides	1971	Transit sonar	Na	Na
	1968	Sparker	Unknown	1900
	1970	Sparker	Unknown	1950
	1972	Pinger	Unknown	2500
	1985	Pinger	25	230

To obtain an approximate depth conversion between Two-Way Travel Time and metres an average sound speed of 1500 m sec^{-1} was used to represent unconsolidated sediment (Wang et al. 2021, McIntyre. 2012). The depth values calculated were used to give an approximate range of depth to the gas front.

4.2.1.1 Loch Linnhe

The original printed seismic records were used for the analysis; these were obtained from the Scottish Association for Marine Science (SAMS). The seismic survey was conducted in 2010 using an Applied Acoustic AA300 surface-tow boomer. Vertical scale lines show the two-way travel time interval of 20 msec measuring 33 mm on paper records. Following a sound speed of 1500 msec for unconsolidated sediment and 2000 msec for consolidated sediment, this provides us with an approximate depth conversion of 1 mm = 0.45 m–0.60 m. Horizontal scale lines record the ‘fixes’, which were recorded at 1-minute time intervals. With an average constant ship speed of 4.5 knots, the approximate distance between fixes is 140 m; this is confirmed by ArcGIS analysis. Seismic profiles were scanned (digitised) and interpreted—building on the existing, unpublished seismostratigraphy (McIntyre 2012).

An ESRI shapefile containing the position of seismic lines and fixes was obtained from the British Geological Survey (BGS) Offshore GeoIndex (Figure 4.1) (<https://www.bgs.ac.uk/map-viewers/geoindex-offshore> (accessed on 29/01/19)).

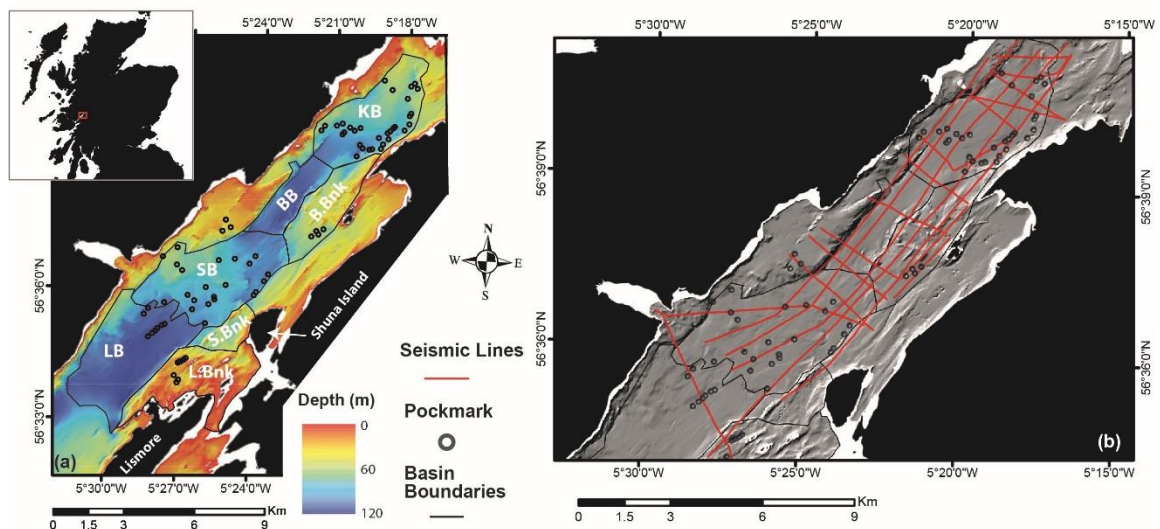


Figure 4.1. Maps of Loch Linnhe; (a) Bathymetry of Loch Linnhe, location of pockmarks sub-regions; KB – Kentallen Basin, BB – Balnagowan Basin, B.Bnk – Balnagowan Bank, SB – Shuna Basin, S.Bnk – Shuna Bank, LB – Lismore Basin, L.Bnk – Lismore Bank; (b) Position of seismic lines within Loch Linnhe. Stornoway Bay

Stornoway Bay was surveyed using a variety of geophysical equipment from 1968 to 1985 during several BGS projects involving the mapping of the seabed of north-western Scotland (Figure 4.2 & Figure 4.3). The first of these surveys began with a reconnaissance cruise by the RRS John Murray in 1968. This survey included the use of a 1000-Joule

sparker seismic-survey system. Subsequent cruises also involved sparker and pinger sub-bottom profilers and were undertaken by MV Whitehorn 1973, RRS Challenger 1977, and MV Gorsethorn 1985. Another survey was conducted in 1983, however although the seismic records exist additional metadata on the cruise is not available, this is similar to cruises between 1973-1985 where cruise reports and metadata are not readily accessible. With information gained from existing cruise metadata, a two-way travel time interval of 100 msec for sparker records and 25 msec for pinger records was assessed. From the position of the seismic lines obtained from the BGS offshore GeoIndex, it is possible to measure the distance between the positional 'fixes'.

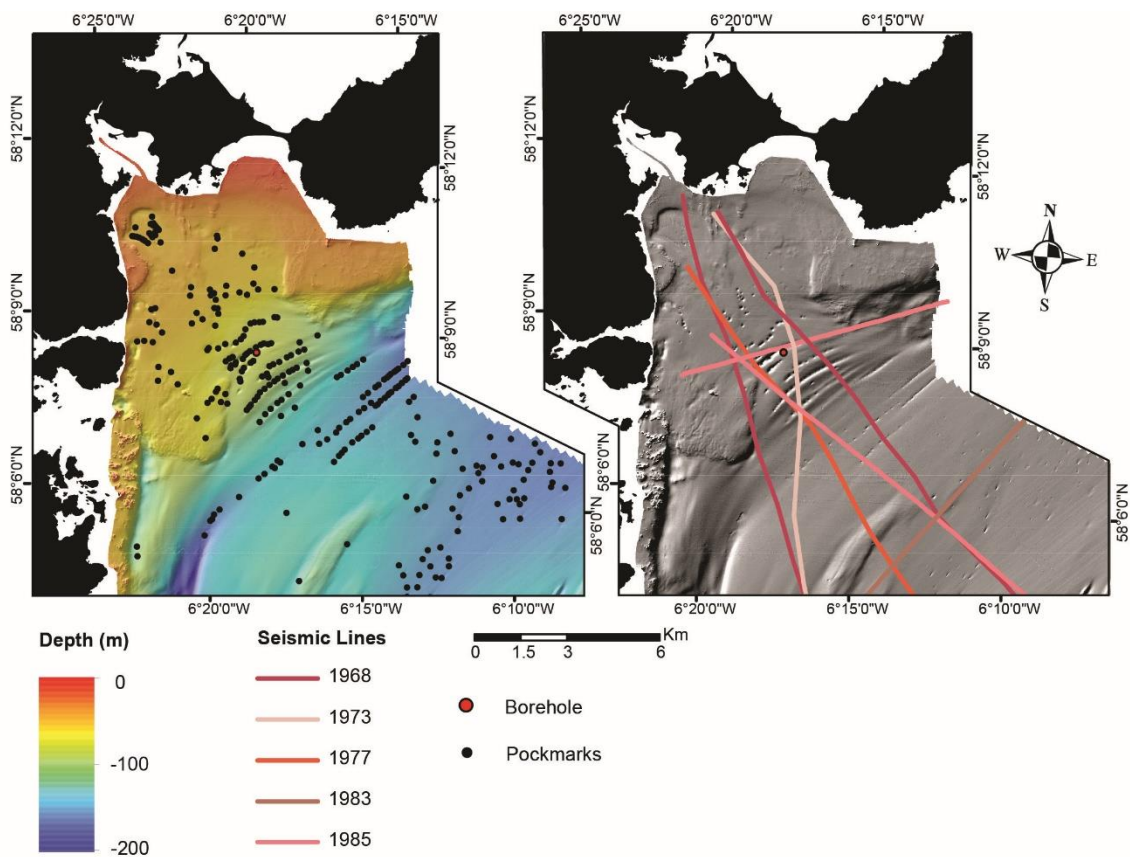


Figure 4.2 Bathymetry and location of seismic lines, pockmarks and BGS borehole 78/4 in Stornoway Bay. Seismic lines include pinger and sparker lines from several years of surveys.

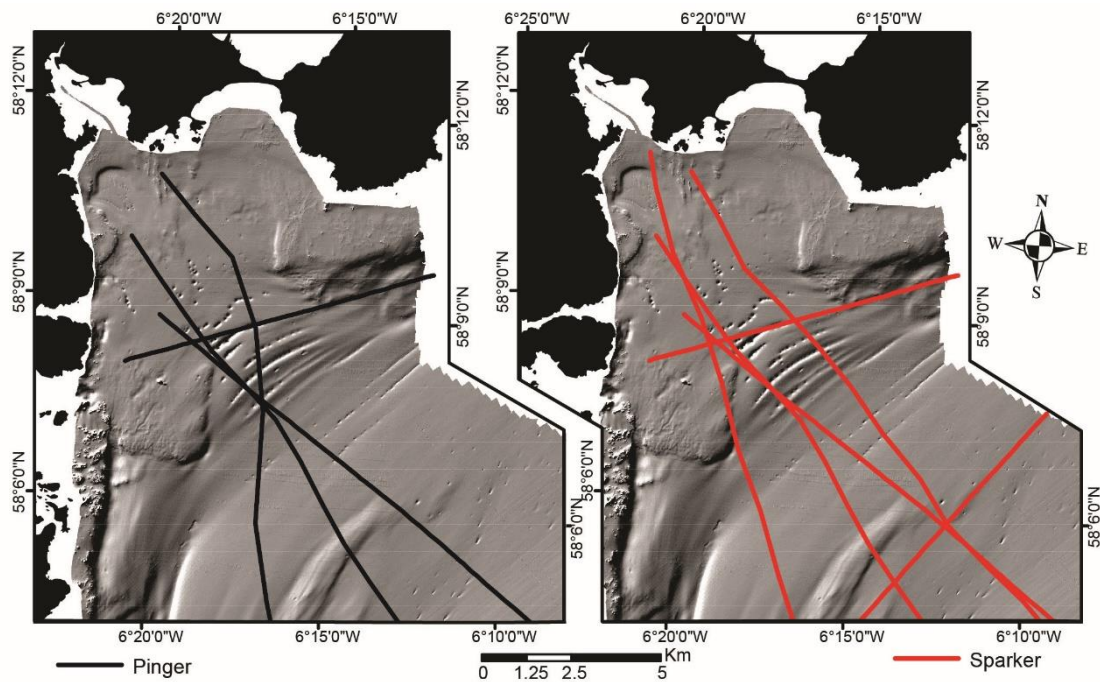


Figure 4.3 Seismic lines from Stornoway Bay separated by instrument type. Contains surveys conducted between 1968 – 1985 as shown in Figure 3.2.

The position of a BGS borehole in Stornoway Bay is also recorded and used in this study (Figure 4.2). Borehole 78/4 was recovered during the 1978 seabed sampling cruise onboard the MV Ferder. The core was retrieved in 80 m of water and represents the most complete sediment succession of Quaternary sediments from the region (Graham *et al.* 1990). The position of the borehole was downloaded from the BGS offshore GeoIndex.

4.2.1.3 Loch Broom

Loch Broom was surveyed using an Applied Acoustics surface tow boomer during a 2012 BGS geophysical survey onboard the RV White Ribbon. The inner Loch Broom basin was chosen as the region of interest due to the presence of pockmarks and the high slope angle of the surrounding topography indicating that this was the primary glacial drainage route and also the deepest part of the bedrock basin. The position of the survey lines and seismic profiles were archived by BGS and available on the BGS offshore GeoIndex (Figure 4.4).

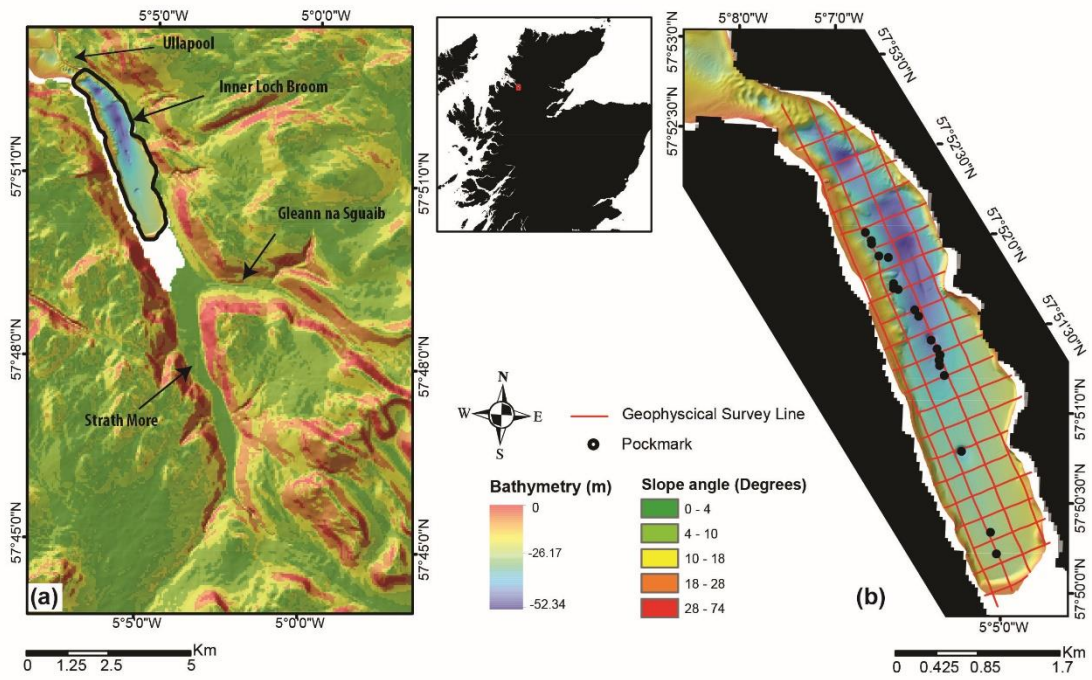


Figure 4.4. Maps of Loch Broom. (a) shows the slope angle of the surrounding topography of Loch Broom. (b) shows the bathymetry of the inner Loch Broom basin, position of pockmarks and the position of Geophysical survey lines.

4.2.1.4 Inner Sea of Hebrides

Several geophysical surveys were conducted within the Inner Sea of Hebrides between 1968 and 1985 (Figure 4.5). The surveys were conducted using several research vessels collecting data using pinger and sparker seismic profilers and transit sonars (Figure 4.6). Metadata from these cruises is not readily available, however published literature from the same region which investigate similar vintage seismic lines have shown that the two-way time interval is 25 msec (Howe *et al.* 2012; Arosio & Howe 2018). The position and digitised images of geophysical records were retrieved from the BGS offshore geosindex.

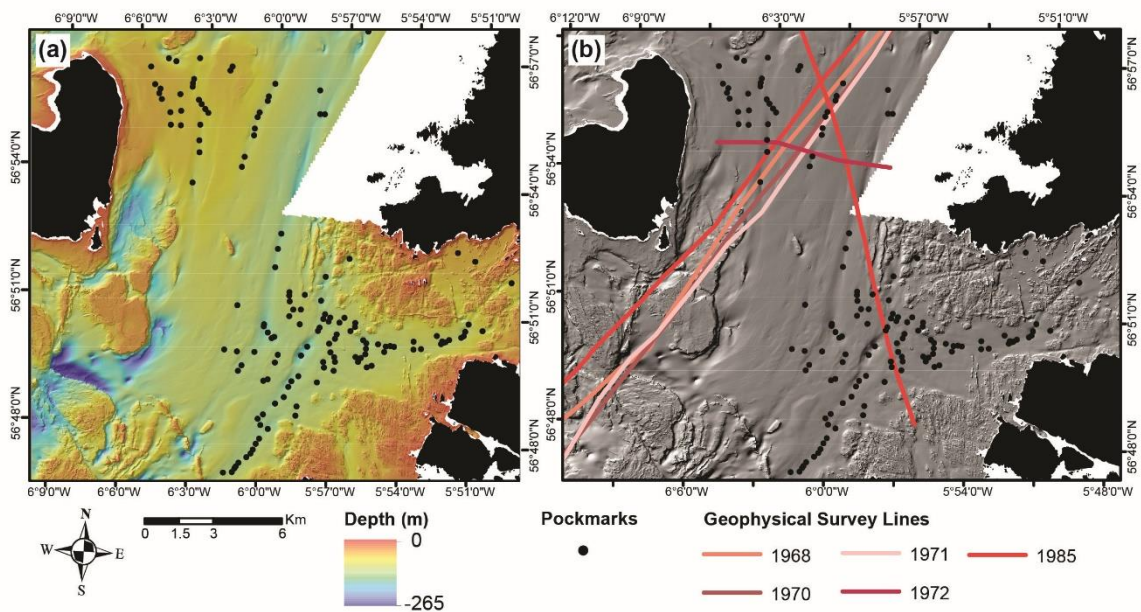


Figure 4.5. Bathymetry and location of geophysical survey lines and pockmarks in the Inner Sea of Hebrides and Arisaig Bay. Geophysical surveys were conducted between 1968 – 1985 and include the use of pinger, sparker and transit sonar geophysical instruments.

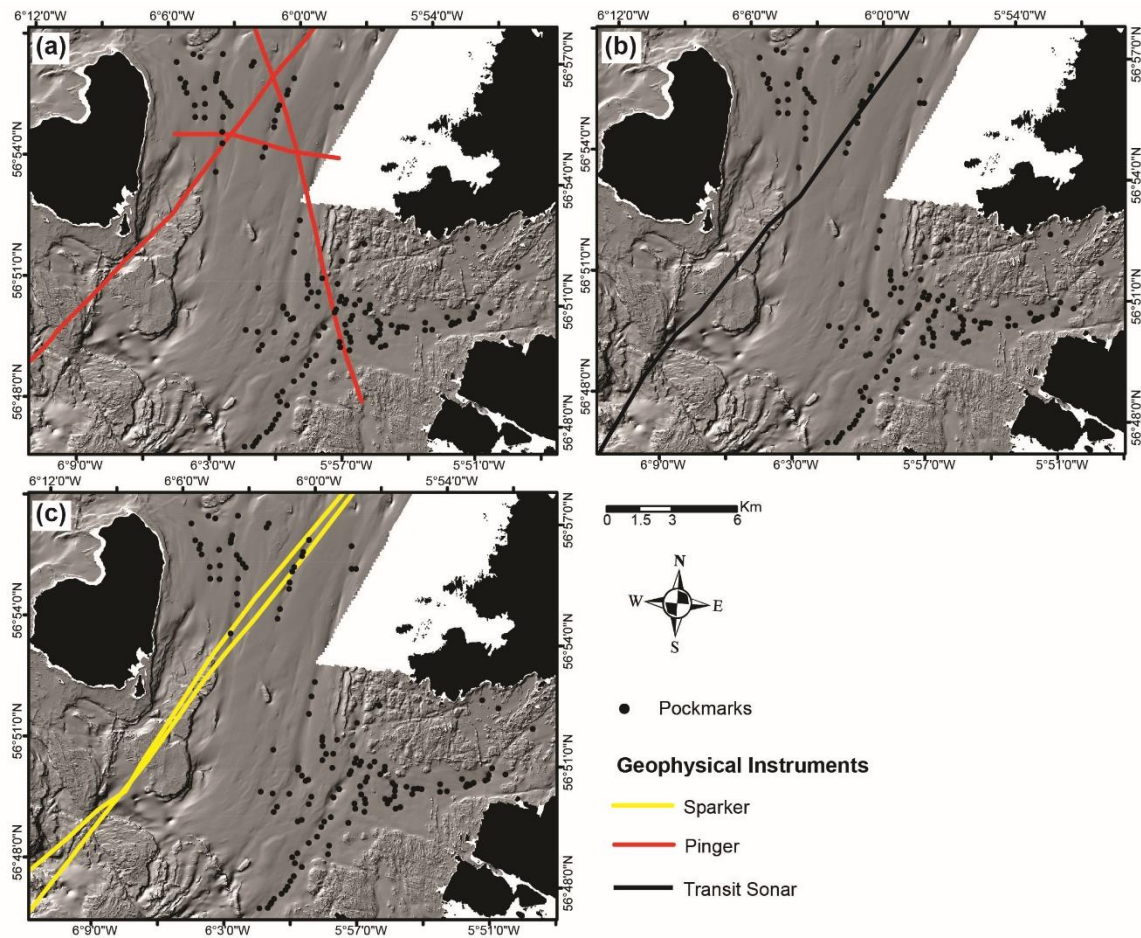


Figure 4.6. Geophysical survey lines from the Inner Sea of Hebrides separated by instrument type. (a) position of pinger seismic lines. (b) position of a transit sonar survey. (c) position of sparker seismic lines. Surveys were conducted between 1968 – 1985 as shown in Figure 3.5.

4.2.2 Inverse distance weighting

Within ArcGIS the inverse distance weighting (IDW) tool was used to interpolate the vertical distance to the acoustic turbidity horizon interpreted as sub-seabed gas. IDW uses the principle that distant points have less of an effect on nearby points and interpolates a surface based on this. The depth to the inferred gas front was measured by recording observations of acoustic turbidity at each seismic fix. If no acoustic turbidity was observed, then an NA value was recorded and not processed during IDW interpolation.

Due to the limited availability of metadata from several cruises within the study region (i.e. Stornoway Bay and Inner Sea of Hebrides) IDW analysis of the depth to gas front was only possible in Loch Linnhe and Loch Broom.

4.2.3 Hot-spot analysis

Optimized hot-spot analysis within ArcGIS was used to identify hot-spots of pockmark formation. The tool uses the Getis-ord G_i^* statistic, which implements the principle that nearby features are more related than distant features. Two main variables can be set by the user: cell size and neighbourhood distance. The default values are calculated by the tool using spatial auto-correlation, which identifies the distance band of peak clustering of the features. This is generally used as a guide to inform the user, but it is recommended that variables are set according to the specific question being tested.

For this analysis, variables were set to test the question whether pockmark hot-spots have formed. Previous studies suggest that when pockmarks form, they act as the primary drainage channels for all surrounding gas up to half the nearest neighbour distance, at which point gas theoretically vents from the 'new' nearest pockmark to reduce pressure (Cartwright *et al.* 2011; Moss *et al.* 2012b). This distance of half the nearest neighbour distance is termed the 'exclusion zone' (Moss *et al.* 2012b) within which theoretically no other pockmarks will form. Nearest neighbour distance was calculated using the average nearest neighbour tool within ArcGIS. If this assumption is violated, we consider this a hot-spot, and by inference, that the volume/pressure of gas within the region is unable to escape effectively through a single pockmark. In these situations, theory would suggest that one pockmark is not able to sufficiently reduce the gas pressure within the area. Using this 'exclusion zone' concept, the cell size for hot-spot analysis was set at half the average distance to the nearest neighbour, and the neighbourhood distance was set as the average distance to the nearest neighbour. Thus, if more than one pockmark occurs within the exclusion zone, then a hot-spot is immediately recognised; if further pockmarks are observed within the neighbourhood distance, then these areas are also considered hot-spots at varying degrees of confidence.

Due to only 19 pockmarks being observed within inner Loch Broom it was not possible to calculate a statistically reliable results using the '*Optimized Hot Spot Analysis*' tool in ArcGIS, which requires a minimum number of 30 features.

4.3 Results

4.3.1 Loch Linnhe

4.3.1.1 Hot-spot analysis

GIS hot-spot analysis was conducted over three scales (Figure 4.7) to identify regions where statistically more pockmarks have formed in the study region and highlight regions that require further investigation. The first targeted all pockmarks within the outer basin of Loch Linnhe. The analysis calculated an average nearest-neighbour distance of 220.4 m, which was used as the analysis neighbourhood with half this distance (110.2 m) used as the cell size. The analysis identifies that the majority of pockmarks are forming in localised hot-spots within basins, with the exception of SB (Figure 3.7a). The second scale of analysis targeted only the pockmarks that are within the region covered by the seismic survey. A nearest-neighbour distance of 285 m was used as the analysis neighbourhood and 142.5 m for the cell size. This hot-spot analysis produced similar results to the first scale of analysis (Figure 4.7b). The third analysis only targeted pockmarks in the region where gas was observed on seismic records. In this case, a nearest neighbour distance of 402 m was used as the analysis neighbourhood and 201 m for the cell size. The third analysis shows hot-spots within LB, KB and B. Bnk (Figure 4.7c). No hot-spots were identified at any scale within BB, and the majority of pockmarks within SB do not form hot-spots at any scale.

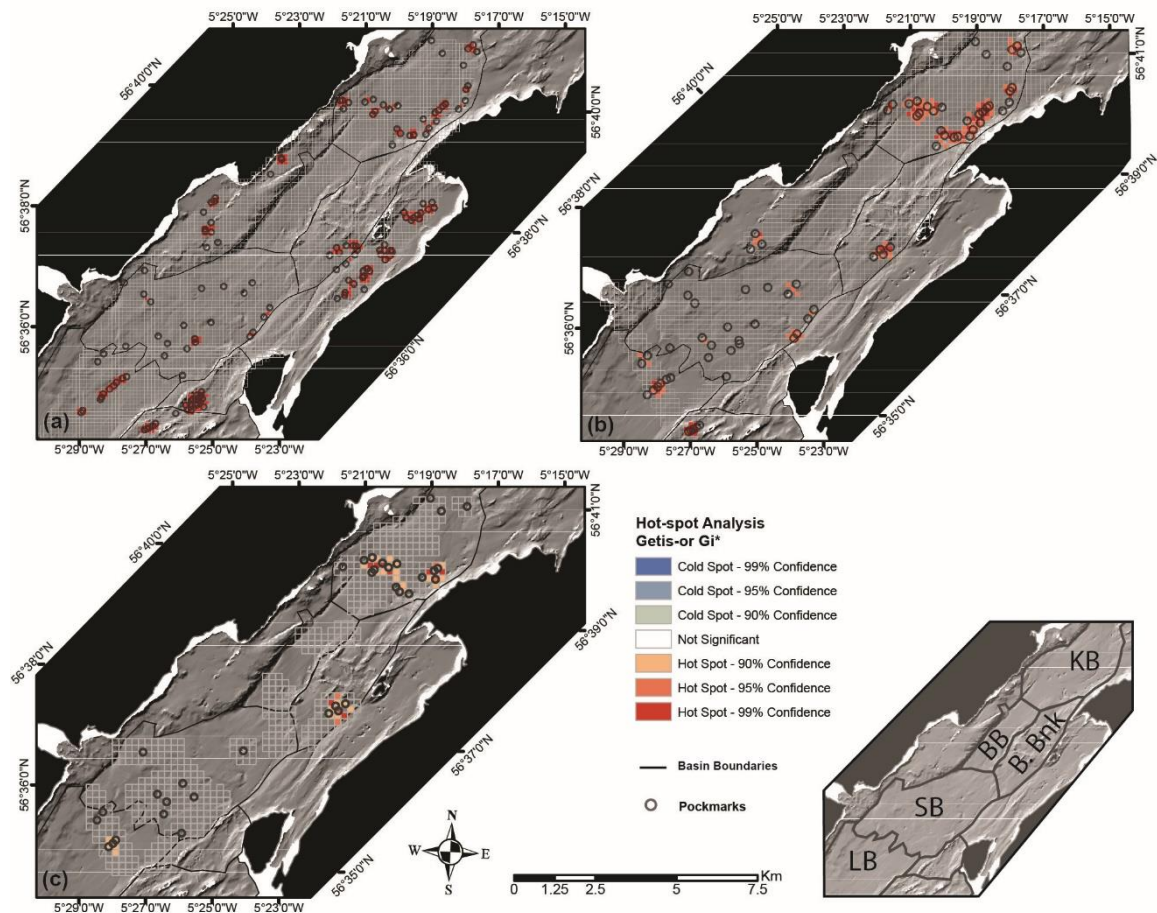


Figure 4.7. Hot-spot analysis using the Getis-ord G_i^* statistic of pockmarks within Loch Linnhe along with an inset map showing main basins mentioned in Figure 1; **(A)** Hot-spot analysis of all pockmarks within Loch Linnhe; **(B)** Hot-spot analysis of pockmarks that occur within the region of the boomer seismic survey; **(C)** Hot-spot analysis of pockmarks where gas was observed in seismic profiles.

4.3.1.2 Seismic facies

Seismic interpretation of Loch Linnhe data has been adapted from (McIntyre 2012). A total of 5 distinct facies, labelled as Loch Linnhe Seismic facies (LLSF) were observed (Table 4.3). A common feature observed within every line was the L1 reflector which occurs at the base of LLSF5.

Table 4.3. Seismic Facies of Loch Linnhe and their interpretations adapted from McIntyre 2012.

Seismic Facies	Seismic Characteristic	Interpretation	Setting
LLSF5	Strong, continuous, parallel reflectors draped over topography.	Youngest unit, 3-4 m thick. Thin or absent on steep slopes. Terrigenous derived, organic/inorganic, deposited under suspension.	(Holocene) Marine
LLSF4	Continuous, parallel, sheeted reflectors, draped in deep basins.	Directly under LLSF5 (L1) reflector. Up to 45 m deep. Thin or absent on bathymetric highs.	(Post Younger Dryas) Glaciomarine (distal)
LLSF3	Strong, continuous to discontinuous. Parallel to sub-parallel.	Occurs below LLSF4, > 80 m deep. Absent from banks and shallows.	(Post Younger Dryas) Glaciomarine (proximal)
LLSF2	Lacking internal structure, chaotic reflections. Sometimes blanks underlying seismic structures.	(a) Present at the base of many slopes, occupying regions which would otherwise contain LLSF3/4. Usually does not, or only partially, obscure underlying facies. (b) Occurs as wide regions with abrupt to diffusive initial reflection. Abrupt vertical boundaries where it obscures LLSF3/LLSF4. Usually completely obscures any other reflectors. May also form as isolated domes. Interpreted as acoustic blanking due to gas scattering or attenuated seismic signal.	(a) Slumps. (b) Gas.
LLSF1	Strongly hyperbolic to chaotic. Discontinuous reflectors.	Present as the basal unit in most regions. In other regions they can occur as discontinuous reflections within LLSF2. Interpreted as ice-contact deposited proglacially as moraines or sub-glacially. Compacted, unsorted clay – boulder in size.	(Younger Dryas) Diamict or bedrock

The clearest representation of gas within the study region is in the form of acoustic turbidity (blanking) as seen within numerous seismic line profiles (Figure 4.8). This is identified as LLSF2b (Table 4.3) and can be observed at the southerly and northerly regions of Loch Linnhe. Acoustic turbidity can be observed in the form of undulating curtains (Figure 4.8 Line A) or associated with reflector pull-downs interpreted as a chimney structure (Figure 3.8 Line B), or as widespread blanket (Figure 4.8 Line C). Regions of acoustic turbidity are often found to be near pockmarks, where gas has vented into the water column during pockmark formation/activity.

Pockmark 2 shown in Figure 4.9 Line A was identified and described as a 'deep' pockmark (Audsley *et al.* 2019); that is a statistically deeper-than-average pockmark (based on depth/area ratio) across the studied sites around western Scotland. The L1 reflector is not present within the centre of this pockmark. No clear signs of gas, LLSF2b, are observed beneath pockmarks 1 and 2 (Figure 4.9 Line A:B). The seismic facies are chaotic and obscure in places; however, they do not have the same acoustic turbidity characteristics commonly attributed to gas. Seismic lines B and C show the classic example of acoustic turbidity (LLSF2b), interpreted as gas. Line B shows a variable depth to the gas front and

contains a pockmark. Line C shows widespread coverage of LLSF2b, here termed a 'gas blanket'.

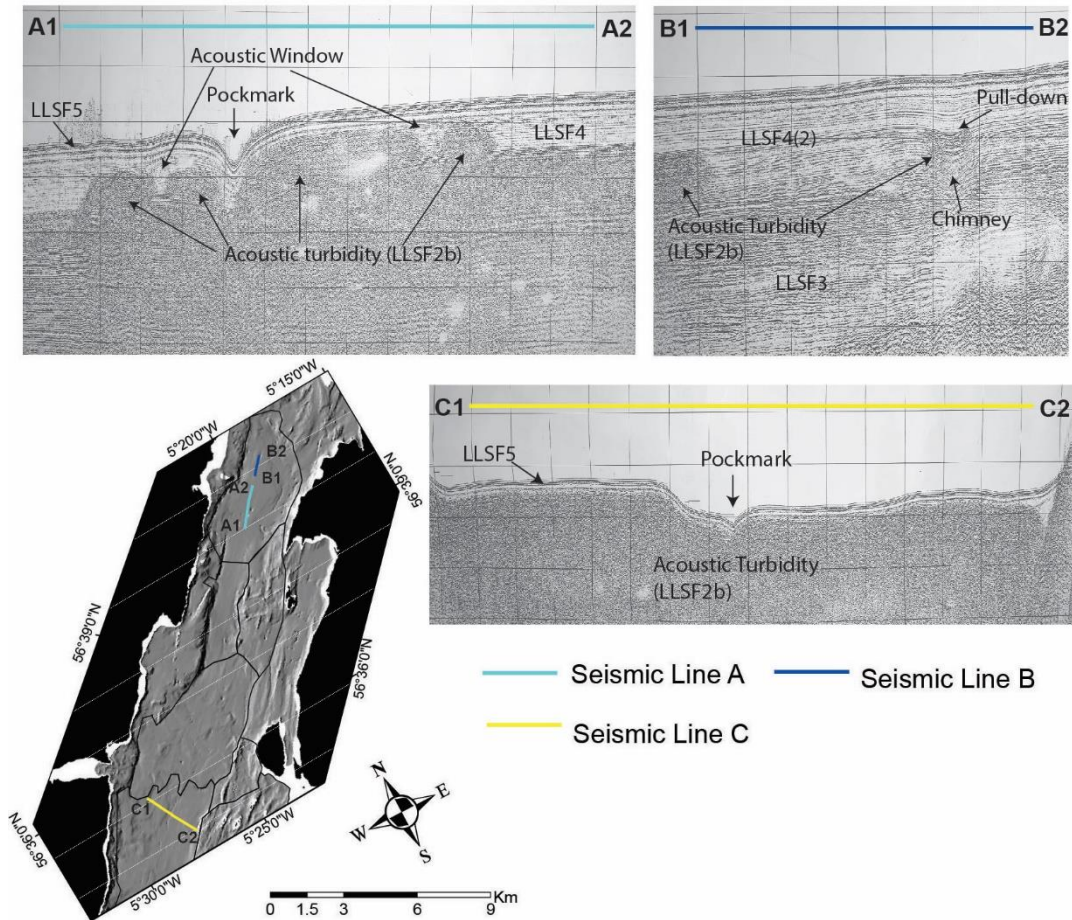


Figure 4.8. Seismic analysis of selected lines that contains evidence of gas/fluid accumulation in the form of acoustic turbidity (LLSF2b), pockmarks and pull downs. Map shows the position of seismic lines to corresponding profile of the same colour.

The seismic line that extends through BB from KB in the north to SB to the south contains several examples of pull-down reflectors (Figure 4.10). The most northern section of Line B (Figure 4.10) shows the clearest evidence of LLSF2b, interpreted as gas at this site. This acoustic turbidity continues at greater depth until it forms the front to a section of LLSF2. This front is very stable but is not parallel to the seabed. It appears to occupy the region that would otherwise be filled with the older LLSF4 (1) unit. We are unable to definitely interpret this facies as gas due to the incomplete blanking of deeper reflectors. Sections of pull-down reflectors are recorded within LLSF3. It is likely that this area of LLSF2 is slump material or sediment that has lost all internal structure due to it becoming

'quick', with occasional pockets of gas. A similar interpretation is made for LLSF2 in Line B. No evidence of LLSF2 is observed in Line C. We interpret this section as not containing gas. A section of acoustically stronger reflectors lies between the boundary of LLSF4 (2) and LLSF4 (1). This is interpreted as a unique lens of higher density material—possibly a short-lived debris flow event. Further clear evidence of pull-down reflectors is present within Line C, extending throughout the depth of LLSF3 and towards the boundary with LLSF1.

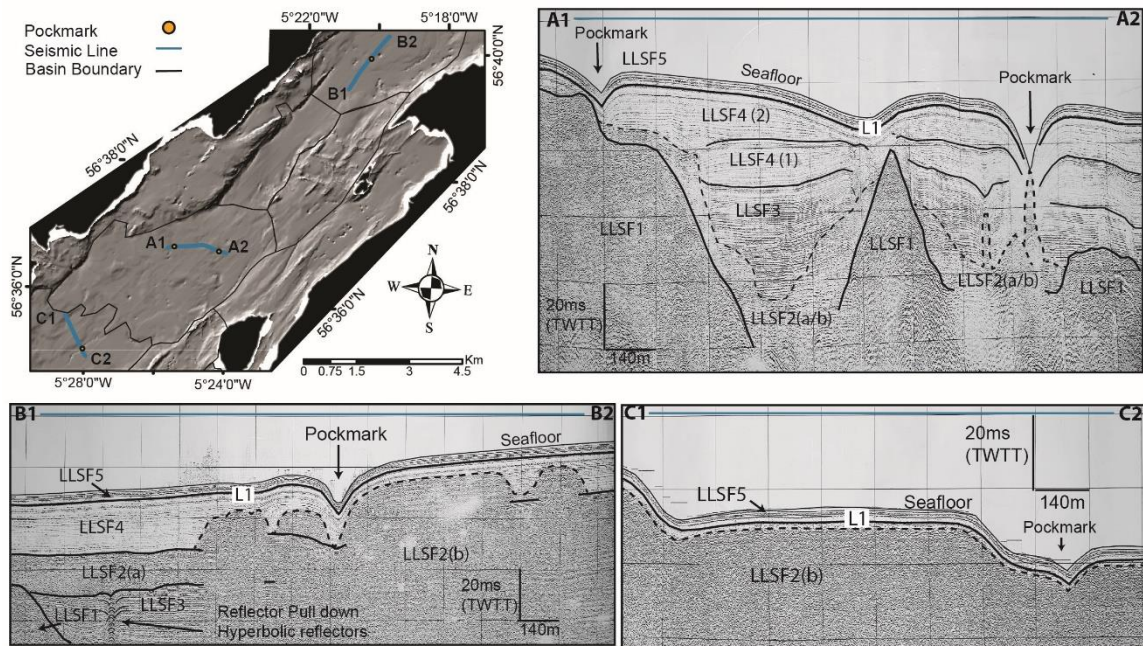


Figure 4.9. Seismic analysis of selected lines that contained pockmarks. Map shows the position of seismic lines, basin boundaries and the location of pockmarks that appear on the seismic line. Labelled seismic lines sections correspond to the seismic profiles A:C. Profiles B and C are also shown in Figure 3.3 where gas associated features are indicated.

Further examples of pull-down reflectors are closely related to the presence of pockmark 6 within KB (Figure 4.11 Line A). The pull-down reflectors are directly below pockmark 6 and extend into the underlying LLSF3. Evidence of gas is seen on either side of the pockmark in this profile but not directly below the pockmark. Further evidence of gas is recorded at the start of Profile H. Pull-down reflectors are also recorded immediately southwest of pockmark 6. The internal reflections at this point of interest are discontinuous and partially obscured, indicating that sediment containing gas may be present here.

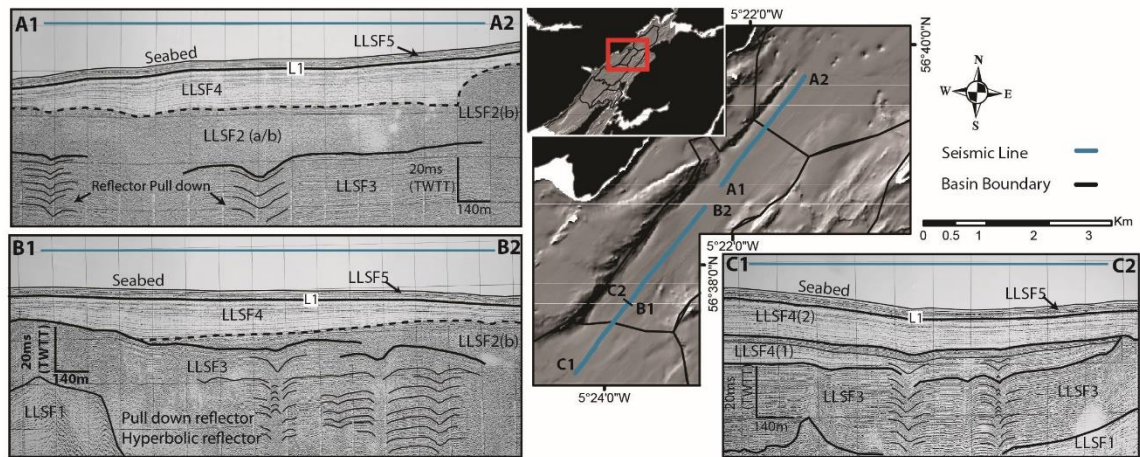


Figure 4.10. Seismic analysis of selected lines that contain pull-down reflectors. Map shows the position of seismic lines and basin boundaries. Labelled seismic lines sections correspond to the seismic profiles A:C. Dotted lines within seismic profiles show the position of the surface reflector for LLSF2. Where LLSF2b indicates acoustic turbidity (Table 3.1).

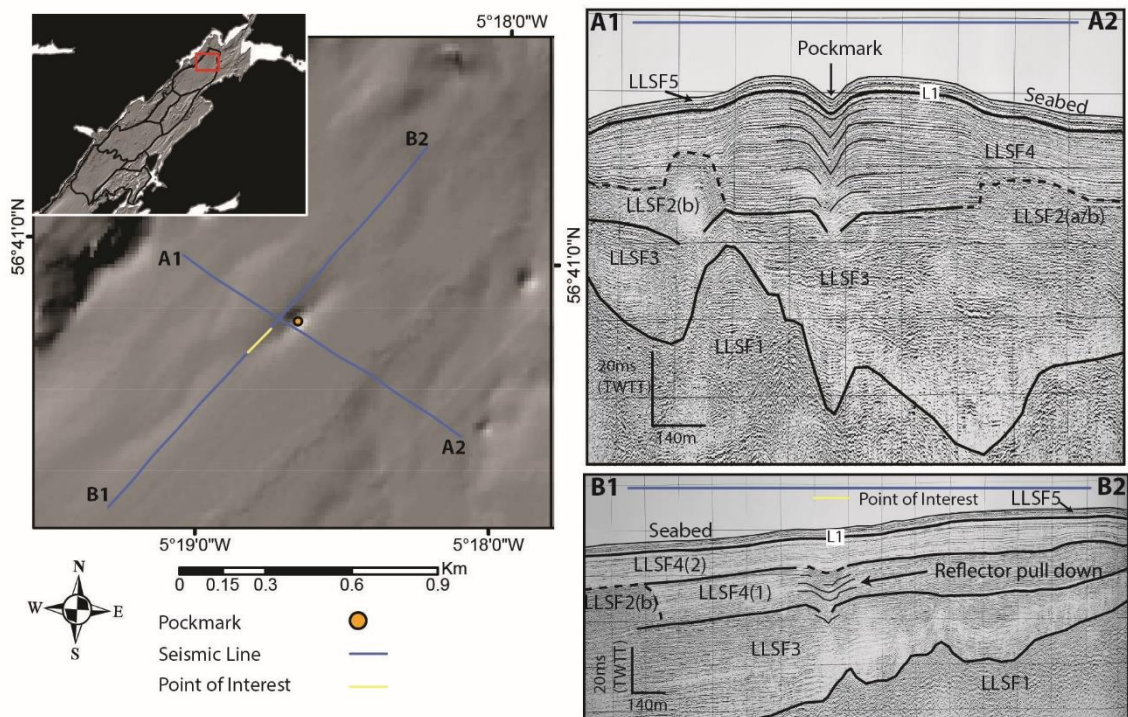


Figure 4.11. Seismic analysis of selected lines that contained a pockmark and nearby pull-down reflectors. Map shows the position of seismic lines, basin boundaries and the location of pockmarks that appear on seismic line. Labelled seismic lines sections correspond to the seismic profiles A:B. Seismic Line B is also shown in Figure 3.3 where gas associated features are indicated.

4.3.1.3 Gas distribution

The interpolated raster shows locations where sub-seabed gas was identified from seismic data. The gas shows a depth range of 3.7–50 milliseconds (msec) two-way travel time (TWTT) (Figure 4.12a). Gas was observed within all regions of the outer basin. The regions of most widespread gas occur in LB and KB; in all other regions, gas forms isolated zones. Generally, gas was seen in close proximity to pockmarks. Figure 4.12b shows the number of pockmarks that lie directly above a region of gas-rich sediment. Thirty-five pockmarks have gas directly beneath their centres. Of these, 29 pockmarks occur above a gas front 3.7–20 msec deep, five pockmarks above a gas front at 20–30 msec depth, and one pockmark is located above possible gas at 40–50 msec depth; this pockmark is further investigated in the discussion. Thirty-two pockmarks occur in regions where gas could not be observed; however, this result largely reflects the incomplete seismic survey coverage in Loch Linnhe, making it not possible to observe the presence/absence of gas between geophysical lines.

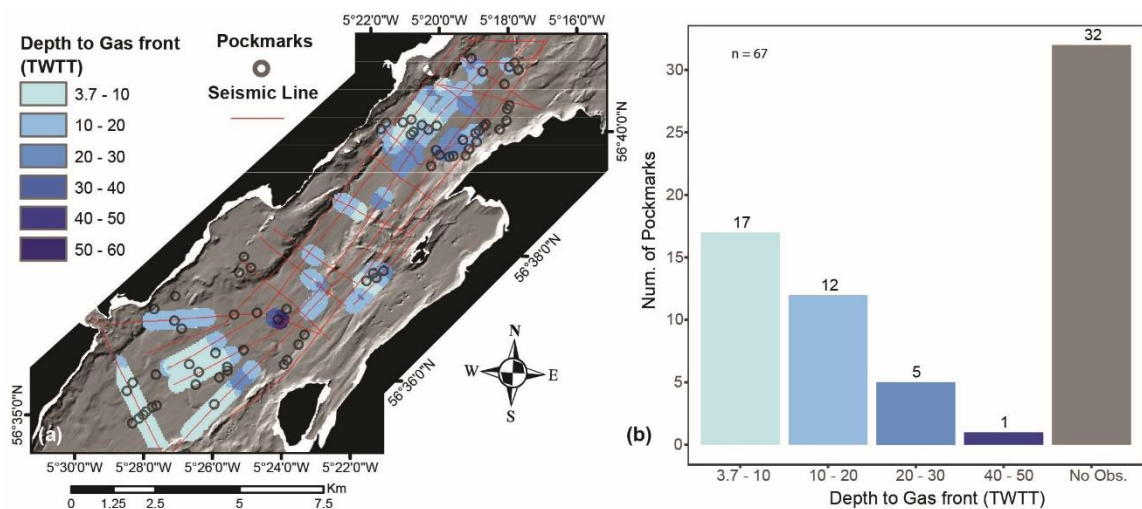


Figure 4.12. Primary study region of Loch Linnhe that includes the boomer seismic survey; (a) Depth to the gas front (msec TWTT) where gas was observed in seismic profiles; (b) Bar-plot showing the number of pockmarks found within each distance band to the gas front.

4.3.2 Stornoway Bay

4.3.2.1 Hot-spot analysis

Hot-spot analysis was conducted within Stornoway Bay using an average nearest neighbour value of 265.5 m, with that value being the neighbourhood distance and 132.75 as the cell size. This has highlighted that the majority of hot-spots are closer to shore with fewer recorded further into the North Minch (Figure 4.13). The analysis clearly captures

the pockmarks which are forming close together and forming linear strings across much of this region. Pockmark hot-spots are less common around the edges of Stornoway Bay where regions of partly exposed bedrock can be observed. Another prominent hot-spot has been recorded within the north westerly bay in the study region, where an isolated cluster of pockmarks has formed. Overall, it is observed that the majority of pockmark hot-spots are forming in the regions of Stornoway Bay which lies close to the suspected region major Minch fault, and within the bathymetrically restricted regions of Stornoway Bay.

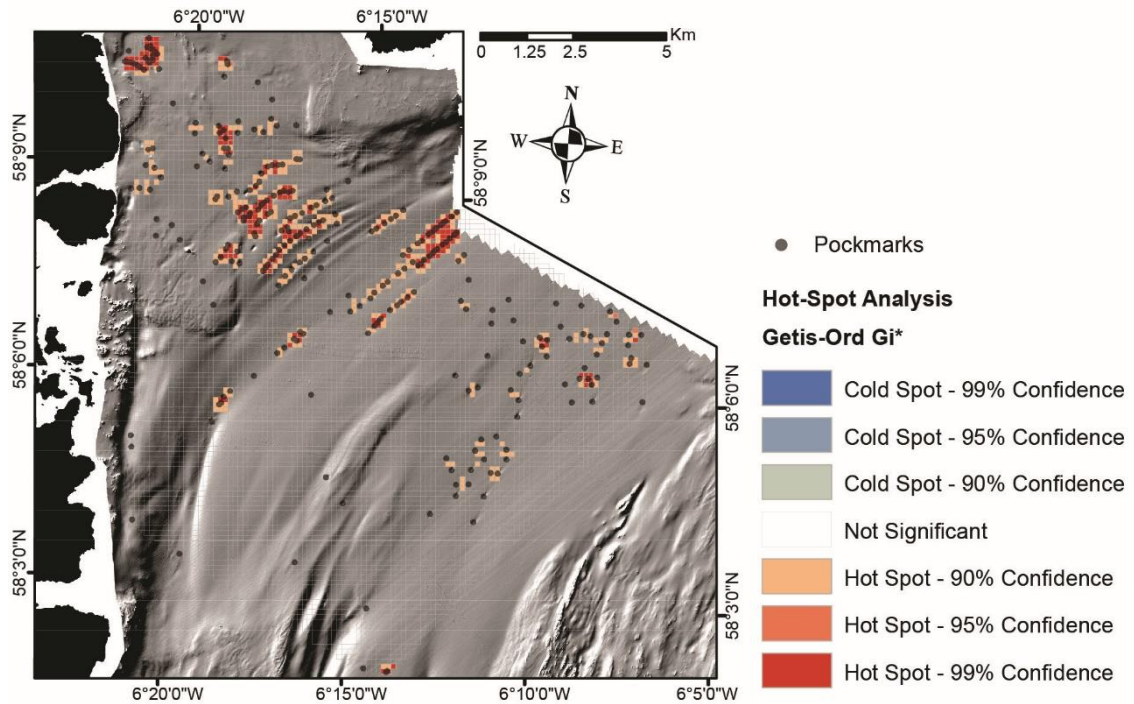


Figure 4.13. Hot-spot analysis using the Getis-ord G_i^* statistic of pockmarks in Stornoway Bay. Map shows the distribution of pockmarks and the results of the hot-spot analysis.

4.3.2.2 Seismic facies

Seismic interpretation of Stornoway Bay has been based on geophysical surveys where both pinger and sparker systems were used on the same line, it is found that 5 separate facies are observed and recorded; these are termed as Stornoway Seismic facies (SSF) (Table 4.4). The acoustic expression of gas is similar to that found in Loch Linnhe where the seismic data becomes chaotic and lacks internal structure, this is recorded as SSF3. SSF3 is observed to occur beneath SSF4, the youngest depositional unit. At times gas can be found directly below SSF4 which is approximately 15m thick, and is not observed at shallower depths than this. It was also found that the distribution of SSF3 can either be as large continuous blankets, such as below pockmark strings, or as more isolated gas curtains such as those found further into the North Minch (Figure 4.14). As previously

stated SSF3 generally obscures any internal reflectors and completely masks any deeper facies, however it is possible at times identify SSF1, interpreted as bedrock, and SSF2 at the 'acoustic edges' of these large gas blankets.

These identified seismic facies within Stornoway Bay can be related to the lithological character of the sediments thanks to borehole 78/4 which penetrated the entire Quaternary sequence and the Jurassic bedrock (Graham *et al.* 1990) (Table 4.5). An interpretation of these sediments has allowed approximate ages of the seismic facies and associated environmental conditions in which they were deposited to be deduced. The main finding here suggests that the gas-bearing SSF3 is likely of similar age and lithology to SSF2 deposited during a distal glaciomarine environment of the Weichselian (or Devensian) stage of the Quaternary period.

Table 4.4. Seismic facies present in Stornoway Bay from Sparker and Pinger profiles. These facies are described according to their appearance and distribution characteristics.

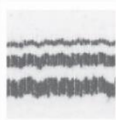
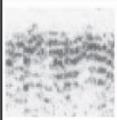
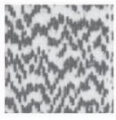
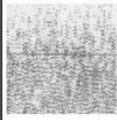
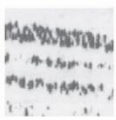

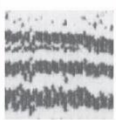
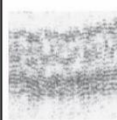

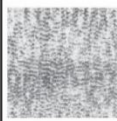
Seismic facies	Example		Reflector Description	Distribution
	Sparker	Pinger		
SSF4			Strong continuous parallel reflectors found at seabed and draped over underlying units.	Youngest depositional unit. A consistent unit present in all seismic lines. Can be 0-15 metres thick.
SSF3			Generally chaotic, lacking internal structure. Some discontinuous reflectors are sometimes present within sparker profiles.	Occurs periodically within seismic lines. Can be in the form of a blanket > 500 metres long, or as curtain feature, < 500 metres long. Present beneath pockmarks. Generally blanks out inter reflectors, however within Sparker records, some internal reflectors of SSF2 can be observed.
SSF2b			Continuous and discontinuous reflectors. Parallel to sub-parallel. Pinger records show an acoustically transparent discontinuous scattered reflectors.	Occurs beneath SSF4, variable thickness, pinches out near bedrock highs.
SSF2a			Strong generally continuous reflectors that are parallel to one another. Pinger show strong discontinuous to continuous reflectors	The older unit of SSF2 and is found beneath SSF2b. Generally found in all seismic lines apart from where it is obscured by SSF3.
SSF1			Strong hyperbolic reflectors or chaotic. The initial reflector is generally discontinuous.	Oldest unit observed within seismic profiles. Occurs at the base of SSF2a, but may also appear as a discontinuous boundary where SSF3 is present.

Table 4.5. Interpretation of seismic facies observed in seismic profiles from Stornoway Bay. The interpretation and lithological character of the facies is adapted from the interpretation of BGS borehole 78/4, Stornoway Bay (Graham et al 1990).

Seismic facies	Lithology	Interpretation
SSF4	Very soft muds, silty clay, 0 -10 m thick	Sediments deposited between the Holocene and Flandrian sequences of the Quaternary. Deposited between 0 - 9860 ± 160 yrs BP. These represent temperate marine conditions.
SSF3	Lithology is similar to background facies, SSF2a/b depending on depth of observed SSF3. Sediment likely contains gas bubbles.	Sediments were deposited during the same period as SSF2a/b depending on which background facies is likely present. This facies is interpreted as sediments containing gas.
SSF2b	Moderately firm silty clay, dark grey in colour. Poorly to slightly bedded.	Sediments deposited during the Devensian stage of the Quaternary period. Deposited between 9860 ± 160 yrs BP to 12785 ± 140 yrs BP. This is interpreted as distal glaciomarine conditions.
SSF2a	Firm silty clay, brownish grey in colour, with occasional pebbles.	Sediment deposited during the earlier stages of the Devensian. Deposited later than 12785 ± 160 yrs BP. This is interpreted as proximal glaciomarine conditions.
SSF1	Soft black shelly mudstone	Jurassic bedrock

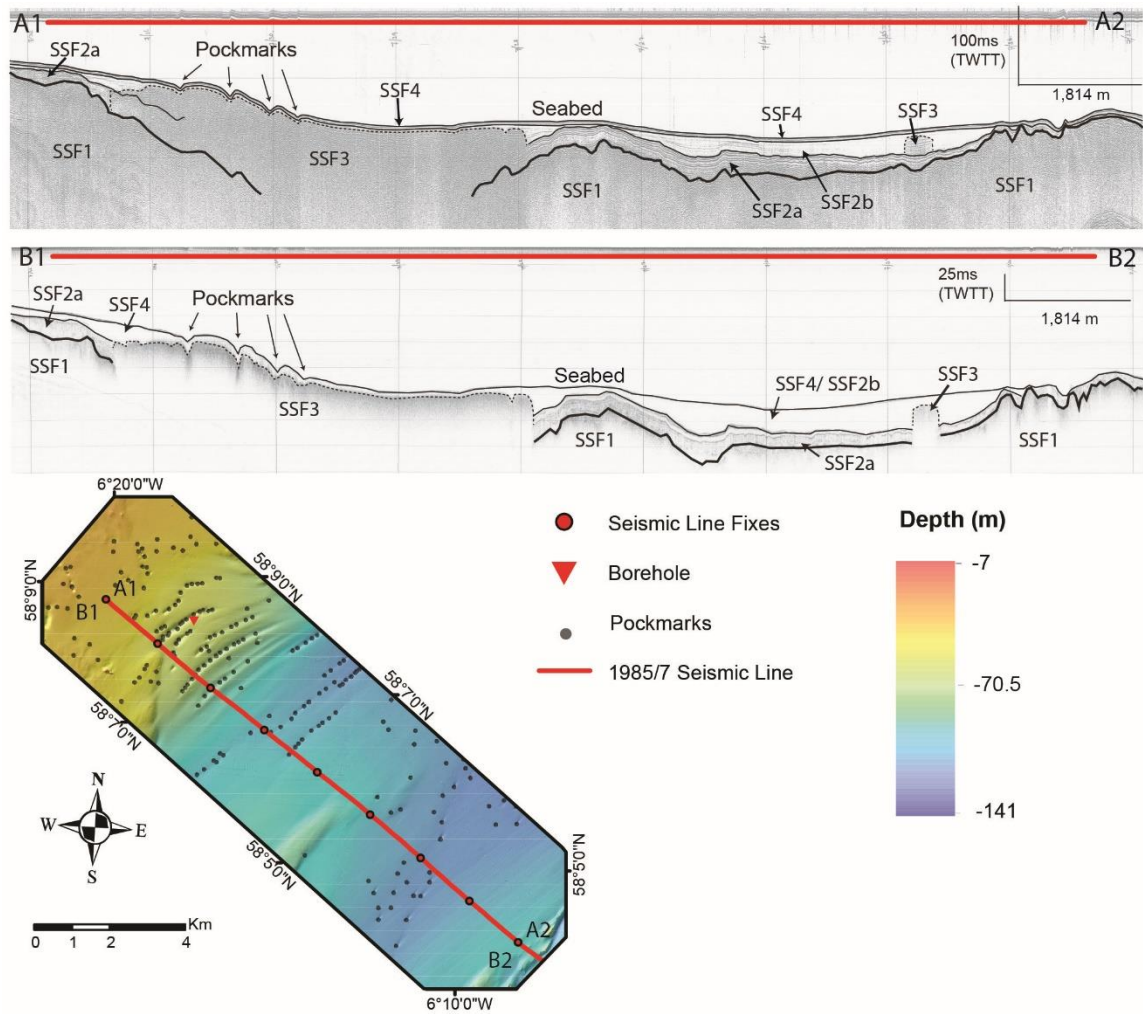


Figure 4.14. Seismic analysis of Seismic line 1985/7 in Stornoway Bay. Line A shows the Sparker seismic profile. Line B shows the Pinger seismic profile. Inset map shows the position of the seismic line, the position of BGS borehole 78/4 and the distribution of pockmarks.

The seismic facies SSF3 associated with gas can be clearly observed within sparker and pinger records (Figure 4.14). It is most commonly observed in the regions with high densities of pockmarks, where hot-spots are identified. Further into the more hydrodynamically exposed region of the North Minch, gas is not as abundant within the records, apart from a single isolated gas curtain observed. The sudden loss of further seismic reflectors directly below SSF3 is the result of the attenuation of the sound wave as a result of gas and can be clearly observed within pinger records (Figure 4.14B). Although it is common for all internal reflectors to be obscured due to the presence of gas, within sparker records it is sometimes possible to track the presence of the bedrock (SSF1) or other strong reflectors, particularly at the edges of these gas rich regions. It is possible to partially track the bedrock within Stornoway Bay below the main gas blanket,

and it can be observed that the depth to bedrock is increased. It therefore appears that the main region of acoustic turbidity and presence of developed pockmark strings occurs in the region where sediment thickness is greatest.

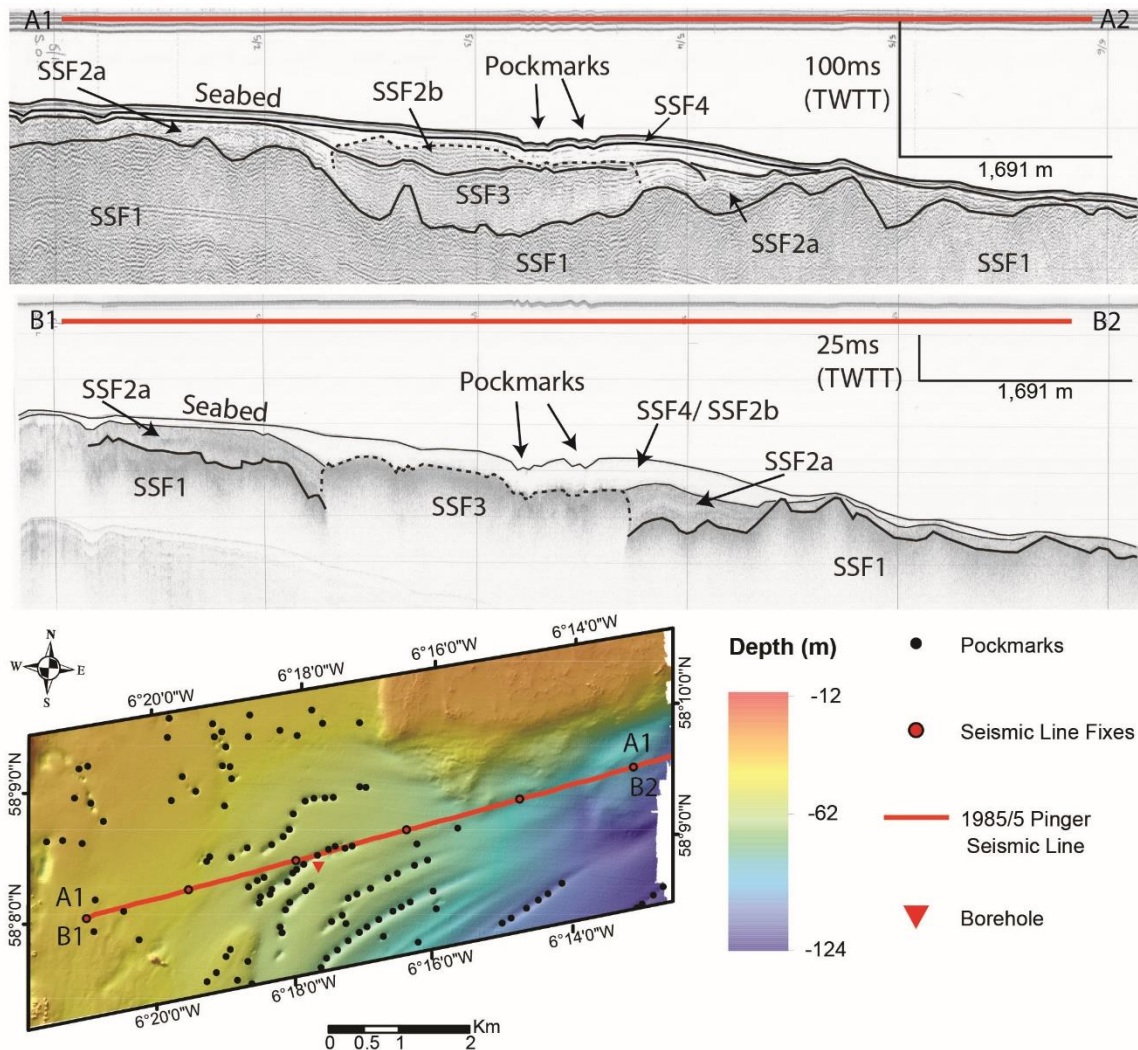


Figure 4.15. Seismic analysis of seismic lines 1985/5 in Stornoway Bay. Line A shows the sparker seismic profile. Line B shows the pinger seismic profile. Inset map shows the position of the seismic line, position of BGS borehole 78/4 and the distribution of pockmarks.

The sparker and pinger seismic lines 1985/5 (Figure 4.15) cross the main basin of Stornoway Bay. Again, the presence of gas has caused a loss of internal seismic reflectors particularly in the pinger record. However, it is possible to partially track the bedrock and SSF2 reflectors within the sparker record. As with line 1985/7, sediment thickness

increases towards the centre of this basin where the majority of pockmarks strings are also observed.

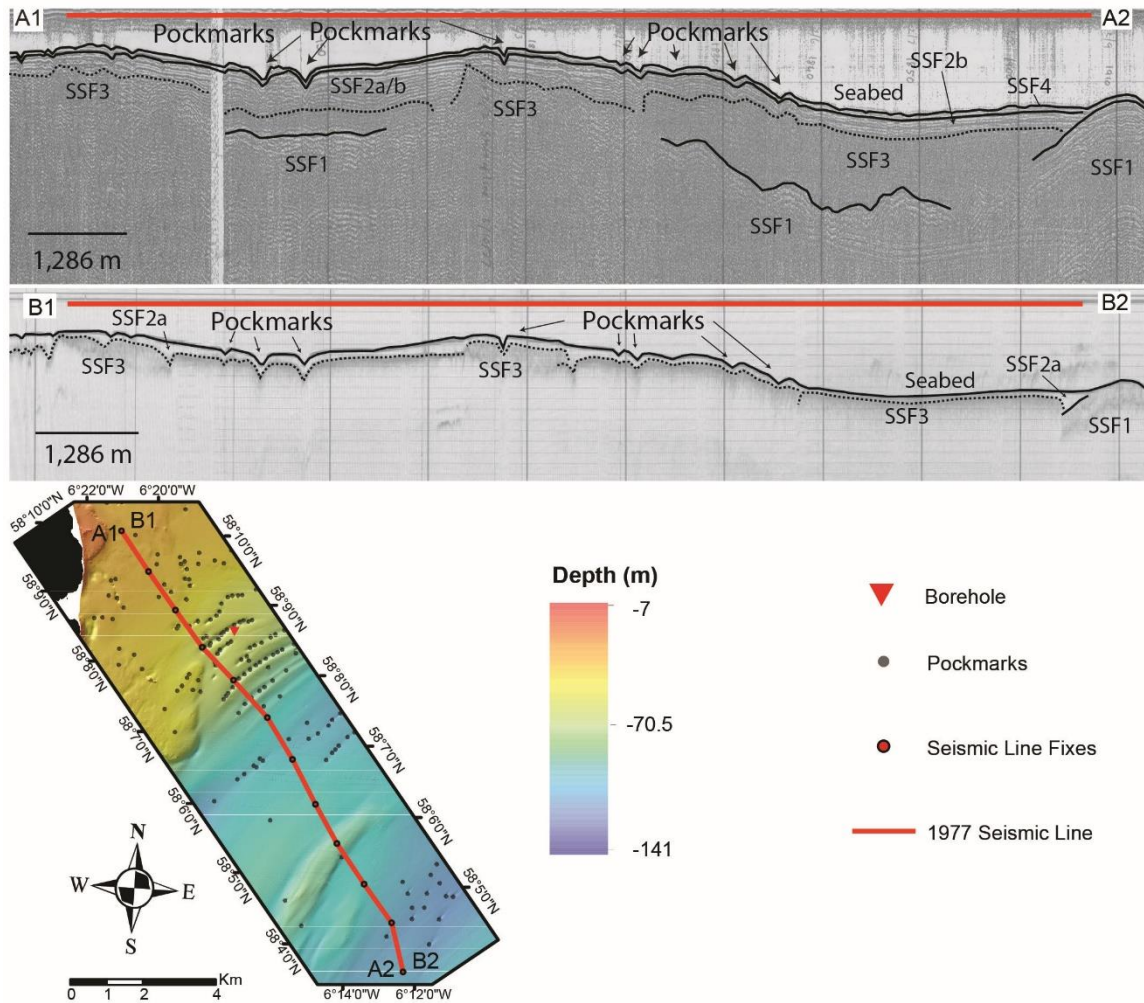


Figure 4.16. Seismic analysis of seismic line 1977/2. Line A shows the sparker seismic profile. Line B shows the pinger seismic profile. Inset map shows the position of the seismic line, the position of BGS borehole 78/4 and the distribution of pockmarks.

The metadata records for the 1977 line were not as readily available as other lines therefore a two way travel time was not recorded. However, it is still possible to observe the gas-bearing SSF3 directly below pockmarks (Figure 4.16). SSF3 is also observed extending slightly further into the North Minch compared to line 1985/7. Within the sparker record it is also possible to track the SSF1 reflector at times even below SSF3. Again, it appears the sediment thickness generally increases within the regions of SSF3 (gas-presence) and in the zone of pockmark hot-spots.

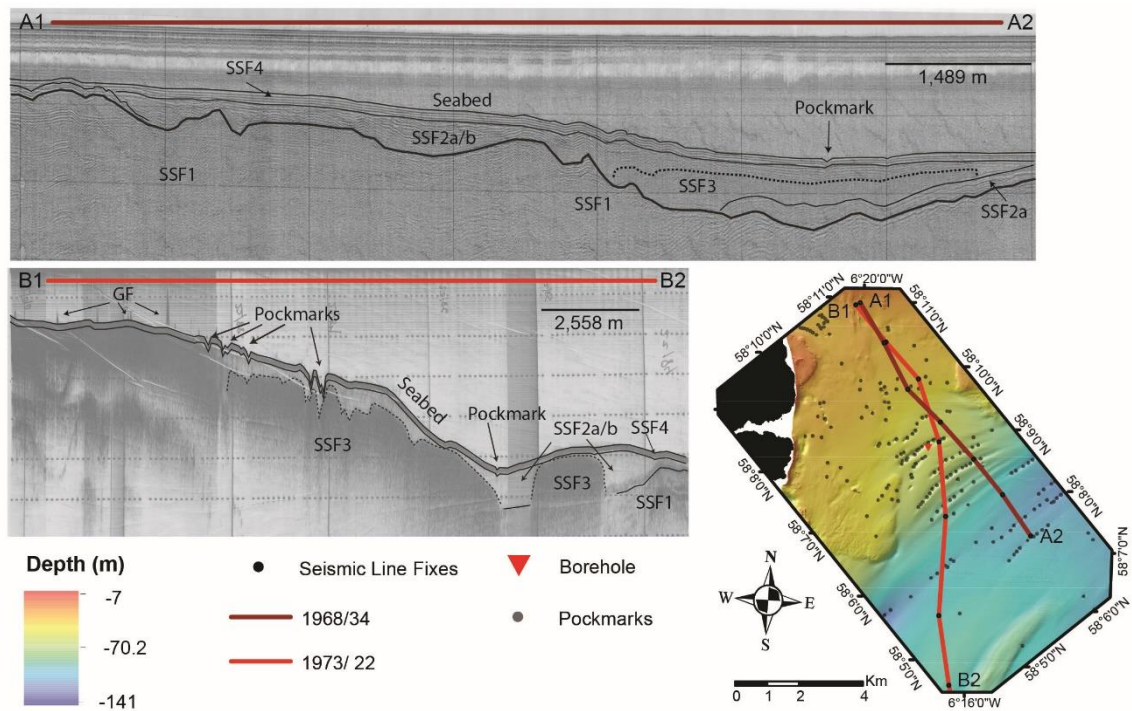


Figure 4.17. Seismic analysis of seismic lines 1973/22 and 1968/34. Line A shows the sparker seismic profile of 1968/34. Line B shows the sparker seismic profile of 1973/22. Maps show possible gas flares (GF) and identified seismic facies. Inset map shows the position of seismic lines, the position of BGS borehole 78/4 and the distribution of pockmarks.

The seismic lines 1973/22 and 1968/34 lack metadata and therefore the two-way travel time could not be determined with confidence. Being the oldest, these are also the poorest quality records in the region (Figure 4.17). However, it is still possible to observe SSF3 in both lines. SSF3 on line 1968/34 seems to be isolated within the outer sections of Stornoway Bay, in the deeper-water areas, and not within the shallower inner sections where it is seen elsewhere (Figure 4.15) close to pockmark hot-spots. By contrast on line 1973/22, SSF3 is more widely distributed within the inner Stornoway Bay and an isolated blanket in deeper water regions of the North Minch. Pockmarks are also not easily observed on the sparker line 1968/34 apart from a single pockmark located in the outer bay / North Minch region. It is possible that the irregular seabed along the middle of the line is the region where we observe the large pockmark strings, however these are not as well developed in this 1968 sparker line as in other seismic records. The 1968 sparker line is the oldest seismic survey from Stornoway Bay where both gas and pockmarks can be observed, this demonstrates that pockmarks have existed here for at least 54 years.

4.3.2.3 Gas distribution

Due to the low density and irregular distribution of seismic lines within the region a reliable interpolated raster for the depth to gas front could not be created. It is however possible to create a simple 2D map showing the general regions where gas is recorded on seismic lines between 1968 and 1985 (Figure 4.18). This map emphasises the results from the hot-spot analysis, with sub-seabed gas accumulations are clearly observed in the main Stornoway Bay region in close spatial association with the strings of pockmarks in the area. It is notable that gas expressions are rarer on seismic lines further offshore, into the North Minch.

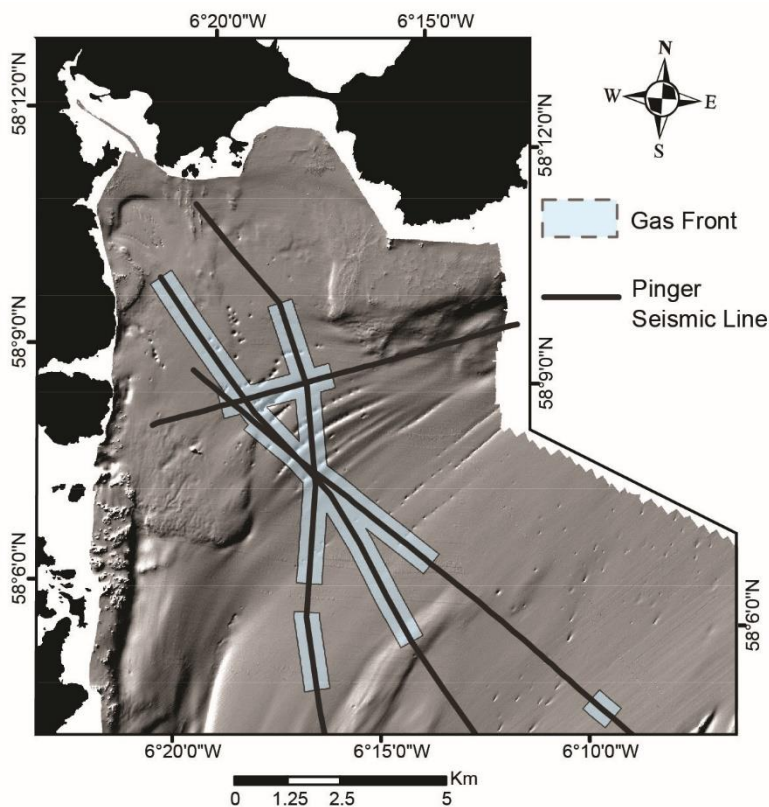


Figure 4.18. Distribution of gas identified from all pinger seismic lines available in Stornoway Bay.

4.3.3 Loch Broom

4.3.3.1 Hotspot analysis

A total of 19 pockmarks were observed within the Loch Broom study area, coinciding with the dense grid of seismic lines. Due to this low number of pockmarks it was not possible to carry out a statistically meaningful hot-spot analysis.

4.3.3.2 Seismic facies

The seismic profiles in Loch Broom do not show as much variety of seismic facies as the other study areas. This is largely due to the presence of acoustic turbidity in the Boomer profiles across the study area obscuring deeper facies. The regions of acoustic turbidity are found to be directly below and/or surrounding pockmarks (Figure 4.19). Based on the seismic facies in the wider region mapped and identified by Stoker *et al.* (2009) it is possible to separate the overlying Summer Isles Formation from the underlying Annat Bay and Assynt Glacigenic Formations (Figure 4.19). Stoker *et al.* (2009) found that gas appears to be associated with sediments within and at the base of the Summer Isles Formation and occasionally obscuring the Annat Bay Formation. This study, based on higher density Boomer data, finds a similar observation.

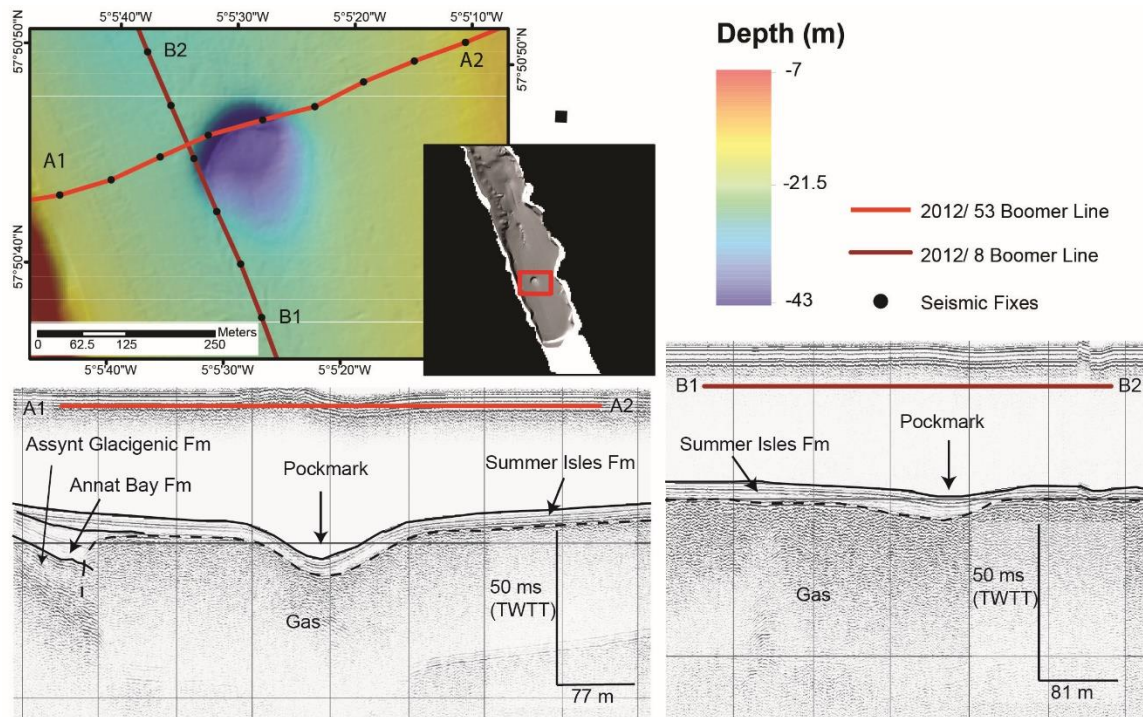


Figure 4.19. Seismic analysis of Boomer seismic lines 2012/53 and 2012/8. Line A shows the boomer seismic profile of line 2012/53. Line B shows the boomer seismic profile of line 2012/8. Inset map shows the area of interest in the inner basin of Loch Broom, the bathymetry and position of seismic lines in relation to the pockmark.

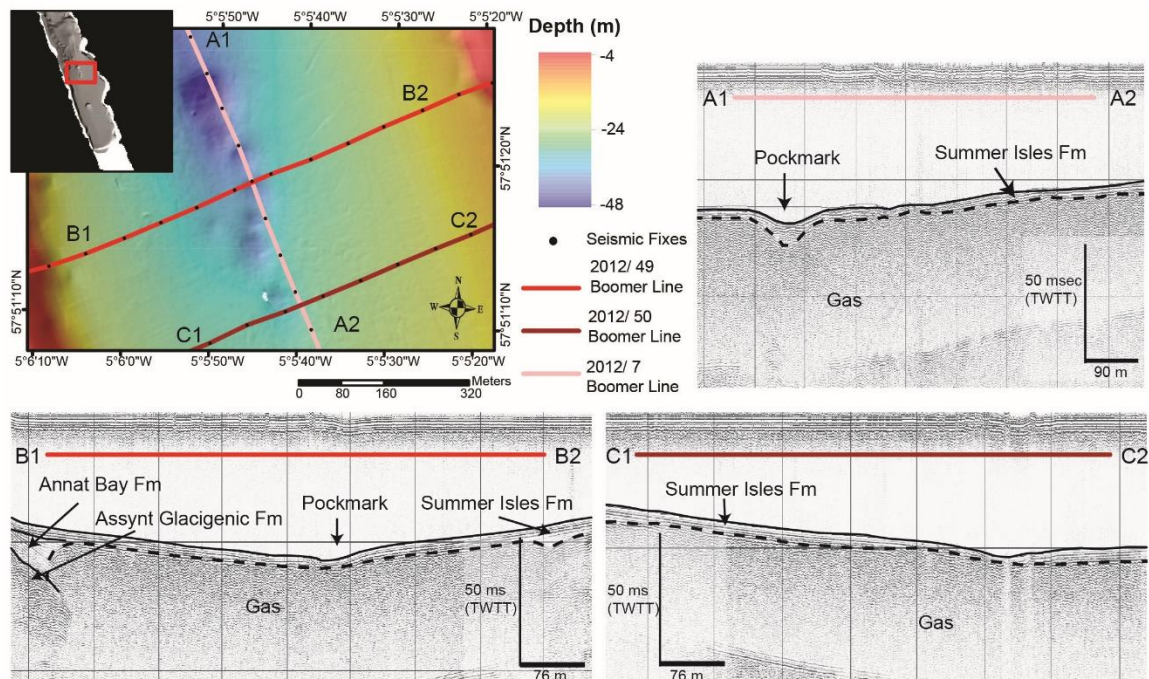


Figure 4.20. Seismic analysis of Boomer seismic lines 2012/49, 2012/50 and 2012/7. Line A shows the Boomer seismic profile of Line 2012/7. Line B shows the boomer seismic profile of line 2012/49. Line C shows the boomer seismic profile of line 2012/50. Inset map shows the region of interest within the inner basin of Loch Broom, the bathymetry and position of seismic lines in relation to pockmarks.

Further evidence of acoustic turbidity is observed around a string of pockmarks in Loch Broom (Figure 4.20). Here there is very little acoustic structure visible due to the presence of gas rich sediments causing acoustic turbidity. In this location gas can be observed close to seabed within or at the base of the Summer Isles Formation and is widely distributed across the Boomer Line.

4.3.3.3 Gas distribution

A total of 19 pockmarks were observed within inner Loch Broom (Figure 4.21). The interpolated raster of the depth to gas front shows that across most of the region has gas very close to seabed, between 3-6 msec (TWTT). The deepest depth to the gas front was recorded as 9 msec. Eight pockmarks were found in regions where no gas was observed in seismic (boomer) data.

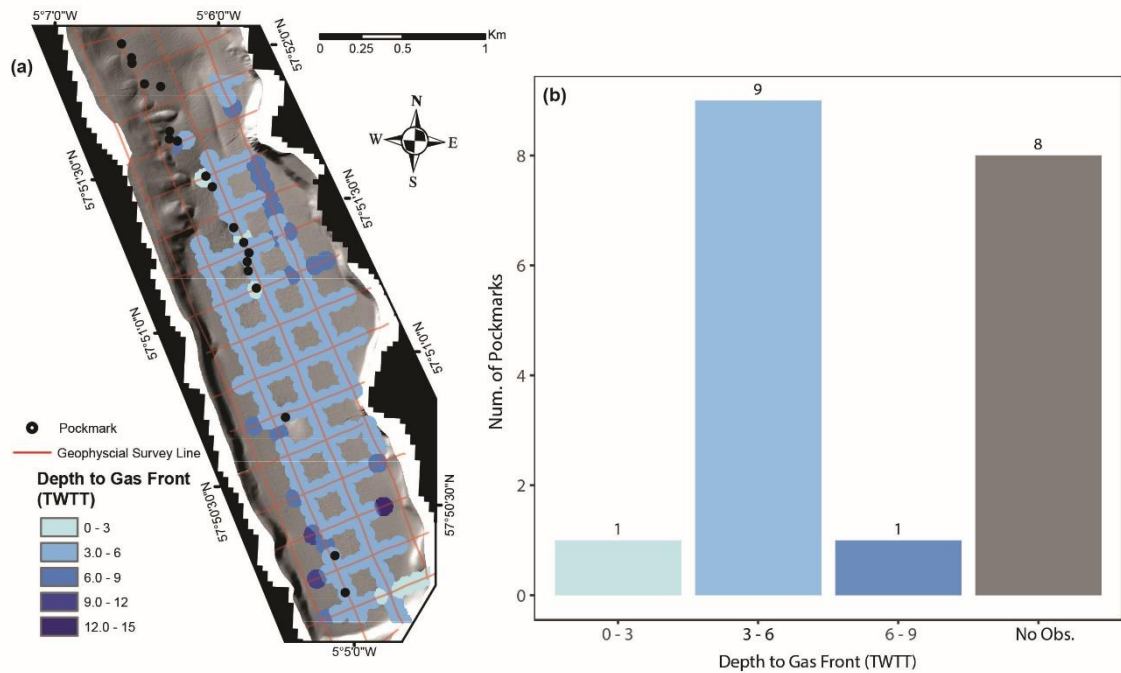


Figure 4.21. Depth to gas front analysis of the Inner Loch Broom study region; (a) Depth to the gas front (TWTT in msec) where gas was observed in seismic profiles; (b) Bar-plot showing the number of pockmarks found in each depth band to the gas front.

4.3.4 Inner Sea of Hebrides and Arisaig Bay

4.3.4.1 Hotspot analysis

Hot-spot analysis was conducted over three scales (Figure 4.22) to identify regions where statistically more pockmarks have formed in the study region and to highlight regions that require further investigation. The first analysis targeted all pockmarks within the ISH study region. The analysis calculated an average nearest-neighbour distance of 384.8 m, which was used as the analysis neighbourhood with half this distance (192.4 m) used as the cell size. Due to the large size of the region including those large areas where pockmarks are absent, the majority of pockmarks have been identified as a hot-spot at this scale of analysis. Because of this it was necessary to conduct a second analysis within discrete areas of interest. This includes the region East of Eigg (Figure 4.22B) and the region of Arisaig Bay (Figure 4.22C). Within these regions a nearest neighbour distance of 398 and 368 m were calculated respectively; the cell size was set as half this distance for each analysis. At this scale, it was possible to detect discrete pockmark hot-spots. The region East of Eigg showed only 5 cells with a hot-spot at the 99% confidence interval. By contrast many more cells were observed as hot-spots in Arisaig Bay.

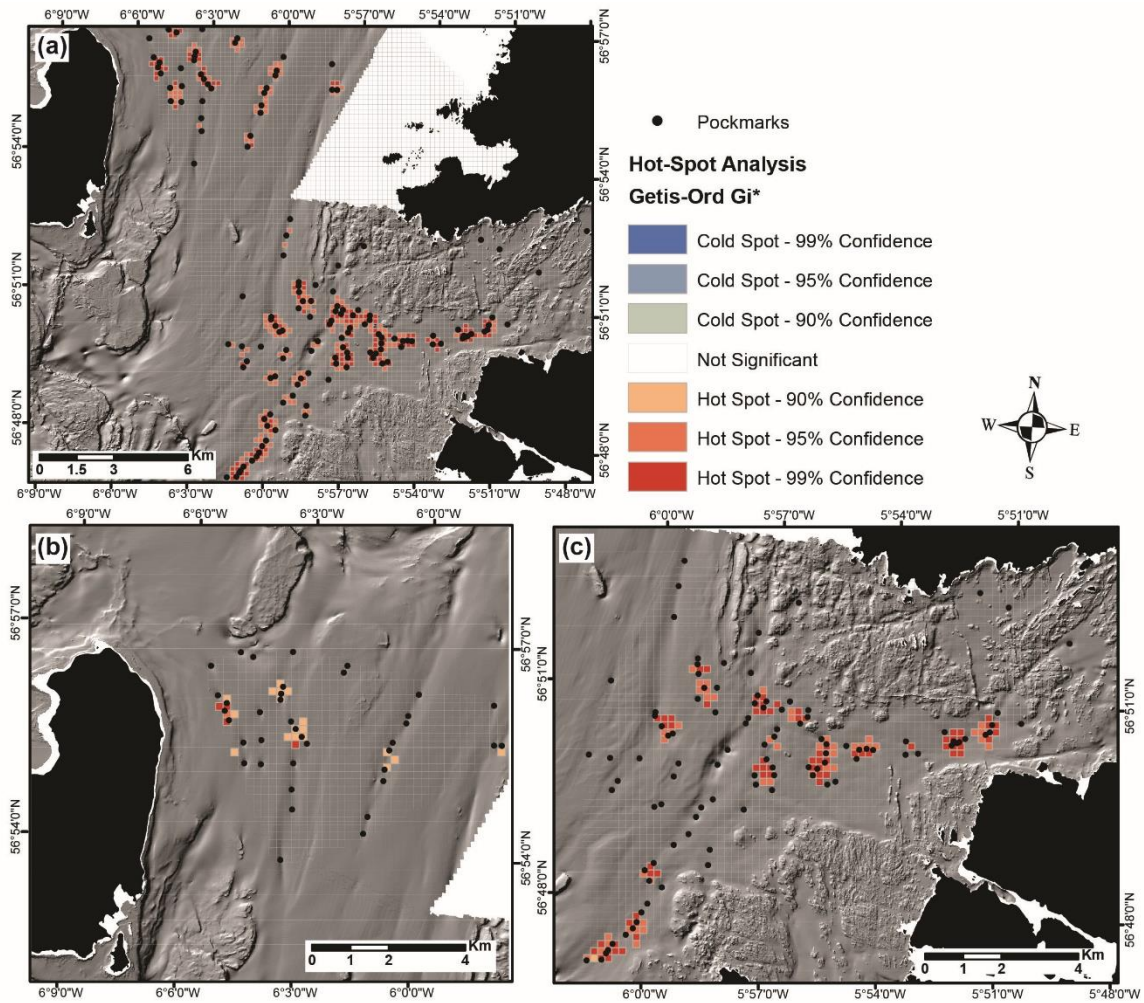


Figure 4.22 Hot-spot analysis using the Getis-ord G_i^* statistic of pockmarks within the Inner Seab of Hebrides and Arisaig Bay. (a) Hot-spot analysis for all pockmarks within the Inner Sea of Hebrides. (b) Hot-spot analysis of pockmarks East of Eigg. (c) Hot-spot analysis of pockmarks in Arisaig Bay only.

4.3.4.2 Seismic facies

From a transit sonar survey conducted in 1971 it is possible to observe several pockmarks on the seabed East of Eigg (Figure 4.23). This demonstrates that these pockmarks formed before 1971.

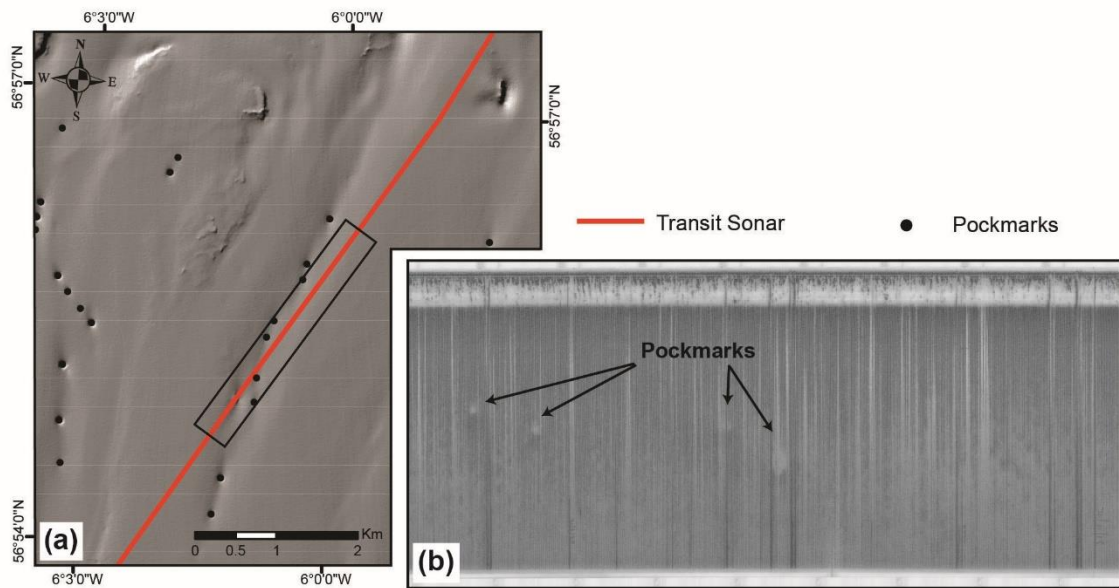


Figure 4.23. Position of a transit sonar survey from 1971 within the Inner Sea of Hebrides. Transit sonar profile shows pockmarks present on the seabed. Map shows the position of the transit sonar survey line, the region of interest shown in the sonar profile and the distribution of mapped pockmarks from high-resolution bathymetry data.

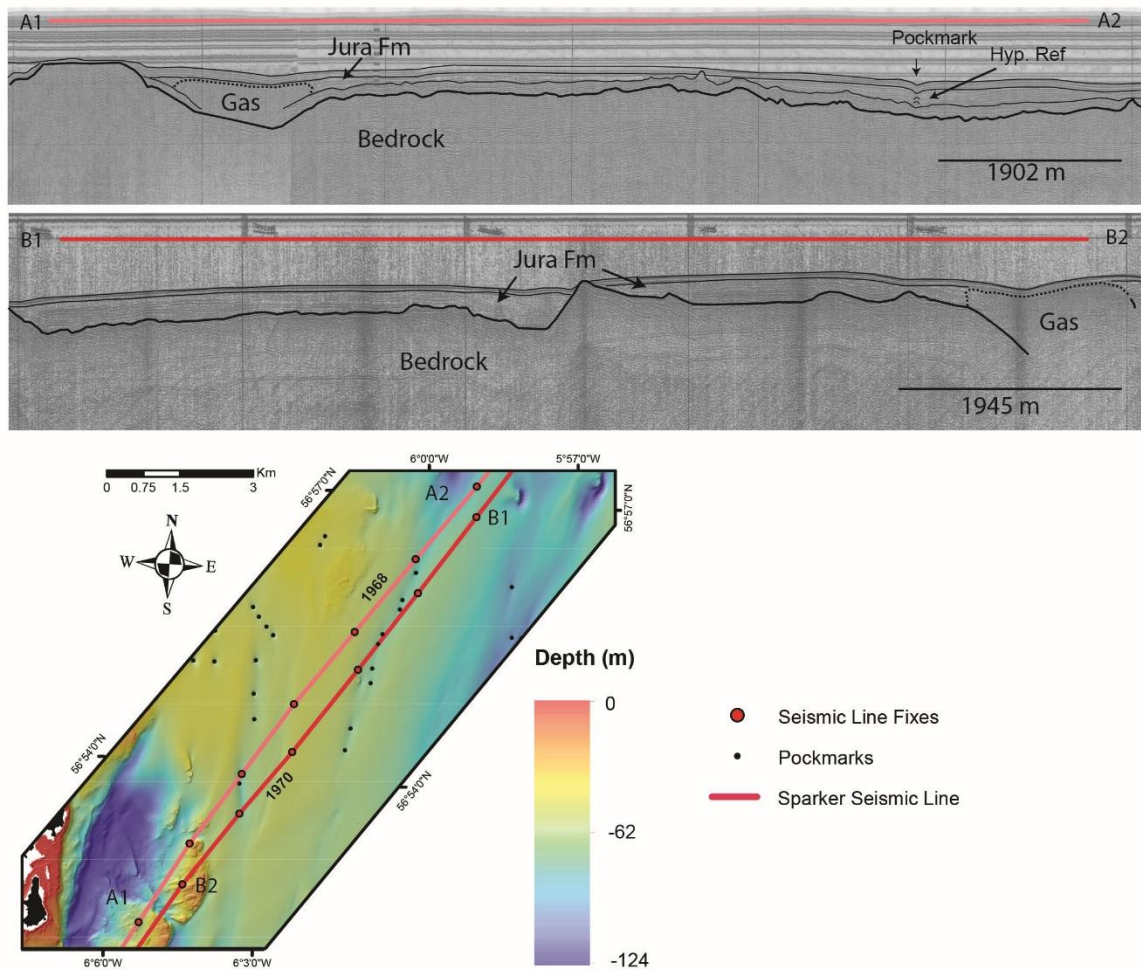


Figure 4.24. Seismic Analysis of sparker seismic lines 1968/27+ (A) and 1970/M29 (B).

The oldest seismic survey line from this region date from 1968 using a sparker system (Figure 4.24, Line A). It shows that gas accumulations, characterised by an acoustically chaotic expression are associated with the Jura Formation mapped by other (Howe *et al.* 2012). Pockmarks are also present in this line 1968/27+, with evidence of hyperbolic reflectors immediately below. The gas present within this is associated with bedrock basins where the Quaternary sediment thickness is greatest. This line shows that gas and pockmarks have been present since before 1968.

Another survey conducted in 1970 shows further evidence of gas (Figure 4.24, Line B). Again, this gas occurs in a region with greater sediment thickness; likely associated with the Jura Formation, no pockmarks are observed on this line.

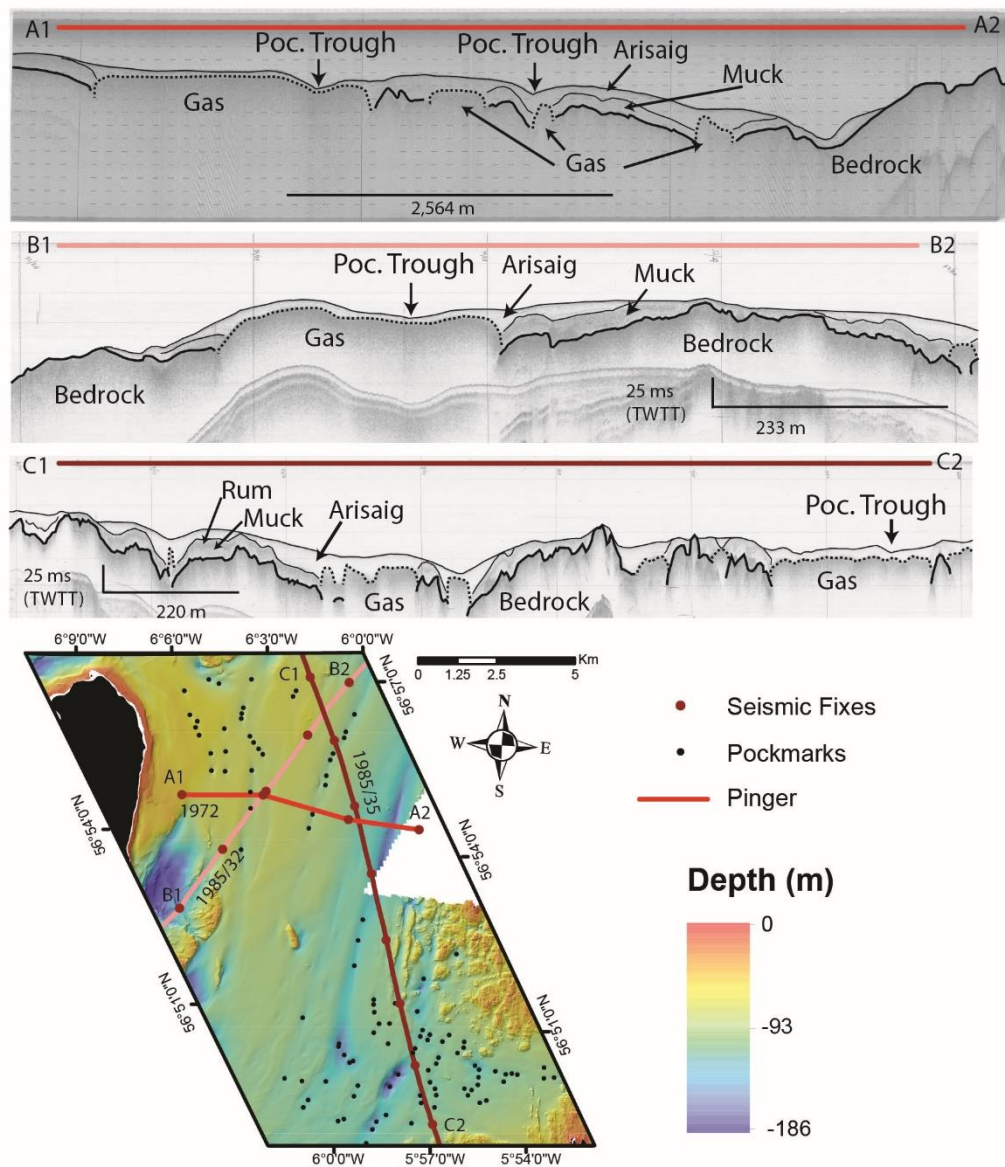


Figure 4.25. Seismic analysis of geophysical surveys using a pinger seismic system. Map shows the position of geophysical survey lines, and distribution of pockmarks. Line A shows the pinger profile from Line 1972/12. Line B shows the pinger profile from Line 1985/32. Line C shows the pinger profile from Line 1985/35. The members of the Jura Formation are also labelled; Muck, Rum and Arisaig Members of the Jura Formation.

Pinger system surveys were also carried out by BGS in 1972 and 1985 (Figure 4.25). As with other pinger surveys the chaotic effect of gas is easily observed. Gas-related acoustic turbidity completely obscures any internal reflectors or deeper acoustic facies. In these survey lines gas can either be observed as widely distributed gas blankets or as isolated curtains in regions where sediment thickness increases. It is possible to separate the Jura Formation into its separate stratigraphic members (Howe *et al.* 2012) on the basis of acoustic character; these include the Arisaig, Muck and Rum Members. It is unclear which

acoustic strata the gas is most likely associated with, but it clearly occurs within the Late Devonian Jura Formation.

4.3.4.3 Gas distribution

Due to the sparse coverage of seismic lines and the lack of metadata within several of these lines it was not possible to create an interpolated raster showing depth to gas front in this region. However, it is possible to create a simple 2D map that shows the general presence of gas within this study area (Figure 4.26). This map shows that the distribution of gas can either be spatially extensive or more localised and discrete regions. Interestingly, the spatial association between sub-seabed gas and pockmarks is not always clear in the Inner Sea of Hebrides.

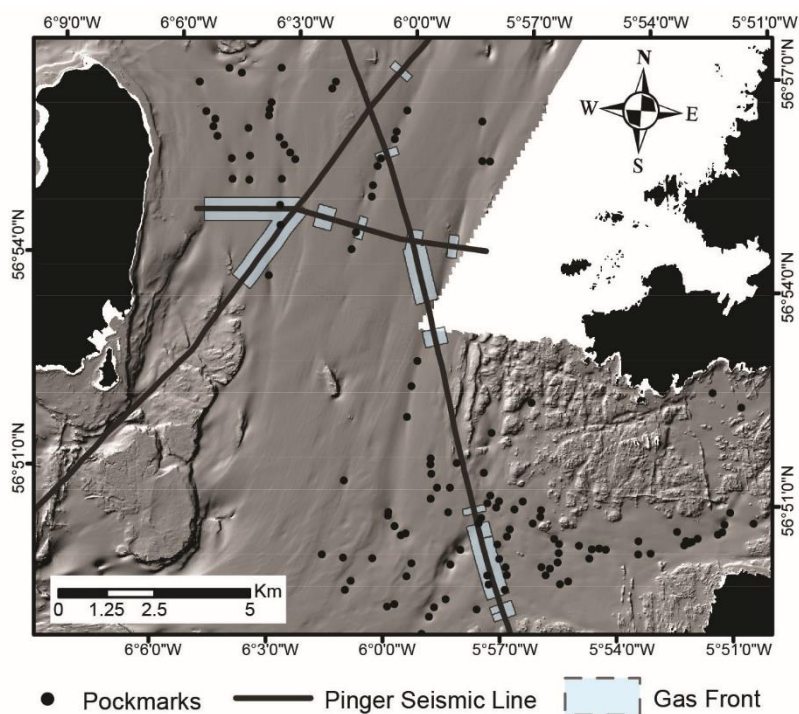


Figure 4.26 Distribution of gas identified from pinger seismic lines in the Inner Sea of Hebrides and Arisaig Bay.

4.4 Discussion

4.4.1 Hot-spot analysis and gas distribution in the study areas

Quantitative hot-spot analysis has been used to investigate whether pockmark hot-spots in Scottish fjords relate to the distribution of sub-seabed gas seen in geophysical data since 1968. An important finding is that a hot-spot analysis based on the principle of an exclusion zone (Moss *et al.* 2012b) can be used to identify regions where organic carbon

required for significant sub-seabed gas formation has been deposited. As a result, it has been found within the results of this PhD project that pockmark hot-spots can be used to identify regions which currently have contained large volumes of stored organic carbon.

In Loch Linnhe it was found that hot-spots were consistently identified at all scales of analysis within the KB, LB and SB sub-basins (Figure 4.7). In these three regions there is widespread evidence of sub-seabed gas, with a gas front between 3.7–30 msec deep (TWTT) which is approximately 2.8 m – 30 m below seabed based on a sound speed of 1500 msec for weak, unconsolidated sediment. By applying the exclusion zone principle (Moss *et al.* 2012b), a suitable model for identifying regional gas-rich sediment through pockmark hot-spot identification can be developed (Figure 4.27). We note that pockmark hot-spots are absent from much of the LB and BB sub-basins of Loch Linnhe. This is likely due to the thinner accumulations of glaciomarine sediments here containing less organic material necessary for the formation of biogenic gas and the generation of pockmarks. The thinning of LLSF4 observed within these regions (McIntyre 2012) is interpreted as areas of non-deposition resulting from stronger bottom currents typical in narrower bathymetric settings.

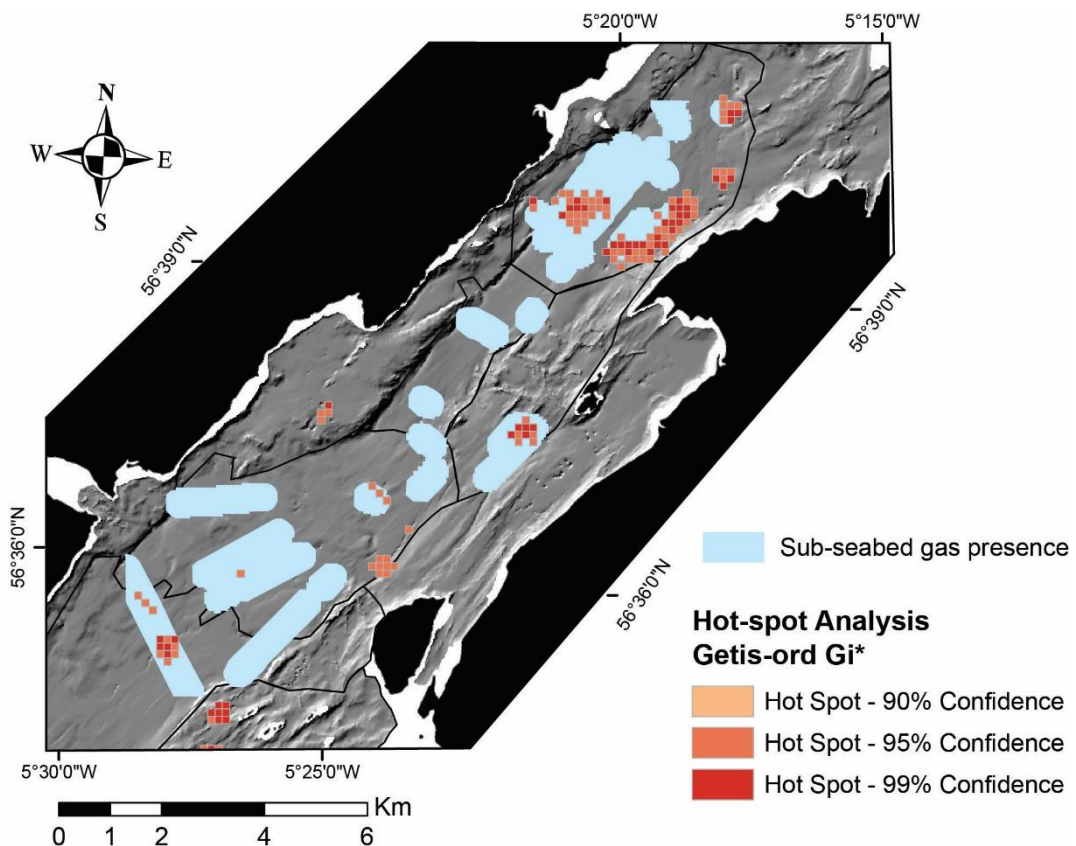


Figure 4.27. Presence of sub-seabed gas identified from zones of acoustic turbidity alongside areas of pockmark hot-spots in Loch Linnhe.

Interpolating a 2D grid (raster) in this way, based on the presence of gas within seismic records is a useful method for not only mapping the distribution of gas within a region but also for identifying its depth range and its spatial association with pockmarks. Sub-seabed gas was mapped throughout the Loch Linnhe study area: either widespread in KB, northwest LB and B.Bnk, or as isolated pockets, such as in BB (Figure 4.12). The depth range to the gas front recorded beneath most pockmark centres is between 3.7–20 msec, equivalent to 2.8 m – 20 m (Figure 4.12b). The analysis of geophysical datasets supports the conclusion that gas-rich sediments, represented in seismic records as LLSF2b, were deposited at the same time as LLSF4, based on the depths of the gas fronts (McIntyre 2012) and surrounding facies. It is therefore likely that the sediments of LLSF2b are similar in origin as LLSF4, however they may contain less organic carbon. Facies LLSF4 is interpreted as distal glaciomarine sediment laid down during ice wastage at the end of the last (Late Weichselian) ice-sheet glaciation or during the Younger Dryas (McIntyre 2012).

Within Loch Linnhe, total carbon content has been estimated at 92.28 Mt (Smeaton *et al.* 2020), but with very low C/N ratios recorded in the uppermost 4 m of sediment (McIntyre 2012). This is likely attributed to relatively high inorganic carbon content resulting in poor preservation of organic carbon (Henrichs & Reeburgh 1987; Ingall & Cappellen 1990). Similar gas-charged sediments of biogenic origin have also been found within the glaciomarine Emerald Silt Formation on the Canadian Atlantic continental shelf (Fader 1991). In that setting, however, the authors argue that thermogenic sources of gas must be present, as they deem it unlikely that the sediment package contained enough organic matter to form a sufficient volume of gas for pockmark formation. Owing to the predominantly metamorphic Precambrian bedrock, a thermogenic source of gas is unlikely in Loch Linnhe. Contrary to the findings on the Canadian Atlantic shelf, distal glaciomarine sediments within fjordic environments off Svalbard can contain enough organic carbon to generate relatively large shallow sub-seabed gas accumulations (Howe *et al.* 2003).

In Stornoway Bay pockmark hot-spots occur primarily in the centre of the main basin of Stornoway Bay (Figure 4.13). Further offshore, in the North Minch proper, they become sparse in number and widely distributed. The cause of this change in distribution likely relates to the thickness of the Quaternary sediment; the greatest sediment accumulation is within the Stornoway Bay as seen in Figure 4.14. As the seismic line progresses eastward, down the slope and into the North Minch, there appears to be a shallowing of the bedrock reflector and a considerably reduced Quaternary sediment thickness. It is interpreted that, overall, the thinner sediment cover within the North Minch probably does not contain enough organic matter to produce sufficient quantities of gas, and form

pockmarks. Instead, gas is observed as isolated curtains (Figure 4.14 & Figure 4.17). This is in stark contrast with Stornoway Bay where large blankets of gas are observed, associated with numerous pockmarks. Hot-spots are also not found along the coastal edges within Stornoway Bay sediment basin. Although seismic lines have not captured this region well, it is possible to observe bedrock highs with limited sediment coverage here (Figure 4.2). It is interpreted that this region does also not contain enough organic matter and/or greater sediment thickness required for the formation of pressurised gas and ultimately lead to pockmark formation. Smeaton *et al.* (2017) calculated carbon content for the innermost basin of Stornoway Bay, known as Cala Steornobhaigh. In this somewhat isolated and hydrodynamically restricted basin 0.27 Mt of organic and 0.34 Mt of inorganic carbon are estimated to be buried (Smeaton *et al.* 2017); of which 17% and 34% is within glacial sediments. Therefore, the majority of this buried carbon is thought to be contained within the overlying post-glacial sediments. It is expected that the total amount of carbon within the Stornoway Bay sediment basin has not been defined until now. The occurrence of numerous pockmark hot-spots also implies a greater volume of buried organic material (carbon) offshore Stornoway than has been previously stated. It is suggested that previous estimates of sedimentary or 'blue' carbon have not included the full areal extent or depth of the Stornoway Bay basin, where the vast majority of carbon is probably stored.

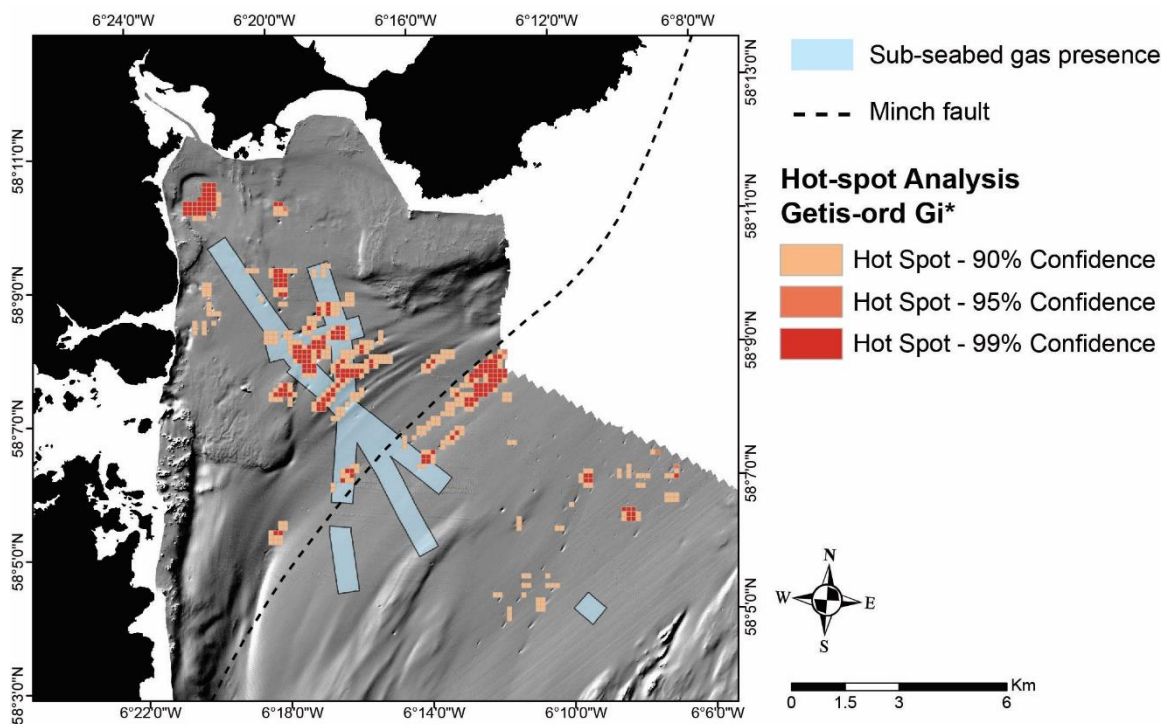


Figure 4.28. Presence of sub-seabed gas identified from zones of acoustic turbidity alongside areas of pockmark hot-spots in Stornoway Bay.

Although an interpolated raster could not be created for Stornoway Bay due to the sparse coverage of seismic lines and the unknown vertical scale (TWTT) it was still possible to create a map showing the general distribution of gas seen in seismic records from BGS surveys conducted between 1968-1985 (Figure 4.18). From this map it is clear that the distribution of gas is similar to the location of pockmark hot-spots. Gas appears widely distributed within the centre of the Stornoway Bay basin, and becomes less so further into the North Minch. Although this could be explained due to the sparse coverage of seismic lines further offshore. From seismic surveys conducted in 1985 the vertical depth scale is known and therefore the depth to the gas front could be calculated. From pinger records where gas can be clearly observed the depth to the gas front ranges between 6.25 msec – 18.75 msec, equivalent to 4.7 m – 18.75 m below seabed. This depth range includes the glaciomarine muds identified in borehole 78/4 (Graham *et al.* 1990). The source of the gas in and around Stornoway Bay is unclear, although a biogenic origin associated with organic-rich glaciomarine muds is the most likely source. However, the presence of Jurassic source rocks and the Minch fault running parallel to the Lewis coastline (Imber *et al.* 2002; Smith 2012) indicates that a thermogenic source and an established migration route are both possible.

Due to the relatively small number of pockmarks ($n = 19$) observed within the inner basin of Loch Broom a hot-spot analysis was not possible. However, it is clear from mapping that pockmarks form towards the west side of the sea loch (or fjord) (Figure 4.4). These pockmarks form in distinct linear strings, but are not as long or deep as those pockmark strings observed within Stornoway Bay. These linear pockmark strings in Loch Broom may elude to a possible geological structure controlling the distribution of pockmarks here; although this cannot be confirmed from the sub-bottom seismic records or from existing geological maps. It is also possible that these strings have formed where the thickness of Quaternary sediments is greatest.

It can be seen (Figure 4.21) that the majority of gas in Loch broom is observed between 3-6 msec (TWTT) depth, this is the equivalent to 2.25 m – 3 m, although gas can also be observed above 2.25 m in a few places. This depth range is also the depth of gas observed directly beneath most pockmarks in Loch Broom. It was found that the majority of pockmarks do not have a gas front observed beneath their centre. This could be due to the pockmarks not being close enough to a seismic line and therefore falls outside the coverage of the interpolated raster. It could also be that no gas actually exists beneath the pockmarked region, as is the case with pockmarks in the outer basin of Loch Broom reported on by Stoker & Bradwell (2009). In this region sediment slumps are observed on the bathymetry data, some of which were mapped by Stoker & Bradwell (2009). It is known

that slumping occurred widely in Loch Broom and Little Loch Broom between 13 ka BP and 14 ka BP (Stoker & Bradwell 2009). It is likely that the most northerly pockmarks in the fjord have formed as a result of sediment slumps and associated degassing / fluid-release.

A carbon inventory was calculated for Loch Broom using the BGS 2012 boomer dataset (Smeaton *et al.* 2017). The carbon content of the entire loch is estimated to be 2.41 Mt organic carbon and 2.69 Mt inorganic carbon; of which 21% and 44% respectively is associated with glacial sediments. Therefore the majority of the carbon in this sea loch is purported to be stored within post-glacial sediment.

In the Inner Sea of Hebrides the hot-spot analysis identified numerous pockmark hot-spots (Figure 4.22). This included an area East of Eigg, where 20 cells were identified as hot-spots above the 90% confidence interval. Pockmarks in this region have also formed in short strings that appear to have been winnowed or modified by currents creating gently sloping seabed troughs. The fact that these pockmarks have formed in strings suggests that there is likely some structural control such as faults or deepened bedrock troughs which have facilitated pockmark formation (Smith 2012). Seismic lines that are available in this region show that these pockmark strings are forming within buried channels where sediment thickness is likely greater (Figure 4.24).

Many hot-spots were identified in the other region of interest, Arisaig Bay (Figure 4.22). Here hot-spots are recorded within the central part of the bay where thicker sediment has preferentially accumulated. Near the coastal fringes where bedrock appears sporadically on the multibeam bathymetry data, pockmarks are absent.

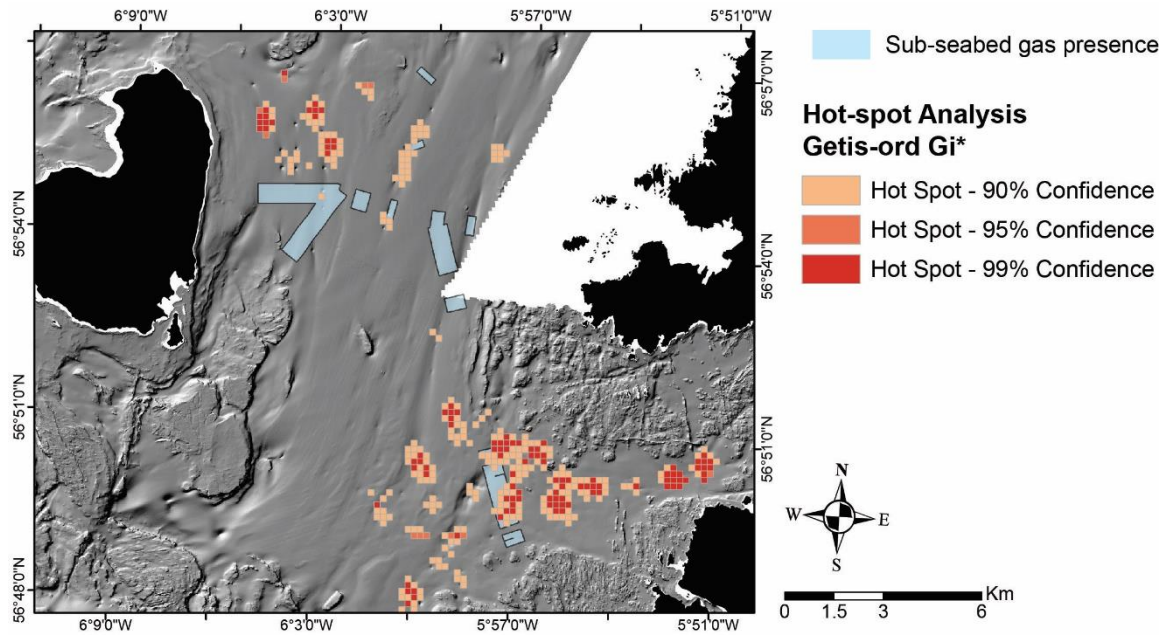


Figure 4.29. Presence of sub-seabed gas identified from zones of acoustic turbidity alongside areas of pockmark hot-spots in the Inner Sea of Hebrides.

Although an interpolated raster showing the depth to the gas front could not be created for the Inner Sea of Hebrides it was possible to create a simple 2D map showing the distribution of sub-seabed gas based on the seismic lines available (Figure 4.26). The map shows that gas is clustered in several small pockets mostly associated with the presence of shallow troughs seen on the bathymetry. Two regions may indicate more extensive regions of gas-rich sediment, one within Arisaig Bay and another in the region just south of the pockmark hot-spots East of Eigg. Due to limited seismic surveys in the region East of Eigg it is not possible to observe gas beneath these pockmark hot-spots, although it is assumed that gas is widespread in this region, possibly associated with the presence of over-deepened channels and basins present within this area (Howe *et al.* 2012; Smith 2012). Here organic-rich sediments accumulated and supported microbial communities that consumed this organic matter and produced gas which led to pockmark formation. A similar interpretation is made for the pockmark hot-spots and gas distribution within Arisaig Bay. Here gas is likely to be more widely distributed across the centre of the bay where sediment thickness is greatest.

With the limited information available from the seismic surveys in the Inner Sea of Hebrides it is possible to observe gas forming approximately 3 m – 15.95 m below seabed and is associated with the Jura Formation (Howe *et al.* 2012). There is no offshore carbon inventory made for this region, however one does exist for Loch Ailort which feeds into Arisaig Bay. In Loch Ailort 0.72 Mt of organic carbon and 0.76 Mt of inorganic carbon is

estimated to be stored in the sub-seabed sediments; of which 17% and 39% is associated with glacial sediments respectively (Smeaton *et al.* 2017). Due to the high number of pockmarks identified here (Audsley *et al.* 2019), and the greater areal extent of the Quaternary sediment basins of Arisaig bay and East of Eigg (extending 5 – 10 km from the mainland coast). It is expected that considerable volumes of stored carbon exist within these regions than has been previously suggested.

The distribution of pockmarks in Arisaig Bay suggest that there is probably some underlying structural control on pockmark formation. Smith (2012) mapped the presence of a conspicuous fault line extending from the Moine Thrust within the region. It is also suggested that Jurassic source rocks are present in this region which might lead to some of the gas in this region having a thermogenic origin (Hesselbo & Coe 2000; Smith 2012). The presence of a major fault in this region may be considered as a structural weakness allowing pockmarks to form, possibly associated with periods of tectonic activity. This relationship is unconfirmed but is presented here as another possible interpretation for the formation and distribution of pockmarks in the Arisaig Bay region.

This study suggests that relatively distal glaciomarine material within fjordic and extra-fjordic settings contains enough organic material to promote the build-up of shallow biogenic gas accumulation (<100 msec deep) (Shmatkova *et al.* 2015). Despite being deposited during deglaciation, these muddy sediments must contain enough organic matter to support microbial communities and produce considerable volumes of gas. Deposition of organic matter in contemporary nearshore glacial settings has been found within the fjords of western Svalbard (Holding *et al.* 2017) where gas-charged sediment is observed resulting from organic matter associated with marine productivity distal to the tidewater glacier margin. Further examples of biogenic gas accumulations within Late Pleistocene (Weichselian) glaciomarine muds are found in the North Sea Basin (Judd *et al.* 1997) and in one or two small nearshore basins of northwest Scotland (Stoker & Bradwell 2009; Stoker *et al.* 2009; Bradwell *et al.* 2021). From these findings, we suggest that biogenic gas can form in nearshore sedimentary basins where sediments containing organic matter were deposited rapidly during the warming events at the end of the last (Weichselian) ice-sheet glaciation and/or at the Younger Dryas/Holocene transition. Rapid sediment accumulation in these time intervals has been reported in Loch Etive, West Scotland (Nørgaard-pedersen *et al.* 2006) and in Loch Broom, Northwest Scotland, where there is similar geophysical evidence of shallow (biogenic) gas below the seabed (Stoker *et al.* 2006). Rapid sedimentation is also reported in numerous presently glaciated high-latitude fjords, such as Kongsfjorden, Svalbard with sedimentation rates as high as 10 cm a⁻¹ (Svendsen *et al.* 2002; Howe *et al.* 2010; McIntyre & Howe 2010).

Organic material would have preferentially accumulated in regions where hydrodynamic flow was restricted by bathymetric obstacles, such as moraines or bedrock highs, or in larger deeper-water basins with weak bottom currents (McIntyre 2012). By identifying pockmark hot-spots and investigating the extent of sediments containing gas it is possible to recognise regions where the complex interactions between hydrodynamics and seabed topography in Loch Linnhe has resulted in the patchwork of gas pockets now present within SB and BB and the more widespread gas accumulations in KB and northwest LB sub-basins – the latter perhaps representing local depocenters for organic material in areas of little or no bottom current. A similar interpretation is made for ISH where organic matter has accumulated around moraines and bedrock highs along with buried sub-seabed channels present in region East of Eigg. An important finding of this study is that within Stornoway Bay, specifically closer to shore where a deeper sedimentary basin is found, and in regions of the Inner Sea of Hebrides where deepened channels and basins are present, sub-seabed gas has been found to be much more widespread. These regions represent much larger depocenters unrestricted by bathymetric obstacles. The deep basin present in Stornoway Bay, possibly associated with the presence of the Minch fault, and the deepened basins of the ISH formed by glacial erosion, can therefore accommodate much larger masses of sedimentary carbon, which have not been accounted for in national carbon inventories.

This study proposes that these regions contain significant quantities of stored 'blue' carbon, much greater than the smaller sea-lochs or fjords which have been reported on (Table 4.2). It is likely that other organic carbon depocentres exist in regions previously not considered due to their distance from shore. This research suggests that significant quantities of stored carbon are present in nearshore / inshore regions around western Scotland. These regions have all experienced intense glaciation and thus contain deep basins or channels which have been subsequently infilled by sedimentation, particularly where these basins are protected from ocean currents by headlands or islands. Norton Sound, Alaska (Park *et al.* 1979; Naidu *et al.* 1993) and Belfast Bay, Maine (Kelley *et al.* 1994; Andrews *et al.* 2010) where large numbers of pockmarks have formed outside local fjords might be other such regions which contain significant quantities of stored carbon and have yet to be included in carbon inventories.

4.4.2 Gas migration and pockmark activity

Loch Linnhe and Loch Broom have the best coverage of seismic lines, however Loch Linnhe has a more complex bathymetry which results in a variety of seismic facies not seen within Loch Broom. For this reason, Loch Linnhe has been chosen as the case study

to interpret the seismic characteristics that can aid the interpretation of gas migration and pockmark formation and/or activity status. It is hoped that the methods proposed here, and their interpretation can be applied to any seabed region where gas is present and could provide a guide to the interpretation of gas migration and assessment of pockmark activity status. The following discussion is based on the specific geophysical characteristics in Loch Linnhe; however these could also be applied to any region with similar facies and references will be made to other study regions where an in-depth analysis is not possible due to the quality and/or type of the geophysical records.

The L1 reflector has been identified on seismic data throughout the Loch Linnhe and is thought to represent the onset of a full interglacial environment in the fjord (McIntyre 2012). Through LLSF4, the environment changes from distal glaciomarine to Early Holocene paraglacial conditions before its transition into full interglacial (Holocene) marine conditions (represented by LLSF5). LLSF5 represents Holocene sedimentation where vegetation has stabilised much of the surrounding terrestrial topography, resembling the present-day landscape. A similar reflector termed E1 was identified in the adjacent fjord of Loch Etive where radiocarbon-dated shells yielded an age of 10,240 +/- 82 ¹⁴C yr BP (Howe *et al.* 2002). Shells from the L1 reflector in Loch Linnhe provide radiocarbon dates of 10,313 +/- 100 and 8347 +/- 73 ¹⁴C yr BP (McIntyre 2012). These data strongly suggest that the transition from late glacial (cold) to interglacial (warm) marine conditions occurred at a broadly similar time across western Scotland ca. 10.5–11.5 cal ky BP.

The results presented in this PhD project show that this Holocene sediment package (LLSF5) is of approximately uniform thickness across Loch Linnhe, even in the majority of pockmarks. This is interpreted to reflect a generally constant, spatially uniform sedimentation rate across the seafloor during the Holocene. Since LLSF5, including the L1 reflector, is present within the majority of pockmarks, it is likely that the majority of Loch Linnhe's pockmarks formed prior to 10.3 cal ky BP and have, at most, only been periodically venting low volumes of gas with insufficient fluid flow to remove or inhibit sedimentation. This is supported by the results on the morphology of pockmarks in the region (Audsley *et al.* 2019), where 51% of pockmarks are classed as 'regular' due to their shallow profile and low depth: area ratio. This class of pockmarks is common in the waters around western Scotland. 'Regular' pockmarks are suggested as being less active than 'deep' pockmarks (Audsley *et al.* 2019). The only pockmark imaged in seismic records where the L1 reflector is not observed is pockmark 2 (Figure 4.9, Line A). Due to the absence of the L1 reflector and the thin cover of LLSF5, we interpret this as the most recently active pockmark within Loch Linnhe. However, the strongly V-shaped depth profile of the pockmark and presence of the L1 reflector in the flanks of the pockmark

suggest that it started forming prior to ~10.3 ky BP and has been regularly active throughout the Holocene. This interpretation is supported by semi-automated classification of pockmarks in this region (Audsley *et al.* 2019). This unusual pockmark was classed as 'deep' by Audsley *et al.* (2019) who interpreted it as one of a number of pockmarks with a longer activity time or possibly more energetic gas/fluid venting. Interestingly, we find little seismic evidence of gas directly below this pockmark. LLSF2 is seen below pockmark 2 (Figure 4.9), as separate narrow vertical zones in the surrounding facies and connecting with the base of the pockmark. However, in this location, this facies does not have the typical acoustic character commonly associated with gas.

Pockmarks can also form through venting of fluids without gas present. Pockmarks forming from non-gas-related fluid discharge have been observed in MacBeth fiord, Baffin Island (Syvitski 1997) and Isfjorden, Svalbard (Roy *et al.* 2015). This phenomenon has been described to occur either in ice-proximal settings, where buried ice can be present in regions of very rapid sediment accumulation or where groundwater is driven under glaciomarine sediments by the hydrostatic pressure of surrounding topography (Syvitski 1997). From this evidence, we conclude that this deep pockmark formed prior to ~10.3 ky BP and has been regularly active throughout the Holocene, although the genesis of this pockmark may be related to fluid discharge and not the expulsion of biogenic gas.

V-shaped pull-down reflectors are observed on seismic records across much of Loch Linnhe, closely related to sub-seabed gas accumulations and/or pockmarks (Figure 4.9 – Figure 4.11). These V-shaped reflectors are generally found in LLSF3 and terminate near the lower boundary of LLSF4 but can also be found directly below pockmarks. Where pull-down reflectors are seen within LLSF3, they were previously interpreted (McIntyre 2012) as examples of faults associated with isostatic rebound or examples of relict fluid-escape pockmarks below the present-day seabed, as seen elsewhere (Syvitski 1997). Where pull-down reflectors are recorded directly below pockmarks in Loch Linnhe, these were interpreted as acoustic artefacts resulting from the attenuation of sound waves due to gas or as the morphology of the former seabed. In the case of pockmark 6 (Figure 4.11, Line A), we find that the reflectors change from steep sided V-shaped to more rounded U-shaped reflectors close to seabed. We conclude that this particular pockmark is probably inactive and that pull-down reflectors here probably represent the palaeo-seabed at depth.

Throughout the Loch Linnhe study area, several examples of gas migration are observed. According to Taylor (1992), these can be either acoustic blankets, curtains (100–500 m wide) or plumes (<50 m wide). It has been suggested (Judd & Hovland 2007) that terms other than acoustic blanket and plume are unnecessary and do not add to the

interpretation of gas migration within marine sediments. It is argued here that additional descriptive terms are useful, as they form a possible continuum of stages potentially showing the progression of gas migration. Where gas blankets are observed (Figure 4.8, Line C), the gas front is uniform and near seabed, even when a pockmark is present; this is thought to represent a region where gas pressure is controlled by the diffusion of gas into the Sulphate Methane Transition Zone (SMTZ), where it is consumed by microbial communities (Albert *et al.* 1998). Within this zone, methane is consumed, which effectively lowers the pressure of the gas-rich fluids stored below. This finding is supported by the diffusive boundary at the gas front below 3.7 msec (Figure 4.8, Line C). At this site, the pockmark is no longer the primary gas-venting site, and the presence of LLSF5 overlying the pockmark indicates that it is no longer active. This pockmark probably formed prior to the widespread migration of gas and provided the only vent in the region to lower the pressure of shallow gas. The present-day distribution of gas blankets at this site is interpreted to have been caused by the vertical migration of gas and the formation of *in situ* gas from microbial communities within younger organic-rich sediments.

Gas curtains are also seen in the seismic data from Loch Linnhe (Figure 4.8, Line B). These curtains (100–500 m wide) are seen at the flanks of pockmarks and can be related to deeper gas blankets (Figure 4.8, Line B). Between these gas curtains are regions where the acoustic signal is not interrupted by gas, these regions are termed ‘acoustic windows’ and provide an insight into the sediment facies otherwise obscured by gas blanking. From this analysis, it is inferred that sub-seabed gas is strongly associated with LLSF4 in Loch Linnhe, consistent with the depth of the gas front (Figure 4.12) and the relative thicknesses of acoustic facies (Table 4.3). It has been shown that gas concentrations in sediment within gas curtains and blankets are significantly higher than within acoustic windows (Jones *et al.* 1986), explaining the acoustic turbidity or blanking effect seen in geophysical profiles. It is also suggested that gas curtains form above the deepest parts of basins where sediment thickness is greatest (Taylor 1992; Baltzer *et al.* 2005). This study suggest that curtains and plumes can form by gas migrating at the flanks of pockmarks. Here, internal weaknesses in the sediment resulting from previous (now inactive) pockmark formation reach close to the seabed allowing the gas to be consumed within the SMTZ. Over time, gas migration and continued *in situ* gas formation, within shallow sediments containing organic carbon, can spread laterally forming a gas blanket. This study suggests that gas curtains probably contain gas at low pressures, particularly if this gas is close to seabed. However, gas plumes should be given special consideration as studies have shown that when a gas plumes is halfway between the seabed and its source, the chance of an intermittent pockmark formation is high (Cathles *et al.* 2010),

especially so in the absence of structural weaknesses or nearby pockmarks. The migration of gas and further gas formation by microbial activity can lead to sufficient pressures to form a new pockmark at seabed. It is possible that pockmarks located where gas is observed within the near-surface sediment are still periodically active (Audsley *et al.* 2019). In these settings, gases such as methane are released into the water column to re-join the marine carbon cycle. The age and activity status of pockmarks in west coast Scottish waters is still unknown, but due to the depth and form of many pockmarks in Loch Linnhe, it is likely that they have experienced a long activity history (Audsley *et al.* 2019). Due to these uncertainties, it is not currently possible to calculate the volumes of 'stored' carbon released into the marine column in Scottish waters. However this should be a key question for future research.

The variation in gas-associated seismic facies present within Loch Linnhe, along with acoustic windows has allowed for the interpretation of sedimentary units that are otherwise obscured by gas. This analysis has made it possible to build a broad interpretation of gas migration pathways and possible pockmark activity status in Loch Linnhe since deglaciation. Using Loch Linnhe as a case study it may be possible to apply these interpretations of gas-rich facies to other pockmarked seabed area where detailed geophysical information is absent.

In Loch Broom the analysis shows that much of the gas is between 2.25 – 6 m (Figure 4.21) and is the shallowest gas observed across any of the study regions in this research project. The sedimentary units associated with this gas includes the Summer Isles Formation which has largely been deposited since 8012 +/- 53 ¹⁴C years BP during the Holocene (Stoker *et al.* 2009) and the Annat Bay Formation. The lithofacies of the Summer Isles Formation are described as homogenous very soft silty clay with sporadic shells, and with a smell of gas; it is mainly found to be ≤ 5 m thick but can be found locally to be up to 12 m thick. The Annat Bay Formation lithofacies is described as homogenous soft silty clay with sporadic shells, 10-25 m thick and was likely deposited between 13 ka BP when the Summer Isles became ice free, and 8012 +/- 53 ¹⁴C years BP when the Summer Isle Formation began to be deposited. Stoker *et al* (2009) also noted the presence of gas associated acoustic turbidity which occasionally obscured Annat Bay Formation. It is noted that the Annat Bay Formation has not been previously observed in the inner basin of Loch Broom, however it has been observed in the deep inner basin of the neighbouring Little Loch Broom. Due to the presence of gas associated acoustic turbidity present throughout much of the inner basin of Loch Broom, which appears within and at the base of the Summer Isles Formation, it is suggested that gas has formed within the distal-glaciomarine muds of the Annat Bay Formation and migrated into the overlying Summer

Isles Formation. The very shallow nature of gas within Loch Broom, the few pockmarks observed and the variations in erosional and depositional processes suggests that gas within Loch Broom is still actively seeping from the seabed and/or being consumed within the SMTZ, similar to the shallow gas observed in Loch Linnhe. The relatively small number of pockmarks in Loch Broom suggests that focused rather than widespread venting of gas has occurred. Although gas has likely vented from these pockmarks it is interpreted that some may have been originally formed as a result of seabed instabilities triggered during the late glacial to interglacial transition. Collapse, displacement and slumping of the seabed and the associated fluid release formed two major depressions recorded elsewhere in Loch Broom (Stoker & Bradwell 2009) and is interpreted that the pockmarks within inner Loch Broom also formed during this time. The source of the gas in Loch Broom is currently unknown, but a biogenic origin is very likely as the sub-surface Precambrian metamorphic geology is not conducive to a thermogenic origin.

In Stornoway Bay seismic facies SSF4, interpreted as Holocene sediments, can be found throughout the entire area covered by seismic lines and appears as a uniform thickness unit. It is interpreted to represent a steady depositional environment. This SSF4 facies is also present within pockmarks in Stornoway Bay, similar to the majority of pockmarks within Loch Linnhe where the L1 reflector is observed. Although these pockmarks include some classed as “deep” (Audsley *et al.* 2019), particularly those that form strings of pockmarks, it is interpreted that most have been inactive for an extended period of time and fluid escape that does still occur is not enough to remove sediment. Despite pockmark formation in Stornoway Bay, gas is clearly still present within the underlying sediment. Since it is not expected that these pockmarks are regularly active this gas is probably under low pressures and/or widely distributed. This gas is in the form of gas blankets, an additional gas curtain is present further offshore into the North Minch. This gas has likely formed in regions where organic content is greatest; with gas able to migrate vertically and laterally across sedimentary layers until pressure is reduced, gas movement is inhibited, or a pre-existing weakness can be exploited. In this specific location pathways or weaknesses for gas escape may be related to neotectonic structures and/or pre-existing faults.

Due to the limited coverage and low quality of geophysical surveys within Inner Sea of Hebrides it is difficult to determine the overall gas migration patterns that might be occurring across this study region. With the geophysical data that is available it has been possible to determine that pockmarks are forming within sub-seabed channels and linear depocentres where organic matter has probably preferentially accumulated during the deposition of the Late Devonian Jura Formation. It is in these channels that microbial

activity consumed this organic material producing methane gas. Pockmarks have formed as gas accumulates and sub-seabed pressure increases. In Arisaig Bay the distribution of pockmarks is similar to those observed in Loch Linnhe. Here gas has formed within local organic matter depocenters that have been typically confined by bathymetric obstacles such as moraines and bedrock highs.

4.4.3 Geohazard assessment

Finally, it is suggested that the identification of pockmarks and shallow sub-seabed gas within a nearshore region should not always be considered as a hazard, particularly when gas is at shallow depth (<100 m deep) (Shmatkova *et al.* 2015). It is likely that shallow (3.7–20 msec) gas curtains and blankets contain only relatively small volumes of low-pressure gas that can be consumed by microbial activity in the SMTZ— seen as a diffusive upper boundary in boomer profiles. In these situations, pockmark formation will release pressure within sub-seabed sediments and could increase overall substrate stability (Riboulot *et al.* 2019). Pockmarks can sometimes form within local depocenters of sediment containing higher proportions of organic carbon compared to surrounding regions, where much of the sediment can be gas free. However, the presence of gas plumes, which are typically deeper, may pose a potential hazard if migration pathways are unavailable, as this gas will have had little opportunity to reduce in pressure as it migrates vertically. Therefore, to inform industry on potential geohazards in fjordic and nearshore environments, both bathymetric and sub-bottom geo-physical surveys are required to identify (i) fluid-release pockmark hot-spots, (ii) thick muds potentially containing high-quantities of organic carbon and (iii) the depth of shallow sub-seabed gas accumulations. Assessing these factors could be used to gauge whether gas pressures and volumes in Quaternary sediments would be potentially hazardous to seabed infrastructure.

4.5 Conclusions

- Hot-spot analysis based on the principle of a pockmark exclusion zone can be used as a technique to identify depocentres of organic carbon within fjordic and extra-fjordic settings.
- Pockmark hot-spots represent areas where high gas volumes have formed from the decomposition of organic carbon. The pressures in these areas have been high enough to force additional pockmarks to form to reduce the gas pressure.

- The identification of acoustic facies associated with the presence of sub-seabed gas can be a useful indicator for pockmark activity status, potential formation and general gas migration patterns in a region.
- Should sub-seabed gas be identified at shallow depth, (0 – 6 msec TWTT) and be widespread in the form of a gas blanket or curtain, it is likely that pockmarks in the area are no longer active and gas venting is not focused at the pockmark vent site but is instead venting at low volumes at various sites on the seabed or is being actively consumed at the SMTZ.
- Should gas be identified deeper within the sediment, and in the form of a curtain or plume, the gas can be under sufficient pressure to cause imminent pockmark formation. Should a gas plume or curtain be found directly below a pockmark it is likely that the pockmark is regularly venting and can be considered still active.

Chapter 5: How pockmarks affect the physical and chemical properties of marine sediments

5.1 Introduction

Pockmarks represent important gateways for carbon to be reintroduced to the marine environment and re-enter the carbon cycle (Panieri *et al.* 2017). Powerful greenhouse gases such as methane can be vented from pockmarks, however our understanding of the activity status and volume of gas emitted from pockmarks is still poorly quantified (Bange *et al.* 1994; Krämer *et al.* 2017). This chapter explores the changes in the physical and chemical properties of marine sediments associated with pockmark activity, past and present. Further information and introduction to physical and chemical properties of marine sediments are provided in Chapter 1.

Changes in grain size can normally be attributed to variations in sediment provenance and/or sediment transport path and can be used as a proxy for the energy of deposition (e.g. current strength, entrainment velocity) (Folk & Ward 1957; Buccianti *et al.* 2006; Flemming 2007). In the case of gas expulsion, pockmarks fluid/gas venting normally disturbs and removes the finer grain sizes, putting them into suspension in the water column whereby they are transported by currents, leading to an overall increase in mean grain size within the pockmark. An increase in grain size within a pockmark can be used as a proxy for pockmark activity (Ravasopoulos *et al.* 2002).

Organic matter is deposited onto the seafloor through sedimentation from a highly productive overlying water column or through the flux of organic rich sediments from terrestrial sources (Romankevich 1984; Bianchi *et al.* 2018). In fjordic environments of Western Scotland organic matter is deposited in relatively high volumes, especially during the periods of abrupt climate change experienced since deglaciation (ca. 13 – 11 ka BP) (Smeaton *et al.* 2020). When deposited on the seafloor bacterial communities are responsible for the conversion of organic matter into CO₂. Organic matter can also be preserved when buried by subsequent sedimentation, and can be stored, this is sometimes referred to as “blue carbon” (Nellemann *et al.* 2009). Blue carbon has been a subject of interest in Scotland recently as it has been found that fjordic environments contain vast amounts of organic carbon and are now seen as important stores of preserved carbon (Burrows *et al.* 2014; Smeaton *et al.* 2016, 2017, 2020).

When deposited on the seafloor bacterial communities are responsible for the conversion of organic matter into CO₂ or its preservation. The process of remineralizing organic

matter is dependent on the availability of electron acceptors. Initially O₂ is consumed through aerobic decomposition of organic matter. Following the consumption of oxygen nitrates are then utilized, followed by Mn and Fe. Once these are no longer available sulphate reduction then remineralizes organic matter (Martens *et al.* 1998). Deeper within the sediment methanogens consume organic matter producing methane gas. (Martens & Berner 1974). From the results presented in this thesis (Chapter 2) it has been shown that many of these fjordic environments also contain pockmarks (Audsley *et al.* 2019) indicating the release of sub-seabed gas, representing incompletely studied gateways for carbon to re-enter the marine carbon cycle.

Studies have shown the importance of Fe and Mn reduction in marine sediments for biogeochemical processes (Burdige 1993; Lalonde *et al.* 2012; Hyun *et al.* 2017). It has been shown that Mn and Fe can account for up to 45% and 20% respectively of organic matter oxidation in the Uleng basin, China (Hyun *et al.* 2017). This potential of Fe for binding organic matter is confirmed from a variety of depositional settings where it was shown that $21.5 \pm 8.6\%$ of organic matter is bound to Fe (Lalonde *et al.* 2012). Iron and Manganese have been recognised as redox sensitive elements (Froelich *et al.* 1979; Naeher *et al.* 2013), and have been used to monitor palaeo-redox conditions. More recently Fe and Mn have been used to assess the changes in redox brought on by the Deep Water Horizon blow out in the Gulf of Mexico (Hastings *et al.* 2016). Fe and Mn have been chosen as the elemental focus for this study as they directly impact the amount of organic carbon preserved within marine sediments and producing methane gas. It is therefore important to observe and characterise changes within the redox potential of marine sediments affected by pockmarks to improve the understanding of how oxic/suboxic sediments can recover from a methane flux and limit the volume of methane gas being reintroduced to the marine environment.

The aim of this chapter is to identify whether changes in redox sensitive elements and grain size can be indicators of pockmark activity. To achieve this non-destructive and destructive methods were used to quantify changes in the geochemical and physical properties of sediment cores retrieved from inside and outside three pockmarks. The specific objectives of this chapter are to:

- Compare Mn/Fe ratios of marine sediments inside and outside pockmarks as a possible proxy for changes in the redox conditions associated with pockmark activity.
- Discuss the impact of changing in redox conditions and pockmark activity over time.

- Identify changes in sediment grain size, inside and outside pockmarks, as an alternative method of identifying former pockmark activity.

5.2 Materials and methods

The following section details the procedures for core collection, physical and chemical data collection and analysis. All analyses were performed by the author unless otherwise stated, for instance when instrument calibration or operation could only be performed by qualified lab technicians. All data presented here is new and currently unpublished, and has been generated specifically for the purposes of this PhD project.

5.2.1 Core collection

A total of 14 sediment cores were collected in 2019 onboard the Marine Scotland research vessel *MRV. Scotia* during the SA1019S science cruise (

Table 5.1). A seabed gravity corer was supplied by the Scottish Association for Marine Science. The corer consists of a 3 m long barrel, weighted with 1.1 tonne metal plates. The deployment involved lowering the corer towards the seabed at 40m/ min. When the corer was 50 m above seabed, the lowering stopped to allow for the ship to be repositioned and for the corer to stop spinning. The corer was then lowered further at 40 m/ min. Once it penetrated the seabed the corer was left for one minute before retrieving at the same rate as it was lowered. Once safely recovered in deck, the core liner containing the sediment was removed from the core barrel and cut into 1.5 m (or less) sections then capped and sealed with electrical tape. Core sections were labelled using the common naming practice ; cruise code – type of corer and core number – core section code. The core section code consists of a letter, where “A” is the top section (i.e. closest to seabed) and a number which relates to the total number of sections (this was normally 2 sections) e.g. SA1019S – GC027 – A/2; SA1019S – GC027 – B/2 [i.e. both section of core GC027].

Table 5.1. Cores collected during the SA1019S onboard the MRV Scotia. Table also records the analysis conducted for each core.

Core	Section	Location	Length	X-Ray	MSCL-S	MSCL-ICS	MSCL-XYZ	ITRAX	PSA/CN
SA1019S GC006	A	Stornoway	0.77	X	X	X	X	X	
	B	Stornoway	1.44	X	X	X	X		
SA1019 GC008	A	Stornoway	0.68	X	X	X	X	X	
	B	Stornoway	1.5	X	X	X	X		
SA1019S GC011	A	Stornoway	0.66	X					
	B	Stornoway	1.5	X					
SA1019S GC012	A	N. Minch	1.5	X					
SA1019S GC014	A	N. Minch	0.89	X	X	X	X		
	B	N. Minch	1.42	X	X	X	X		
SA1019S GC015	A	N. Minch	0.9	X	X	X	X		
	B	N. Minch	1.43	X	X	X	X		
SA1019S GC018	A	Loch. Eishart	0.89	X	X	X	X		
	B	Loch. Eishart	1.43	X	X	X	X		
SA1019S GC019	A	Loch. Eishart	0.4	X	X	X	X		
	B	Loch. Eishart	1.44	X	X	X	X		
SA1019S GC020	A	Loch Eishart	0.41	X	X	X	X		
	B	Loch Eishart	1.42	X	X	X	X		
SA1019S GC021	A	East Eigg	0.8	X	X	X	X	X	X
	B	East Eigg	1.4	X	X	X	X	X	X
SA1019S GC022	A	East Eigg	0.8		X	X	X		
	B	East Eigg	1.4	X	X	X	X		
SA1019S GC023	A	East Eigg	0.37	X	X	X	X	X	X
	B	East Eigg	1.5	X	X	X	X	X	X
SA1019S GC024	A	Summer Isles	0.9	X					
	B	Summer Isles	1.5	X					
SA1019S GC027	A	N. Sea	0.79	X	X	X	X	X	X
	B	N. Sea	1.45	X	X	X	X	X	X

Key coring sites were chosen from Stornoway Bay and East of Eigg, Western Scotland, and in the Scanner Pockmarks SAC, North Sea (Figure 5.1). These sites were selected on the basis of high density pockmark clusters, location of unusually “deep” pockmarks, identified during the morphological classification in Chapter 2, and also somewhat by time constraints of the cruise. One core was retrieved from inside the pockmark of interest, close to the deepest point; and one core from a nearby area outside the pockmark that is assumed to be unaffected by gas venting (Figure 5.2). Due to the protection status of the Scanner SAC and the limited timeframe on the cruise, only one core was taken from *inside* the Scotia pockmark, North Sea.

During initial hydrographic surveying of the Scotia Pockmark, a 50 m high acoustic flare was observed in the water column, emanating from the pockmark centre (Figure 5.3). On the initial hydroacoustic echosounder survey over the pockmark at 01:11 of 29/7/2019 a 50 m high acoustic flare can be seen emanating from the pockmark depression. A second pass over the pockmark at 01:45 shows the flare has decreased in height, yet still be present after 34 minutes. This acoustic flare is the result of gas and sediment being vented into the water column. Due to the presence of this acoustic flare, a coring site was prioritised for the centre of the Scotia’s southern pockmark within the Scotia pockmark complex.

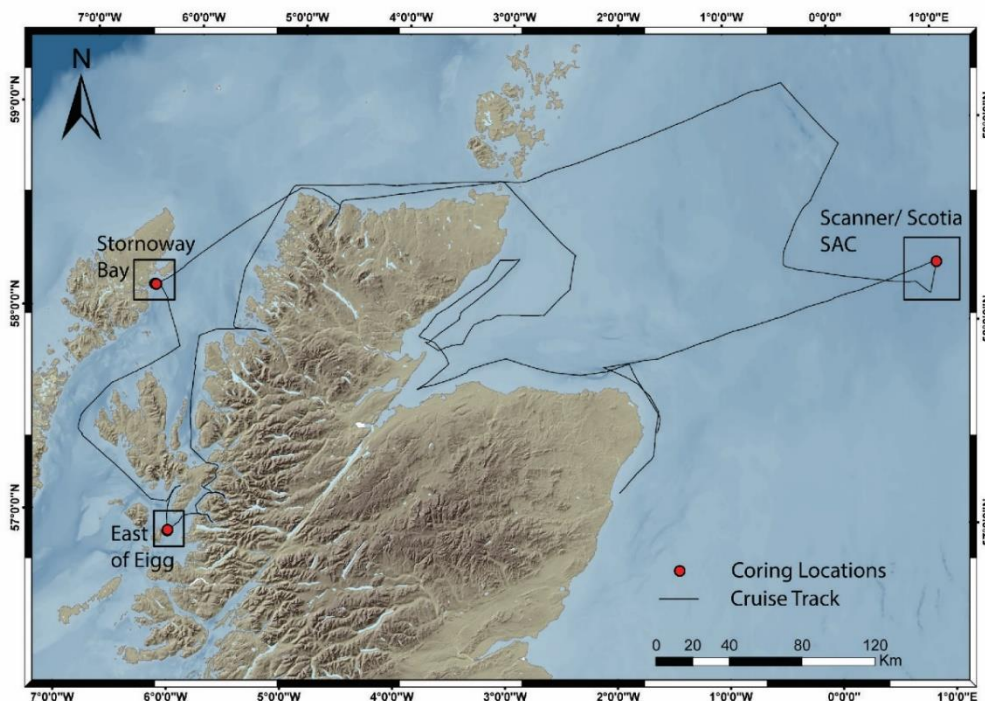


Figure 5.1. Map showing the location of selected cores used in this study and the course taken by the MRV. Scotia on cruise SA1019S.

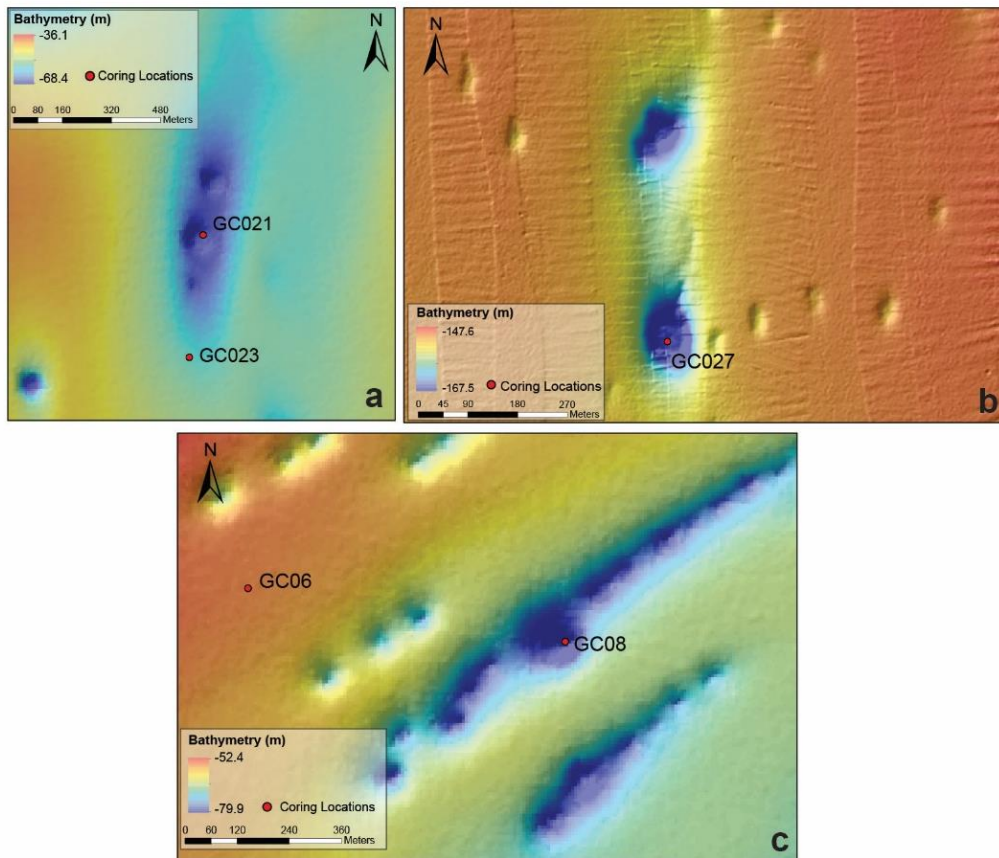


Figure 5.2 Maps showing the coring locations within key pockmarks of (a) East of Eigg, (b) Scotia Pockmark, North Sea, (c) Stornoway Bay.

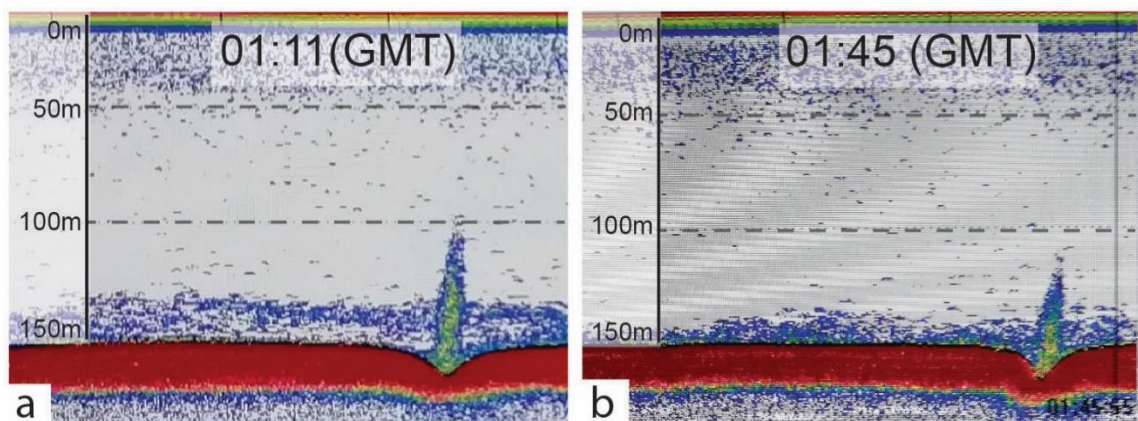


Figure 5.3. Acoustic flare emanating from Scotia Pockmark, North Sea surveyed on 29/7/19 using a EK60 echosounder. (a) image taken at 01:11 (GMT) showing acoustic flare rising 50 m from seabed. (b) image taken at 01:45 (GMT) showing the acoustic flare rising 30-40 m from seabed.

5.2.2 Core X-radiography

The cores were taken to Geotek Ltd. in Daventry (UK), which has a vertical X-ray and CT core scanning and imaging system (Geotek VXCT). This system was used to acquire full-length continuous 2D X-radiographs of 10 whole (unsplit) core sections at 57-micron resolution. Some core were scanned in two different planes (0 and 90) to compare X-radiographs at 90 degrees. The X-ray source was a 65W Thermo Kevex with variable focus. A lead slit was used to obtain a higher resolution image of the cores, as this has been shown to reduce the amount of radiation scattering that can obscure the image (Barnes 1991). The upper sections (A section) are variable in length, depending on total core recovery (from 0.3 to 1.0 m) and are mostly composed of wet sediment with a high-water content and low density. Therefore it is essential that this analysis is conducted before the core is split and with minimum disturbance to the core. Splitting the core would also allow the sediments to de-gas and possibly destroy any gas related voids and structures.

5.2.3 Multi Sensor Core Logger – Standard

The cores were then taken to the British Ocean Sediment Core Facility (BOSCORF) at the National Oceanography Centre (NOC) Southampton. A Geotek standard multi-sensor core logger – (MSCL-S) was used on whole (unsplit) cores. All cores were allowed to reach room temperature at least 12 hours before scanning. The instrument was calibrated, by BOSCORF staff, using an empty (air filled) core liner and a water filled core liner following BOSCORF standard calibration procedures. The instrument sensors employed were as follows: gamma-ray attenuation, p-wave velocity, magnetic susceptibility (MS) and electrical sensitivity. All measurements were made at 1cm downcore resolution. These non-destructive sensors will provide valuable high-resolution information on the bulk density of sediment, possible sediment origin, stratigraphic correlation between cores, and acoustic velocity of sediment and grain-size variations (Rothwell & Rack 2006).

After MSCL-S analysis, the cores sections were split along their long axis, into two equal halves, using a Geotek core splitter. This machine uses a vibrating blade and a fixed, slightly hooked blade to split the core liner and ensure minimum sediment contamination by plastic debris.

5.2.4 Multi Sensor Core Logger – Core Imaging System

Immediately after being split, the core surface was cleaned and smoothed using a 35mm wide blade. The archive half of each core was then photographed in a Geotek MSCL-Core Imaging System (CIS) at BOSCORF. It is essential that this is done very soon on

split cores as the colour of sediment can change rapidly as it oxidises. The powerful LED light system allows for the acquisition of colour-calibrated high-resolution 5k line-scan images. These images capture a precise photographic record enabling the precise correlation of geophysical and geochemical characteristics based on sediment physical appearance or optical properties.

5.2.5 *Multi Sensor Core Logger – XYZ*

A Geotek MSCL-XYZ was used to measure two key variables, magnetic susceptibility, and spectrophotometry of split core sections. The instrument uses a Bartington magnetic susceptibility point sensor, allowing for 0.5 mm resolution. Data from the point sensor and the lower-resolution loop sensor on the MSCL-S can be compared using inter-instrument calibration and regression analysis for increased accuracy. The MSCL-XYZ instrument is also fitted with a Konica Minolta spectrophotometer, the results from which can accurately quantify the colour or lightness of the core surface. This technique measure the wavelength spectra of reflected light to derive absolute colour, or lightness values, in a number of different colour spaces. This technique can permit the identification of small-scale laminations and light-dark sediment variability often associated with palaeo-climatic events. The results from the spectrophotometer were used to reconstruct a simulated core image based on the internationally recognised Munsell colour system.

A simulated true-colour coded core image based on the relative Munsell colour changes was constructed using R packages: *Munsell* and *aqp*. The Munsell package can only use a limited number of hue values; the colour value must also be an integer and chroma must be a multiple of 2. Due to these limitations, results from the MSCL-XYZ had to be rounded to the nearest applicable colour value. Therefore, the resulting colour-simulated core can only be considered to showing the relative colour changes.

5.2.6 *Manual core logging*

At this stage cores were visually logged, whereby their physical appearance was observed and recorded. General colour changes were noted along with changes in grain size determined by the texture of the core section. The descriptions of the terms used to describe the core textures are as follows: homogenous silty/clay covers the smaller grain sizes of clay and silt fraction which compose mud, these were observed to have a smooth texture with occasional grit between the fingers; sandy silt was observed in sections of the cores whereby the texture of the sediment was coarser than the silty/clay fraction and yet not as coarse as sand; coarse sandy silt described the sediment type found in some cores, this was observed from the texture of the sediment along with a visual change where

sediment grains could be easily seen with the eye. The presence of any larger particles such as shell fragments or lithic fragments were also recorded in the core logs.

5.2.7 ITRAX – XRF Core Scanner

The Cox Analytical Systems (Sweden AB) ITRAX, housed at BOSCORF-NOC, is a high-resolution micro-XRF elemental analyser for measuring geochemical elemental abundance of elements with atomic numbers from 13 (Aluminium) to 92 (Uranium) (Croudace & Rothwell 2015). The instrument uses a molybdenum X-ray tube to detect elements using variable count time (5-60 secs), at 30 Kv and 40 Ma. The XRF system works by the X-ray exciting a sample, the resulting fluorescent X-rays emitted are unique to an element. The peaks in a XRF energy spectra can be assigned to specific element and be used to calculate the relative abundance of elements, represented as counts per second (cps). In this study these results were normalised using the X-ray scatter calculated from the ratio of incoherent and coherent scattering values (Boyle *et al.* 2015; Woodward & Gadd 2019) with the exception of Mn (normalised to Fe) and Sulphur (normalized to Cl); used for the analysis of redox conditions and organic content. Normalizing to X-ray scatter accounts for the effect of changing water content on elemental data. Downcore analysis was performed at 1 mm intervals, with a 30-second count time per interval. Archive sections were scanned for a wide elemental suite (Al to U) focusing on the following elements: Ca, Fe, Mn, S, Sr and Cl.

5.2.8 Particle size analysis

Particle size analysis (PSA) was conducted using the Beckman Coulter LS 230 multi-frequency laser diffraction analyser at the University of Stirling (Biological & Environmental Sciences). The Beckman Coulter LS 230 used laser diffraction and polarisation intensity differential scattering (PIDS) to calculate the percentage volume of grain sizes between 0.04 – 2000 microns. Small sediment samples were taken from working halves from cores GC027, GC021 and GC023 at 5 cm downcore intervals. Samples were weighed and dried in an oven set to 60°C overnight. Samples were then reweighed. A small subsample was taken for organic carbon and nitrogen analysis, the remaining sediment was reweighed and sieved to remove the >2 mm grain size fraction.

The <2 mm fraction was treated with the anti-flocculant agent Calgon (Sodium Hexametaphosphate) and placed on a shaking table overnight to displace sediment grains and effectively mix the sample to produce a representative sample. A magnetic stirrer was added, and the sample was mixed for an additional 30 minutes before analysis. A plastic

pipette was used to agitate the sample and transfer a representative sample into the fluid module. This module contains filtered water, which is circulated, keeping the sediment in suspension. More sample is added to the fluid module until an obscuration value of 40 – 60% is achieved which indicates the desired level of light scattered by particles. A control sample with a known particle size distribution of sand, silt and clay was run at the start of every session. Three runs were conducted for each sample and the results averaged.

Averaged results were analysed within the statistical software R and the commonly used grain size statistics Microsoft Excel package *gradistat* version (Blott & Pye 2001). R packages *G2SD* and *rioja* use the same grain size principles as *gradistat*. The grain size classification principles are based on the sediment descriptions of Folk and Ward (1957) and further adapted from Udden (1914) and Wentworth (1922). Output statistics can be used to define the sorting of grain sizes and accurately classify the sediment fractions of clay, silt, and sand.

5.2.9 Organic carbon and nitrogen analysis

Organic carbon and Nitrogen (CN) analysis was performed using the Thermo Scientific Flash Smart NC-org elemental analyser at the University of Stirling (Biological & Environmental Sciences). Sediment samples were taken from cores GC027, GC023 and GC021 at 5cm downcore intervals. Sub-samples were taken from samples initially taken for PSA after they were dried. Sub-samples for the CN analysis were ground using a pestle and mortar into a fine powder. 2 – 15 mg of the fine powder was then placed in a tin container and weighed using a 5-point balance. This tin capsule was carefully folded into a sphere, ensuring that it was sealed, and no holes were made. Samples were then placed into the NC-org elemental analyser. The analyser was operated by qualified lab technicians (Ian Washbourne and Lorna English).

5.3 Results

Only gravity cores that were retrieved *inside* and *outside* selected pockmarks of interest were analysed, interpreted, and reported – namely, cores from Stornoway Bay (GC008 and GC006) and East of Eigg (GC021 and GC023). As well as a single core which was retrieved from inside the Scotia pockmark, North Sea (GC027). The core logs, particle size analysis and geochemical (ITRAX-derived) stratigraphy for each of these 5 cores are presented in the following sections.

5.3.1 GC006

Core GC006 was retrieved outside a pockmark in Stornoway Bay (Figure 5.2) and is 225 cm long. Core log GC006 (Figure 5.5) shows a very homogenous silty/clay sediment with no lithographic changes. Few notable colour changes are observed except for the seabed interface where yellow value increases along with the hue and chroma, giving an overall darker appearance. Numerous shell fragments are recorded within the core; most of which are bivalves, with a single gastropod shell recorded at 40 cm. A single vertical fracture, flame like in appearance, recorded at 150 – 190 cm, is attributed to gas expansion within the sediment (Figure 5.4).

Samples for grain size analysis were not taken from GC006 due to time constraints and restricted lab access in 2020 during the Covid19-pandemic. Therefore the core logs are relied upon to identify general change in grain size which can be detected by physical appearance. No clear grain size change was observed in core GC006, as the core is composed of predominantly homogenous silt/clay.

Data loss within the P-wave plots are noted between 70 – 80 cm and 160 – 200 cm (Figure 5.6). The first loss of data occurs at the position the core was separated and therefore can be explained by damage to core material during the cutting of the core liner and movement of sediment. The second loss in P-wave data occurs at 160 – 200 cm, this coincides with fractures noted within the X-ray images (Figure 5.4a, Figure 5.5). This fracture has been interpreted as a gas fracture which developed as gas migrated through the sediment during core retrieval.

It is important to note the change in the scale between the MS and chemical profiles, only the A section of the core was analysed using the ITRAX (Figure 5.7). The MS values range from 12 – 21 SI x 10⁻⁵. The profile shows three main peaks at 10, 45 and 205 cm with a smaller peak recorded at 115 cm. These seem to coincide with an increase in Mn/Fe ratio in the upper A-section of the core. These MS also seem to occur at a similar depth to p-wave inferred increase in grain size. The largest Mn/Fe ratio is from the core section appears at the seabed with value of 0.012, and decreases to 0.01 at 5 cm. A second Mn/Fe peak is recorded 7.5 cm with a value of 0.011, before decreasing again. Sulphur values are initially low, increasing to a peak at 12.5 cm with a secondary peak at 17.5 cm. The content of Ca gradually increases to a peak at 42.5 cm before decreasing rapidly to a minimum at 47 cm. The content of Ca values are likely reflecting the proportion of calcium-carbonate microfossils (e.g. foraminifera) deposited in this marine environment, which is present throughout this core section. Sr values could show a similar trend as Ca with a decrease recorded at 47 cm. Sr values could help to discriminate between

carbonates and represent those associated with pteropods, again reflecting a marine environment (Croudace & Rothwell 2015). S/Cl ratio has been used in this core to give an indication of high organic content, a technique employed by others (Thomson *et al.* 2006). Samples for C/N analysis were not taken in this core therefore the S/Cl ratio is used to reflect the organic matter within the core (Thomson *et al.* 2006). S/Cl values range from 0.03 – 0.09 and show a generally increasing trend with depth, with numerous peaks throughout.

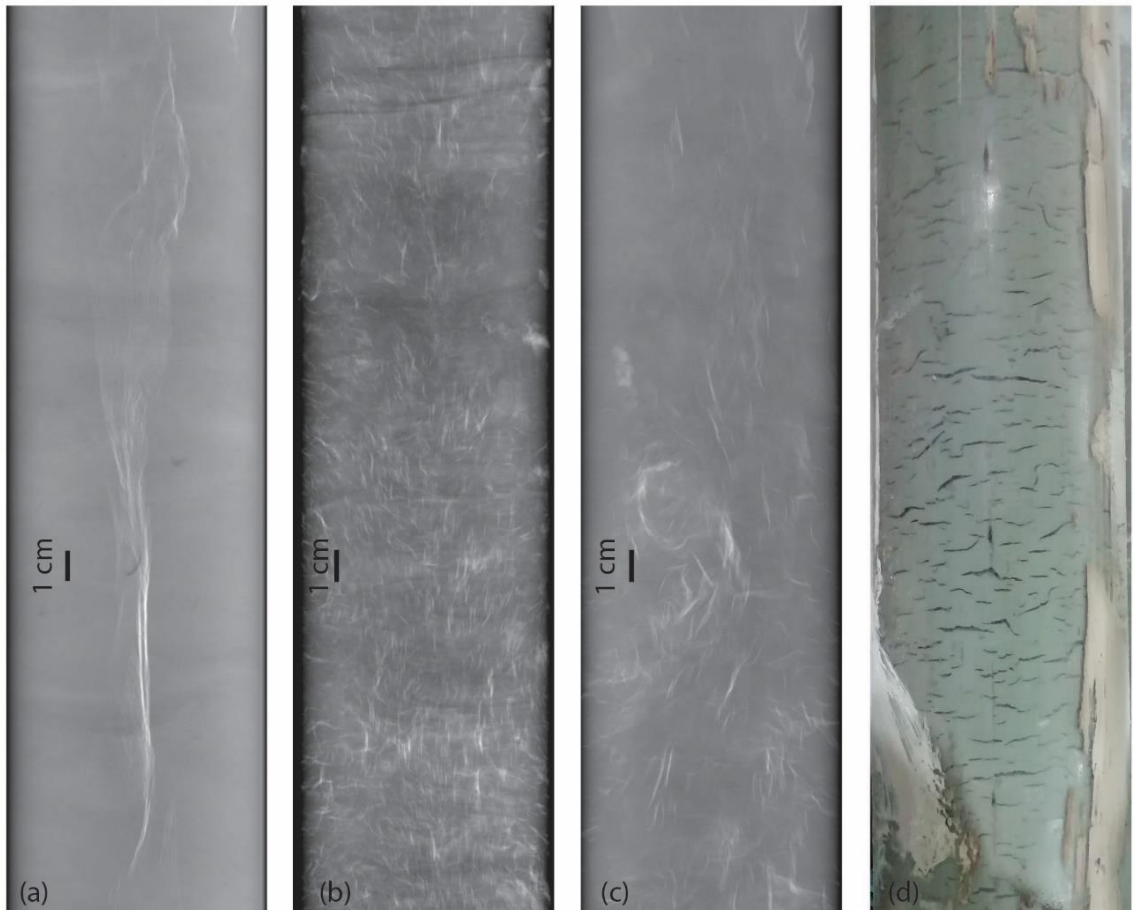


Figure 5.4 Gas fractures observed within sediment cores from Western Scotland. (a) Gas fractures in core GC006 imaged using X-radiography.(b) Gas fractures in core GC023 imaged using X-radiography.(c) Gas fractures in core GC021 imaged using X-radiography.(d) Gas fractures in GC019 as seen through core liner after core recovery.

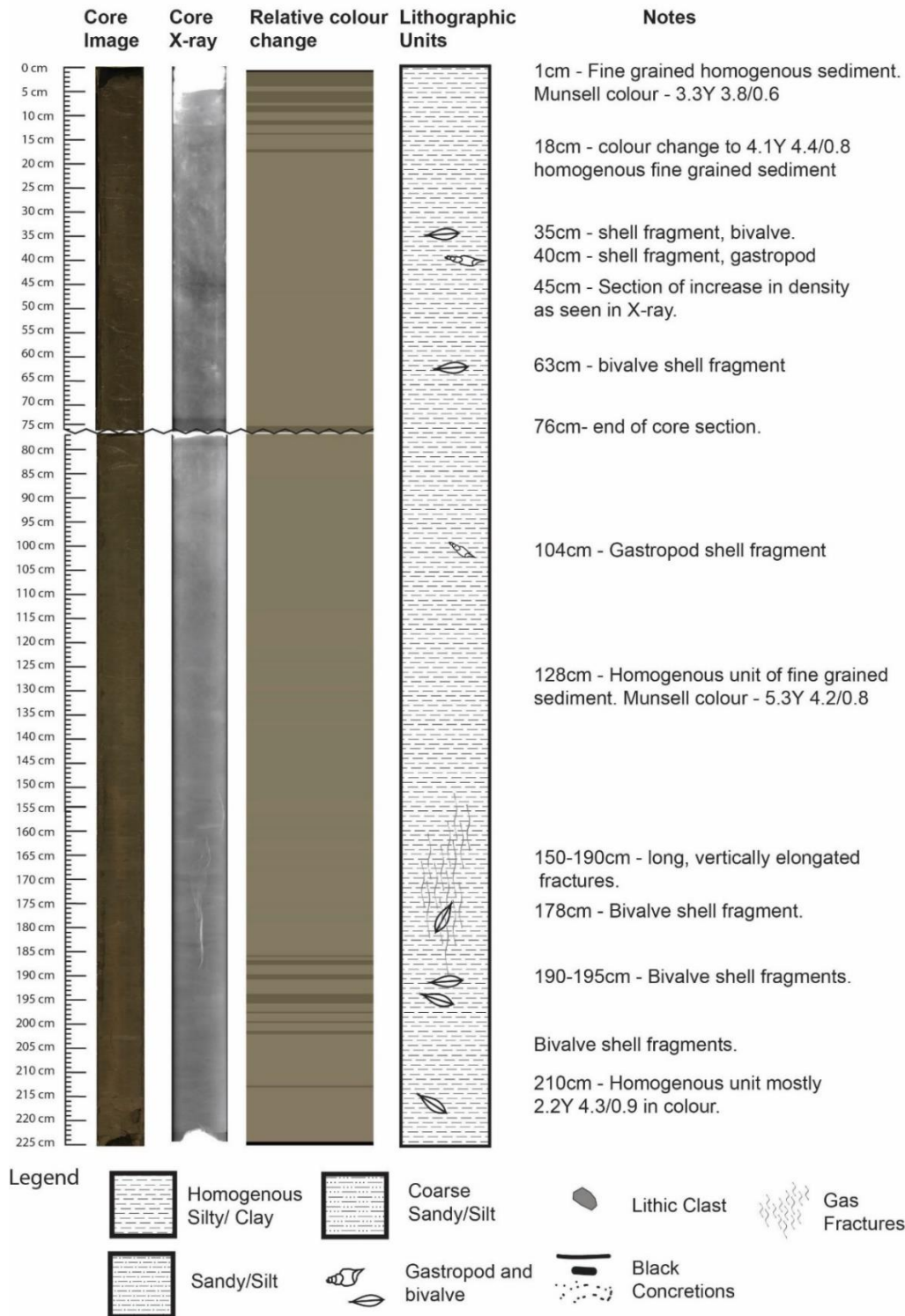


Figure 5.5 GC006 core log. (From left to right) High-resolution core photograph from MSCL-CIS, core X-radiograph from Geotek – VXCT; relative colour change derived from the Munsell colour values measured by the MSCL-XYZ spectrophotometer; core log showing the main lithological units and core features; other core notes from sediment logging

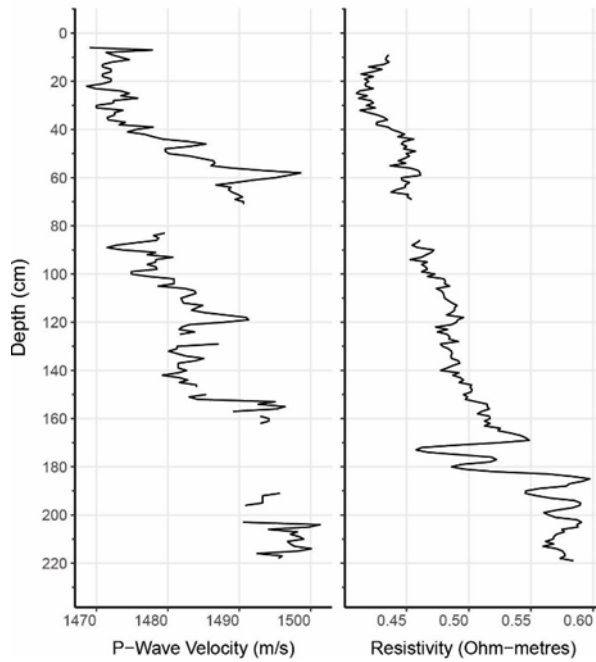


Figure 5.6. GC006; p-wave velocity and resistivity data from MSCL-S. Data loss at 75 cm are due to end caps.

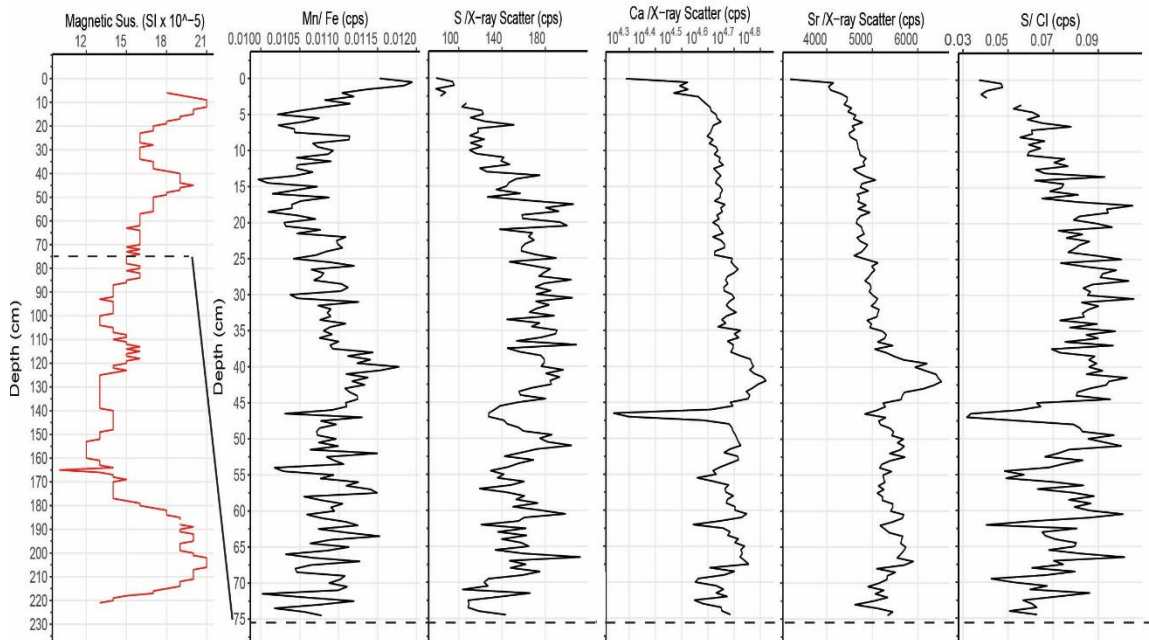


Figure 5.7. GC006: physical and chemical properties derived MSCL-XYZ and ITRAX respectively. Note different vertical scale values between Magnetic susceptibility and elemental abundance. (From left to right) magnetic susceptibility from MSCL-S, Manganese/Iron, Sulphur, Calcium, Strontium, Sulphur/Chlorine. Dashed line indicates break in the core sections (A & B).

5.3.2 GC008

Core GC008 was retrieved from inside a pockmark in Stornoway Bay (Figure 5.2) and is 223 cm long. Core log GC008 (Figure 5.8) shows a 160 cm thick upper unit of homogenous silt/clay. From 160 – 223 cm, the sediment become slightly coarser, this is represented by a gradational change downcore. This coarser unit is also recognisable in the X-ray where it appears darker (denser). Throughout the core are numerous colour changes. The most distinct change is near the base of the core, at 205 cm, where the yellow hue increases, appearing slightly green/blue in the relative colour profile. Like GC006 there are several shells scattered throughout the core but only bivalves are recorded.

Unfortunately, grain size analysis was not undertaken for GC008, owing to time constraints and lab access restriction in 2020. Instead, core logs are relied upon to show observed change in grain size (Figure 5.8). From 0 – 160 cm the core is observed to consist of homogenous silt/clay. At 160 cm the grain size is observed to become coarser, where it is described as sandy silt. The observed change in grain size alongside the colour change probably indicates a gradual transition from distal glaciomarine to marine conditions up core at 160-120 cm.

The P-wave velocity and resistivity plots (Figure 5.9) show that there is a signal loss at 60 – 80 cm. This is likely due to the depth at which the core sections were separated and the resulting movement of core material effecting the data at this region. No other regions of data loss are observed and no evidence of gas fractures are observed within this core.

MS values in GC008 range from 14 - 24 SI x 10⁻⁵ which are higher than values recorded within GC006 (Figure 5.10). The minima at 70-75 cm may be an artefact due to the where the cores sections were cut or may represent a real decrease in MS values at this core depth. MS values are generally consistent in the A section of the core (0-70 cm). The largest value is recorded at 15 cm, however this does not coincide with any noticeable changes in any of the geochemical profiles. The Mn/Fe ratio show a generally decreasing trend with depth (Figure 5.10). The initial results from 0 – 5 cm fluctuate between the maximum and minimum recorded values; these are likely outliers due to the highly mobile seabed interface causing sediment mixing. An initial peak in the ratio is observed at 5 cm with a value of 0.0137. These values then decrease with scattered fluctuations towards other minima at 12 cm and at 32.5 cm, both minimum values are 0.011. Little structure is observed within the S profile. These values show a slight increase with depth, although with numerous fluctuations and marked variability. A minimum value of 75 cps is recorded at 15.5 cm. Ca and Sr values are both highly variable, showing fluctuations of values

between 25,118 – 44,668 cps and 3500 – 5000 cps, respectively. These ranges are similar to those observed in GC006 and probably attest to these sediments having a marine origin. C/N analysis were not undertaken for GC008, and therefore the S/Cl ratio are used as a proxy for organic matter. These values range from 0.03 – 0.07, peaking at 55 – 65 cm, and like other elemental abundances in this core show a generally increasing trend with depth.

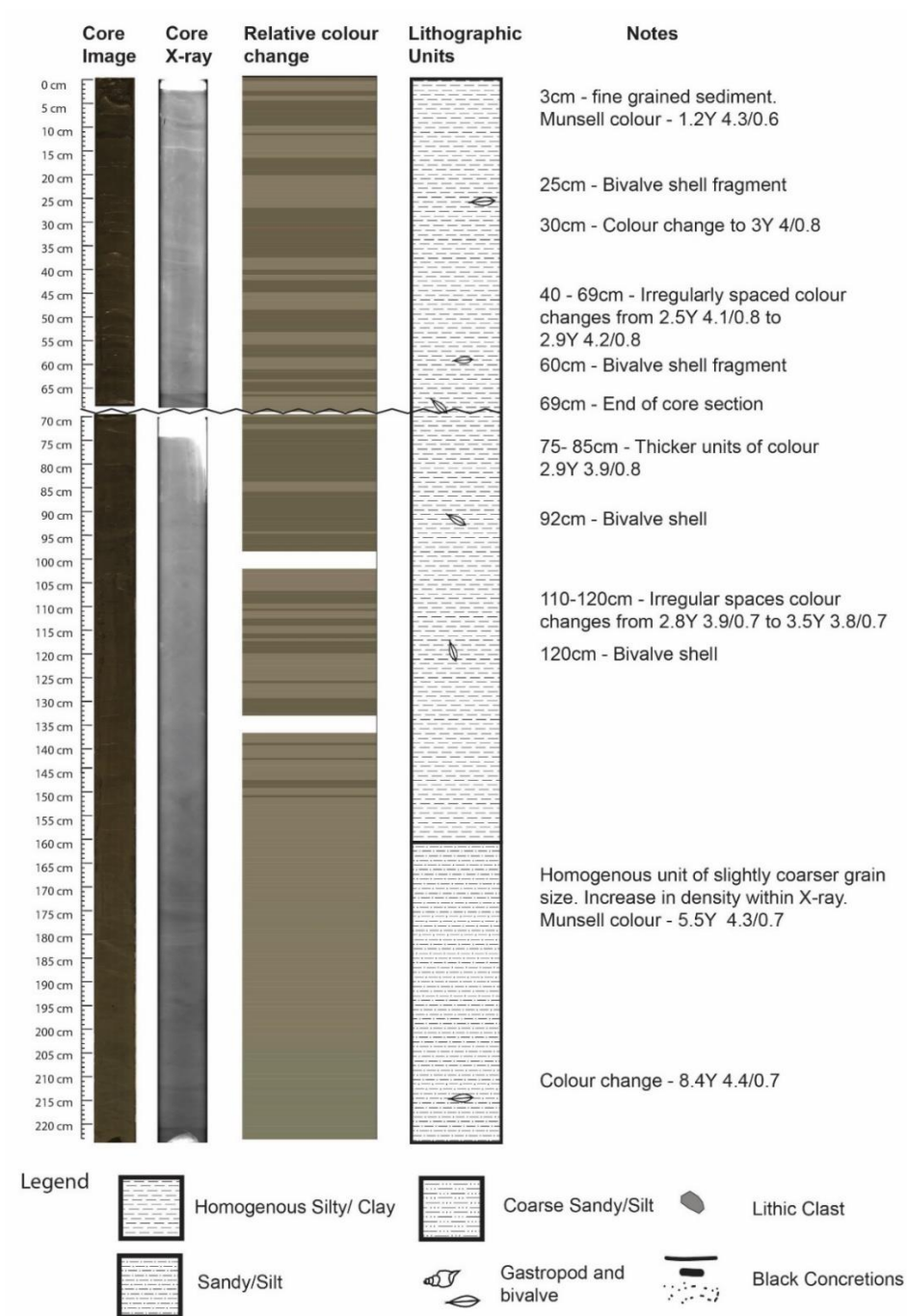


Figure 5.8 GC008 core log. (From left to right) High-resolution core photograph from MSCL-CIS, core X-radiograph from Geotek – VXCT; relative colour change derived from the Munsell colour values measured by the MSCL-XYZ spectrophotometer; core log showing the main lithological units and core features; other core notes from sediment logging.

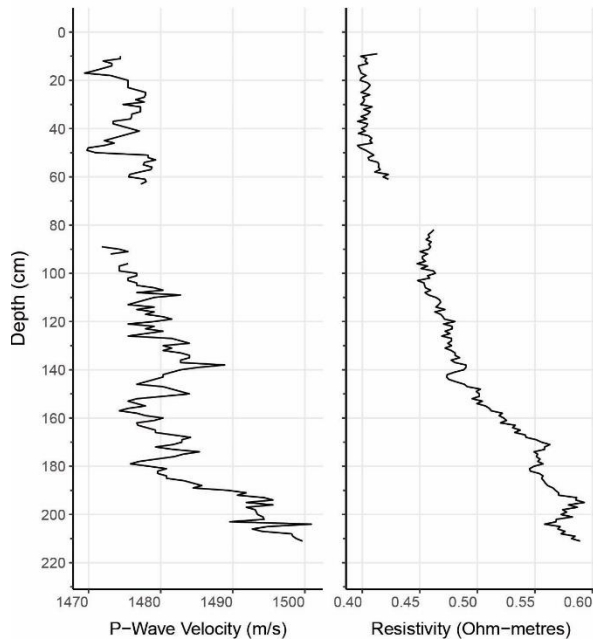


Figure 5.9. GC008: p-wave velocity and resistivity. Breaks are missing data due to end caps or no signal return.

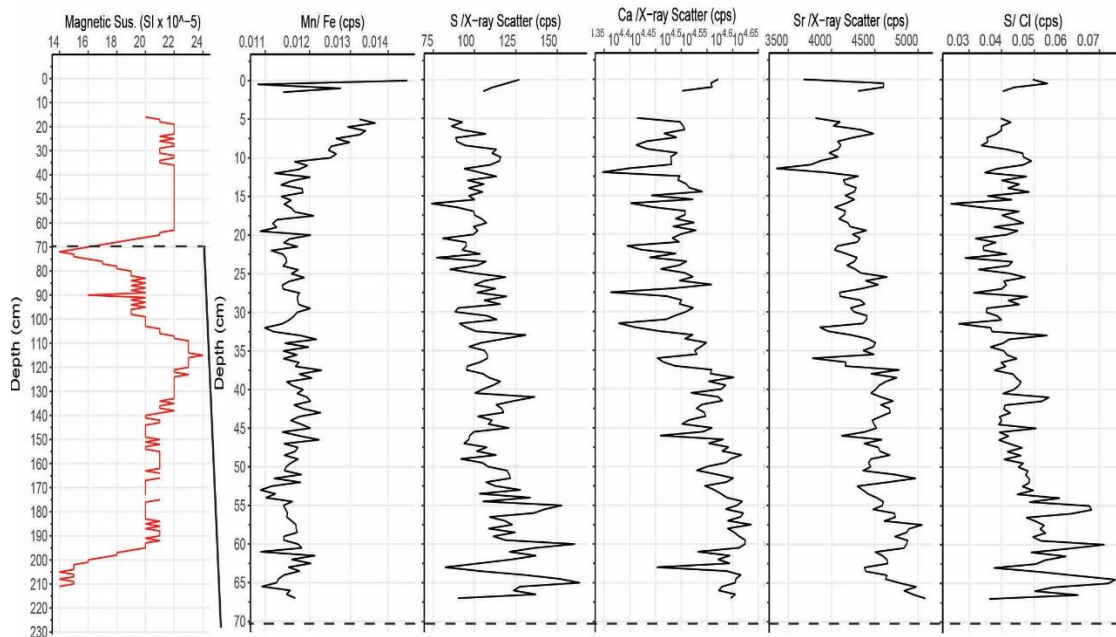


Figure 5.10. GC008: physical and chemical properties derived MSCL-XYZ and ITRAX respectively. Note change in vertical scale values between Magnetic susceptibility and chemical content. (From left to right) magnetic susceptibility from MSCL-S, Manganese/Iron, Sulphur, Calcium, Sulphur/Chlorine content. Dashed line indicates break in the core sections (A & B).

5.3.3 GC021

Core GC021 was retrieved from inside a pockmark east of Eigg (Figure 5.2) and is 250 cm in length. Core log GC021 (Figure 5.11) shows a fine-grained uppermost top lithological unit composed of silt/clay which gradually coarsens below 50 cm where sediment becomes very fine sand/silt. This unit gradually fines back to silt/clay at 90 cm. Another lithological change is present towards the base of the core where the grain size again gradually coarsens to a very fine sand/coarse medium silt below 205 cm. very few shells are present within this core, and these are mainly bivalve shells present at 50 and 97 cm. There are three main colour units within this core and are separated as follows: 0-20 cm sediment colour is 2.8Y 3.1/0.9, from 20-146 cm the colour is generally homogenous grey/brown with a Munsell values of 1.7Y 4.2/0.9, the most distinct relative colour change is seen below 146 cm where a gradational change to a green/yellow hue, the base of the core has a Munsell value of 3.4GY 4.3/0.6. Numerous sub-horizontal to vertically aligned fractures are scattered throughout the lowermost 75 cm of the core, and extending from 185 cm to the core base (250 cm) (Figure 5.4). These internal fractures are clearly visible on the X-rays forming a network of small open (low density) cracks mainly oriented with their long axis vertically. These are interpreted as gas-filled fractures that have expanded (opened) and began to extend through the sediment as the core was recovered from sub-seabed and brought onboard. These fractures are also attributed to the loss of data observed within the P-wave velocity between 160 – 240 cm.

Particle size analysis (PSA) was conducted on GC021. The PSA data shows that the mean grain size is between 8-24 microns (Figure 5.12), which is classified as fine to medium silt (Wentworth 1922). Two notable peaks are seen in the mean grain size at 75 cm and 210 cm, these show an increase in the percentage of silt and sand fractions at these depths. The break in the p-wave velocity at 80 – 95 cm is likely due to where the core was separated into A and B sections. The lower region of missing p-wave (>160 cm) attributable to the dense network of gas fractures observed in Figure 5.12. The notable peak in p-wave velocity appears at a similar depth as the peak in the mean grain size. A similar peak is also seen in the resistivity. These changes in grain size coincide with the changes in grain size recorded during visual sediment core logging.

MS values range from 10 – 24 $\text{SI} \times 10^{-5}$, the highest values are recorded between 10 – 110 cm, after which MS values decrease to a minimum value at 155 cm, remaining low to the core base at 230 cm (Figure 5.13). C/N analysis shows a generally increasing trend with depth. C/N values range from 20-25 in the surface sediments (>15 cm deep) increasing to 30-34 below 110 cm and remaining at this level to the base of the core.

Mn/Fe ratios show a rather unstructured 'noisy' profile; values range from 0.011 – 0.013 cps. Sulphur values show an increasing trend with values ranging from 100 cps in surface sediments until an increase to around 175 cps at 100 cm. These values then increase more markedly (200-275 cps) below 100 to core base – 240 cm. Ca and Sr values show an increasing trend with depth. S/Cl also show an increasing trend with depth. Notable changes in all these non-destructive elemental profiles are seen to show a rapid decrease at 80 cm followed by a rapid increase at 95 cm, which mirrors the destructively sampled C/N ratios.

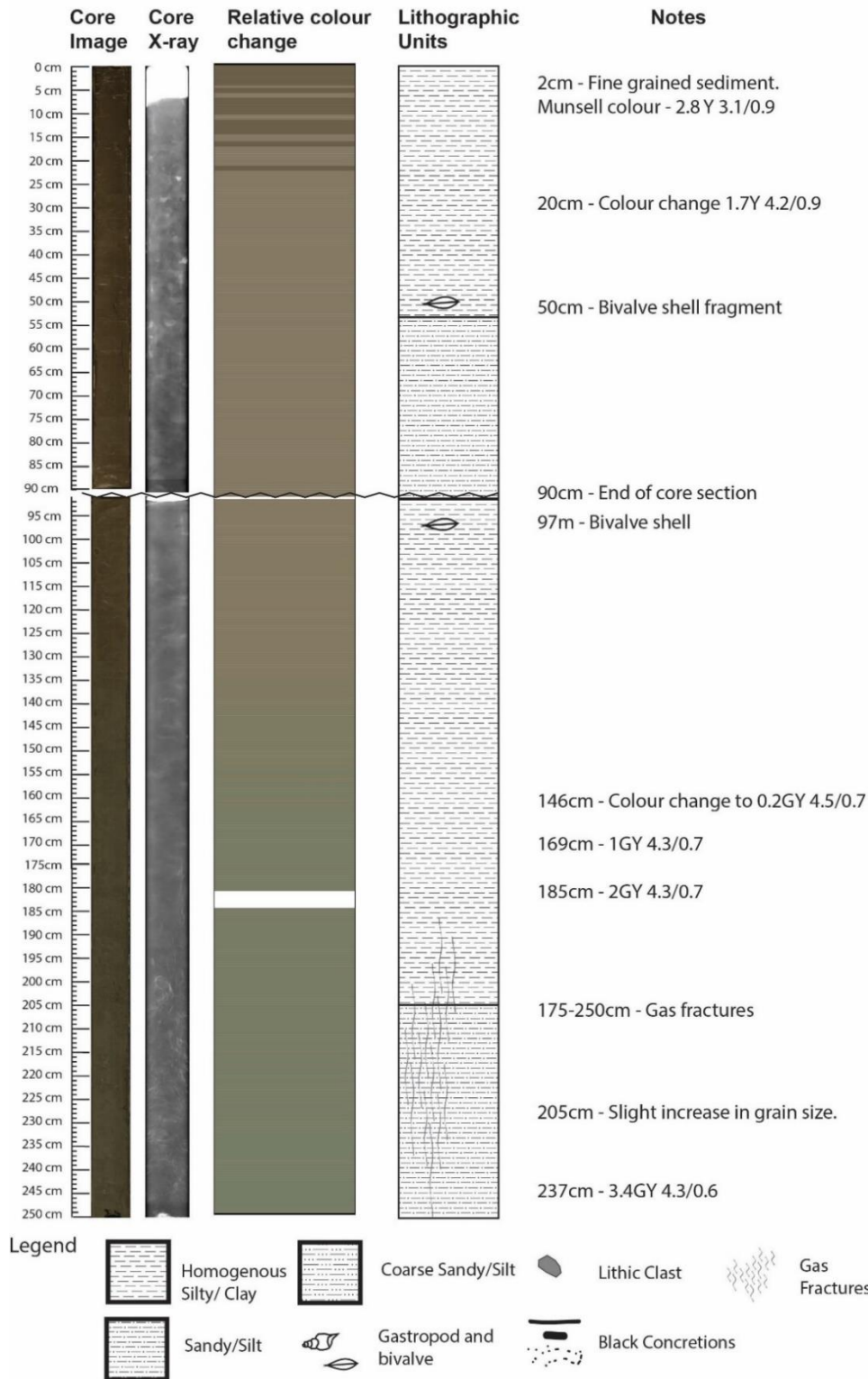


Figure 5.11 GC021 core log. (From left to right) High-resolution core photograph from MSCL-CIS, core X-radiograph from Geotek – VXCT; relative colour change derived from the Munsell colour values measured by the MSCL-XYZ spectrophotometer; core log showing the main lithological units and core features; other core notes from sediment logging.

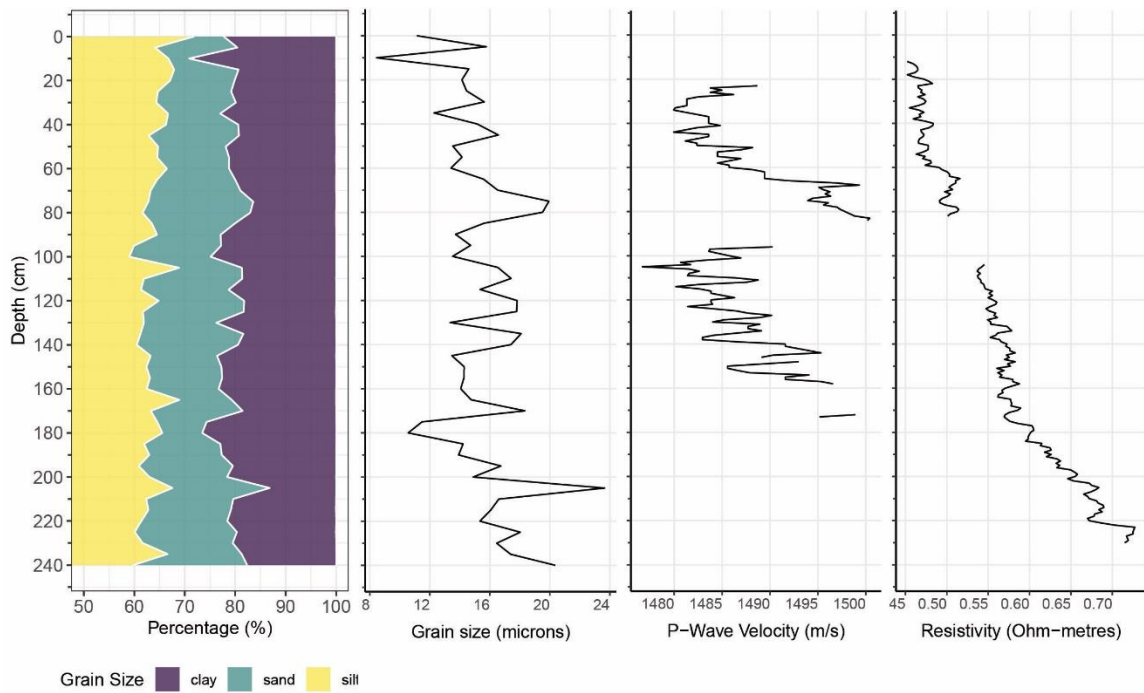


Figure 5.12. GC021 particle size plot. (From left to right) cumulative percentage grain size fractions, mean grain size, P-wave velocity from MSCL-S, resistivity from MSCL-S. Breaks are missing data due to end caps or no signal return.

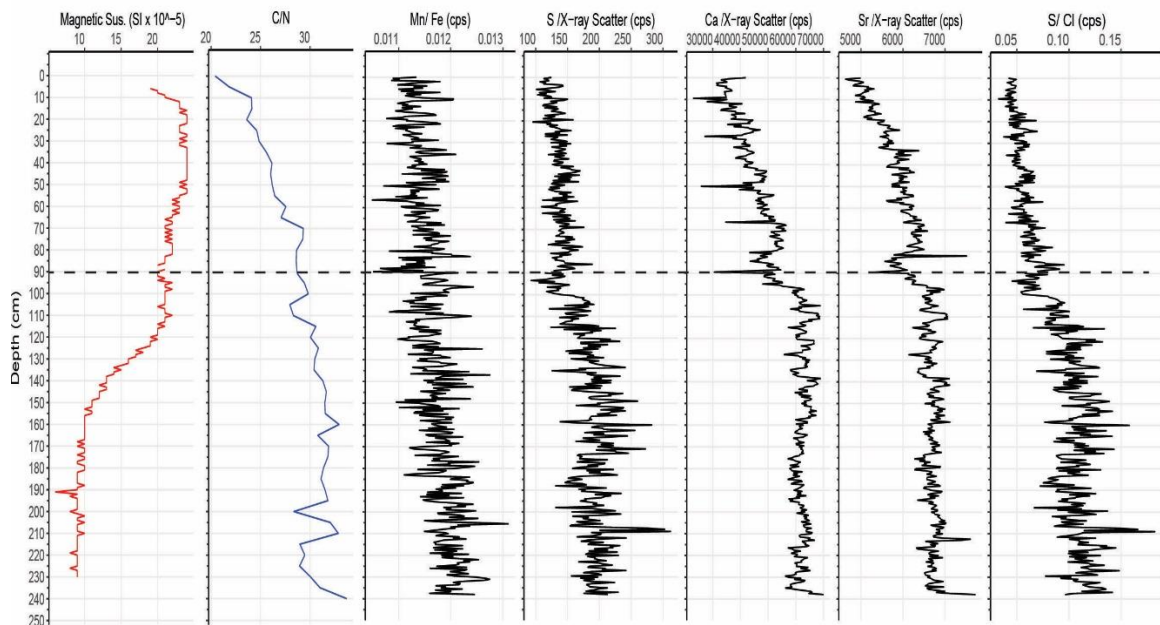


Figure 5.13. GC021: physical and chemical properties derived MSCL-XYZ and ITRAX respectively. (From left to right) magnetic susceptibility from MSCL-S, Manganese/Iron, Sulphur, Calcium, Sulphur/Chlorine content. Dashed line indicates break in the core sections (A & B).

5.3.4 GC023

Core GC023 was retrieved outside a pockmark east of Eigg (Figure 5.2) and is 210cm in length. Core log GC023 (Figure 4.13) shows two main lithological units. The upper unit is 45-50 cm thick and is composed of fine-grained silty/clay. This unit is almost completely contained within section A of the core. Core section B contains the second lithological unit identified which shows an increase in grain size to very fine sand/ silt. There are numerous colour changes throughout the core, these are broadly correlated with denser material as seen on the X-ray. The colour changes can also be seen clearly in the core image, in the form of laminations of varying thickness (mm to several cm). These laminations appear indistinguishable from the surrounding sediment, apart from their colour. There are numerous open fractures scattered throughout the B section of the core, from 90 cm to the core base (210 cm); these appear as a network of internal, sub-horizontal to vertically aligned, short (<1 cm) fractures on X-radiographs (Figure 5.4). As in core GC021 these are interpreted as gas-related expansion fractures.

PSA was conducted on core GC023. The mean grain size ranges between 10-24 microns (Figure 5.14), corresponding to fine to medium silt (Wentworth 1922). Peaks within the mean grain size generally correspond to peaks in the percentage of the sand fraction. The clay fraction in the sediment appears to be highest in the uppermost units, between 0 – 50 cm core depth. The changes in the clay percentage confirm the lithological observations made during visual core logging. P-wave velocity data is discontinuous and missing in much (>50%) of this core. The first gap in p-wave velocity data is likely due to the break in core sections. However, the main loss of p-wave data from 85 cm downcore occurs in the region where numerous small fractures associated with gas-escape seen in the X-radiography image (Figure 5.14). The electrical resistivity values are initially low before data-break (no signal returned) values then increase in the B section of the core, this is likely associated with the increase in mean grain size. An important observation is that a similar mean grain size is recorded between GC023 and GC021 at 50-190 cm and 100-240 cm respectively (Figure 5.12 & Figure 5.15). These could allow stratigraphic correlation between these two adjacent cores and will be discussed later in this chapter.

MS values range between 22 – 29 $\text{SI} \times 10^{-5}$. A small peak in values occurs at 20 cm depth, values then decrease possibly associated with the end of the core section. In core section B, MS values increase again with numerous peaks between 26 – 29 $\times 10^{-5}$ (Figure 5.16). C/N ratios range from 18 – 25. An initial peak is observed at 20cm which coincides with a peak in the MS. A prominent peak reaching the max value is recorded at 75 cm. C/N ratios generally increase to the depth of 75 cm, before showing a gradual

decreasing trend. Mn/Fe values range from 0.012 – 0.018. Values at surface are low but rapidly increase to the prominent peak at 27.5 cm, this increase occurs at the same depth as the peaks noted in the C/N and MS. Smaller, secondary peaks are also observed at 5 cm and 10 cm. Mn/Fe values rapidly decrease after 27.5 cm to 45cm, from this depth the Mn/Fe ratio ranges between 0.013 – 0.016, showing a fluctuating but generally increasing trend. Values of S are in the range of 75 – 175 cps, showing an increasing trend to a peak at 52.5 cm. Below this depth, values become sporadic and numerous sections missing data. Ca and Sr values show an increasing trend, especially in the uppermost 50cm, with depth showing a range of 20000 – 50000 cps, and 4000 – 7000 cps, respectively. Little overall structure is observed in this geochemical data with numerous peaks scattered throughout the core at varying intervals. S/Cl values range from 0.02 to 0.08, with an increasing trend to a prominent peak at 52.5 cm, this peak does not coincide with peaks in C/N values. Below 52.5 cm there are numerous regions with data loss associated with poor counts in Sulphur.

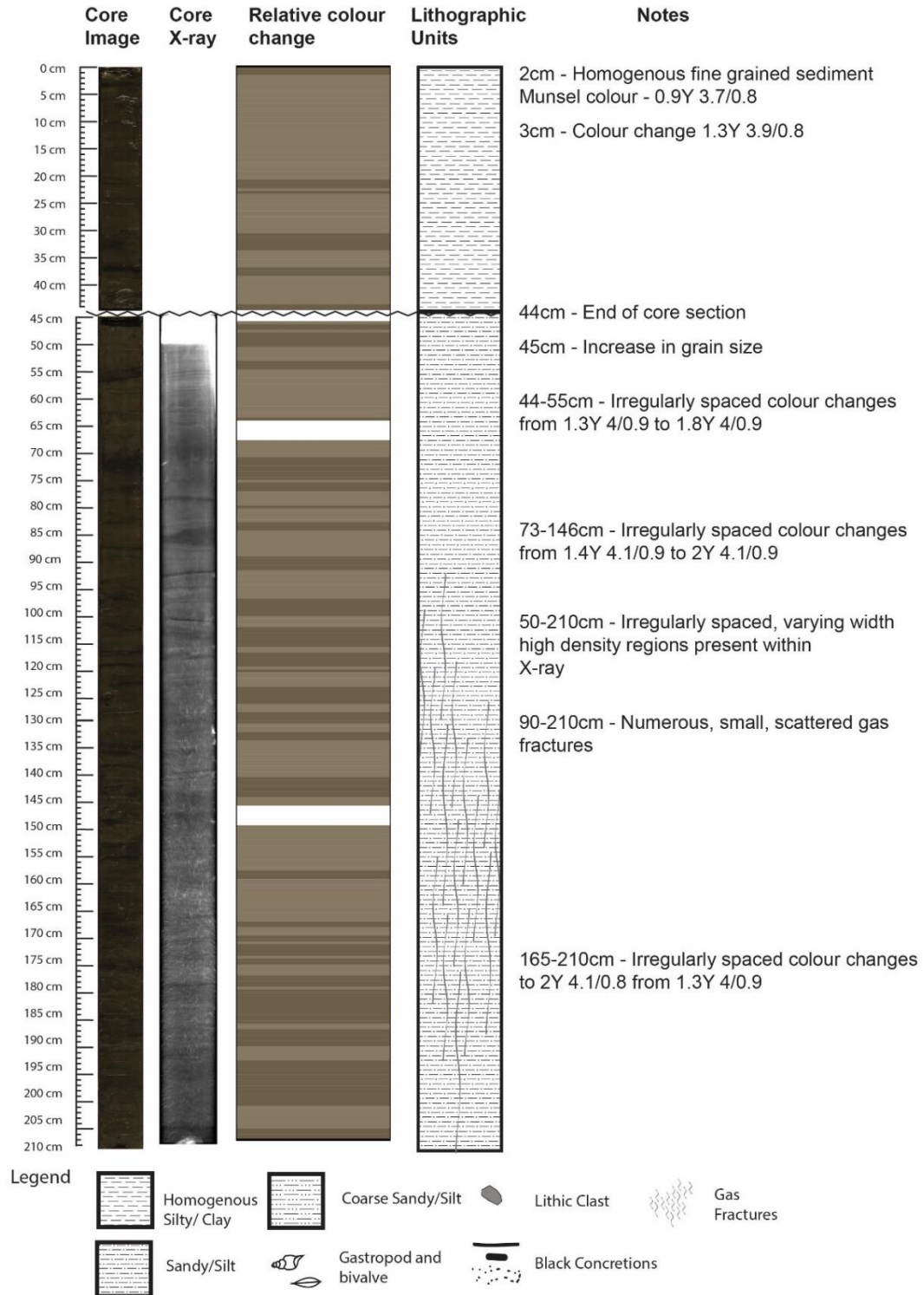


Figure 5.14 GC023 core log. (From left to right) High-resolution core photograph from MSCL-CIS, core X-radiograph from Geotek – VXCT; relative colour change derived from the Munsell colour values measured by the MSCL-XYZ spectrophotometer; core log showing the main lithological units and core features; other core notes from sediment logging.

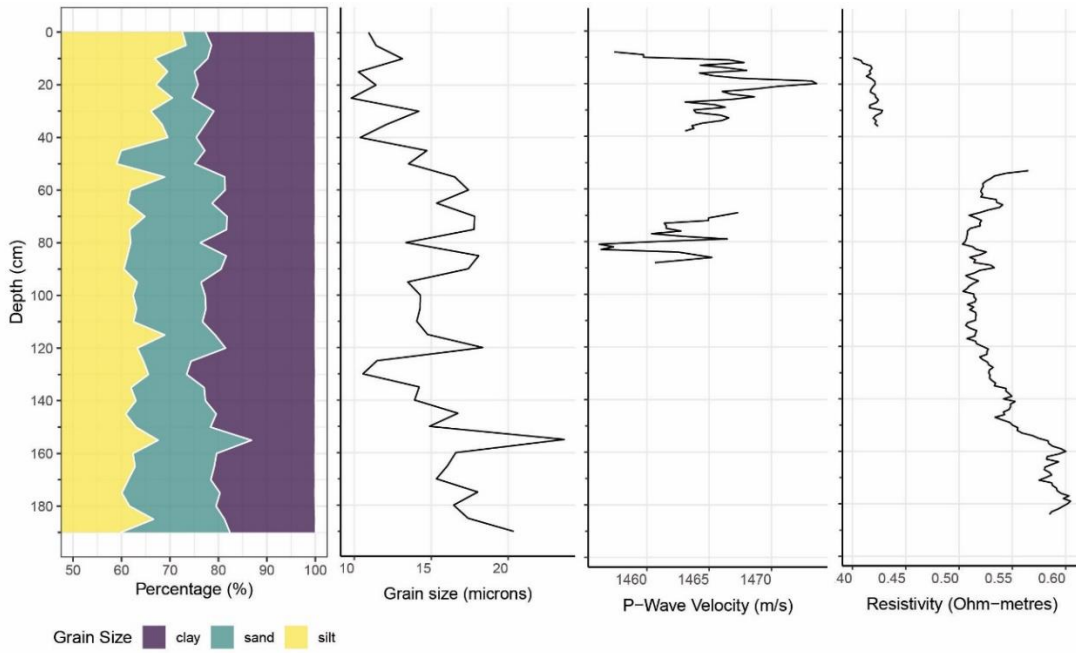


Figure 5.15 Particle size plot for core GC023. (From left to right) cumulative percentage grain size fractions, mean grain size, P-wave velocity from MSCL-S, resistivity from MSCL-S.

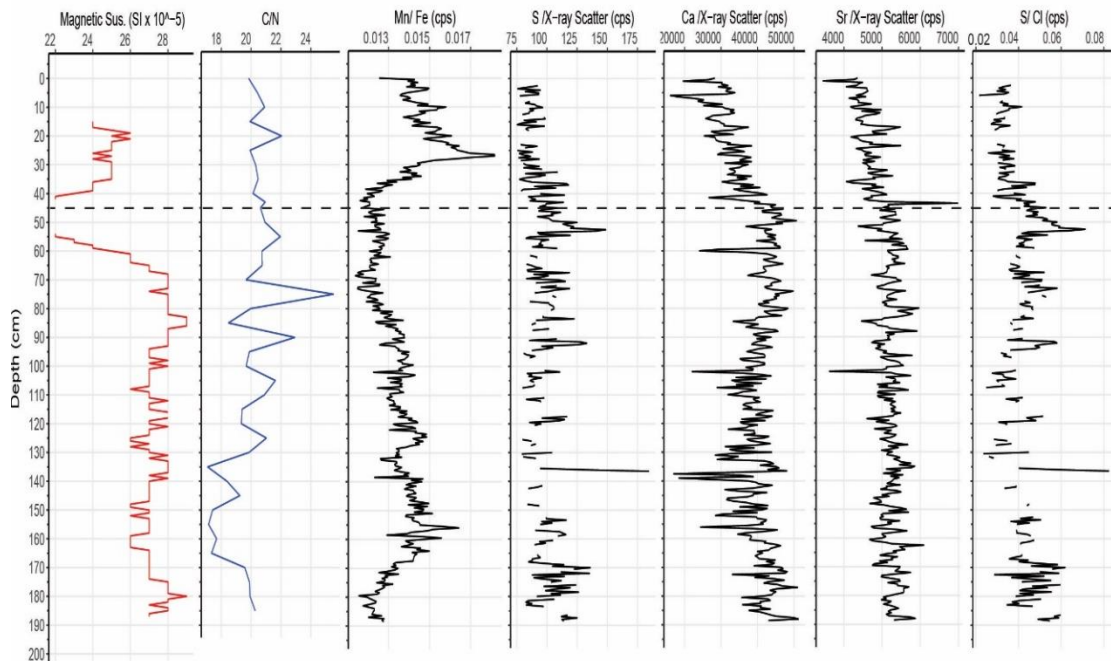


Figure 5.16 GC023: physical and chemical properties derived MSCL-XYZ and ITRAX respectively. (From left to right) magnetic susceptibility from MSCL-S, Manganese, Iron, Calcium, Sulphur, Chlorine content. Dashed line indicates the position where core sections were separated.

5.3.5 GC027

Core GC027 was retrieved inside the South pockmark within the Scotia pockmark complex, North Sea (Figure 5.2). The core is 226 cm in length. It is clear from initial observations of the core log (Figure 5.17/Figure 4.16) that this sediment is from a different environment. The sediment cores appearance differs greatly from all other cores recovered from two different west coast regions of Scotland. In GC027 the uppermost unit is composed of fine-grained grey/brown sediment (silt/clay) with Munsell colours between 4.4Y 4.2/0.9 and 6.1Y 4.4/0.9. This unit is stratigraphically the most recent and has the lowest density in the X-radiographs indicating that this is of Holocene marine muds. From 30 – 40 cm depth there is a small increase in grain size, very fine sand/ silt, with a slight decrease again from 40-60 cm depth. Below 60 cm downcore there is a clear change to a coarser sediment, fine sand/ very fine sand, with a large lithic clast at the base at 90 cm. The basal contact of this unit seems to dip at a shallow angle. From 90 – 169 cm depth the mean grain size returns to a silt/clay. The final lithological change is seen at 169 cm and extends to the base of the core. The grain size increases once again to a very fine sand/silt. Colour returns to a yellow hue before turning to blue and green hues, Munsell values of 5B 3.7/0.2 and 5.1G 4.1/0.2, at 191 cm. The most distinguishing features of this lower unit are the colour changes, from yellow hues to green and blue/green hues, with Munsell values of 5.9G 4.1/0.2 and 2.8BG 4.2/0.2. Also within this unit are layers, or clusters, of black clasts/concretions that are scattered in the mud and can occur as large as gravel sized clasts. These are identified in the X-radiography images as discrete areas of higher density. A lithic clast is also present at 190 cm. Shells are absent from the uppermost and lowermost unit but are otherwise found in various locations throughout the core. Surprisingly, despite being in a known to be an active pockmark (Figure 5.3) there are no gas fractures observed in this core.

Particle size analysis was undertaken on GC027 It shows that the mean grain size is 15-63 microns (Figure 5.18), which corresponds to fine to coarse silt before it becomes very fine sand (Wentworth 1922). This particle size range is notably coarser than sediments in GC021 and GC023. Two main peaks can be observed in the mean grain size at 35 cm and 65 cm depth which are due to an increase in the sand fraction percentage. These correspond to the increase in grain size noticed during visual logging (Figure 5.17). Several large gaps in the p-wave velocity are observed, however no gas fractures can be seen in the X-radiographs or visual core log. P-wave velocity increases in the region where we observe a peak in grain size. The slight increases in resistivity are likely attributed to variation in grain size or downcore compaction. Despite numerous clasts/concretions being observed within the core log, particularly between 90-225 cm, they do not affect the

grain size data. It is likely that the process of oven drying, wet sieving and the effect of the anti-flocculent (Calgon) along with the action of the magnetic stirring, broke these fragile concretions into finer grained constituent particles. Therefore, we cannot rely solely on the mean grain size and percentage grain size in this case. The electrical resistivity measurements are also likely giving an indication of the presence of these discrete concretions.

The MS values in core GC027 range between 0 – 30 SI x 10⁻⁵ (Figure 5.19). An initial slight increase in values occurs in the A section of the core rising to 9 x 10⁻⁵ at 30cm depth, below this values decrease slightly. Within the B section of the core (78-226 cm), MS values rapidly increase to peaks at 95 cm and 110 cm to a value of 20 x 10⁻⁵. Further peaks occur downcore at 170 cm and 207 cm peaking at 30 x 10⁻⁵ and 27 x 10⁻⁵ SI units respectively. C/N ratios within the core range from 25 to 55; these are the highest values recorded in any of the analysed cores. An initial peak in C/N at 35 cm coincides with a rise in MS. Below 35 cm C/N ratios decrease before rising again to a peak at 70 cm. Another prominent peak is recorded at 150 cm with a smaller peak at 190 cm depth. Two minimums are observed at 170 cm and 200 cm, these coincide with two peaks in MS at these depths. Conversely, apart from these peaks, the general increase in C/N in the B section is related to the increase in MS values recorded. Mn/Fe ratio ranges between 0.009 – 0.013, with surface values of 0.011. Values increase below 0 cm to a depth of 40 cm, where the values are 0.013. Between these depths a rise in values occurs at 11 cm before rapidly decreasing again. Below 45 cm depth, values notably decrease rapidly and remain low until a prominent peak at 145 cm and another at 160 cm. Sulphur values are the highest within this core that any of the other cores analysed, ranging from 250 – 1000 cps. An initial rise in S counts occurs at 45 cm, just below the peaks in Mn/Fe. Ca and Sr values show similar trends, with the highest values associated with the first 85 cm of the core. Below 90 cm, the counts decrease abruptly and remain low to the core base. This abrupt change correlates well with the rise in MS ~90 cm, and below a lithological change observed between 60 cm – 90 cm. This is likely related to a change in the depositional environments, one that is not observed in any of the other cores analysed. Finally, S/Cl values do not seem to correlate well with the C/N ratios, showing an initial rise in values at 40-50 cm, which is below the initial peak in C/N values.

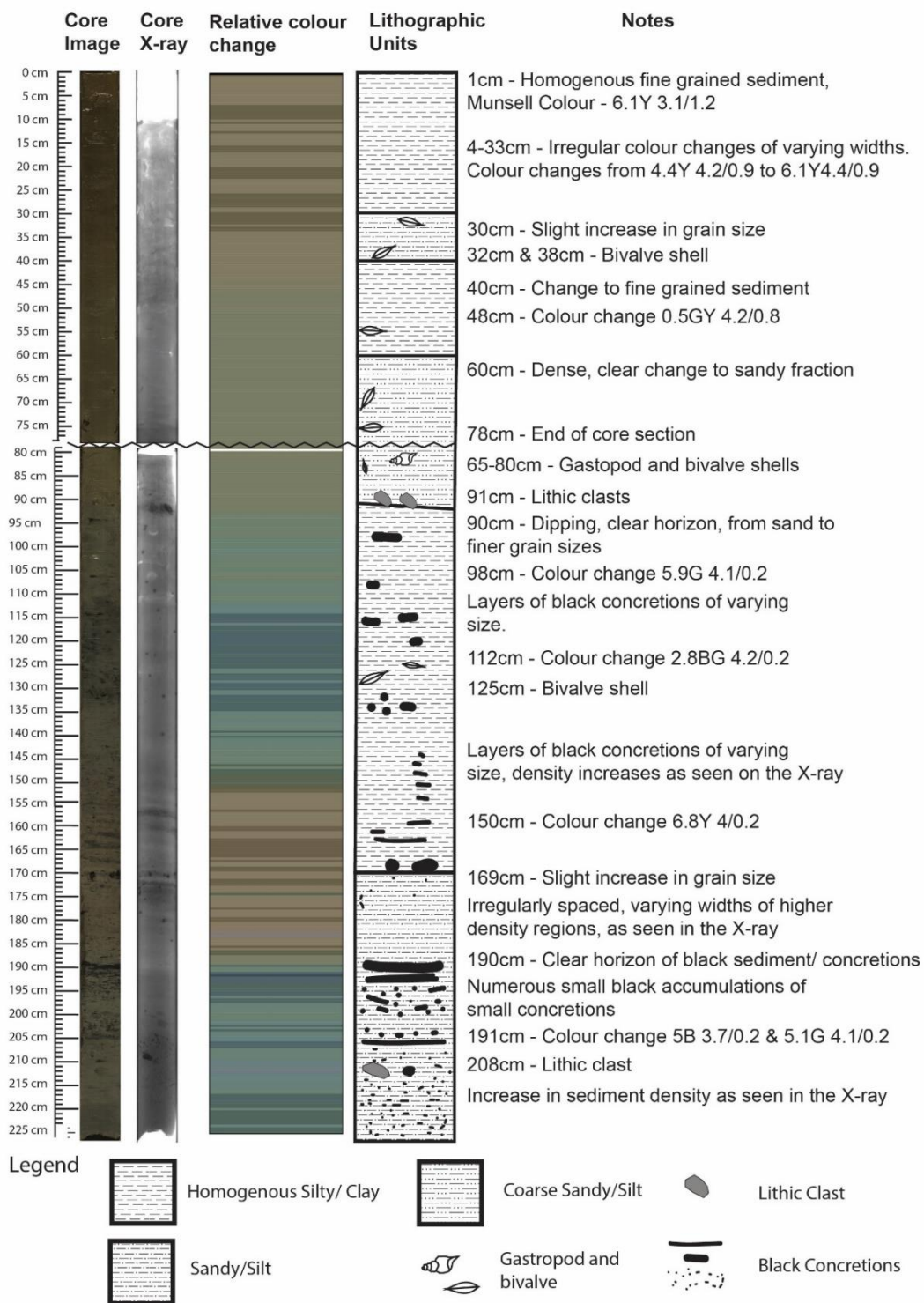


Figure 5.17. GC027 core log. (From left to right) High-resolution core photograph from MSCL-CIS, core X-radiograph from Geotek – VXCT; relative colour change derived from the Munsell colour values measured by the MSCL-XYZ spectrophotometer; core log showing the main lithological units and core features; other core notes from sediment logging.

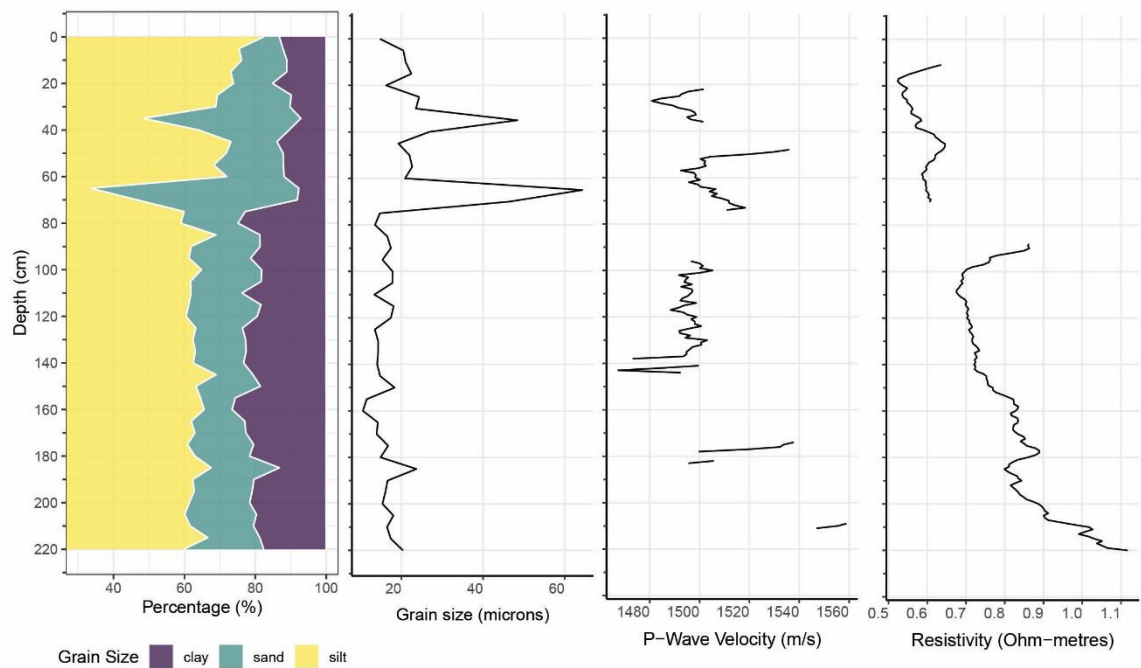


Figure 5.18. GC027 particle size plot. (From left to right) cumulative percentage grain size fractions, mean grain size, P-wave velocity from MSCL-S, resistivity from MSCL-S.

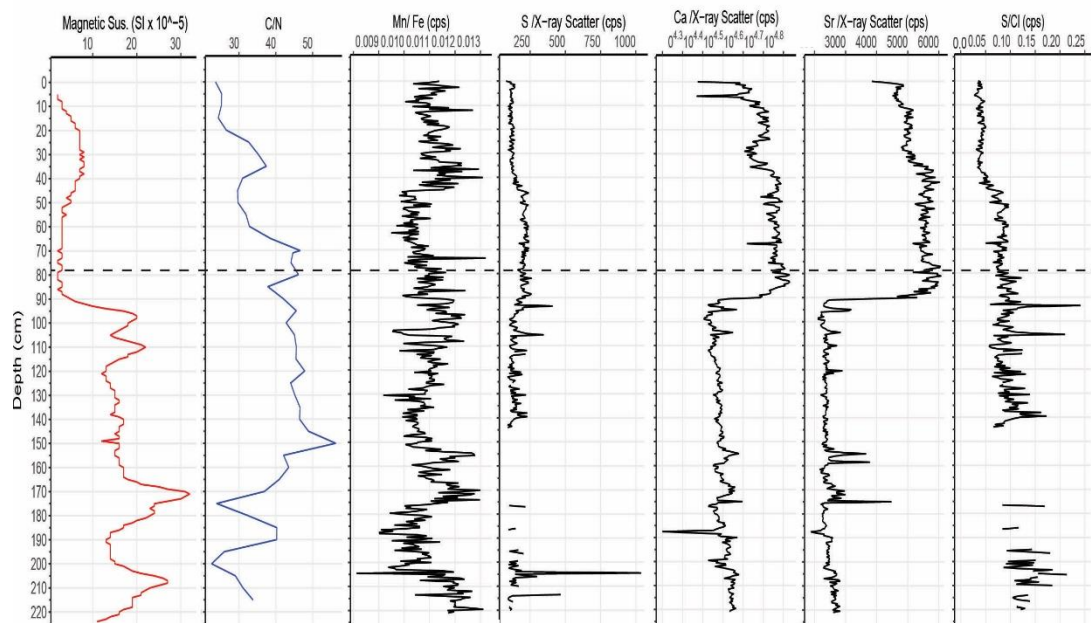


Figure 5.19. GC027: physical and chemical properties derived MSCL-XYZ and ITRAX respectively. (From left to right) magnetic susceptibility from MSCL-S, Manganese/Iron, Sulphur, Calcium, Sulphur/Chlorine content. Dashed line indicates break in the core sections (A & B).

5.4 Discussion

5.4.1 East of Eigg pockmark.

This following section includes the interpretations of cores GC021 and GC023 retrieved from inside and outside a pockmark to the East of Eigg.

A possible stratigraphic correlation can be made between these two cores when observing similarities in mean grain size derived from PSA at 5 cm downcore intervals. The trends in means grain size from 50 – 190 cm in GC023 and 100 – 240 cm in GC021, correlate well with one another (Figure 5.20a). GC023 preserves a record of Holocene sediments, deposited during full marine conditions, defined here as unit H1. This interpretation is supported by the homogenous, muddy sediment, bioturbation and shells, fine grain size and lack of clasts or ice rafted debris. This same unit (H1) can also be observed in core GC021 based on the near identical mean grain size. At 80 cm depth in GC021 these two cores differ in mean grain size, where the percentage of sand increases, resulting in an increased mean grain size. This is defined as unit P1 in GC021. As core GC021 is located inside a pockmark, this increase in mean grain size is interpreted to indicate a period of pockmark activity. Similar interpretations of pockmark activity relate to changes in grain size have been reported for pockmarks in the Aegean Sea, Greece (Ravasopoulos *et al.* 2002) and OsloFjord, Norway (Hammer & Webb 2010) and on the Indian continental shelf (Dandapath *et al.* 2010). As gas or fluid is released from seabed the resulting force sends the finer grain sizes into suspension leaving behind the larger grain sizes. The sediment grain size data within the upper part of core GC021, between 0 – 60 cm, does not correlate with the mean grain size of core GC023. This material may be the result of pockmark activity and/or the slumping of the pockmark side. This is identified as unit S/P2. Unit H2, recorded in GC023, seems to be missing from GC021, indicating that pockmark formation and/or related slumping activity may have occurred in recent times, therefore obscuring or reworking this unit. It is difficult to determine the timing of pockmark activity without any chronological control (e.g. radiocarbon dating), however, pockmark formation has likely occurred during the transition between H1 and H2 at 40 cm depth in core GC023. It is important to note that no obvious correlation can be made between cores based on the colour of the sediment. It is possible that despite the correlation between grain sizes that these cores cannot be stratigraphically correlated completely. Within GC021 a transition to green/yellow sediment colour is apparent indicating a possible change to sediments deposited during glaciomarine conditions. A similar colour change in GC023 cannot be observed, therefore the base of these core may not completely correlate well with one another.

The geochemical Mn/Fe ratio data can provide further insights into recent pockmark activity (Figure 5.20b). Under stable redox conditions it would be expected to see a single peak in Mn and Fe, indicating the redoxcline between the reduction and oxidation zone (Burdige 1993). It has been shown by other workers that a low Mn/Fe ratio indicates low oxygen concentration (Naehler *et al.* 2013; Makri *et al.* 2020). These low oxygen concentrations are associated with reducing conditions in marine sediments and would be expected within an active pockmark as expelled gas drives minerals and oxygen vertically into the water column (Panieri *et al.* 2017). GC023, retrieved from just outside the pockmark (~300 m to the South) shows a prominent peak in Mn/Fe at 30cm. This is interpreted as a long-lasting redox zone (Burdige 1993). Smaller peaks are also observed at 5 cm and 10 cm indicating that this redox zone has migrated in the past, possibly as a result of seasonal variations in hydrographic conditions (Burdige 1993; Makri *et al.* 2021). Overall, the sediment zone above 40 cm is considered sub-oxic and above 20 cm the sediment probably contains higher oxygen concentrations. The low surface values of Mn/Fe and structureless data from core GC021, indicate that reduction and release of Mn is probably occurring. Sulphur values are equally 'noisy' and lacking a clear trend in GC021, with only a subtle increase recorded at 40 cm and another increase at 100 cm, further emphasising that anaerobic reactions are probably taking place at various depths throughout this core. Taken together these anoxic conditions at the seabed (GC021) and comparing it to the sub-oxic to oxic sediments just outside the pockmark (GC023) it is believed that this indicates that this pockmark has probably been active recently.

Results also show that C/N values generally increase with depth in core GC021 up to a max value of 30, whereas there is no overall C/N trend in core GC023 with a single prominent peak to a value of 24 at 0.75 m depth. This provides an insight into the potentially rich organic content of sediments found at 0.5 - 2 m below seabed inside this pockmark where organic matter is available for microbial communities to consume and form carbon rich gases such as methane and CO₂. The possible high content of organic matter found at depth within pockmark sediments indicate that these sediments have also acted as suitable stores of 'blue carbon' over an extended period. However, with the remobilisation and reduction of metals the longer-term preservation of carbon is uncertain. It has also been shown that low Mn/Fe ratios correlate with high organic carbon content (Koinig *et al.* 2003), further confirming that reducing conditions occur near seabed in this pockmark East of Eigg. As MS values increase due to the presence of magnetic material, such as ferromagnetic minerals, this may provide a generally good indicator of the depth at which Fe sensitive redox reactions are occurring (Doh *et al.* 1988; Seeberg-Elverfeldt *et al.* 2005). What is also clear from this dataset is that gas-rich sediment is not confined

to the pockmark itself. Gas fractures within core GC023 are also observed, perhaps indicating that the potential for pockmark formation/ activity within the region of East of Eigg still exists. Based on the analysis of different datasets from cores GC021 and GC023, it is concluded that the pockmark of interest to the East of Eigg has been active within the Mid-Late Holocene (last 5000 years) due to the observed peak in mean grain size at 80 cm. After this fluid-release activity, the sides of the pockmark probably slumped due to the angle being greater than the sediments internal cohesive strength. The Mn/Fe profiles inside the pockmark (GC021) show low surface values, when compared to those of Core GC023, located just outside the pockmark. This is interpreted as showing that redox reactions within the pockmark have been significantly altered due to the venting of carbon-rich gases and the high content of organic matter. The future of preservation of this organic carbon (i.e. 'blue carbon') within the pockmark is uncertain. Although pockmarks, once inactive, can become suitable depocenter for sediments (Pau & Hammer 2013), without the sediment becoming oxidised again, oxidative reduction of organic matter may not occur for an extended time period. Studies have shown that the shallowing of the redoxcline happens over a shorter time frame than the downward migration of oxygen into the sediment column unless bioturbation or other mixing occurs (Hastings *et al.* 2016).

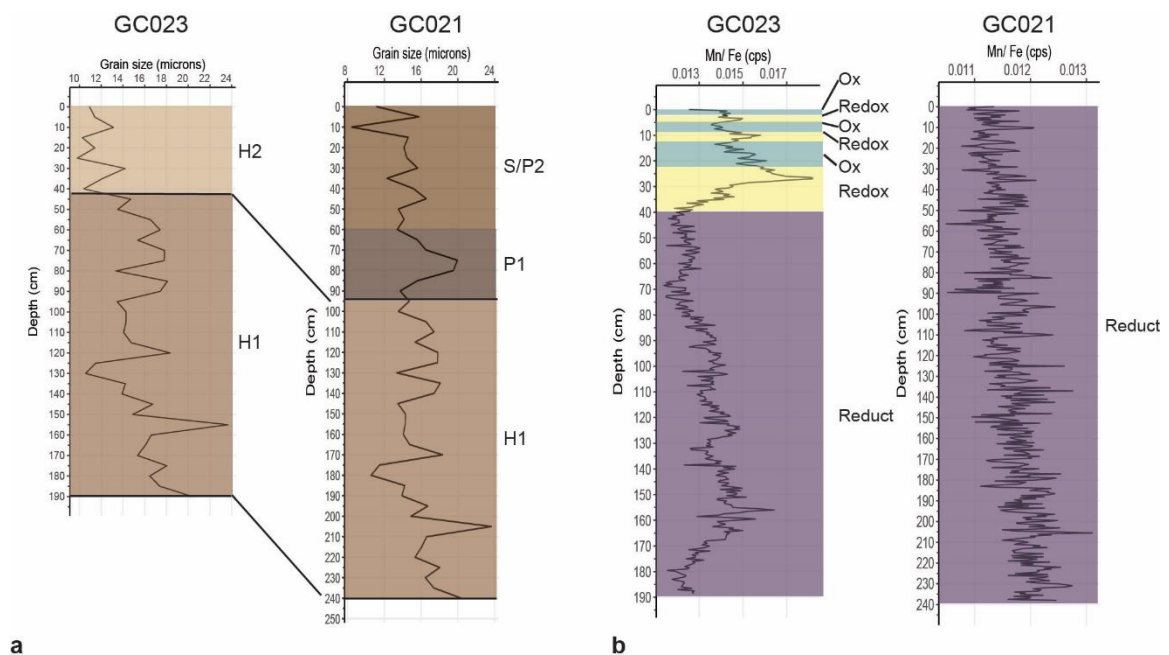


Figure 5.20. Interpretation of cores GC021 and GC023 from east of Eigg. **(a)** Mean grain size plots showing identified lithological units: H1:H2 – Sediments deposited within marine conditions during the Holocene, P1 – Pockmark activity, S/P2 – Slumping/ pockmark activity. **(b)** Manganese/Iron ratio profiles, showing identified Redox Zones: Ox – Oxidation zone, Reduct – reduction zone, Redox – Redox zone.

5.4.2 *Stornoway Bay pockmarks.*

This following section interprets the results from core GC006 and GC008, retrieved from outside and inside a pockmark in Stornoway Bay respectively.

Core logs of GC006 and GC008 show a similar lithological composition of homogenous clays/silt in both cores to a point. This changes at 160 cm depth in GC008 where the sediment becomes gradually coarser. This may be an indication of a change to glaciomarine conditions or alternatively indicate pockmark activity. This coarser unit is not present within GC006; however gas fractures are noted from 160 cm downcore. PSA was not conducted on this core and therefore stratigraphic correlation based on mean grain size (as above) is not possible. Since it is difficult to correlate the stratigraphy of these two cores it cannot be said with any confidence that these cores capture the same sediment record, especially since GC008 was taken within a pockmark where sediment has probably been expelled and has also experienced subsequent slumping and sedimentation. What the cores do show, is that shallow gas is located within these muddy sediments even outside regions of pockmark formation (GC006). Since no gas related fractures are present within GC008 it is difficult to tell whether the pockmark has been active recently or has the potential to be active. The likelihood is that this pockmark has sealed itself as material slumps from the pockmark walls, preventing gas from migrating to seabed at the same vent site, instead gas will preferentially migrate towards the weakened sediment structure along the pockmark sides; this could account for the deep and wide structure of this pockmark (Chapter 3). The self-sealing nature of pockmarks has been recorded from pockmarks in the North Sea (Hovland 2002; Gafeira & Long 2015a; Gafeira *et al.* 2018), northern Irish Sea (Coughlan *et al.* 2021) and northern Danish waters (Andresen *et al.* 2021), where it is believed to be the key process for the widening of pockmarks.

Micro-XRF data was analysed from cores GC008, and GC006 allowing interpretation to be made on the current redox state of these sediments (Figure 5.21). Since GC006 was retrieved from outside a pockmark it has not been affected by the flux of minerals and gas through the sediment column and therefore the redox conditions present here are interpreted as typical conditions for Stornoway Bay. This non-pockmarked site shows high surface values of Mn/Fe ratio measuring 0.012. Based on the downcore Mn/Fe profile the depth range of 0 – 5 cm is interpreted as sediment with a higher content of oxygen, where oxidation reactions are taking place. The secondary peak of Mn/Fe values indicates the depth at which redox reactions are taking place (<15 cm) therefore below this it is suggested that reduction reactions are dominant and the environment is considered

anoxic. The surface values of Mn/Fe ratio within core GC008 are highly variable covering the entire range of values for this core from 0.011 – 0.014. Since these values are equal to and greater to the surface values shown in GC006 the depth range of 0 – 5 cm is interpreted as oxic sediment. The decrease from a peak between 5 – 12.5 cm is interpreted as the minimum depth at which redox reactions are occurring and are likely to be sub-oxic. Below 12.5 cm is the range where reductions reactions are predominately taking place; this is characteristic of an anoxic environment.

C/N samples were not analysed for cores GC006 and GC008, therefore the S/Cl ratio is used as a proxy to indicate the organic matter content (Thomson *et al.* 2006). The ratio values for GC006 are similar to those found in core GC023 and ranges from 0.03 – 0.09. This may indicate a similar organic matter content between these two sites. However, the ratio for core GC008 is less than core GC021, 0.03 – 0.07 compared with 0.05 – 0.015,. Since S/Cl ratios are low inside the pockmark from Stornoway Bay (GC008), this could indicate that the organic matter has been removed by pockmark activity or the source of the gas is found deeper within the sediment. In the case of the first scenario, this indicates that pockmarks are important gateways for carbon to be reintroduced to the marine carbon cycle and therefore deserve special attention when quantifying the volume of blue carbon stored within shallow (<200 m) marine settings. The second scenario, where the possible source of gas is found deeper in the sediment indicates that pockmarks and their associated sedimentary facies could be used to identify possible thermogenic sources of gas deeper in the sediment sequence. It is well known that geological faults are present within the North Minch, parallel to the coast of Lewis near Stornoway, within potential thermogenic, hydrocarbon-bearing source rocks (Morton 1993). Seismic activity has been recorded as a possible trigger mechanism for pockmark formation elsewhere (Hasiotis *et al.* 1995; Kuşçu *et al.* 2005) but the close spatial association between the Stornoway Bay pockmarks and the underlying faults is highly suggestive of a link between seismicity and a gas-release source for pockmark formation. It is currently uncertain which scenario is most applicable to the Stornoway Bay pockmark strings, although a seismic origin for deeper-sealed gas escape is very possible.

Since Mn/Fe values are similar in both cores the investigated pockmark in Stornoway Bay is interpreted to be currently inactive and has probably been so for a long time. As the re-oxygenation of sediment happens over longer time scales than the consumption of organic matter via reduction reactions.

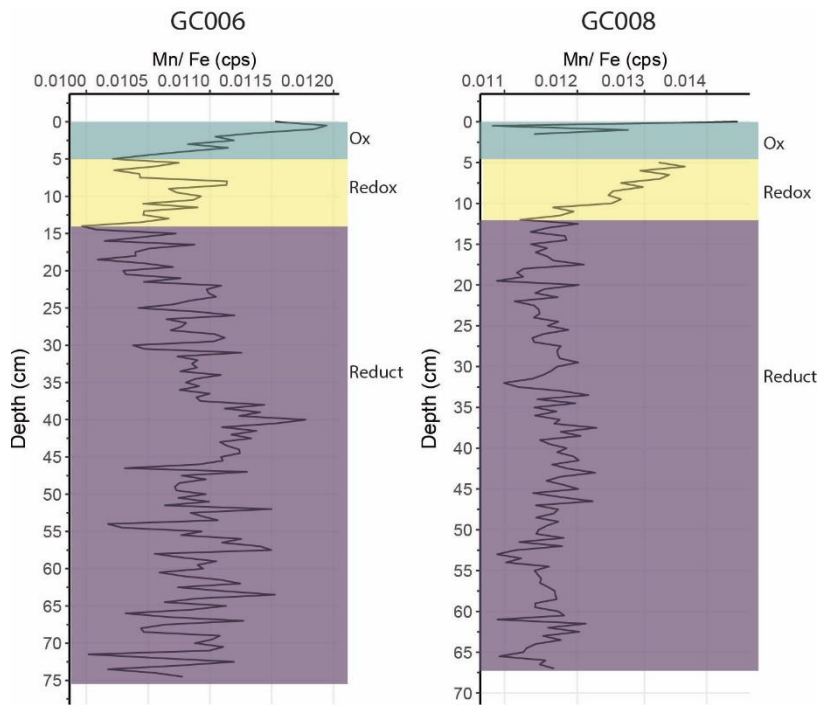


Figure 5.21. Interpretation of cores GC006 and GC008 from Stornoway Bay. Plots show the Manganese/Iron ratio profile, identifying Redox zones: Ox – oxidation zone, Reduct – reduction zone, Redox – redox zone.

5.4.3 Scotia pockmark.

The following section interprets the results from GC027, retrieved from inside the southern pockmark in the Scotia pockmark complex, North Sea.

Core GC027 clearly shows a more varied lithology and a different stratigraphic history from the cores taken in West coast waters. Since active venting of the Scotia pockmark (Figure 5.3) was observed on the science cruise in July 2019, it would be expected that the particle size analysis and various chemical profiles would reflect this. Mean grain size is greater than cores from around the West coast of Scotland, despite GC027 being located further offshore (>100 km). It is suggested that this coarser grain size range, from 20 – 60 microns, shows that this pockmark is regularly venting and removing the fine grain sizes, particularly within the uppermost 80 cm where the lowest percentage of clay was measured. The particle size analysis of core GC027 shows two primary mean grain size peaks at 35 cm and 65 cm where an increase in sand fraction is seen. These peaks are taken to reflect periods of sustained venting in this pockmark. Despite known activity during core recovery of the Scotia pockmark, no gas or gas related fractures are observed within the core. This may be due to this pockmark having a very focused venting site where gas is utilizing a pre-existing weakness. Due to the established self-sealing nature

of some pockmarks, it is expected that the venting sites of pockmarks to be mobile and probably migrate towards the flanks of the pockmark where weaknesses developed due to slumping. As such the pockmark can increase in diameter. This might explain the atypical size of the Scotia pockmark compared to the numerous smaller pockmarks located nearby (Gafeira & Long 2015b; Böttner *et al.* 2019). Therefore, it is suggested that the two peaks observed from the particle size analysis may reflect a time when the vent site was situated closer to the location of core GC027.

What is not captured in the PSA analysis is the increased grain size associated with the formation of magnetic, minerogenic particles or concretions below 90 cm (Figure 5.22). These magnetic concretions are interpreted as authigenic ferromanganese nodules that have formed around a small granular nucleus such as tephra or a shell. These concretions may have been inadvertently broken down during the analysis method and therefore their impact on grain size is not captured. Instead, the p-wave velocity and resistivity indicate a possible increase of mean grain size between 150 and 180 cm. This increase in grain size may not be associated with pockmark activity. The clear and abrupt change in the MS, Ca and Sr profiles at 90 cm indicate that this is a different lithological unit. The presence of lithic fragments from 91 cm depth provides further clues as to the origin of this lower unit. Due to the distance from shore, it is likely that these lithic fragments represent dropstones deposited by drifting icebergs during the retreat of glaciers from the last British and Fennoscandian ice sheets after the Last Glacial Maximum (Carr *et al.* 2006; Chiverrell & Thomas 2010). This unit between 90 cm and 225 cm depth in core GC027 is therefore interpreted as a glaciomarine sediment facies, deposited during the later stages of North Sea deglaciation. Although not dated in this core, this sediment unit is similar in character and physical properties to the Late Weichselian glaciomarine sediment deposited ca. 18-25 ka BP on the seafloor around the Shetland Islands and in the northern North Sea Basin (Bradwell *et al.* 2021). A similar trend in elemental profiles to that seen here is found in cores from the Scanner pockmark to the South of Scotia pockmark by Böttner *et al.* (2019). They also interpret this abrupt transition at Scanner pockmark as a change from glaciomarine to marine dominated sediments of the Holocene.

Because the Scotia pockmark is still (periodically) active and was cored during a period of gas-venting, it would be expected that the Mn/Fe ratio to capture the impact of migrating fluids on redox reactions at this site. From these results, the surface values are measured to be in the range of 0.011 – 0.013 (Figure 5.22). Based on these low values and the known activity status of the Scotia pockmark, these must reflect, at least, a suboxic zone where redox reactions are taking place. Below 50 cm the Mn/Fe ratio decreases rapidly

before plateauing and then increasing to a secondary peak at 95cm. This initial decrease is probably reflecting the occurrence of reduction reactions taking place within anoxic sediments. This is further supported by the initial rise in Sulphur content (Figure 5.19). Sulphur is reduced after Mn and Fe and therefore the peak in sulphur values is normally found stratigraphically beneath that of Mn and Fe (Albert *et al.* 1998). This is the case in this core, supporting the interpretation that this is the depth of where redox reactions are currently taking place.

The results from the C/N ratio show the highest recorded values in all the five cores analysed. The ratio of S/Cl is also the greatest, ranging between 0.05 – 0.25, with an increase at 40 cm, below this depth there is then an observed increase in C/N. These values and trends show that this setting is possibly an important store of carbon, potentially even more so than the fjordic environments. The volume of carbon stored further offshore Scotland is poorly quantified compared to the nearshore fjordic environments around western Scotland (Burrows *et al.* 2014; Smeaton *et al.* 2016, 2017, 2020). Consequently, future studies may need to focus on the importance of these offshore continental shelf environments as long term stores of sedimentary carbon.

It has been shown from the observation of a distinct acoustic flare emanating from the southern Scotia pockmark and the shallow redox conditions seen in core GC027, that this pockmark is still active. Due to the reduced height of this plume during the 30+ minutes of the survey it is suggested these are probably periodic events that are only active when gas pressure increases or a trigger mechanism such as seismic activity causes the release of gas.

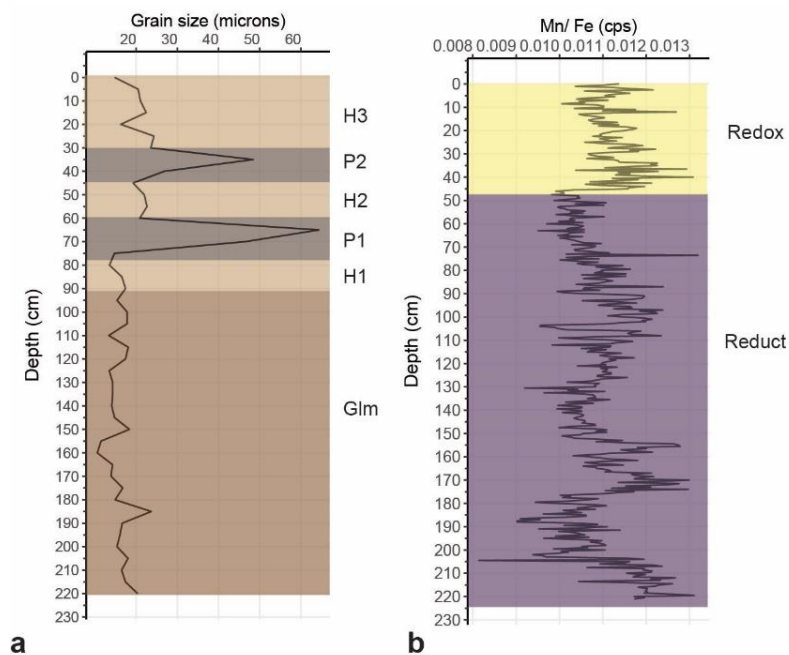


Figure 5.22. Interpretation of core GC027 from Scotia Pockmark, N. Sea. (a) Mean grain size, showing identified lithological units: G1m – Sediments deposited during glaciomarine conditions, H1:H3 – Sediments deposited during marine conditions of the Holocene, P1:P2 – Pockmark activity. (b) Manganese/Iron ratio profile, showing identified redox zones.

5.5 Conclusions

- It has been concluded that the use of X-ray, micro-XRF, and grain size analysis are useful tools to investigate pockmark activity status.
- It has been interpreted that the pockmark located East of Eigg in the Inner Sea of Hebrides has been recently active due to the differences observed in mean grain size and Mn/Fe profiles. This highlights the usefulness of grain size data and analysis of sediment cores using XRF methods.
- Clear signs of possible pockmark activity were not observed in the core logs or Mn/Fe profiles for the sediment core taken from a pockmark within Stornoway Bay. It is interpreted that this pockmark has not seen recent gas venting and is considered to be inactive over a considerable period of time.
- Despite clear signs of pockmark activity from the Scanner pockmark (North Sea) no signs of gas fractures are found within the core X-ray images. This suggests that the physical characteristics of the sediment at this site create highly focused venting sites that were not captured during coring.

Chapter 6: Discussion

6.1 Introduction

This PhD research investigates the formation, distribution and activity status of pockmarks in the nearshore waters of western Scotland. These have been achieved by focusing on three important areas of research: (i) the morphological characteristics of pockmarks; (ii) the distribution of pockmarks and free gas within sub-seabed sediments; and (iii) the chemical and physical stratigraphy of sediments from inside and outside pockmarks. The results and interpretation of these research topics are reported fully in Chapters 3, 4 and 5 respectively.

This chapter will focus on collating the findings from Chapter 3, 4 and 5 and discuss their significance regarding the formation and activity status of pockmarks. This first part of this chapter has been subdivided into sections discussing what the distribution of pockmarks and sub-seabed gas can tell us on the formation of pockmarks and how they can be used to identify organic rich sediments. The other subsection will discuss how morphological character and sediment stratigraphy can be used to infer pockmark activity. The second part of this chapter will discuss the relevance of pockmark research to geohazard assessment, benthic ecology and marine conservation. Finally, this chapter will suggest possible future research avenues and summarise the key findings of this PhD project.

6.2 Formation and distribution of pockmarks around western Scotland

6.2.1 *Distribution of pockmarks and its implications to their formation and organic carbon research.*

This research has mapped a total of 1015 pockmarks from high-resolution multibeam - echosounder bathymetry data in twelve study areas around western Scotland (Audsley *et al.* 2019). This has greatly extended the known number and distribution of pockmarks in Scottish waters (Howe *et al.* 2002; Stoker *et al.* 2006; McIntyre & Howe 2010; McIntyre 2012; Gordon *et al.* 2016). These pockmarks have been mapped within classic fjordic regions such as Loch Broom and Loch Linnhe, but also in fjord adjacent and extra-fjordic regions such as the Inner Sea of Hebrides and Stornoway Bay. The seafloors of fjordic regions have already been recognised as very important stores of organic carbon (Nellemann *et al.* 2009; Burrows *et al.* 2014; Smeaton *et al.* 2017, 2020). Western Scotland is therefore a very important region for research into the global sedimentary

carbon inventory. As this carbon is consumed by microbial activity, gases such as carbon dioxide and methane are produced (Whiticar *et al.* 1986; Flury *et al.* 2016). As these gases increase in volume and pressure builds beneath the surface, it is possible for pockmarks to form (Hovland 1989; Wessels *et al.* 2010; Szpak *et al.* 2015). Therefore these marine sedimentary stores can be characterised and may even be identified, by locations in which pockmarks were formed. This relationship in fjords has been suggested by others (Taylor 1992; Baltzer *et al.* 2005; Judd & Hovland 2007) and confirmed in this PhD project – with numerous pockmarks observed in gas-rich sediments on the floor of Loch Linnhe, Loch Broom and Loch Spelve.

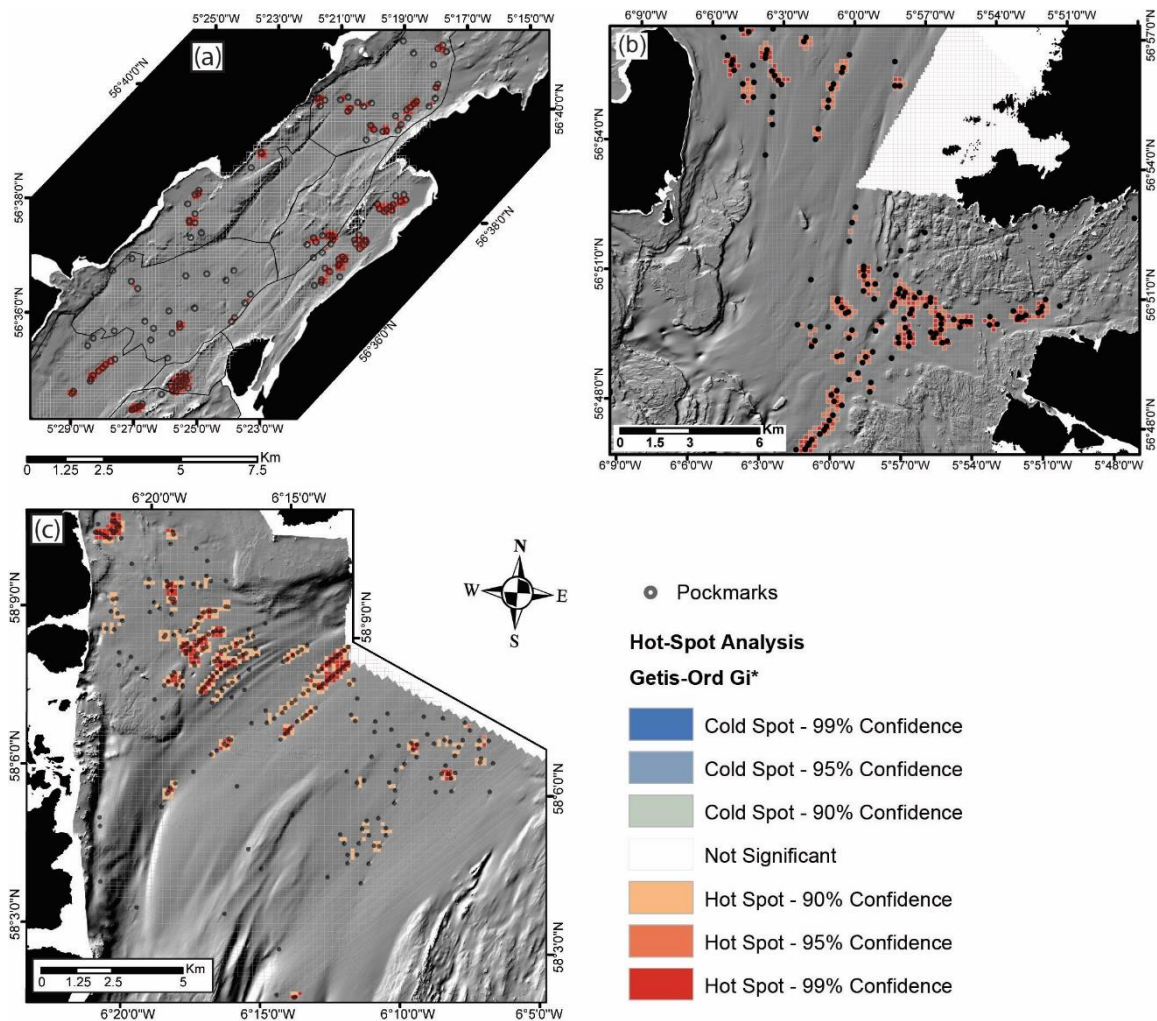


Figure 6.1 Pockmark hotspots in fjordic and extra-fjordic regions. (a) Loch Linnhe. (b) Inner Sea of Hebrides. (c) Stornoway Bay and North Minch.

However, a new and important finding from this PhD project, is that pockmarks have also formed on the seabed outside fjords, and in non-fjordic settings, such as those found within Stornoway Bay, the Inner Sea of Hebrides and the North Minch (Figure 6.1). Since

these seabed regions are further offshore and more exposed to currents they have previously not been considered as potentially large stores of organic carbon. Large distributions of pockmarks have been recorded in Maine, North America in regions described as temperate estuaries (Andrews *et al.* 2010; Brothers *et al.* 2012). Due to the distance from shore it could be argued that these regions could also be described as extra-fjordic, in that they exist outside the classical fjordic environment of an enclosed valley separated from open water by a series of sills. It was found that within these areas large numbers of pockmarks have formed in areas where the sediment thickness is greatest (Andrews *et al.* 2010). The sediment consists of buried peat stores and therefore contain a high mass of organic carbon (Brothers *et al.* 2012). This PhD project has mapped numerous pockmarks in these extra-fjordic environments of western Scotland; these can be atypically deep and even form large complex seabed features such as the strings of pockmark in the North Minch and Stornoway Bay. As a result of this mapping, these regions are also expected contain large stores of sedimentary organic carbon, which have not been previously considered in the accounting of national carbon inventories (Smeaton *et al.* 2017, 2020). Due to the findings from Western Scotland and in North American temperate estuaries it is likely that in regions adjacent to mid-high latitude fjordic settings, described here as extra-fjordic, containing large distributions of pockmarks are considered to be important stores of organic carbon.

The results from Chapter 3 show that it is important to consider the localised distribution and density of pockmarks, as this can indicate regions where high organic content sediment exists (Audsley *et al.* 2021). The statistical GIS-based analysis of pockmark distribution employed the concept of an exclusion zone (Cartwright *et al.* 2011; Moss *et al.* 2012b). This concept was applied to identify pockmarks 'hot-spots'; that is where more pockmarks were formed within the exclusion zone than would be expected (Moss *et al.* 2012b). Occurrence of these hotspots is interpreted to indicate regions where a single pockmark was unable to sufficiently reduce the gas pressure and therefore, to compensate, another pockmark formed within the exclusion zone to reduce the pressure. This is clearly the case in Loch Linnhe and the Inner Sea of Hebrides where pockmarks appear in discrete isolated clusters indicating localised depocentres of organic carbon rich sediments. This research suggests that organic carbon has been preferentially deposited in areas restricted by currents or in the lee of bathymetric obstacles such as moraines and bedrock highs (Audsley *et al.* 2021). In these locations gas build-ups have not been able to migrate laterally and reduce the pressure because of the constricting submarine geology. The only method of pressure release is gas-venting to seabed and the formation of a pockmark.

Conversely, in Loch Broom, Northwest Scotland, relatively few pockmarks are observed and yet the entire inner basin shows gas-rich sediment in geophysical (boomer) profiles. In this case the over-deepened inner basin of Loch Broom is the depocentre for organic carbon deposited during deglaciation. Presumably the gas pressures are low in Loch Broom and sub-seabed gas has been able to migrate laterally across the entire inner basin as it is not restricted by topographic/bathymetric obstacles. The few pockmarks that have formed in Loch Broom are likely the result of increased gas generation where sediment thickness is greatest or where slumping/ slope collapse has triggered the release of gas creating sudden pressure changes (Stoker & Bradwell 2009). Another possible mechanism is by rapid gas escape through hydrostatic pressure increase from sea-level changes. It has been suggested that Quaternary sea level changes are an important control mechanism for gas seep activity (Brothers *et al.* 2012; Riboulot *et al.* 2014). The complex and widely recorded evidence of sea level changes in Scotland (Smith *et al.* 2017) suggest that this is also a possible trigger mechanism for pockmarks in the studied regions.

Other seabed features formed due to the unique distribution of pockmarks can also provide clues to the formation mechanisms of pockmarks (Hovland 1981b; Pilcher & Argent 2007; Velayatham *et al.* 2018). In Stornoway Bay large curvilinear strings of pockmarks have formed and further eroded by currents to produce trough like features. These troughs are a particularly unique feature observed on the seabed across western Scotland, which deserve to be recorded within reports on the geodiversity of Scotland and encourage future research into their formation. These features may allude to the cause of pockmark formation being related to the presence of the major Minch fault present in this region (Hesselbo *et al.* 2010). This spatial relationship indicates that pockmark activity in Stornoway Bay may have been triggered by tectonic activity. Additionally, the presence of organic rich Jurassic source rocks are recorded within the bedrock sequence in Stornoway Bay (Graham *et al.* 1990; Smith 2012) and probably in the Inner Sea of Hebrides (Hesselbo *et al.* 2010; Smith 2012), which may indicate a possible, deeper-seated, thermogenic source of gas. However, this has not been proven in this study and other gas release trigger mechanisms must also be considered for Stornoway Bay, such as sea-level change. The location of pockmarks in Stornoway Bay is in the region of increased sediment thickness. This is likely high in organic carbon deposited distal to the glacier front, and could be the source of the gas found here. The trigger for the release of the gas could be changes in sea level (Smith *et al.* 2017) similar to the pockmark fields of Maine, North America (Brothers *et al.* 2012).

6.2.2 *Distribution of free gas in sub-seabed sediments*

Generally, the distribution of free gas in fjordic sub-seabed sediments, identified as acoustic turbidity in geophysical records, is similar to the distribution of pockmarks (Audsley *et al.* 2021). This finding is not surprising as pockmarks are taken by some previous workers as an indicator of shallow gas presence in sub-seabed sediments (Camargo *et al.* 2019). Geophysical records can, however, tell more about the likely source of the gas and the method of gas migration to seabed (Baltzer *et al.* 2005), as well as whether a pockmark is still likely to be active. Due to the shallow depth of the gas front in all regions around western Scotland, it is likely that the gas is mainly of biogenic origin. But there is still the possibility that gas within Stornoway Bay, the North Minch and the Inner Sea of Hebrides could contain thermogenic sources due to the presence of major faults and Jurassic source rocks (Graham *et al.* 1990; Smith 2012). However, it is most likely that even in these regions the gas is biogenic in origin – resulting from very high volume of organic matter deposited during the late Pleistocene and Early Holocene. Interestingly, the unusual strings of pockmarks that occur in Stornoway Bay is also where the sediment thickness is greatest, according to geophysical records.

Gas can be described as blankets in most regions around western Scotland due to the large lateral extent (>500m). Although it can also, locally, be found as curtains (100 m – 500 m wide) and plumes (<50 m wide) (Taylor 1992). It has been argued that the terms blanket and curtain do not add to our understanding of how gas migrates (Judd & Hovland 2007). However, this research has not only shown that these terms can allow for the identification of sub-seabed regions which are likely higher in organic content and could therefore be important when accounting for national offshore carbon inventories, but also give an indication to the activity status of pockmarks.

Using this understanding of how gas can migrate within marine sediments and the depth of the gas front it is possible to interpret whether pockmarks are inactive, likely to become active or still active. The most common example of gas presence, which is widely distributed in each study site is that of a 'gas blanket' or 'gas curtain'. A gas blanket is described as regions of acoustic turbidity which are >500m wide and gas curtain is a region of acoustic turbidity <500m wide (Taylor 1992). If the gas front is very shallow (0 – 6 msec TWTT) and widespread, in the form of a gas blanket or curtain, it is likely that the sediment has allowed the widespread lateral distribution of gas and is therefore probably of low pressure and not able to vent from the seabed; alternatively, it could be being consumed by microbial activity responsible for redox reactions (Figure 6.2a). As a result the pockmark may no longer be regularly active due to gas supply being of low pressure.

Gas is likely escaping in low volumes at the pockmark but also widely across the sedimentary basin where gas is observed. Similar interpretations are made in Eckernforde Bay where a well-studied region of acoustic turbidity exists (Abegg & Anderson 1997). This acoustic turbidity is in the form of an acoustic blanket and is located at approximately 1 m depth. Whiticar (2002) has shown that this methane is actively consumed at the SMTZ. It is therefore likely that regions presenting very shallow and widespread gas blankets are not responsible for pockmark formation or pockmark activity and are instead only emitting low volumes of gas not necessarily at the pockmark vent site. The interpretation of shallow gas curtains is the same as that of gas blankets. However, gas curtains may provide further indication as to the local geological controls on the distribution of gas. In the case of Loch Linnhe numerous gas curtains are observed to be limited in distribution due to local geological obstacles such as bedrock or glacial moraines (Figure 6.2b). In these settings localised depocentres of organic carbon have been developed leading to increased gas pressure. Therefore pockmarks which are fed by gas curtains within isolated sub-basins may be more regularly active.

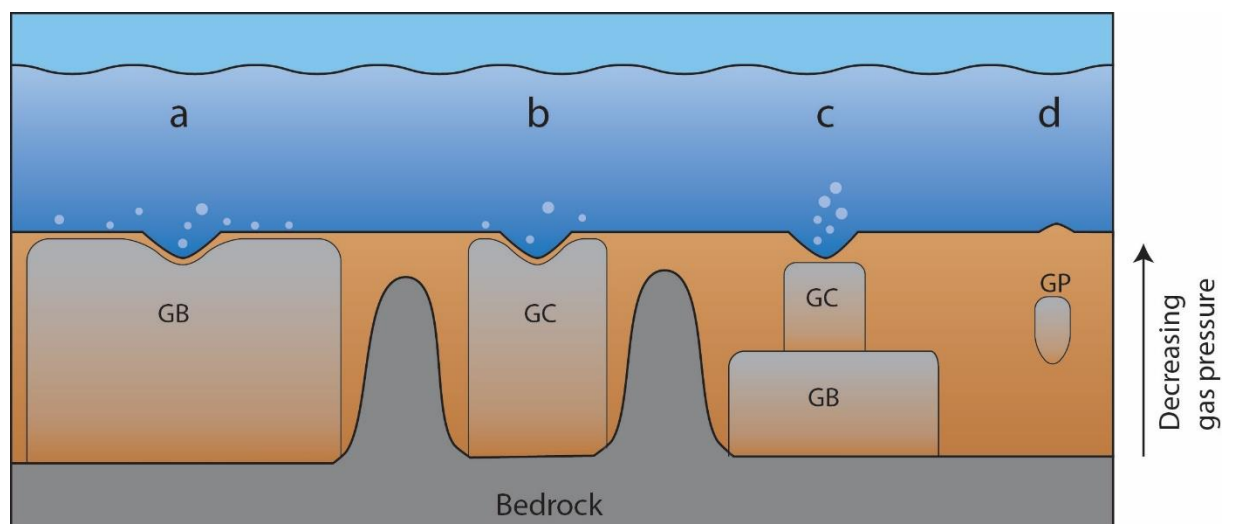


Figure 6.2. Conceptual model of acoustic facies associated with gas. GB – Gas Blanket, GC – Gas Curtain, GP – Gas Plume.

One form of acoustic turbidity which Hovland & Judd (2007) draw attention to is acoustic plume or gas plume. Gas plumes are used to describe a situation where the gas has made clear vertical migration path above the underlying gas front. However, this PhD project has shown that gas curtains should also be considered as an important distinguishing feature of acoustic turbidity that should be identified during analysis. This is of particular importance should the gas front be located deeper within the sediment (>10 msec TWTT) where the pressure is likely to be greater and, if a pockmark has not been formed

previously, pockmark formation could be imminent (Figure 6.2d). In Loch Linnhe, Western Scotland and in areas of the Norwegian Trench, North Sea and Irish Sea (Hovland & Judd 1988; Judd & Hovland 2007) areas of acoustic curtains can be seen rising from underlying gas fronts and therefore represent the vertical migration of gas considered of high importance by Hovland & Judd (2007). In Loch Tay, East Scotland a particular example of a gas curtain can be observed connecting the gas curtain with a pockmarks centre (Duck & Herbert 2006). In this case the identification of the gas curtain is of great importance as it suggests that this is directly feeding the pockmark resulting in gas release into the water column (Figure 6.2c).

6.2.3 The use of morphological characteristics for interpreting pockmark formation and activity status.

An important question when researching pockmarks is whether they are currently active or not. This is particularly relevant when considering a region for potential offshore development (Hovland *et al.* 2002; Andresen *et al.* 2021) and the possible role pockmarks have in supporting vulnerable biological biotopes (Webb *et al.* 2009b, a; Sánchez *et al.* 2021). The best evidence to answer the question of pockmark activity comes from images of active gas flares observed from acoustic imaging of the water column (Schneider von Deimling *et al.* 2015; Idczak *et al.* 2020). Pockmarks are generally considered to be, at most, periodically active and to observe an active gas flare from a pockmark is considered to be a rare event (Judd *et al.* 1997; Anderson *et al.* 1998). The problem is therefore how to interpret a pockmark's activity status solely based on other proxies such as morphology and/or sedimentological data.

In order to develop our understanding of pockmark activity status in the absence of observed gas flares, this PhD research measured the morphological characteristics of 1015 pockmarks around Western Scotland. There is growing agreement that the morphology of a pockmark is controlled by its activity status, development history and/or the hydrographic conditions of the region (Hovland 1983; Gafeira *et al.* 2012; Audsley *et al.* 2019; Coughlan *et al.* 2021). This PhD research used a statistically robust classification methodology of variations in pockmark morphology to develop a transferable classification system. By focussing on the vertical relief, elongation and/or area it has been found that it is possible to identify groups of similar morphologies which can shed light on pockmarks activity status and development history (Figure 6.3). Of the 1015 pockmarks mapped in western Scotland's waters, 176 belong to the "deep" class. It is inferred that these pockmarks have seen very low (or zero) sedimentation in the pockmark, whilst the surrounding seabed as seen normal sedimentation rates over relatively long periods of

time. This indicates that these pockmarks may have formed recently and/or been regularly or periodically active since formation. Such a classification system may aid future research in targeting specific pockmarks of interest and, with long-term monitoring, it should be able to observe periods of activity and calculate volumes of gas released. This statistically derived classification system will also enable a glossary of pockmark forms to be created, defined by robust morphological criteria (Audsley *et al.* 2019). This should remove numerous descriptive terms for pockmarks from literature which are sometimes synonymous and confuses the research, obscuring important forms of pockmarks which deserve further analysis (Judd & Hovland 2007; Chen *et al.* 2015).

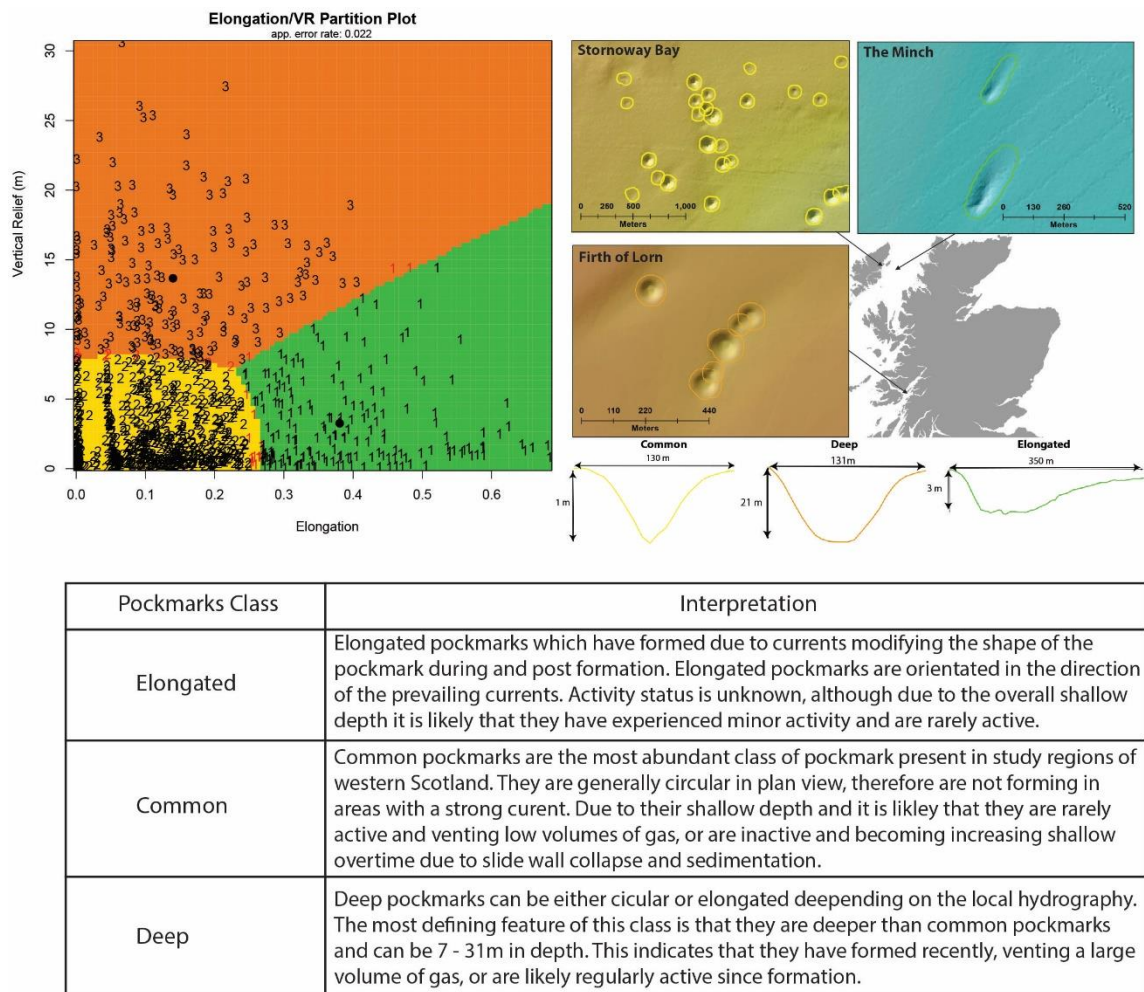


Figure 6.3 Classes of pockmarks around western Scotland. Determined from morphological classification. Table records the interpretation of these classes in terms of their development and possible activity status.

Pockmarks are also very abundant in the Witch Ground Basin, North Sea, UK and Norwegian sectors (Long 1992; Gafeira *et al.* 2012; Böttner *et al.* 2019). Other workers have shown that these pockmarks can be separated into two classes determined solely

by their morphological characteristics (Böttner *et al.* 2019). These are: Class 1 pockmarks, which are greater than 6 m deep, 250 m long and 75 m wide; and Class 2 pockmarks, which are <3 m deep, 26-140 m long and 14-57 m wide. According to these classes, the majority of pockmarks around western Scotland would be included within Class 2. There are pockmarks which are greater than 6 m deep around western Scotland such as those found in Stornoway Bay, Inner Sea of Hebrides and Loch Linnhe. Following the classification system developed for pockmarks of the North Sea, the 'deep' pockmarks of western Scotland would be defined as a Class 1 pockmark. However, in comparison to the Class 1 counterparts in the Witch Ground Basin, North Sea, the pockmarks of western Scotland can be much deeper than 6 m. Therefore this would suggest that the 'deep' pockmarks of western Scotland are actually a class of their own, and cannot be directly related to Class 1 / Class 2 Pockmarks of Witch Ground Basin, North Sea. In fact it is likely that these deep west-coast pockmarks have experienced much greater levels of gas-venting than those Class 1 pockmarks in the North Sea. This highlights the need for an advanced classification system for pockmarks, which takes into account the morphological characteristics of pockmarks from different geographic areas.

6.2.4 Pockmark activity status inferred from physical and chemical stratigraphy of sub-seabed sediments

This PhD research has also collected, for the first-time sediment cores from inside and outside pockmarks from around Scotland. Because of the time and lab constraints only two pockmarks could be targeted for further analysis. These pockmarks were identified as belonging to the "deep" class during the morphological analysis and are therefore considered to have been recently and/or periodically active. Using a variety of analytical instruments, measuring physical and chemical properties at mm-scale resolution, it was possible to investigate whether gas migration has left an imprint within the sedimentological properties. This project found that gas can be present in the uppermost 2 metres of the seabed sediment, within and near pockmarks, as evidenced in numerous distinctive gas fractures captured in X-ray images. These images show that gas fractures appear as either sub-vertical 'flame-like' structures within the centre of the sediment core (typically 1 mm wide and 20-140 mm long), or as small randomly scattered (expansion) fractures (typically 0.4 mm wide and 2-6 mm long).

This project also found that gas venting has probably caused a shallowing of the redox zone, using Mn/Fe as a proxy (Froelich *et al.* 1979; Naeher *et al.* 2013). From this interpretation it is thought that the studied pockmark analysed from the East of Eigg has likely been active recently, although the timing for this event is still unknown. The studied

pockmark in Stornoway Bay does not show this shallow redox zone and is therefore believed to no longer be (regularly) active. Interestingly, although both of these pockmarks are classed as “deep” (Audsley *et al.* 2019) this high-resolution geochemical analyses suggest that the depth profile may not always be indicative of recent activity status.

The deep pockmarks of Stornoway Bay and Inner Sea of Hebrides are comparable to the giant Class 1 pockmarks of the North Sea (Böttner *et al.* 2019). These North Sea pockmarks include the Scanner, Scotia and Challenger pockmarks which are thought to have formed by the release of biogenic **and** thermogenic gases (Hovland & Sommerville 1985; Böttner *et al.* 2019). Although it is unlikely that all “deep” pockmarks of western Scotland have a possible thermogenic gas source, the recorded presence of organic-rich Jurassic source rocks in these locations means that this source cannot be ruled out (Graham *et al.* 1990; Hesselbo & Coe 2000; Hesselbo *et al.* 2010; Smith 2012). A possible thermogenic origin of gas at these sites may also account for their linear distribution patterns. This could be a key avenue for future research interested in the formation of deep pockmarks and their activity status.

6.3 Active venting of the Scotia Pockmark

The Scotia pockmark, Central North Sea, fell outside the original study area of this project, however it provided some of the best evidence of pockmark activity in UK waters. During MRV Scotia cruise (SA1019S) in July 2019, good sea conditions and efficient core recovery allowed for additional areas of interest to be added to the cruise plan. This included a cruise track to survey the Scanner and Scotia pockmark SAC (JNCC 2018). During the initial survey, the EK60 echo sounder imaged a distinct gas flare in the water column emanating from the Scotia pockmark (Figure 6.4). Most observations of pockmark activity in this region come from the Scanner pockmark, South of the Scotia pockmark, known to contain MDAC (Hovland & Sommerville 1985; Gafeira & Long 2015b; JNCC 2018). The gas-venting captured by SA1019S from the Scotia pockmark is probably the first detection of gas flaring since the pockmark was discovered in 1983 (Hovland & Sommerville 1985). The images from the two EK60 transits across the Scotia pockmarks have shown that this period of activity lasted >30 minutes. Due to the perceived rarity of observing active gas venting, it is believed that the Scotia pockmark is therefore regularly active. The return period between active venting is still unknown, along with the volume of gas emitted. Future research at this large and active pockmark should focus on obtaining a detailed understanding of the long-term activity status and the implications it may have on biological communities present. Obtaining new data on well known, large

pockmarks in the North Sea Basin, such as this could provide an interesting comparison between the nearshore / fjordic pockmarks of western Scotland and those further offshore.

Interestingly a single gravity core retrieved from the Scotia pockmark showed no gas fracturing in X-radiographic images. The geochemical XRF stratigraphy of the core also did not prove conclusively whether the redox zone is atypically shallow due to gas release which would be expected, and yet the pockmark is most definitely active based on the echosounder images of an active gas flare in the water column. This may be due to the glacial and geological history of the region and the resulting sediment stratigraphy (Böttner *et al.* 2019). Cohesive glaciomarine muds are found as shallow as 90 cm within the Scotia pockmark. These muds are highly cohesive with a high shear strength, meaning gas pressures would have to be high enough in order to overcome this. It is believed that gas venting at the Scotia pockmarks and other giant pockmarks of the North Sea occurs at highly focused vent sites. This could explain the lack of gas fracturing within the core, which may not have directly cored the vent site, and yet the observation of an active gas flare present.

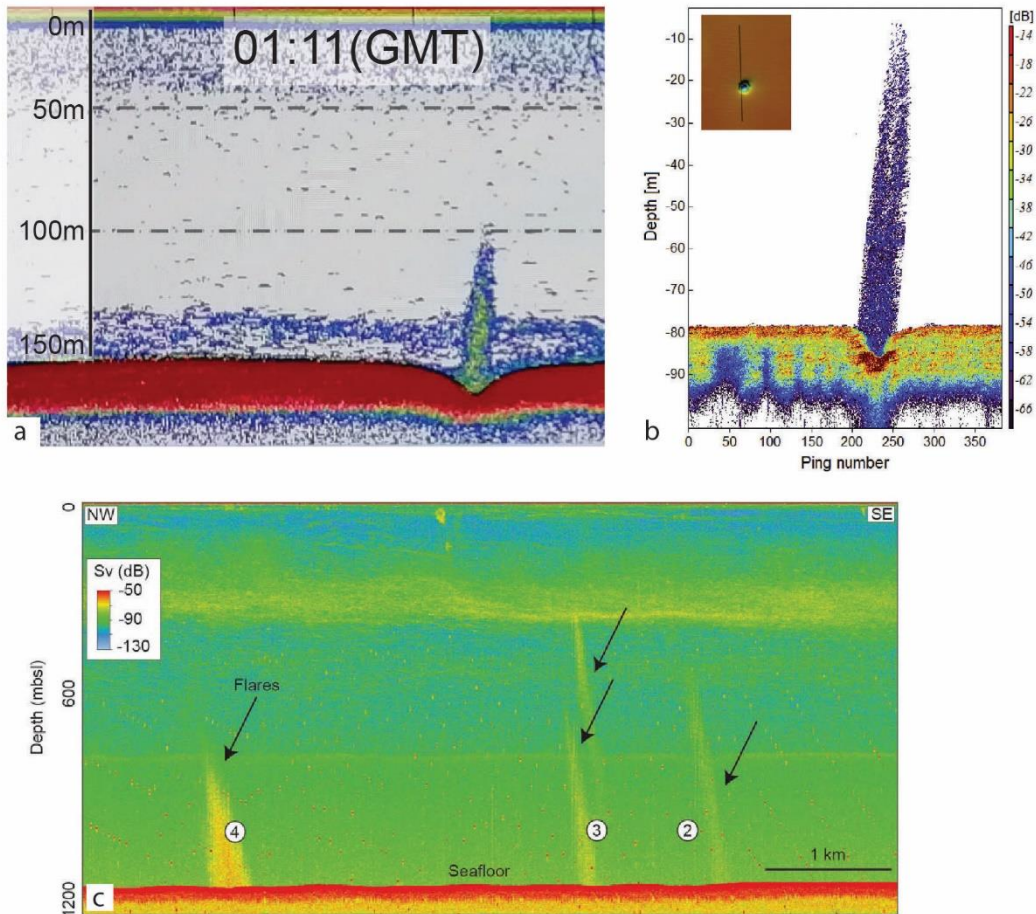


Figure 6.4 Echograms showing gas flares released from seafloor. (a) Gas flare released from Scotia pockmark, North Sea captured during this PhD and is likely biogenic/thermogenic. (b) Gas flare released from the MET1-BH pockmark, Baltic Sea (Idczak *et al.* 2020) and is likely biogenic. (c) Gas flares from Vestnesa Ridge Svalbard, gas is from dissociated gas hydrates (Smith *et al.* 2014)

6.4 Implications of pockmark formation

6.4.1 Geohazard

Pockmarks are generally considered to be geohazards due to their formation by gas release and associated decreased stability of sediments (Fannin 1979; Camargo *et al.* 2019). The identification of shallow gas and assessment of its potential risk to offshore infrastructure is vitally important during geohazard evaluation as it can lead to gas-blowouts or undermine infrastructure leading to loss of property or even life (Hovland 2002; Orange *et al.* 2005; Camargo *et al.* 2019). The oil and gas industry will meander pipelines through pockmarks fields in order to avoid pressurized shallow gas accumulations which adds to the cost of pipeline construction (Hovland *et al.* 2002).

Additionally whenever there is a need to install anchors for drilling vessels and offshore platforms be they for the oil and gas industry or renewables, pockmark occurrences must be assessed and taken into consideration (Shmatkova *et al.* 2015; Camargo *et al.* 2019).

Although the historical assessment of pockmarks is that they are to be considered geohazards, recent studies have argued that in some cases pockmarks can actually enhance seafloor stability (Riboulot *et al.* 2019). In an area of mass-movement and slope failure, 65 km offshore Nigeria, a small pockmark field was observed to have diverted the flow of sediment. It is believed that this was due to the pockmarks modifying the shear strength of surrounding sediments (Riboulot *et al.* 2019). Although it is suggested that this may only occur when sub-seabed sediments have been cemented by carbonate precipitation or when a weak basal shear layer has been drained of fluids and becomes more consolidated (Locat *et al.* 2014; Riboulot *et al.* 2019). Theoretically pockmarks act as natural vent sites that formed as a means to reduce gas pressures in a region. The resulting vertical heterogeneities or chimneys created by gas-escaping from a pockmark enable it to become the preferred pathway for future gas venting. This hypothesis is based on the concept of an exclusion zone around pockmarks (Cartwright *et al.* 2011; Moss *et al.* 2012b). Gas within an exclusion zone will preferably migrate towards the closest pockmark making it an effective sub-seabed fluid drainage cell (Moss *et al.* 2012b).

The results of this PhD research suggest that pockmarks around western Scotland are not necessarily dangerous geohazards and may not pose potential risk to seabed infrastructure. This conclusion stems from the fact that the majority of pockmarks mapped are small in area and shallow in depth and are therefore likely to be inactive. The larger pockmarks mapped identified in this study may potentially, at most, only be periodically active, although due to the widespread distribution and shallow depth to the gas front, it is likely that only low volumes of low pressurized gas is released. Typically, low energy fluid seeping is more likely than high energy venting around western Scotland. Therefore, the pockmarks around western Scotland should be considered as a logistical obstacle to offshore developments such as submarine cables. Regions with pockmarks should not be presumed as geohazards whereby limiting the areas possible for offshore infrastructure but should be assessed on a case by case basis.

Pockmarks are also known to form in areas affected by mass movement, slope failure events and earthquakes (Hovland *et al.* 2002; Judd & Hovland 2007). It has been recorded that pockmarks can become active and form before and during earthquakes and could act as a early warning system for earthquakes in regions which are vulnerable by such natural disasters such as in the Gulf of Corinth (Soter 1999; Hovland *et al.* 2002), Gulf of

Patras, Greece (Hasiotis *et al.* 1995; Marinaro *et al.* 2006) and the Gulf of Izmit, Turkey (Kuşçu *et al.* 2005). However, this type of early-warning system would require the deployment of long-term moorings capable of measuring temperature and pressure changes at pockmarks associated with major faults. Such systems have been developed and deployed at certain pockmarks in Greece (Marinaro *et al.* 2004, 2006) and in several locations of the Mediterranean (Monna *et al.* 2013). The use of these “benthic observatories” were the first long-term monitoring of gas venting from pockmarks – recording more than 60 events associated with gas venting over 6.5 months (Marinaro *et al.* 2006). Using a system similar to the ‘benthic laboratory’ it would be possible to monitor key pockmarks, identified in this research, which are believed to be still active. Pockmarks around western Scotland are also in regions effected by earthquakes, such as those recently recorded near Loch Linnhe and beneath Loch broom (https://earthquakes.bgs.ac.uk/earthquakes/recent_uk_events.html [accessed 14/12/2021]). Use of a gas monitoring array, deployed at selected pockmarks in Scottish inshore and offshore waters would make it possible to identify and measure periods of gas-venting activity, the concentration of released methane, and identify specific triggers for gas venting such as storm surges and earthquakes.

6.4.2 *Biological communities*

It has been suggested that pockmarks can be an important ecological niche for marine communities which require a heterogenous substrate and can utilize nutrients made available by seabed fluid release (Webb *et al.* 2009b; Champilou *et al.* 2019; Sánchez *et al.* 2021). Ecological studies on the giant pockmarks of the North Sea, namely Scanner, Scotia and Challenger have shown that the abundance of marine life is doubled within pockmarks when compared to the surrounding seabed (Webb *et al.* 2009b). Some of these giant pockmarks can also host exposed hard concretions, likely Methane Derived Authigenic Carbonates (MDAC) (Hovland & Sommerville 1985; Gafeira & Long 2015b; JNCC 2018). These provide a unique shelter and structure for colonisation. These pockmarks have been designated as Special Areas of Conservation due to the presence of geological structures (MDAC) made by fluid release. Thanks to the protection status such as SACs and the presence of hard substrates, these giant pockmarks of the North Sea provide a good level of protection from trawling activity. This is essential for slow-growing vulnerable benthic species such as gorgonian corals, present within the Scanner pockmark (Webb *et al.* 2009b) or the recently designated OSPAR threatened and declining species of *Haploops* present in pockmarks offshore Brittany (Champilou *et al.* 2019).

For western Scotland's pockmarks, there is little understanding of what role they provide if any, for supporting biological communities. Some pockmarks, identified in this study, have shown to be deep and steep sided, therefore it is very possible that marine life in these pockmarks have been protected from the damaging effects of trawling. The *Nephrops* (*Nephrops norvegicus*), or Scottish langoustine, fishery of western Scotland is the second most valuable fishery in Scotland, upon which many coastal communities depend (Williams & Carpenter 2016; Scottish Government 2019). Income from the Scottish *Nephrops* fishery in 2018 was £63 million; which is 11% of the total value of all landed species (Scottish Government 2019); with certain west-coast fishing towns / pots depending very heavily on the *Nephrops* sector.

Much of the seabed around western Scotland is considered to be a suitable habitat for *Nephrops* (Figure 6.5(a)). However this is based on analysis undertaken in the 1990s (Coull *et al.* 1998) and now outdated in terms of our understanding of seabed habitats (Vasquez *et al.* 2021). Numerous towed-camera surveys have been used to observe and estimate *Nephrops* burrows and populations such as those conducted within the Firth of Clyde (Campbell *et al.* 2009). Additionally, the UK Vessel Monitoring System (VMS) can be used as a proxy for the location of *Nephrops* habitats (Figure 6.5(b)). This shows that regions where *Nephrops* have been observed using underwater cameras are also the most visited by fishing boats and are greatly affected by trawling. The figures show that the highest densities of *Nephrops* burrows are located in the Firth of Clyde (Figure 6.5(c)).

Pockmarks around western Scotland are an abundant seabed feature in regions where high intensity trawling activity occurs. (Audsley *et al.* 2019). *Nephrops* have been recorded within North Sea pockmarks (Rance *et al.* 2017) and the Irish Sea (Reilly *et al.* 2012) but no studies currently exist on *Nephrops* in the nearshore Scottish pockmarks. It is unclear from the ecological literature whether pockmarks can be isolated oases for unusual levels of marine species abundance. However, anecdotal evidence from fisherman in the North Sea (Judd & Hovland 2007) and the few studies on the marine biological impact of pockmarks (Rance *et al.* 2017) seem to suggest they might be breeding grounds for numerous benthic species depending on activity status. If pockmarks do provide a suitable environment as breeding/ nursery grounds for *Nephrops*, where they are protected from trawling, they might be providing an essential ecosystem service for sustaining the valuable fishery. The possible link between pockmarks as unique benthic biotope for marine life should be the focus of future research when seeking to establish new marine protected areas in Scottish waters on geoconservation or biodiversity grounds.

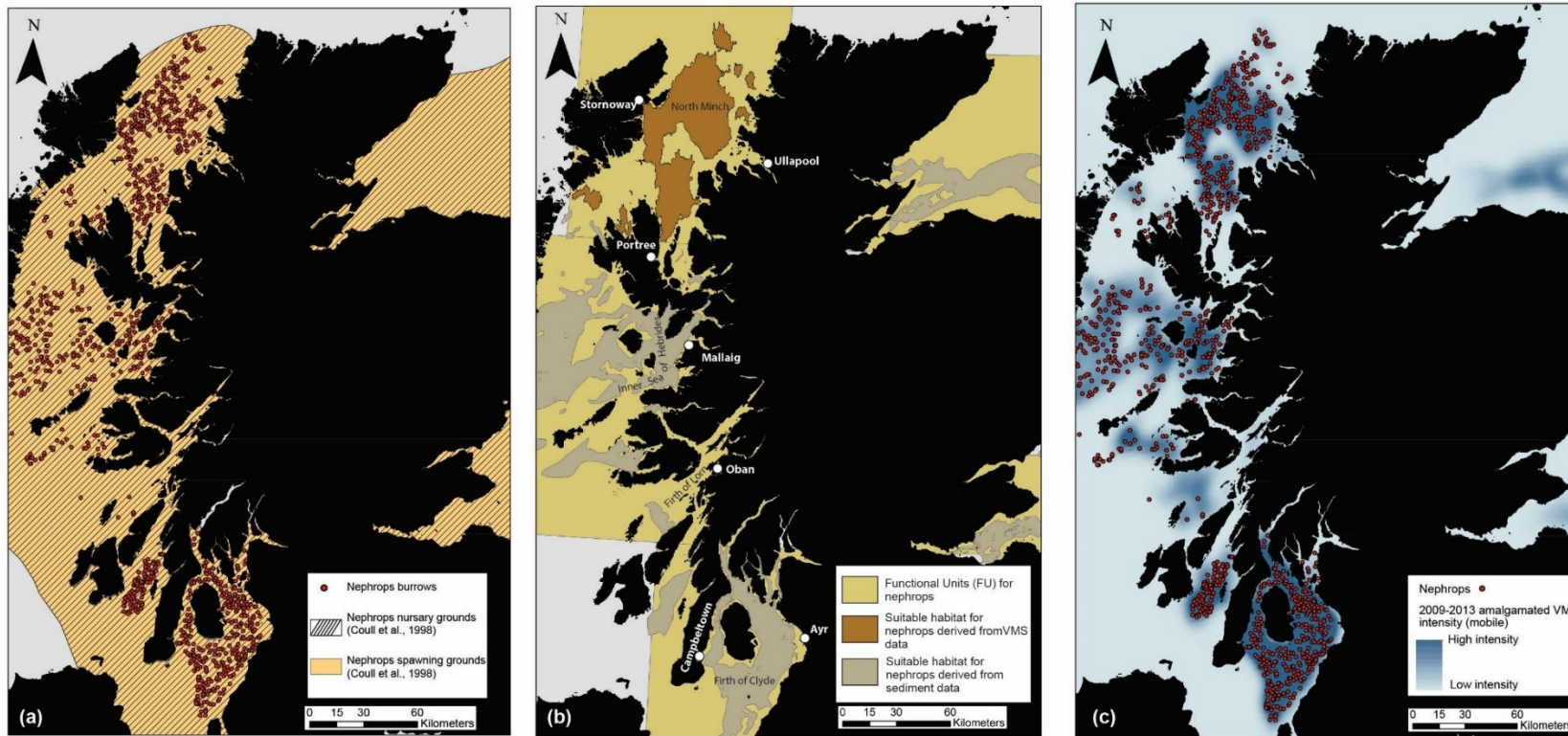


Figure 6.5(a) Spawning and nursery grounds for *Nephrops* (Coull et al. 1998) and *Nephrops* burrows identified from Underwater Television (UWTV) surveys. (b) Suitable habitats for *Nephrops* identified from ICES Functional Units, Vessel Monitoring System (VMS) and distribution of muddy sediment. (c) *Nephrops* burrows identified from UWTV and trawling intensity derived from VMS data.

6.5 Future Research

Future research into pockmarks on the seabed around Scotland and elsewhere should focus on developing a standardised glossary of pockmark types which are defined by set morphological criteria. This would simplify the identification and description of pockmarks and highlight unique morphologies that require further research. This would be especially important when investigating pockmark activity status by identifying pockmarks which are atypically deep when compared to surrounding pockmarks and may have formed recently and/or remained periodically active.

This PhD research has also highlighted the usefulness of acoustic instruments, such as EK60 echo-sounders, to observing active gas flares. Such equipment can be found on all UK research vessels and similar systems, referred to colloquially as “fish-finders”, are present on most commercial fishing vessels. Should a database be created to collect and store these datasets, combined with the updated dataset presented here showing the location of pockmarks, the chances of capturing pockmark venting in UK waters would greatly increase. These results would not only provide valuable information on the activity status of pockmarks but most importantly provide information on the approximate volumes of gas emitted.

Long-term “benthic observatories” could also be deployed to target specific pockmarks, believed to be active. These would be designed to measure the duration of venting periods and the concentration of methane being emitted. These instruments would shed valuable light on the difference in venting patterns and could establish, the most likely triggers of gas release (e.g. storms, seismic activity etc.). By developing a statistically robust methodology able to predict pockmark activity status based on morphology it would be possible to estimate volume of gas release and help to target pockmarks which require habitat surveys and potentially protection status.

Targeting these areas of research would aid our understanding of pockmark activity status and volumes of gas being released from the sub-seabed. Such research would be necessary to answer the following specific questions:

- Do different classes of pockmark experience different levels of gas venting?
- Where does gas venting take place within an existing pockmark field, and how widespread across the UK EEZ does gas venting occur?
- What volume of gas is released in the water column on an annual scale, and is it affected by storm or earthquake activity?

This is not an exhaustive list as the understanding of pockmarks within the carbon cycle remains unclear.

6.6 Summary and Conclusions

The aim of this PhD project was to investigate the formation, distribution and activity status of pockmarks around western Scotland. This was achieved by focusing on three areas of research detailed in Chapters 3, 4 and 5. The results of these chapters have significantly increased our understanding of how the distribution of pockmarks in Scottish waters can aid our understanding of their formation and indicate the presence of carbon rich sediments. These research results have also shown that it is possible to infer the activity status of pockmarks based on morphological characteristics and geochemical sediment stratigraphy. The findings are directly relevant to the development of offshore marine industries, especially where pockmarks are considered as geohazards. These findings also have far-reaching implications for marine protection and conservation efforts, as pockmarks are likely to be important, possibly unique, sites of benthic diversity.

The key findings of this PhD are as follows:

- The locations of 1015 pockmarks have been mapped in 12 study areas of western Scotland. Using a robust statistical classification methodology, it is possible to separate pockmarks into classes based on their morphological characteristics; these include: deep, common and elongated pockmarks. These pockmark classes can be used to infer the activity status/ development history. 'Deep' pockmarks are of particular interest as they may have recently formed and/or have experienced regular periods of activity.
- Pockmark hot-spots have been identified in fjordic and extra-fjordic settings around western Scotland. These hot-spots may indicate areas where there is a higher volume of organic carbon stored. These can be found as localised depocentres such as in Loch Linnhe, or more widely distributed such as in Stornoway Bay. This analysis highlights that important and possibly large volumes of organic carbon can be found in extra-fjordic regions, which have not been previously accounted for in national marine carbon inventories.
- The activity status of a pockmark can be potentially inferred from the geochemical/ physical stratigraphy of sediment cores recovered from inside a

pockmark. This is possible by measuring the Mn/Fe ratio which I used as a proxy for sub-seabed redox conditions. It is interpreted that an active pockmarks will cause anoxic sediments which is indicated by a shallow redox zone. It is also found that gas can be present in the first 2 metres of seabed sediments, which can be seen as low-density sub-vertical fractures in X-radiography images.

- This research has observed perhaps the first recorded gas flare emanating from the Scotia pockmark, North Sea since its discovery in 1983. The flare can be seen to reach heights of ~50 m above seabed and can last for periods of 30 minutes or greater. This highlights the functionality of echosounders found on most research and commercial vessels for capturing gas-venting events.

References

- Abegg, F. & Anderson, A.L. 1997. The acoustic turbid layer in muddy sediments of Eckernförde Bay, Western Baltic: Methane concentration, saturation and bubble characteristics. *Marine Geology*, **137**, 137–147, [https://doi.org/10.1016/S0025-3227\(96\)00084-9](https://doi.org/10.1016/S0025-3227(96)00084-9).
- Albert, D.B., Martens, C.S. & Alperin, M.J. 1998. Biogeochemical processes controlling methane in gassy coastal sediments - Part 2: Groundwater flow control of acoustic turbidity in Eckernförde Bay Sediments. *Continental Shelf Research*, **18**, 1771–1793, [https://doi.org/10.1016/S0278-4343\(98\)00057-0](https://doi.org/10.1016/S0278-4343(98)00057-0).
- Algar, C.K. & Boudreau, B.P. 2009. Transient growth of an isolated bubble in muddy, fine-grained sediments. *Geochimica et Cosmochimica Acta*, **73**, 2581–2591, <https://doi.org/10.1016/j.gca.2009.02.008>.
- Algar, C.K. & Boudreau, B.P. 2010. Stability of bubbles in a linear elastic medium: Implications for bubble growth in marine sediments. *Journal of Geophysical Research: Earth Surface*, **115**, 1–12, <https://doi.org/10.1029/2009JF001312>.
- Anderson, A.L., Abegg, F., Hawkins, J.A., Duncan, M.E. & Lyons, A.P. 1998. Bubble populations and acoustic interaction with the gassy floor of Eckernförde Bay. *Continental Shelf Research*, **18**, 1807–1838, [https://doi.org/10.1016/S0278-4343\(98\)00059-4](https://doi.org/10.1016/S0278-4343(98)00059-4).
- Andresen, K.J., Dahlin, A., Kjeldsen, K.U., Røy, H., Bennike, O., Nørgaard-Pedersen, N. & Seidenkrantz, M.S. 2021. The longevity of pockmarks – A case study from a shallow water body in northern Denmark. *Marine Geology*, **434**, <https://doi.org/10.1016/j.margeo.2021.106440>.
- Andrews, B.D., Brothers, L.L. & Barnhardt, W.A. 2010. Automated feature extraction and spatial organization of seafloor pockmarks, Belfast Bay, Maine, USA. *Geomorphology*, **124**, 55–64, <https://doi.org/10.1016/j.geomorph.2010.08.009>.
- Arosio, R. & Howe, J. 2018. Lateglacial to Holocene palaeoenvironmental change in the Muck Deep, offshore western Scotland. *Scottish Journal of Geology*, **54**, 99–114.
- Arosio, R., Dove, D., Ó Cofaigh, C. & Howe, J.A. 2018. Submarine deglacial sediment and geomorphological record of southwestern Scotland after the Last Glacial Maximum. *Marine Geology*, **403**, 62–79, <https://doi.org/10.1016/j.margeo.2018.04.012>.

- Atwood, T.B., Witt, A., Mayorga, J., Hammill, E. & Sala, E. 2020. Global Patterns in Marine Sediment Carbon Stocks. *Frontiers in Marine Science*, **7**, 1–9, <https://doi.org/10.3389/fmars.2020.00165>.
- Audsley, A., Bradwell, T., Howe, J.A. & Baxter, J.M. 2019. Distribution and classification of pockmarks on the seabed around western Scotland. *Journal of Maps*, **15**, 807–817, <https://doi.org/10.1080/17445647.2019.1676320>.
- Audsley, A., Bradwell, T., Howe, J. & Baxter, J. 2021. Spatial Relationships between Pockmarks and Sub-Seabed Gas in Fjordic Settings : Evidence from Loch Linnhe , West Scotland. *Geosciences*, **11**.
- Baltzer, A., Tessier, B., Nouzé, H., Bates, R., Moore, C. & Menier, D. 2005. Seistec seismic profiles: A tool to differentiate gas signatures. *Marine Geophysical Researches*, **26**, 235–245, <https://doi.org/10.1007/s11001-005-3721-x>.
- Bange, H.W., Bartell, U.H., Rapsomanikis, S. & Andreae, M.O. 1994. Methane in the Baltic and North Seas and a reassessment of the marine emissions of methane. *Global Biogeochemical Cycles*, **8**, 465–480, <https://doi.org/https://doi.org/10.1029/94GB02181>.
- Barnes, G.T. 1991. Contrast and scatter in x-ray imaging. *Radiographics*, **11**, 307–323, <https://doi.org/10.1148/radiographics.11.2.2028065>.
- Barry, M.A., Boudreau, B.P., Johnson, B.D. & Reed, A.H. 2010. First-order description of the mechanical fracture behavior of fine-grained surficial marine sediments during gas bubble growth. *Journal of Geophysical Research*, **115**, 1–10, <https://doi.org/10.1029/2010JF001833>.
- Best, A.I., Richardson, M.D., et al. 2006. Shallow Seabed Methane Gas Could Pose Coastal Hazard. *EOS, Transactions, American Geophysical Union*, **87**, 216–217, <https://doi.org/10.1130/G21259.1>.Fleischer.
- Bianchi, T.S., Cui, X., Blair, N.E., Burdige, D.J., Eglinton, T.I. & Galy, V. 2018. Centers of organic carbon burial and oxidation at the land-ocean interface. *Organic Geochemistry*, **115**, 138–155, <https://doi.org/10.1016/j.orggeochem.2017.09.008>.
- Blackford, J., Stahl, H., et al. 2014. Detection and impacts of leakage from sub-seafloor deep geological carbon dioxide storage. *Nature Climate Change*, **4**, 1011–1016, <https://doi.org/10.1038/nclimate2381>.
- Blott, S.J. & Pye, K. 2001. Gradistat: A grain size distribution and statistics package for

- the analysis of unconsolidated sediments. *Earth Surface Processes and Landforms*, **26**, 1237–1248, <https://doi.org/10.1002/esp.261>.
- Bolstad, P. V & Lillesand, T.M. 1992. Improved Classification of Forest Vegetation in Northern Wisconsin Through a Rule-Based Combination of Soils, Terrain, and Landsat Thematic Mapper Data. *Forest Science*, **38**, 5–20, <https://doi.org/10.1093/forestscience/38.1.5>.
- Böttner, C., Berndt, C., et al. 2019. Pockmarks in the Witch Ground Basin, Central North Sea. *Geochemistry, Geophysics, Geosystems*, **20**, 1698–1719, <https://doi.org/10.1029/2018GC008068>.
- Boudreau, B.P., Algar, C., et al. 2005. Bubble growth and rise in soft sediments. *Geology*, **33**, 517–520, <https://doi.org/10.1130/G21259.1>.
- Boyle, J.F., Chiverrell, R.C. & Schillereff, D. 2015. Approaches to Water Content Correction and Calibration for XRF Core Scanning: Comparing X-ray Scattering with Simple Regression of Elemental Concentrations. *In: Croudace, I. W. & Rothwell, R. G. (eds) Micro-XRF Studies of Sediment Cores: Applications of a Non-Destructive Tool for the Environmental Sciences*. Dordrecht, Springer Netherlands, 373–390., https://doi.org/10.1007/978-94-017-9849-5_14.
- Bradwell, T. & Stoker, M.S. 2015. Submarine sediment and landform record of a palaeo-ice stream within the British-Irish ice sheet. *Boreas*, **44**, 255–276, <https://doi.org/10.1111/bor.12111>.
- Bradwell, T., Stoker, M. & Larter, R. 2007. Geomorphological signature and flow dynamics of The Minch palaeo-ice stream, northwest Scotland. *Journal of Quaternary Science*, **22**, 609–617, <https://doi.org/10.1002/jqs>.
- Bradwell, T., Fabel, D., et al. 2021. Pattern, style and timing of British–Irish Ice Sheet advance and retreat over the last 45 000 years: evidence from NW Scotland and the adjacent continental shelf. *Journal of Quaternary Science*, **36**, 871–933, <https://doi.org/10.1002/jqs.3296>.
- Brothers, L.L., Kelley, J.T., Belknap, D.F., Barnhardt, W.A., Andrews, B.D., Legere, C. & Hughes Clarke, J.E. 2012. Shallow stratigraphic control on pockmark distribution in north temperate estuaries. *Marine Geology*, **329–331**, 34–45, <https://doi.org/10.1016/j.margeo.2012.09.006>.
- Brown, D.J., Holohan, E.P. & Bell, B.R. 2009. Sedimentary and volcano-tectonic processes in the British Paleocene Igneous Province: A review. *Geological*

- Magazine*, **146**, 326–352, <https://doi.org/10.1017/S0016756809006232>.
- Buccianti, A., Mateu-Figueras, G. & Pawlowsky-Glahn, V. 2006. Compositional Data Analysis in the Geosciences: From Theory to Practice. *Geological Society, London, Special Publications*, **264**.
- Burdige, D.J. 1993. The biogeochemistry of manganese and iron reduction in marine sediments. *Earth Science Reviews*, **35**, 249–284, [https://doi.org/10.1016/0012-8252\(93\)90040-E](https://doi.org/10.1016/0012-8252(93)90040-E).
- Burrows, M.T., Kamenos, N.A., Hughes, D.J., Stahl, H., Howe, J.A. & Tett, P. 2014. Assessment of carbon budgets and potential blue carbon stores in Scotland's coastal and marine environment. *Scottish Natural Heritage Commissioned Report No. 761*.
- Bussmann, I., Schlömer, S., Schlüter, M. & Wessels, M. 2011. Active pockmarks in a large lake (Lake Constance, Germany): Effects on methane distribution and turnover in the sediment. *Limnology and Oceanography*, **56**, 379–393, <https://doi.org/10.4319/lo.2011.56.1.0379>.
- Camargo, J.M.R., Silva, M.V.B., Júnior, A.V.F. & Araújo, T.C.M. 2019. Marine geohazards: A bibliometric-based review. *Geosciences*, **9**, <https://doi.org/10.3390/geosciences9020100>.
- Campbell, N., Dobby, H. & Bailey, N. 2009. Investigating and mitigating uncertainties in the assessment of Scottish Nephrops norvegicus populations using simulated underwater television data. *ICES Journal of Marine Science*, **66**, 646–655.
- Carr, S.J., Holmes, R., van der Meer, J.J.M. & Rose, J. 2006. The Last Glacial Maximum in the North Sea Basin: Micromorphological evidence of extensive glaciation. *Journal of Quaternary Science*, **21**, 131–153, <https://doi.org/10.1002/jqs.950>.
- Cartwright, A., Moss, J. & Cartwright, J. 2011. New statistical methods for investigating submarine pockmarks. *Computers and Geosciences*, **37**, 1595–1601, <https://doi.org/10.1016/j.cageo.2011.02.013>.
- Cathles, L.M., Su, Z. & Chen, D. 2010. The physics of gas chimney and pockmark formation, with implications for assessment of seafloor hazards and gas sequestration. *Marine and Petroleum Geology*, **27**, 82–91, <https://doi.org/10.1016/j.marpetgeo.2009.09.010>.
- Cevatoglu, M., Bull, J.M., Vardy, M.E., Gernon, T.M., Wright, I.C. & Long, D. 2015. Gas migration pathways, controlling mechanisms and changes in sediment acoustic

- properties observed in a controlled sub-seabed CO₂ release experiment. *International Journal of Greenhouse Gas Control*, **38**, 26–43, <https://doi.org/10.1016/j.ijggc.2015.03.005>.
- Champilou, J.B., Baltzer, A., Murat, A., Reynaud, M., Maillet, G.M., Nardelli, M.P. & Metzger, É. 2019. New evidence of perfect overlapping of Haploops and pockmarks field: Is it a coincidence? *Marine Geology*, **415**, 105961, <https://doi.org/10.1016/j.margeo.2019.105961>.
- Chen, J., Song, H., et al. 2015. Morphologies, classification and genesis of pockmarks, mud volcanoes and associated fluid escape features in the northern Zhongjiannan Basin, South China Sea. *Deep-Sea Research Part II: Topical Studies in Oceanography*, **122**, 106–117, <https://doi.org/10.1016/j.dsr2.2015.11.007>.
- Chiverrell, R.C. & Thomas, G.S.P. 2010. Extent and timing of the Last Glacial Maximum (LGM) in Britain and Ireland: A review. *Journal of Quaternary Science*, **25**, 535–549, <https://doi.org/10.1002/jqs.1404>.
- Çifçi, G., Dondurur, D. & Ergün, M. 2003. Deep and shallow structures of large pockmarks in the Turkish shelf, Eastern Black Sea. *Geo-Marine Letters*, **23**, 311–322, <https://doi.org/10.1007/s00367-003-0138-x>.
- Coughlan, M., Roy, S., O'Sullivan, C., Clements, A., O'Toole, R. & Plets, R. 2021. Geological settings and controls of fluid migration and associated seafloor seepage features in the north Irish Sea. *Marine and Petroleum Geology*, **123**, 104762, <https://doi.org/10.1016/j.marpetgeo.2020.104762>.
- Coull, K.A., Johnstone, R. & Rogers, S.I. 1998. Fisheries Sensitivity Maps in British Waters. *UKOOA Ltd.*, <https://doi.org/10.16309/j.cnki.issn.1007-1776.2003.03.004>.
- Croudace, I.W. & Rothwell, R.G. 2015. Micro-XRF Studies of Sediment Cores. *Micro-XRF Studies of Sediment Cores: Applications of a non-destructive tool for the environmental sciences*, **17**, <https://doi.org/10.1007/978-94-017-9849-5>.
- Dandapath, S., Chakraborty, B., et al. 2010. Morphology of pockmarks along the western continental margin of India: Employing multibeam bathymetry and backscatter data. *Marine and Petroleum Geology*, **27**, 2107–2117, <https://doi.org/10.1016/j.marpetgeo.2010.09.005>.
- Dando, P.R. 1991. Ecology of a North Sea pockmark with an active methane seep. *Marine Ecology Progress Series*, **70**, 49–63, <https://doi.org/10.3354/meps070049>.

- Davies, B.J., Roberts, D.H., Bridgland D.R. et al. 2011. Provenance and depositional environments of the Quaternary sediments from the western North Sea basin. *Journal of Quaternary Science*, **26**: 59–75.
- Davies, H.C., Dobson, M.R. & Whittington, R.J. 1984. A revised seismic stratigraphy for Quaternary deposits on the inner continental shelf west of Scotland between 55°30'N and 57°30'N. *Boreas*, **13**, 49–66, <https://doi.org/10.1111/j.1502-3885.1984.tb00059.x>.
- de Mahiques, M.M., Schattner, U., Lazar, M., Sumida, P.Y.G. & Souza, L.A.P. de. 2017. An extensive pockmark field on the upper Atlantic margin of Southeast Brazil: spatial analysis and its relationship with salt diapirism. *Heliyon*, **3**, <https://doi.org/10.1016/j.heliyon.2017.e00257>.
- Diesing, M. & Thorsnes, T. 2018. Mapping of cold-water coral carbonate mounds based on geomorphometric features: An object-based approach. *Geosciences*, **8**, <https://doi.org/10.3390/geosciences8020034>.
- Diesing, M., Green, S.L., Stephens, D., Lark, R.M., Stewart, H.A. & Dove, D. 2014. Mapping seabed sediments: Comparison of manual, geostatistical, object-based image analysis and machine learning approaches. *Continental Shelf Research*, **84**, 107–119, <https://doi.org/10.1016/j.csr.2014.05.004>.
- Diesing, M., Thorsnes, T. & Rún Bjarnadóttir, L. 2021. Organic carbon densities and accumulation rates in surface sediments of the North Sea and Skagerrak. *Biogeosciences*, **18**, 2139–2160, <https://doi.org/10.5194/bg-18-2139-2021>.
- Doh, S.-J., King, J.W. & Leinen, M. 1988. A rock-magnetic study of giant piston core LL44-GPC3 from the central North Pacific and its paleoceanographic implications. *Paleoceanography*, **3**, 89–111, <https://doi.org/https://doi.org/10.1029/PA003i001p00089>.
- Dove, D., Arosio, R., Finlayson, A., Bradwell, T. & Howe, J.A. 2015. Submarine glacial landforms record Late Pleistocene ice-sheet dynamics, Inner Hebrides, Scotland. *Quaternary Science Reviews*, **123**, 76–90, <https://doi.org/10.1016/j.quascirev.2015.06.012>.
- Duck, R.W. & Herbert, R.A. 2006. High-resolution shallow seismic identification of gas escape features in the sediments of Loch Tay, Scotland: Tectonic and microbiological associations. *Sedimentology*, **53**, 481–493, <https://doi.org/10.1111/j.1365-3091.2006.00778.x>.

- Evans, J., Oakleaf, J. & Cushman, S. 2014. An ArcGIS Toolbox for Surface Gradient and Geomorphometric Modeling.
- Evans, D., Roberts, M., Bateman., et al. 2021. Retreat dynamics of the eastern sector of the British-Irish Ice Sheet during the last glaciation. *Journal of Quaternary Science*, 1–29.
- Fader, G.B.J. 1991. Gas-related sedimentary features from the eastern Canadian continental shelf. *Continental Shelf Research*, **11**, 1123–1153, [https://doi.org/10.1016/0278-4343\(91\)90094-M](https://doi.org/10.1016/0278-4343(91)90094-M).
- Fannin, N. 1979. The use of regional geological surveys in the North Sea and adjacent areas in the recognition of offshore hazards. *In: In: Offshore Site Investigations, Proceedings of the Society of Underwater Technology Symposium*. London, Graham and Trotman.
- Fleischer, P., Orsi, T.H., Richardson, M.D. & Anderson, A.L. 2001a. Distribution of free gas in marine sediments: A global overview. *Geo-Marine Letters*, **21**, 103–122, <https://doi.org/10.1007/s003670100072>.
- Fleischer, P., Orsi, T.H., Richardson, M.D. & Anderson, A.L. 2001b. Distribution of free gas in marine sediments: A global overview. *Geo-Marine Letters*, **21**, 103–122, <https://doi.org/10.1007/s003670100072>.
- Flemming, B.W. 2007. The influence of grain-size analysis methods and sediment mixing on curve shapes and textural parameters: Implications for sediment trend analysis. *Sedimentary Geology*, **202**, 425–435, <https://doi.org/10.1016/j.sedgeo.2007.03.018>.
- Floodgate, G.D. & Judd, A.G. 1992. The origins of shallow gas. *Continental Shelf Research*, **12**, 1145–1156, [https://doi.org/10.1016/0278-4343\(92\)90075-U](https://doi.org/10.1016/0278-4343(92)90075-U).
- Flury, S., Røy, H., et al. 2016. Controls on subsurface methane fluxes and shallow gas formation in Baltic Sea sediment (Aarhus Bay, Denmark). *Geochimica et Cosmochimica Acta*, **188**, 297–309, <https://doi.org/10.1016/j.gca.2016.05.037>.
- Folk, R.. & Ward, W.. 1957. Brazos River Bar: A Study in the Significance of Grain Size Parameters. *Journal of Sedimentary Petrology*, **27**, 3–26.
- Froelich, P.N., Klinkhammer, G.P., et al. 1979. Early oxidation of organic matter in pelagic sediments of the eastern equatorial Atlantic: suboxic diagenesis. *Geochimica et Cosmochimica Acta*, **43**, 1075–1090, [https://doi.org/https://doi.org/10.1016/0016-7037\(79\)90095-4](https://doi.org/https://doi.org/10.1016/0016-7037(79)90095-4).

- Fyfe, J.A., Long, D. & Evans, D. 1993. *The Geology of the Malin–Hebrides Sea Area*. HMSO for the British Geological Survey. London.
- Gafeira, J. & Long, D. 2015a. Geological investigation of pockmarks in the Braemar Pockmarks and surrounding area. *JNCC Report No 571, JNCC Peter*, 1–92.
- Gafeira, J. & Long, D. 2015b. Geological investigation of pockmarks in the Scanner Pockmark SCI area. *JNCC Report No. 570*.
- Gafeira, J., Long, D. & Diaz-Doce, D. 2012. Semi-automated characterisation of seabed pockmarks in the central North Sea. *Near Surface Geophysics*, **10**, 303–315, <https://doi.org/10.3997/1873-0604.2012018>.
- Gafeira, J., Dolan, M. & Monteys, X. 2018. Geomorphometric Characterization of Pockmarks by Using a GIS-Based Semi-Automated Toolbox. *Geosciences*, **8**, 154, <https://doi.org/10.3390/geosciences8050154>.
- García-García, A., Vilas, F. & García-gil, S. 1999. A seeping sea-floor in a Ria environment: Ria de Vigo (NW Spain). *Environmental Geology*, **38**, 296–300.
- Gold, T. & Soter, S. 1982. Abiogenic Methane and the Origin of Petroleum. *Energy Exploration & Exploitation*, **1**, 89–104, <https://doi.org/10.1177/014459878200100202>.
- Golledge, N.R., Hubbard, A.L. & Sugden, D.E. 2009. Mass balance, flow and subglacial processes of a modelled Younger Dryas ice cap in Scotland. *Journal of Glaciology*, **55**, 32–42, <https://doi.org/10.3189/002214309788608967>.
- Gordon, J.. 2016. Geological and geomorphological features of SSSIs contributing to the MPA network in Scotland's seas. *Scottish Natural Heritage Commissioned Report No. 892*.
- Gordon, J.E., Brooks, A.J., et al. 2016. Progress in marine geoconservation in Scotland's seas: assessment of key interests and their contribution to Marine Protected Area network planning. *Proceedings of the Geologists' Association*, **127**, 716–737, <https://doi.org/10.1016/j.pgeola.2016.10.002>.
- Graham, D.K., Harland, R., Gregory, D.M., Long, D. & Morton, A.C. 1990. The biostratigraphy and chronostratigraphy of BGS Borehole 78/4, North Minch. *Scottish Journal of Geology*, **26**, 65–75, <https://doi.org/10.1144/sjg26020065>.
- Greene, D. 1995. *The Loch Lomond Stadial Ice Cap in Western Lochaber* ,. University of Edinburgh.

- Hammer, Ø. & Webb, K.E. 2010. Piston coring of inner Oslofjord pockmarks, Norway: Constraints on age and mechanism. *Norsk Geologisk Tidsskrift*, **90**, 79–91.
- Hasiotis, T., Papatheodorou, G., Kastanos, N. & Ferentions, G. 1995. A pockmark field in the Patras Gulf (Greece) and its activation during the 14/7/93 seismic event. *Marine geology*, **130**, 333–344, [https://doi.org/10.1016/0025-3227\(95\)00131-X](https://doi.org/10.1016/0025-3227(95)00131-X).
- Hastings, D.W., Schwing, P.T., et al. 2016. Changes in sediment redox conditions following the BP DWH blowout event. *Deep-Sea Research Part II: Topical Studies in Oceanography*, **129**, 167–178, <https://doi.org/10.1016/j.dsr2.2014.12.009>.
- Henrichs, S.M. & Reeburgh, W.S. 1987. Anaerobic mineralization of marine sediment organic matter: Rates and the role of anaerobic processes in the oceanic carbon economy. *Geomicrobiology Journal*, **5**, 191–237, <https://doi.org/10.1080/01490458709385971>.
- Hesselbo, S.P. & Coe, A.L. 2000. Jurassic sequences of the Hebrides Basin, Isle of Skye, Scotland. *Field trip guidebook, International Association of Sedimentologists regional meeting, Dublin*, 41–58.
- Hesselbo, S.P., Oates, M.J. & Jenkyns, H.C. 2010. The lower Lias Group of the Hebrides Basin. *Scottish Journal of Geology*, **34**, 23–60, <https://doi.org/10.1144/sjg34010023>.
- Hillman, J.I.T., Gorman, A.R. & Pecher, I.A. 2015. Geostatistical analysis of seafloor depressions on the southeast margin of New Zealand's South Island - Investigating the impact of dynamic near seafloor processes on geomorphology. *Marine Geology*, **360**, 70–83, <https://doi.org/10.1016/j.margeo.2014.11.016>.
- Hinrichs, K.U. & Boetius, A. 2002. The Anaerobic Oxidation of Methane: New Insights in Microbial Ecology and Biogeochemistry. In: WEFER, G., BILLET, D., HEBBELN, D., JØRGENSEN, B., SCHLUTERM, M. & VAN WEERING, T. (eds) *Ocean Margin Systems*. Berlin Heidelberg, Springer-Verlag, 457–477., https://doi.org/10.1007/978-3-662-05127-6_28.
- Holding, J.M., Duarte, C.M., et al. 2017. Autochthonous and allochthonous contributions of organic carbon to microbial food webs in Svalbard fjords. *Limnology and Oceanography*, **62**, 1307–1323, <https://doi.org/10.1002/lno.10526>.
- Hovland, M. 1981a. A classification of pockmark related features in the Norwegian Trench. *Continental Shelf Research*, **106**.
- Hovland, M. 1981b. Characteristics of pockmarks in the Norwegian Trench. *Marine*

- Geology*, **39**, 103–117, [https://doi.org/10.1016/0025-3227\(81\)90030-X](https://doi.org/10.1016/0025-3227(81)90030-X).
- Hovland, M. 1983. Elongated depressions associated with pockmarks in the Western Slope of the Norwegian Trench. *Marine Geology*, **51**, 35–46, [https://doi.org/10.1016/0025-3227\(83\)90087-7](https://doi.org/10.1016/0025-3227(83)90087-7).
- Hovland, M. 1989. The formation of pockmarks and their potential influence on offshore construction. *Quarterly Journal of Engineering Geology*, **22**, 131–138, https://doi.org/10.2208/jscej.1987.388_13.
- Hovland, M. 2002. On the self-sealing nature of marine seeps. *Continental Shelf Research*, **22**, 2387–2394, [https://doi.org/10.1016/S0278-4343\(02\)00063-8](https://doi.org/10.1016/S0278-4343(02)00063-8).
- Hovland, M. & Judd, A. 1988. *Seabed Pockmarks and Seepages: Impact on Geology, Biology and the Marine Environment*. London, Graham & Trotman.
- Hovland, M. & Sommerville, J.. 1985. Characteristics of two natural gas seepages in the North Sea. *Marine and Petroleum Geology*, **2**, 319–326, [https://doi.org/10.1016/0264-8172\(85\)90027-3](https://doi.org/10.1016/0264-8172(85)90027-3).
- Hovland, M., Judd, A.G. & King, L.H. 1984. Characteristic features of pockmarks on the North Sea Floor and Scotian Shelf. *Sedimentology*, **31**, 471–480.
- Hovland, M., Talbot, M., Olausen, S. & Aasberg, L. 1985. Recently formed methane-derived carbonates from the North Sea. *Journal of Sedimentary Petrology*.
- Hovland, M., Talbot, M.R., Qvale, H., Olausen, S. & Aasberg, L. 1987. Methane-related carbonate cements in pockmarks of the North Sea. *Journal of Sedimentary Petrology*, **57**, 881–892, <https://doi.org/10.1306/212f8c92-2b24-11d7-8648000102c1865d>.
- Hovland, M., Gardner, J. V. & Judd, A.G. 2002. The significance of pockmarks to understanding fluid flow processes and geohazards. *Geofluids*, **2**, 127–136, <https://doi.org/10.1046/j.1468-8123.2002.00028.x>.
- Hovland, M., Svensen, H., et al. 2005. Complex pockmarks with carbonate-ridges off mid-Norway: Products of sediment degassing. *Marine Geology*, **218**, 191–206, <https://doi.org/10.1016/j.margeo.2005.04.005>.
- Hovland, M., Heggland, R., De Vries, M.H. & Tjelta, T.I. 2010. Unit-pockmarks and their potential significance for predicting fluid flow. *Marine and Petroleum Geology*, **27**, 1190–1199, <https://doi.org/10.1016/j.marpetgeo.2010.02.005>.
- Howe, J.A., Shimmield, T., Austin, W.E.N. & Longva, O. 2002. Post-glacial depositional

- environments in a mid-high latitude glacially-overdeepened sea loch, inner Loch Etive, western Scotland. *Marine Geology*, **185**, 417–433, [https://doi.org/10.1016/S0025-3227\(01\)00299-7](https://doi.org/10.1016/S0025-3227(01)00299-7).
- Howe, J.A., Moreton, S.G., Morri, C. & Morris, P. 2003. Multibeam bathymetry and the depositional environments of Kongsfjorden and Krossfjorden, western Spitsbergen, Svalbard. *Polar Research*, **22**, 301–316, <https://doi.org/10.3402/polar.v22i2.6462>.
- Howe, J.A., Austin, W.E.N., Forwick, M., Paetzel, M., Harland, R. & Cage, A.G. 2010. Fjord systems and archives: a review. *Geological Society, London, Special Publications*, **344**, 5–15, <https://doi.org/10.1144/SP344.2>.
- Howe, J.A., Dove, D., Bradwell, T. & Gafeira, J. 2012. Submarine geomorphology and glacial history of the Sea of the Hebrides, UK. *Marine Geology*, **315–318**, 64–76, <https://doi.org/10.1016/j.margeo.2012.06.005>.
- Howe, J.A., Anderton, R., et al. 2015. The seabed geomorphology and geological structure of the Firth of Lorn, western Scotland, UK, as revealed by multibeam echosounder survey. *Earth and Environmental Science Transactions of the Royal Society of Edinburgh*, **105**, 273–284, <https://doi.org/10.1017/S1755691015000146>.
- Hyun, J.H., Kim, S.H., Mok, J.S., Cho, H., Lee, T., Vandieken, V. & Thamdrup, B. 2017. Manganese and iron reduction dominate organic carbon oxidation in surface sediments of the deep Ulleung Basin, East Sea. *Biogeosciences*, **14**, 941–958, <https://doi.org/10.5194/bg-14-941-2017>.
- Idczak, J., Brodecka-Goluch, A., et al. 2020. A geophysical, geochemical and microbiological study of a newly discovered pockmark with active gas seepage and submarine groundwater discharge (MET1-BH, central Gulf of Gdańsk, southern Baltic Sea). *Science of the Total Environment*, **742**, <https://doi.org/10.1016/j.scitotenv.2020.140306>.
- Iglesias, J., Ercilla, G., García-Gil, S. & Judd, A.G. 2010. Pockforms: An evaluation of pockmark-like seabed features on the Landes Plateau, Bay of Biscay. *Geo-Marine Letters*, **30**, 207–219, <https://doi.org/10.1007/s00367-009-0182-2>.
- IHO. 2020. International Hydrographic Organization Standards for Hydrographic Surveys. *Standards for Hydrographic Surveying*, **S44**, 51.
- Imber, J., Strachan, R.A., Holdsworth, R.E. & Butler, C.A. 2002. The initiations and early tectonic significance of the Outer Hebrides Fault Zone, Scotland. *Geological Magazine*, **139**, 609–619, <https://doi.org/10.1017/S0016756802006969>.

- Ingall, E.D. & Cappellen, P. Van. 1990. Relation between sedimentation rate and burial of organic phosphorus and organic carbon in marine sediments. *Geochimica et Cosmochimica Acta*, **54**, 373–386, [https://doi.org/10.1016/0016-7037\(90\)90326-G](https://doi.org/10.1016/0016-7037(90)90326-G).
- Jensen, P. 1992. ‘Bubbling reefs’ in the Kattegat: submarine landscapes of carbonate-cemented rocks support a diverse ecosystem at methane seeps’. *Marine Ecology Progress Series*, **83**, 103–112, <https://doi.org/10.3354/meps083103>.
- JNCC. 2018. Offshore Special Area of Conservation: Scanner Pockmark (SAC). *SAC Selection Assessment Document*, 32.
- Johnson, B.D., Boudreau, B.P., Gardiner, B.S. & Maass, R. 2002. Mechanical response of sediments to bubble growth. *Marine Geology*, **187**, 347–363, [https://doi.org/10.1016/S0025-3227\(02\)00383-3](https://doi.org/10.1016/S0025-3227(02)00383-3).
- Jones, G.B., Floodgate, G.D. & Bennell, J.D. 1986. Chemical and microbiological aspects of acoustically turbid sediments: Preliminary investigations. *Marine Geotechnology*, **6**, 315–332, <https://doi.org/10.1080/10641198609388193>.
- Josenhans, H.W., King, L.H. & Fader, G.B. 1978. Side-Scan Sonar Mosaic of Pockmarks on the Scotian Shelf. *Can J Earth Sci*, **15**, 831–840, <https://doi.org/10.1139/e78-088>.
- Joseph, A. 2017. *Secrets of Bermuda Triangle and Formation of Polymetallic Nodules*, <https://doi.org/10.1016/b978-0-12-809357-3.00002-3>.
- Judd, A. & Hovland, M. 2007. *Seabed Fluid Flow: The Impact on Geology, Biology and the Marine Environment Seabed Fluid Flow Impact of Geology, Biology and The*. Cambridge University Press.
- Judd, A., Davies, G., Wilson, J., Holmes, R., Baron, G. & Bryden, I. 1997. Contributions to atmospheric methane by natural seepages on the UK continental shelf. *Marine Geology*, **137**, 165–189, [https://doi.org/10.1016/S0025-3227\(96\)00087-4](https://doi.org/10.1016/S0025-3227(96)00087-4).
- Judd, A., Croker, P., Tizzard, L. & Voisey, C. 2007. Extensive methane-derived authigenic carbonates in the Irish Sea. *Geo-Marine Letters*, **27**, 259–267, <https://doi.org/10.1007/s00367-007-0079-x>.
- Judd, A.G. 2001. Pockmarks in the UK sector of the North Sea. *UK Department of Trade and Industry Strategic Environmental Assessment*, 71.
- Judd, A.G. 2003. The global importance and context of methane escape from the seabed. *Geo-Marine Letters*, **23**, 147–154, <https://doi.org/10.1007/s00367-003-0136-z>.

- Judd, A.G., Long, D., Sankey, M. 1994. Pockmark formation and activity, UK block 15/25, North Sea. *Bulletin of the Geological Society of Denmark*, **41**, 34–49.
- Kelley, J.T., Dickson, S.M., Belknap, D.F., Barnhardt, W.A. & Henderson, M. 1994. Giant sea-bed pockmarks: evidence for gas escape from Belfast Bay, Maine. *Geology*, **22**, 59–62, [https://doi.org/10.1130/0091-7613\(1994\)022<0059:GSBPEF>2.3.CO;2](https://doi.org/10.1130/0091-7613(1994)022<0059:GSBPEF>2.3.CO;2).
- Kennedy, W.Q. 1946. The Great Glen Fault. *Quarterly Journal of the Geological Society*, **102**, 41 LP – 76, <https://doi.org/10.1144/GSL.JGS.1946.102.01-04.04>.
- King, L.H. & Maclean, B. 1970. Pockmarks on the Scotian Shelf. *Geological Society of America Bulletin*, **81**, 3141–3148.
- Koinig, K.A., Shotyk, W., Lotter, A.F., Ohlendorf, C. & Sturm, M. 2003. 9000 Years of geochemical evolution of lithogenic major and trace elements in the sediment of an alpine lake - The role of climate, vegetation, and land-use history. *Journal of Paleolimnology*, **30**, 307–320, <https://doi.org/10.1023/A:1026080712312>.
- Krämer, K., Holler, P., et al. 2017. Abrupt emergence of a large pockmark field in the German Bight, southeastern North Sea. *Scientific Reports*, **7**, 1–8, <https://doi.org/10.1038/s41598-017-05536-1>.
- Krooss, B.M., Leythaeuser, D. & Schaefer, R.G. 1992. The Quantification of Diffusive Hydrocarbon Losses Through Cap Rocks of Natural Gas Reservoirs—A Reevaluation: Reply1. *AAPG Bulletin*, **76**, 1842–1846, <https://doi.org/10.1306/BDFF8AF6-1718-11D7-8645000102C1865D>.
- Kuşçu, I., Okamura, M., et al. 2005. Seafloor gas seeps and sediment failures triggered by the August 17, 1999 earthquake in the Eastern part of the Gulf of İzmit, Sea of Marmara, NW Turkey. *Marine Geology*, **215**, 193–214, <https://doi.org/10.1016/j.margeo.2004.12.002>.
- Lalonde, K., Mucci, A., Ouellet, A. & Gélinas, Y. 2012. Preservation of organic matter in sediments promoted by iron. *Nature*, **483**, 198–200, <https://doi.org/10.1038/nature10855>.
- Leifer, I. & Judd, A. 2015. The UK22/4b blowout 20 years on: Investigations of continuing methane emissions from sub-seabed to the atmosphere in a North Sea context. *Marine and Petroleum Geology*, **68**, 706–717, <https://doi.org/10.1016/j.marpetgeo.2015.11.012>.
- Locat, J., Leroueil, S., Locat, A. & Lee, H. 2014. Weak Layers: Their Definition and

- Classification from a Geotechnical Perspective. *In*: Krastel, S., Behrmann, J.-H., et al. (eds) *Submarine Mass Movements and Their Consequences: 6th International Symposium*. Cham, Springer International Publishing, 3–12., https://doi.org/10.1007/978-3-319-00972-8_1.
- Lohrberg, A., Schmale, O., Ostrovsky, I., Niemann, H., Held, P. & Deimling, J.S. Von. 2020. Discovery and quantification of a widespread methane ebullition event in a coastal inlet (Baltic Sea) using a novel sonar strategy. *Scientific Reports*, **10**, 1–13, <https://doi.org/10.1038/s41598-020-60283-0>.
- Long, D. 1992. Devensian late-glacial gas escape in the central North Sea. *Continental Shelf Research*, **12**, 1097–1110, [https://doi.org/10.1016/0278-4343\(92\)90071-Q](https://doi.org/10.1016/0278-4343(92)90071-Q).
- Luo, M., Dale, A.W., Wallmann, K., Hensen, C., Gieskes, J., Yan, W. & Chen, D. 2015. Estimating the time of pockmark formation in the SW Xisha Uplift (South China Sea) using reaction-transport modeling. *Marine Geology*, **364**, 21–31, <https://doi.org/10.1016/j.margeo.2015.03.006>.
- MacQueen, J. 1967. Some methods for classification and analysis of multivariate observations. *In*: *Proceedings of the Fifth Symposium on Math, Statistics, and Probability*. Berkeley, CA, University of California Press, 281–297., <https://doi.org/10.1007/s11665-016-2173-6>.
- Makri, S., Rey, F., Gobet, E., Gilli, A., Tinner, W. & Grosjean, M. 2020. Early human impact in a 15,000-year high-resolution hyperspectral imaging record of paleoproduction and anoxia from a varved lake in Switzerland. *Quaternary Science Reviews*, **239**, 106335, <https://doi.org/10.1016/j.quascirev.2020.106335>.
- Makri, S., Wienhues, G., et al. 2021. Variations of sedimentary Fe and Mn fractions under changing lake mixing regimes, oxygenation and land surface processes during Late-glacial and Holocene times. *Science of the Total Environment*, **755**, 143418, <https://doi.org/10.1016/j.scitotenv.2020.143418>.
- Marchant, J. 2000. Swallowing Ships. *New Scientist*.
- Marinaro, G., Etiope, G., et al. 2004. GMM - A gas monitoring module for long-term detection of methane leakage from the seafloor. *Environmental Geology*, **46**, 1053–1058, <https://doi.org/10.1007/s00254-004-1092-2>.
- Marinaro, G., Etiope, G., et al. 2006. Monitoring of a methane-seeping pockmark by cabled benthic observatory (Patras Gulf, Greece). *Geo-Marine Letters*, **26**, 297–302, <https://doi.org/10.1007/s00367-006-0040-4>.

- Martens, C.S. & Berner, R.A. 1974. Methane Production in the Interstitial Waters of Sulfate-Depleted Marine Sediments. *Science*, **185**, 1167–1169.
- Martens, C.S. & Klump, J. V. 1984. Biogeochemical cycling in an organic-rich marine basin-4. An organic carbon budget for sediments dominated by sulfate reduction and methanogenesis. *Geochimica et Cosmochimica Acta*, **48**, 1987–2004.
- Martens, C.S., Albert, D.B. & Alperin, M.J. 1998. Biogeochemical processes controlling methane in gassy coastal sediments - Part 1. A model coupling organic matter flux to gas production, oxidation and transport. *Continental Shelf Research*, **18**, 1741–1770, [https://doi.org/10.1016/S0278-4343\(98\)00056-9](https://doi.org/10.1016/S0278-4343(98)00056-9).
- Martins, V.A., Dias, J.A., et al. 2013. The ITRAX core scanner, a useful tool to distinguish anthropic vs. climatic influences in lagoon of Aveiro (N Portugal) . *Journal of Coastal Research*, **65**, 70–75, <https://doi.org/10.2112/si65-013.1>.
- McGinnis, D.F., Greinert, J., Artemov, Y., Beaubien, S.E. & Wüest, A. 2006. Fate of rising methane bubbles in stratified waters: How much methane reaches the atmosphere? *Journal of Geophysical Research: Oceans*, **111**, 1–15, <https://doi.org/10.1029/2005JC003183>.
- McIntyre, K.L. & Howe, J.A. 2010. Scottish west coast fjords since the last glaciation: a review. *Geological Society, London, Special Publications*, **344**, 305 LP – 329, <https://doi.org/10.1144/SP344.21>.
- McIntyre, K.L. 2012. *Offshore Records of Ice Extent and Deglaciation , Loch Linnhe , Western Scotland*. University of Aberdeen.
- McQuillin, R. & Fannin, N. 1979. Explaining the North Sea's lunar floor. *New Scientist*.
- Meldahl, P., Heggland, R., Bril, B. & De Groot, P. 1999. The chimney cube, an example of semi-automated detection of seismic objects by directive attributes and neural networks: Part I; methodology. In: *SEG Technical Program Expanded Abstracts*. Tulsa, OK, USA, Society of Exploration Geophysicists., <https://doi.org/10.1190/1.1821263>.
- Michel, G., Dupré, S., et al. 2017. Pockmarks on the South Aquitaine Margin continental slope: The seabed expression of past fluid circulation and former bottom currents. *Comptes Rendus - Geoscience*, **349**, 391–401, <https://doi.org/10.1016/j.crte.2017.10.003>.
- Monna, S., Falcone, G., et al. 2013. Underwater geophysical monitoring for European

- Multidisciplinary Sea floor and water column Observatories. *Journal of Marine Systems*, 0–19, <https://doi.org/10.1016/j.jmarsys.2013.09.010>.
- Morton, N. 1993. Potential reservoir and source rocks in relation to upper triassic to middle jurassic sequence stratigraphy, Atlantic margin basins of the British Isles. *Petroleum Geology Conference Proceedings*, **4**, 285–297, <https://doi.org/10.1144/0040285>.
- Moss, J.L., Cartwright, J. & Moore, R. 2012a. Evidence for fluid migration following pockmark formation: Examples from the Nile Deep Sea Fan. *Marine Geology*, **303–306**, 1–13, <https://doi.org/10.1016/j.margeo.2012.01.010>.
- Moss, J.L., Cartwright, J., Cartwright, A. & Moore, R. 2012b. The spatial pattern and drainage cell characteristics of a pockmark field, Nile Deep Sea Fan. *Marine and Petroleum Geology*, **35**, 321–336, <https://doi.org/10.1016/j.marpetgeo.2012.02.019>.
- Naeher, S., Gilli, A., North, R.P., Hamann, Y. & Schubert, C.J. 2013. Tracing bottom water oxygenation with sedimentary Mn/Fe ratios in Lake Zurich, Switzerland. *Chemical Geology*, **352**, 125–133, <https://doi.org/10.1016/j.chemgeo.2013.06.006>.
- Naidu, A.S., Scalan, R.S., et al. 1993. Stable organic carbon isotopes in sediments of the north Bering-south Chukchi seas, Alaskan-Soviet Arctic Shelf. *Continental Shelf Research*, **13**, 669–691, [https://doi.org/10.1016/0278-4343\(93\)90099-J](https://doi.org/10.1016/0278-4343(93)90099-J).
- Nellemann, C., Corcoran, E., Duarte, C.M., Valdés, L., De Young, C., Fonseca, L. & Grimsdith, G. 2009. *Blue Carbon. A Rapid Response Assessment*, (Eds). United Nations Environment Programme, GRID-Arendal.
- Nørgaard-pedersen, N., Austin, W.E.N., Howe, J.A. & Shimmield, T. 2006. The Holocene record of Loch Etive, western Scotland: Influence of catchment and relative sea level changes. *Marine geology*, **228**, 55–71, <https://doi.org/10.1016/j.margeo.2006.01.001>.
- O'Hara, S.C.M., Dando, P.R., et al. 1995. Gas seep induced interstitial water circulation: observations and environmental implications. *Continental Shelf Research*, **15**, 931–948, [https://doi.org/10.1016/0278-4343\(95\)80003-V](https://doi.org/10.1016/0278-4343(95)80003-V).
- Orange, D.L., García-García, A., McConnell, D., Lorenson, T., Fortier, G., Trincardi, F. & Can, E. 2005. High-resolution surveys for geohazards and shallow gas: NW Adriatic (Italy) and Iskenderun Bay (Turkey). *Marine Geophysical Research*, **26**, 247–266, <https://doi.org/10.1007/s11001-005-3722-9>.
- Panieri, G., Bünz, S., et al. 2017. An integrated view of the methane system in the

- pockmarks at Vestnesa Ridge, 79°N. *Marine Geology*, **390**, 282–300, <https://doi.org/10.1016/j.margeo.2017.06.006>.
- Papatheodorou, G., Hasiotis, T. & Ferentinos, G. 1993. Gas-charged sediments in the Aegean and Ionian Seas, Greece. *Marine Geology*, **112**, 171–184, [https://doi.org/10.1016/0025-3227\(93\)90167-T](https://doi.org/10.1016/0025-3227(93)90167-T).
- Park, M., Sciences, S., Angeles, L. & Park, M. 1979. Modern biogenic gas-generated craters (sea-floor " pockmarks ") on the Bering Shelf , Alaska. 1144–1152.
- Parkes, R.J., Cragg, B.A., Fry, J.C., Herbert, R.A. & Wimpenny, J.W.T. 1990. Bacterial biomass and activity in deep sediment layers from the Peru margin. *Philosophical Transactions of the Royal Society of London. Series A, Mathematical and Physical Sciences*, **331**, 139–153, <https://doi.org/10.1098/rsta.1990.0061>.
- Pau, M. & Hammer, T. 2013. Sediment mapping and long-term monitoring of currents and sediment fluxes in pockmarks in the Oslofjord, Norway. *Marine Geology*, **346**, 262–273, <https://doi.org/10.1016/j.margeo.2013.09.012>.
- Picard, K., Radke, L., et al. 2018. Origin of High Density Seabed Pockmark Fields and Their Use in Inferring Bottom Currents. *Geosciences*, **8**, 195, <https://doi.org/10.3390/geosciences8060195>.
- Pilcher, R. & Argent, J. 2007. Mega-pockmarks and linear pockmark trains on the West African continental margin. *Marine Geology*, **244**, 15–32, <https://doi.org/10.1016/j.margeo.2007.05.002>.
- Rance, J., Froján, B., Schinaia, C. & Ju, S. 2017. JNCC/Cefas Partnership Report Series CEND 19x/12: Offshore seabed survey of Braemar Pockmarks SCI and Scanner Pockmark SCI.
- Ravasopoulos, J., Papatheodorou, G., Kapolos, J., Geraga, M., Koliadima, A. & Xenos, K. 2002. A promising methodology for the detection of pockmarks activation in nearshore sediments. *Instrumentation Science and Technology*, **30**, 139–155, <https://doi.org/10.1081/CI-120003894>.
- Reilly, S.O., Kelleher, B., Szpak, M. & Monteys, X. 2012. *Carbon Cycling in Dunmanus Bay Pockmarks*.
- Riboulot, V., Yannick, T., Serge, B., Gwenael, J. & Cattaneo, A. 2014. Control of Quaternary sea-level changes on gas seeps. *Geophysical Research Letters*, **41**, 4970–4977, <https://doi.org/10.1002/2014GL060460>.

- Riboulot, V., Imbert, P., Cattaneo, A. & Voisset, M. 2019. Fluid escape features as relevant players in the enhancement of seafloor stability? *Terra Nova*, **31**, 540–548, <https://doi.org/10.1111/ter.12425>.
- Rise, L., Bellec, V.K., Ch, S. & Bøe, R. 2014. Pockmarks in the southwestern Barents Sea and Finnmark fjords. *Norsk Geologisk Tidsskrift*, **94**, 263–282, <https://doi.org/10.17850/njg94-4-02>.
- Roberts, N., Allcock, S.L., et al. 2016. A tale of two lakes: a multi-proxy comparison of Lateglacial and Holocene environmental change in Cappadocia, Turkey. *Journal of Quaternary Science*, **31**, 348–362, <https://doi.org/10.1002/jqs.2852>.
- Roelofse, C., Alves, T.M., Gafeira, J. & Omosanya, K.O. 2019. An integrated geological and GIS-based method to assess caprock risk in mature basins proposed for carbon capture and storage. *International Journal of Greenhouse Gas Control*, **80**, 103–122, <https://doi.org/10.1016/j.ijggc.2018.11.007>.
- Rogers, J.N., Kelley, J.T., Belknap, D.F., Gontz, A. & Barnhardt, W.A. 2006. Shallow-water pockmark formation in temperate estuaries: A consideration of origins in the western gulf of Maine with special focus on Belfast Bay. *Marine Geology*, **225**, 45–62, <https://doi.org/10.1016/j.margeo.2005.07.011>.
- Romankevich, E.A. 1984. Sources of Organic Matter in the Ocean. *In: Geochemistry of Organic Matter in the Ocean*. Berlin, Heidelberg, Springer Berlin Heidelberg, 4–26., https://doi.org/10.1007/978-3-642-49964-7_3.
- Rothwell, G.R. & Rack, F.R. 2006. New techniques in sediment core analysis: an introduction. *Geological Society, London, Special Publications*, **267**, 1–29, <https://doi.org/10.1144/GSL.SP.2006.267.01.01>.
- Roy, S., Senger, K., Braathen, A., Noormets, R., Hovland, M. & Olaussen, S. 2014. Fluid migration pathways to seafloor seepage in inner isfjorden and Adventfjorden, Svalbard. *Norsk Geologisk Tidsskrift*, **94**, 99–199.
- Roy, S., Hovland, M., Noormets, R. & Olaussen, S. 2015. Seepage in Isfjorden and its tributary fjords, West Spitsbergen. *Marine Geology*, **363**, 146–159, <https://doi.org/10.1016/j.margeo.2015.02.003>.
- Roy, S., Senger, K., Hovland, M., Römer, M. & Braathen, A. 2019. Geological controls on shallow gas distribution and seafloor seepage in an Arctic fjord of Spitsbergen, Norway. *Marine and Petroleum Geology*, **107**, 237–254, <https://doi.org/10.1016/j.marpetgeo.2019.05.021>.

- Sánchez, N., Zeppilli, D., et al. 2021. A threefold perspective on the role of a pockmark in benthic faunal communities and biodiversity patterns. *Deep-Sea Research Part I: Oceanographic Research Papers*, **167**, <https://doi.org/10.1016/j.dsr.2020.103425>.
- Schattner, U., Lazar, M., Souza, L.A.P., ten Brink, U. & Mahiques, M.M. 2016. Pockmark asymmetry and seafloor currents in the Santos Basin offshore Brazil. *Geo-Marine Letters*, **36**, 457–464, <https://doi.org/10.1007/s00367-016-0468-0>.
- Schneider von Deimling, J., Linke, P., Schmidt, M. & Rehder, G. 2015. Ongoing methane discharge at well site 22/4b (North Sea) and discovery of a spiral vortex bubble plume motion. *Marine and Petroleum Geology*, **68**, 718–730, <https://doi.org/10.1016/j.marpetgeo.2015.07.026>.
- Schuller, V.F. 1952. Untersuchungen über die Mächtigkeit von Schlickschichten mit Hilfe des Echographen. *Deutsche Hydrographische Zeitschrift*, **Band 5**.
- Scottish Government. 2019. *Scottish Sea Fisheries Statistics 2018*.
- Seeborg-Elverfeldt, I.A., Lange, C.B., Pätzold, J. & Kuhn, G. 2005. Laminae type and possible mechanisms for the formation of laminated sediments in the Shaban Deep, northern Red Sea. *Ocean Science*, **1**, 113–126, <https://doi.org/10.5194/os-1-113-2005>.
- Seiter, K., Hensen, C., Schröter, J. & Zabel, M. 2004. Organic carbon content in surface sediments—defining regional provinces. *Deep Sea Research Part I: Oceanographic Research Papers*, **51**, 2001–2026, <https://doi.org/https://doi.org/10.1016/j.dsr.2004.06.014>.
- Shmatkova, A.A., Shmatkov, A.A., Gainanov, V.G. & Buenz, S. 2015. Identification of geohazards based on the data of marine high-resolution 3D seismic observations in the Norwegian Sea. *Moscow University Geology Bulletin*, **70**, 53–61, <https://doi.org/10.3103/S0145875215010068>.
- Siddiquie, H.N., Rao, D.G., Vora, K.H. & Topgi, R.S. 1981. Acoustic masking in sediments due to gases on the western continental shelf of India. *Marine Geology*, **39**, M27–M37, [https://doi.org/https://doi.org/10.1016/0025-3227\(81\)90023-2](https://doi.org/https://doi.org/10.1016/0025-3227(81)90023-2).
- Smeaton, C., Austin, W.E.N., Davies, A.L., Baltzer, A., Abell, R.E. & Howe, J.A. 2016. Substantial stores of sedimentary carbon held in mid-latitude fjords. *Biogeosciences*, **13**, 5771–5787, <https://doi.org/10.5194/bg-13-5771-2016>.
- Smeaton, C., Austin, W.E.N., Davies, A.L., Baltzer, A., Howe, J.A. & Baxter, J.M. 2017.

- Scotland's forgotten carbon: a national assessment of mid-latitude fjord sedimentary carbon stocks. *Biogeosciences*, **14**, 5663–5674, <https://doi.org/10.5194/bg-14-5663-2017>.
- Smeaton, C., Austin, W. & Turrell, W. 2020. *Re-Evaluating Scotlands Sedimentary Carbon Stocks*, 2nd ed. Edinburgh, UK, Marine Scotland, Scottish Marine and Freshwater Science, <https://doi.org/10.7489/12267-1>.
- Smeaton, C., Hunt, C.A., Turrell, W.R. & Austin, W.E.N. 2021. Marine Sedimentary Carbon Stocks of the United Kingdom's Exclusive Economic Zone. *Frontiers in Earth Science*, **9**, 1–21, <https://doi.org/10.3389/feart.2021.593324>.
- Smith, A., Mienert, J., Bunz, S. & Greinert, J. 2014. Thermogenic methane injection via bubble transport into the upper Arctic Ocean from the hydrate-charged Vestnesa Ridge, Svalbard. *Geochem. Geophys. Geosyst.*, **15**, 1945–1959, <https://doi.org/10.1002/2013GC005179>.Received.
- Smith, D.E., Barlow, N.L.M., Bradley, S.L., Firth, C.R., Hall, A.M., Jordan, J.T. & Long, D. 2017. *Quaternary Sea Level Change in Scotland*, <https://doi.org/10.1017/S1755691017000469>.
- Smith, K. 2012. The Fascaidale Fault: A tectonic link between the Cenozoic volcanic centres of Rum and Ardnamurchan, Scotland, revealed by multibeam survey. *Scottish Journal of Geology*, **48**, 91–102, <https://doi.org/10.1144/sjg2012-440>.
- Solheim, A. & Elverhøi, A. 1993. Gas-related sea floor craters in the Barents Sea. *Geo-Marine Letters*, **13**, 235–243, <https://doi.org/10.1007/BF01207753>.
- Soter, S.L. 1999. Macroscopic seismic anomalies and submarine pockmarks in the Corinth Patras rift, Greece. *Tectonophysics*, **308**, 275–290.
- Stahl, H. 2012a. *Current Status & Knowledge about Potential Sequestration Capacity for 'Blue Carbon' Sinks in Scotland*.
- Stahl, H. 2012b. *Fate of Terrestrial Carbon in the Scottish Coastal Environment*.
- Stoker, M.S., Long, D. 1984. A relict ice-scoured erosion surface in the central North Sea, *Marine Geology*, **61**, 85–93.
- Stoker, M. & Bradwell, T. 2009. Neotectonic deformation in a Scottish fjord, Loch Broom, NW Scotland. *Scottish Journal of Geology*, **45**, 107–116, <https://doi.org/10.1144/0036-9276/01-393>.
- Stoker, M., Bradwell, T., Wilson, C., Harper, C., Smith, D. & Brett, C. 2006. Pristine fjord

- landsystem revealed on the sea bed in the Summer Isles region, NW Scotland. *Scottish Journal of Geology*, **42**, 89–99, <https://doi.org/10.1144/sjg42020089>.
- Stoker, M.S., Bradwell, T., Howe, J.A., Wilkinson, I.P. & McIntyre, K. 2009. Lateglacial ice-cap dynamics in NW Scotland: evidence from the fjords of the Summer Isles region. *Quaternary Science Reviews*, **28**, 3161–3184, <https://doi.org/10.1016/j.quascirev.2009.09.012>.
- Sun, Q., Alves, T., Xie, X., He, J., Li, W. & Ni, X. 2017. Free gas accumulations in basal shear zones of mass-transport deposits (Pearl River Mouth Basin , South China Sea): An important geohazard on continental slope basins. *Marine and Petroleum Geology*, **81**, 17–32, <https://doi.org/10.1016/j.marpetgeo.2016.12.029>.
- Svendsen, H., Beszczynska-Møller, A., et al. 2002. The physical environment of Kongsfjorden-Krossfjorden, and Arctic fjord system in Svalbard. *Polar Research*, **21**, 133–166, <https://doi.org/10.1111/j.1751-8369.2002.tb00072.x>.
- Syvitski, J.P. 1997. Water-Escape Sea Floor Depressions. In: Davies, T. A., Bell, T., et al. (eds) *Glaciated Continental Margins: An Atlas of Acoustic Images*. Dordrecht, Springer Netherlands, 160–161., https://doi.org/10.1007/978-94-011-5820-6_64.
- Syvitski, J.P.M., Burrell, D.C. & Skei, J.M. 1987. *Fjords – Processes and Products*. New York, Springer.
- Szpak, M.T., Monteys, X., et al. 2012. Geophysical and geochemical survey of a large marine pockmark on the Malin Shelf, Ireland. *Geochemistry, Geophysics, Geosystems*, **13**, 1–18, <https://doi.org/10.1029/2011GC003787>.
- Szpak, M.T., Monteys, X., et al. 2015. Occurrence, characteristics and formation mechanisms of methane generated micro-pockmarks in Dunmanus Bay, Ireland. *Continental Shelf Research*, **103**, 45–59, <https://doi.org/10.1016/j.csr.2015.04.023>.
- Taylor, D.I. 1992. Nearshore shallow gas around the U. K. coast. *Continental Shelf Research*, **12**, 1135–1144, [https://doi.org/10.1016/0278-4343\(92\)90074-T](https://doi.org/10.1016/0278-4343(92)90074-T).
- Thomson, J., Croudace, I.W. & Rothwell, R.G. 2006. A geochemical application of the ITRAX scanner to a sediment core containing eastern Mediterranean sapropel units. *Geological Society, London, Special Publications*, **267**, 65 LP – 77, <https://doi.org/10.1144/GSL.SP.2006.267.01.05>.
- Tizzard, L. 2008. *The Contribution to Atmospheric Methane from Sub-Seabed Sources in*

the UK Continental Shelf. University Of Newcastle.

- Tryon, M., Brown, K., Dorman, L.R. & Sauter, A. 2001. A new benthic aqueous flux meter for very low to moderate discharge rates. *Deep-Sea Research Part I: Oceanographic Research Papers*, **48**, 2121–2146, [https://doi.org/10.1016/S0967-0637\(01\)00002-4](https://doi.org/10.1016/S0967-0637(01)00002-4).
- Udden, J.A. 1914. Mechanical composition of clastic sediments. *Geological Society of America Bulletin*, **25**, 655–744, <https://doi.org/10.1130/gsab-25-655>.
- Valentine, D.L., Kessler, J.D., et al. 2010. Propane Respiration Jump-Starts Microbial Response to a Deep Oil Spill. *Science*, **330**, 208–211, <https://doi.org/10.1126/science.1196830>.
- Van Weering, T., Jansen, J.H.F. & Eisma, D. 1973. Acoustic reflection profiles of the norwegian channel between oslo and bergen. *Netherlands Journal of Sea Research*, [https://doi.org/10.1016/0077-7579\(73\)90016-1](https://doi.org/10.1016/0077-7579(73)90016-1).
- Vasquez, M., Allen, H., et al. 2021. EUSeaMap 2021. A European broad-scale seabed habitat map. 149.
- Velayatham, T., Holford, S.P. & Bunch, M.A. 2018. Ancient fluid flow recorded by remarkably long, buried pockmark trains observed in 3D seismic data, Exmouth Plateau, Northern Carnarvon Basin. *Marine and Petroleum Geology*, **95**, 303–313, <https://doi.org/10.1016/j.marpetgeo.2018.05.007>.
- Wagstaff, K., Cardie, C., Rogers, S. & Schroedl, S. 2001. Constrained K-means Clustering with Background Knowledge. In: *Proceedings of the Eighteenth International Conference on Machine Learning*. 577–584., <https://doi.org/10.1109/TPAMI.2002.1017616>.
- Walbridge, S., Slocum, N., Pobuda, M. & Wright, D.. 2018. Unified Geomorphological Analysis Workflows with Benthic Terrain Modeler. *Geosciences*, **8**, <https://doi.org/https://doi.org/10.3390/geosciences8030094>.
- Webb, K.E., Barnes, D.K.A. & Gray, J.S. 2009a. Benthic ecology of pockmarks in the Inner Oslofjord, Norway. *Marine Ecology Progress Series*, **387**, 15–25, <https://doi.org/10.3354/meps08079>.
- Webb, K.E., Barnes, D.K.A. & Plankea, S. 2009b. Pockmarks: Refuges for marine benthic biodiversity. *Limnology and Oceanography*, **54**, 1776–1788, <https://doi.org/10.4319/lo.2009.54.5.1776>.
- Wentworth, C.K. 1922. A Scale of Grade and Class Terms for Clastic Sediments. *The*

- Journal of Geology*, **30**, 377–392.
- Wessels, M., Bussmann, I., Schloemer, S., Schlüter, M. & Böder, V. 2010. Distribution, morphology, and formation of pockmarks in Lake Constance, Germany. *Limnology and Oceanography*, **55**, 2623–2633, <https://doi.org/10.4319/lo.2010.55.6.2623>.
- Wheeler, S.J. 1988. A conceptual model for soils containing large gas bubbles. *Géotechnique*, **38**, 389–397, <https://doi.org/10.1680/geot.1988.38.3.389>.
- Wheeler, S.J. 1989. The undrained shear strength of soils containing large gas bubbles. *Geotechnique*.
- Wheeler, S.J. 1990. Movement of large gas bubbles in unsaturated fine-grained sediments. *Marine Geotechnology*, **9**, 113–129, <https://doi.org/10.1080/10641199009388234>.
- Whiticar, M.J. 2002. Diagenetic relationships of methanogenesis, nutrients, acoustic turbidity, pockmarks and freshwater seepages in Eckernförde Bay. *Marine Geology*, **182**, 29–53, [https://doi.org/10.1016/S0025-3227\(01\)00227-4](https://doi.org/10.1016/S0025-3227(01)00227-4).
- Whiticar, M.J. & Werner, F. 1981. Pockmarks: Submarine vents of natural gas or freshwater seeps? *Geo-Marine Letters*, **1**, 193–199, <https://doi.org/10.1007/BF02462433>.
- Whiticar, M.J., Faber, E. & Schoell, M. 1986. Biogenic methane formation in marine and freshwater environments: CO₂ reduction vs. acetate fermentation-Isotope evidence. *Geochimica et Cosmochimica Acta*, **50**, 693–709, [https://doi.org/10.1016/0016-7037\(86\)90346-7](https://doi.org/10.1016/0016-7037(86)90346-7).
- Wiggins, S.M., Leifer, I., Linke, P. & Hildebrand, J.A. 2015. Long-term acoustic monitoring at North Sea well site 22/4b. *Marine and Petroleum Geology*, **68**, 776–788, <https://doi.org/10.1016/j.marpetgeo.2015.02.011>.
- Williams, C. & Carpenter, G. 2016. The Scottish Nephrops fishery: Applying social, economic, and environmental criteria. **44**, 73.
- Withjack, M.O. & Scheiner, C. 1982. Fault patterns associated with domes: an experimental and analytical study. *Am. Assoc. Pet. Geol., Bull.; (United States)*, **66**.
- Woodward, C.A. & Gadd, P.S. 2019. The potential power and pitfalls of using the X-ray fluorescence molybdenum incoherent: Coherent scattering ratio as a proxy for sediment organic content. *Quaternary International*, **514**, 30–43, <https://doi.org/10.1016/j.quaint.2018.11.031>.

Yu, K., Miramontes, E., et al. 2021. Incision of submarine channels over pockmark trains in the South China Sea. *Geophysical Research Letters*, **48**, <https://doi.org/10.1029/2021GL092861>.

Yuan, F., Bennell, J.D. & Davis, A.M. 1992. Acoustic and physical characteristics of gassy sediments in the western Irish Sea. *Continental Shelf Research*, **12**, 1121–1134, [https://doi.org/10.1016/0278-4343\(92\)90073-S](https://doi.org/10.1016/0278-4343(92)90073-S).

Yvon-Durocher, G., Allen, A.P., et al. 2014. Methane fluxes show consistent temperature dependence across microbial to ecosystem scales. *Nature*, **507**, 488–491, <https://doi.org/10.1038/nature13164>.

Appendix A

Report submitted to Marine Scotland detailing the results of the successful analysis of cores retrieved during the SA1019S MRV. Scotia cruise (July 2019).

Scotland's Pockmarks: understanding the link between gas-escape features and buried carbon in fjordic systems

Scottish Government & Marine Scotland Report

Allan Audsley



A report on Blue Carbon Research funded by the Scottish government

Project:

Scotland's Pockmarks: understanding the link between gas-escape features and buried carbon in fjordic systems

Report produced by:

Allan Audsley, PhD Student, University of Stirling

Dr Tom Bradwell, Primary Supervisor, University of Stirling

Dr John Howe, Supervisor, Scottish Association for Marine Science

Prof John Baxter, Supervisor, Scottish Blue Carbon Research Forum

1. Introduction

Scotland's fjords and firths are globally important stores of carbon, naturally sequestering organic-rich material in seafloor sediment basins (Burrows *et al.* 2014; Smeaton *et al.* 2016, 2017). Despite fjordic environments being recognised three decades ago as major carbon stores (Syvitski *et al.* 1987), quantifying the carbon in Scotland's fjordic and nearshore sedimentary systems has remained a largely neglected topic. The cores collected during the MRV Scotia 2019 'Blue carbon in the marine ecosystem' cruise were specifically retrieved from gas-charged organic-rich pockmarked sediments in fjords and fjord approaches (Audsley *et al.* 2019). The coring sites included Stornoway Bay, the North Minch and east of Eigg, as well as the Scanner-Scotia Pockmark SAC within the central North Sea Basin (Fig.1). Currently, there is very little information on the formation mechanism, age or activity status of pockmarks in the waters around western Scotland. However, important new data from the MRV Scotia 2019 cruise has already demonstrated that certain pockmarks are currently venting fluids into the water column. The proposed analyses will go a long way to filling existing knowledge gaps by exploring fundamental processes within the terrestrial-to-marine carbon cycle and by examining the impact of pockmarks on marine ecosystems – with emphasis on designated Marine Protected Areas and Special Areas of Conservation. The proposed analytical work sits firmly within the Scottish Blue Carbon Forum research landscape and forms a central part of my MASTS-SNH-SBCF-funded PhD at the University of Stirling.

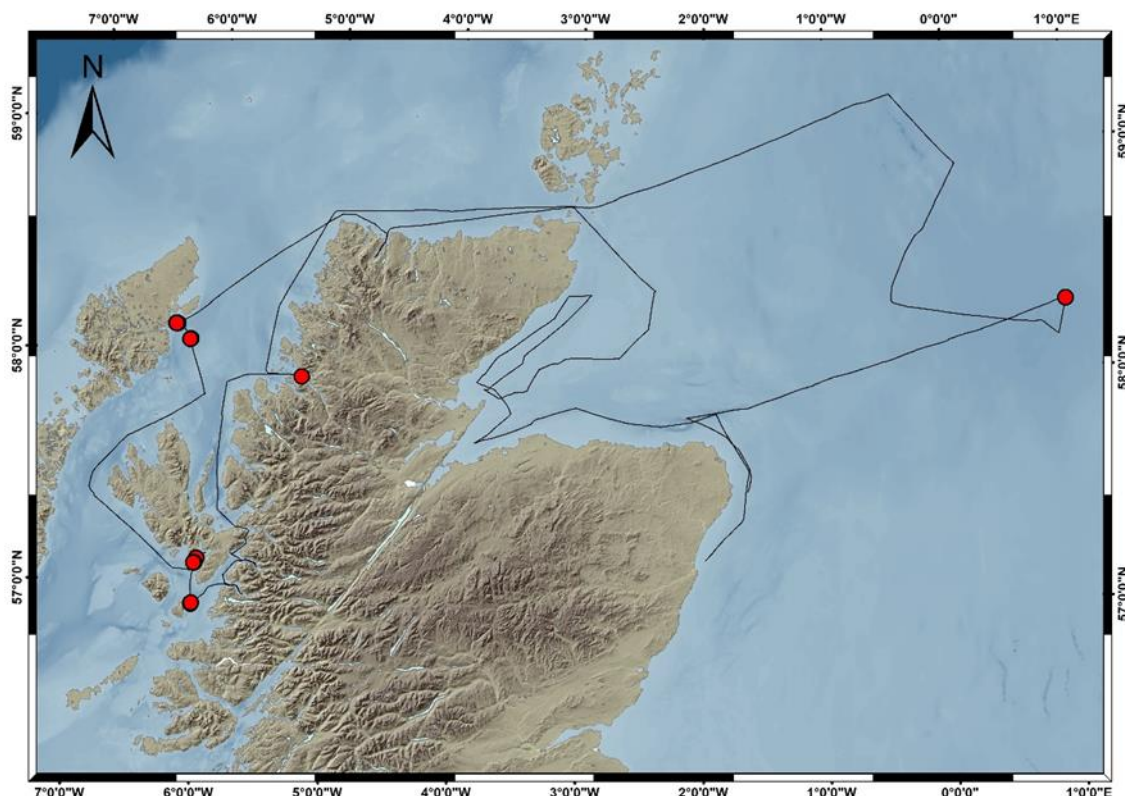


Figure 1. Map of SA1019S MRV Scotia Cruise 2019; cruise track and coring locations (in red)

2. Objectives

This funding will be used exclusively to obtain bespoke non-destructive biogeochemical analyses of valuable sediment cores collected during science cruise SA1019S (MRV Scotia) in July 2019. The analyses, conducted at Geotek (Daventry) and NOC-BOSCORN (Southampton) in 2019, will be used to gain a comprehensive understanding of the geophysical and biogeochemical properties of sediment cores, taken using the SAMS 3-m gravity corer, from within and adjacent to seabed gas-escape features (pockmarks) in Scottish waters. The analyses will include: X-ray computer tomography (CT) scanning, geophysical properties and geochemical spectroscopy using MSCL and ITRAX- μ XRF core scanners. High-resolution (100 μ m) X-radiography will allow the internal structure of intact cores to be imaged, showing how gas is stored and migrates through the sediments; with migration paths (voids, fractures and escape structures) used to estimate specific gas volumes. Geophysical MSCL data will provide bulk density, porosity and acoustic transmissivity information to quantify and understand sediment heterogeneity, sedimentation history and sediment origin (terrigenous or marine). High-resolution XRF

spectroscopy data will reveal the elemental composition of the sediment cores. Specifically, the relative abundance of certain elements (e.g. Ca, Fe, Co, Cu, Mn, Pb, Zn) has been used to gauge the activity status of pockmarks elsewhere (Ravasopoulos *et al.* 2002).

3. Logistics

To complete the objectives mentioned in this report 27 sediment core sections were transported to the Geotek facility in Daventry and then to the British Ocean Sediment Core Facility (BOSCORF) at the National Oceanography Centre (NOC) in Southampton (Fig. 2). In order to reduce vehicle emissions and make efficiency savings it was the University of Stirling team agreed to transport an additional 15 sediment core sections for St Andrews University, needed for analysis at BOSCORF-NOC later in the year. This analysis of the St Andrews sediment cores has also been funded by the Scottish Government.

The length and logistics of the journey, and the multiple analyses, necessitated a two-night stay in Daventry and a further seven nights in Southampton. Following analyses, the cores would all be returned and stored in the University of Stirling cold-store research facility.

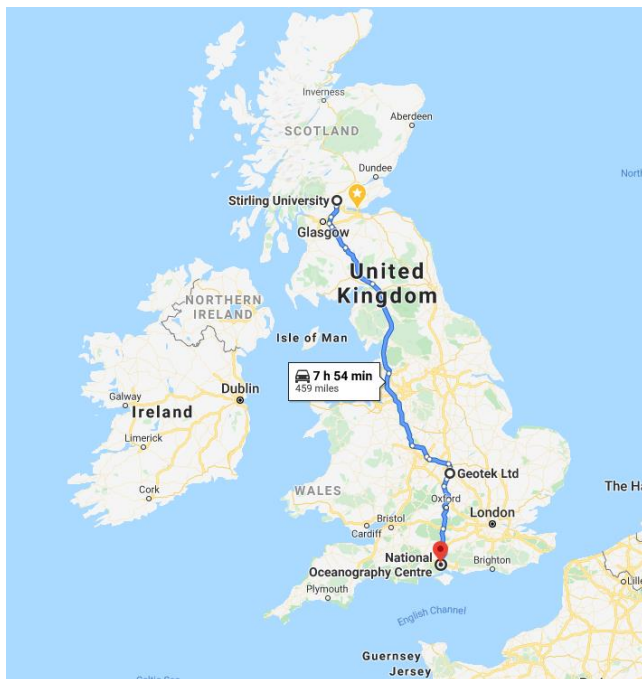


Figure 2. Map of the UK showing locations travelled to for reported analysis (Google Maps).

4. Methodology

4.1. X-radiography

The Geotek vertical X-ray and CT system (VXCT) was used to acquire full-length continuous 2D X-radiographs of 26 whole (uncut) core sections at 57-micron resolution. The x-ray source was a 65W Thermo KeveX with variable focus. A lead slit was used to obtain a higher resolution image of the cores, as this has been shown to reduce the amount of scattering radiation that can obscure the image (Barnes 1991). Additional full 3D CT X-radiographic images were taken of 1 core section. The lower core sections (known as the B section), were imaged along two planes, 0 degrees and 90 degrees to the zero plane, to give a basic 3D representation of the core. The B sections were chosen for this analysis as they were the longest sections (1.5 m in length) and were deemed most likely to contain gas-charged sediment. The upper sections (A section) are variable in length, depending on total core recovery (from 0.3 to 1.0 m) and are mostly composed of wet sediment with a high water content and low density. It is therefore likely that any gas within the A sections escaped on recovery, removing any physical evidence of trapped gas.

4.2. MSCL-S

The multi-sensor core logger – Standard (MSCL-S) at BOSCORF-NOC in Southampton was used on whole cores. Cores were allowed to reach room temperature at least 12 hours before logging. The instrument was calibrated, by BOSCORF staff, using an empty (air filled) core liner and a water filled core liner following standard calibration procedures. The instrument sensors employed were as follows: gamma-ray attenuation, p-wave velocity, magnetic susceptibility and electrical sensitivity all at 1 cm resolution. These non-destructive sensors will provide valuable high-resolution information on the bulk density of sediment, possible sediment origin, stratigraphic correlation between cores, and acoustic velocity of sediment and grain-size variations.

Cores were then split using the BOSCORF precision core-splitting apparatus. The core surface was smoothed using spatulas to create an even and clear surface for optical (photographic) imaging.

4.3. MSCL-CIS

Immediately after cores were split and the surfaces were smoothed they were placed in the MSCL-Core Imaging System (CIS). It is essential that this is done on recently split cores as the colour of sediment can change rapidly as it oxidises. The powerful LED light system allows for the acquisition of high-resolution 5k linescan images. These images

preserve a precise photographic record enabling the correlation of geophysical and geochemical characteristic base on the physical appearance of sediment.

4.4. *MSCL-XYZ*

The MSCL-XYZ measures two variables, magnetic susceptibility and spectrophotometry of split core section. The instrument uses a Bartington magnetic susceptibility point sensor, allowing for 0.5 cm resolution. Data from the point sensor and the lower-resolution loop sensor on the MSCL-S can be compared using inter-instrument calibration and regression analysis for increased accuracy. The MSCL-XYZ instrument is also fitted with a Konica Minolta spectrophotometer, the results from which can quantifying the lightness of the core surface. This can permit the identification of small-scale laminations and sediment variability associated with palaeoclimatic events and other natural forcing cycles. The results of the spectrophotometer can be used to reconstruct a synthetic core image based on the internationally recognised Munsell colour system.

4.5. *ITRAX*

The ITRAX, housed at BOSCORF-NOC, is a high-resolution micro-XRF elemental analyser measuring presence of elements with atomic numbers from 14 (Silicon) to 92 (Uranium). The instrument uses a molybdenum X-ray tube to detect elements using a 30 sec count time, at 30Kv and 40Ma. Downcore analysis was performed at 1mm intervals. Element abundance is represented in counts per second. Archive sections were scanned with the following elements in mind: Ca, Fe, Co, Cu, Mn, Pb, Zn.

4.6. *Carbon and particle size analysis*

Carbon: Nitrogen ratio was measured using Flash smart N: C_{org}-elemental analyser at the University of Stirling. Particle-size analysis was carried out using a Beckman Coulter LS 230. Samples were taken for analysis from the working halves of selected cores at 5 cm downcore intervals.

5. Results

5.1. X-radiograph

Figure 3 shows the imagery from the vertical x-ray scanning of whole core GC027. The x-radiographs show no clear evidence of free gas. They do however show dense objects throughout the core represented by the darkest spots on the x-radiograph image. Towards the base of GC027-B/2 these dense objects are much smaller but more abundant and appear to be in discrete layers.

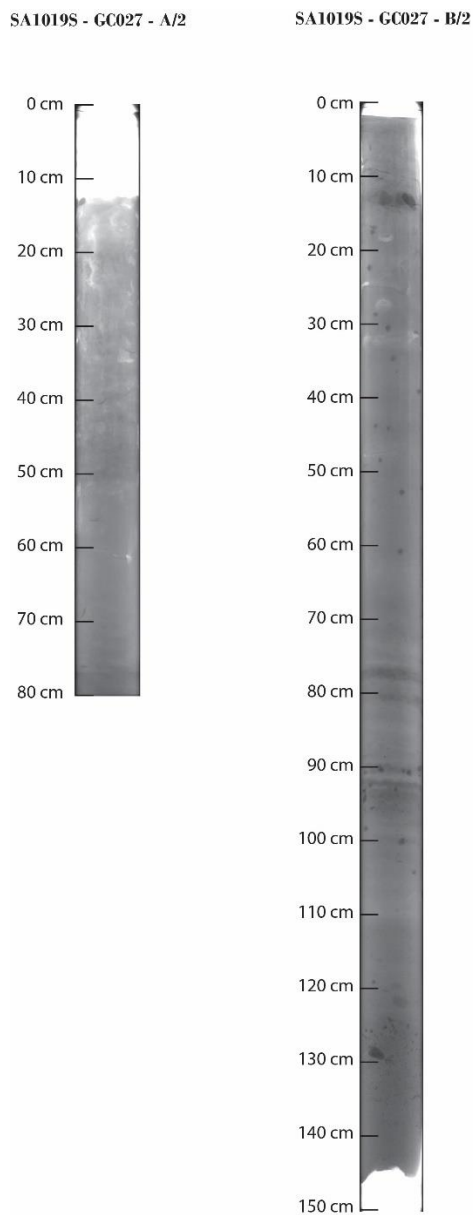


Figure 3. X-ray images for core GC027.

5.2. MSCL-S / MSCL-CIS

Figure 4 shows the results from the MSCL-S and the MSCL-CIS. The mean P-wave velocity is 1501 m/s. Three main units can be identified in the magnetic susceptibility data and the gamma-ray attenuation (density) data. The first unit, from core top to 50 cm downcore is distinguished by low but increasing values of magnetic susceptibility, with a maximum value of $9 \text{ SI} \times 10^{-5}$, and increasing density, from 1.2 to 1.4 g/cm^3 . The second unit, between 50 cm and 90 cm downcore, is characterised by the very low magnetic susceptibility values ($<5 \text{ SI} \times 10^{-5}$). The third unit, from 90 cm to core bottom (225 cm) is the largest unit and is characterised by an abrupt 2-3x step increase in magnetic susceptibility, with a peak of at $32 \text{ SI} \times 10^{-5}$ at 170 cm. This unit is also characterised by increasing density values, to a maximum of 1.55 g/cm^3 near the core base. These units may indicate a marked change from glaciomarine ($>90 \text{ cm}$) to predominately marine conditions (0-90 cm) as far-travelled fine-grained terrigenous material (mud/silt) from wasting ice sheets is replaced by predominantly biogenic/pelagic mud-grade sediments of marine origin.

Black sulphide spots and dark-coloured reduced horizons can be clearly seen in the sediment captured in the MSCL-CIS image. These features probably reflect variable anoxic/oxic conditions at seabed, and may be associated with the dense 'precipitate' objects recorded within the x-radiographic images (Fig. 2).

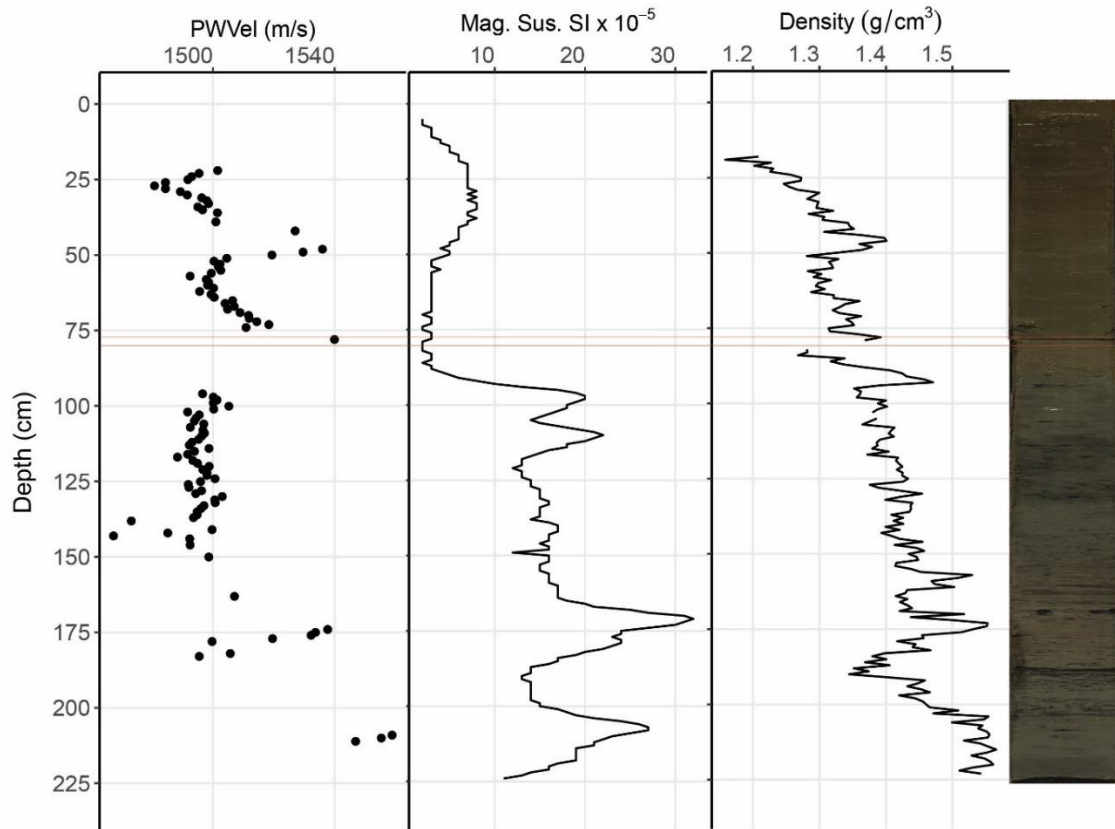


Figure 4. MSCL-S and MSCL-CIS image of gravity ore GC027. From left to right, P-wave velocity, magnetic susceptibility, density, high-resolution linescan image. Horizontal, red lines indicate the region where the two core sections meet.

5.3. ITRAX micro-XRF data

Figure 5 show the results from the ITRAX analysis of core GC027. Selected elements and elemental ratios have been chosen that are optimal proxies for carbon content, grain-size and potential pockmark activity (Croudace & Rothwell 2015). The elemental ratio of manganese to iron has been shown to indicate pockmark activity in the Aegean Sea, Greece (Ravasopoulos *et al.* 2002). Bromine counts per second and the ratio of coherent to incoherent readings from the ITRAX are often used as proxies for organic carbon in sediments (Roberts *et al.* 2016). The trends indicate an increase in organic carbon content from around 90 cm to core top / seabed (0 cm). The Zirconium to rubidium ratio has been used by others as a proxy for grain size (Roberts *et al.* 2016). These results indicate a marked change from finer to coarser grain sizes at ca. 90 cm. Sulphur and iron elemental counts per second point towards important redox reactions occurring above 90 cm, within the surface sediments (Martins *et al.* 2013). Analysis of these elements, alongside organic carbon and other heavy metals, may provide insight on the fate of methane suspected to be migrating towards the seabed surface.

It is clear that the stratigraphic units identified within the MSCL-S data are also represented within the geochemical stratigraphic record. The abrupt boundary between unit 3 and 2 at 90 cm is most striking. Preliminary data suggest that this may indicate an abrupt climatic change or a discrete event occurred at this site, at the same time as the transition from glaciomarine to predominantly marine sediments. It is possible that this abrupt change reflects venting activity of the Scotia pockmark. Increased grain size within this unit (Zr/Rb ratio) is consistent with venting activity, as gas emissions mobilise the finer-grained sediment component transporting it away from the region. The marked drop in Fe values at 90 cm (to core top) would also support this hypothesis.

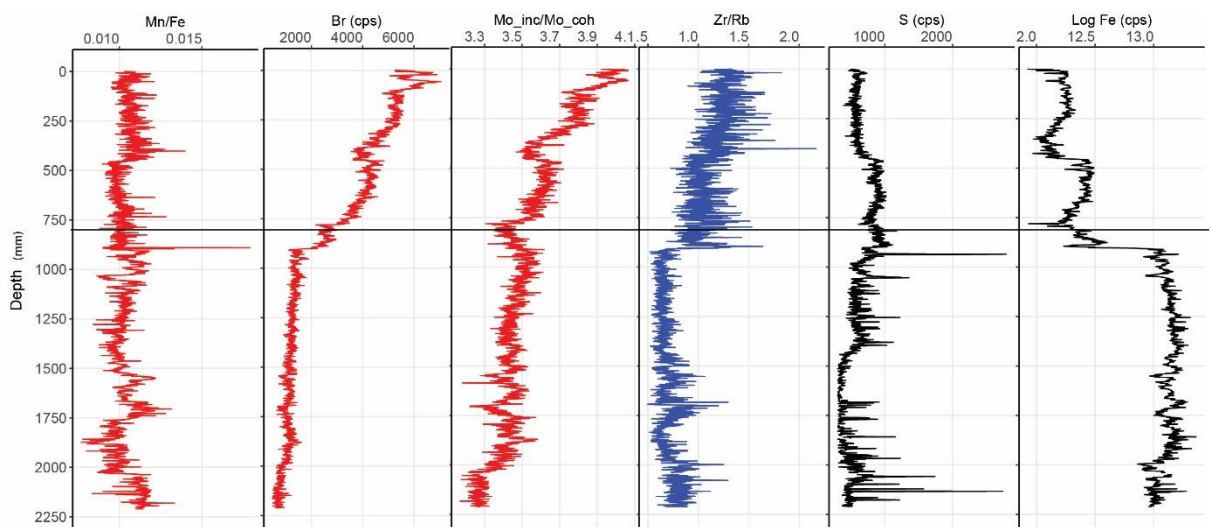


Figure 5. ITRAX results from gravity core GC027; selected element only. Horizontal line indicates the region where the two core sections meet.

5.4. Carbon and particle-size analysis

See section 6. Limitations.

6. Limitations

Due to the enforced lockdown introduced in the UK (from March to July), following the global COVID-19 pandemic, further analysis at the University of Stirling labs has not been possible. It is planned to subsample sediment cores of most interest and measure the amount of organic carbon present. This will allow consolidation of the proxy results from the ITRAX data. Hopefully tests will show whether certain elements or elemental ratios can be used as valid proxies for organic carbon content in sediment. Further lab work will also include particle-size analysis. It is hoped that this will confirm and strengthen proxy grain-size data from the MSCL-S and ITRAX datasets. Together these results will aid our

understanding of how pockmark formation can affect the physical characteristics of seabed sedimentation, and how pockmark activity is preserved in the sediment record. This work is currently scheduled to re-start in early September as staff are gradually allowed to undertake lab work under the new restrictions.

7. Outcomes

The main outcome from this Scottish-Government-funded research project is the outstanding quality of data collected from a large number of high-quality seabed sediment cores ($n = 14$). The x-radiography results are excellent in clarity, resolution and standard allowing a non-destructive internal analysis of all core sections. Only the highest quality x-radiography allows the micro-scale gas fractures to be imaged prior to core splitting and further analysis. For a complete record of the analysis conducted on the cores see Appendix. 1.

The data collected, both onboard the MRV Scotia and as part of these funded activities, will form a large part of the authors' PhD thesis shedding valuable light on our understanding of pockmark formation and gas-venting activity in Scottish waters. This Scottish Government funding has allowed large steps to be taken towards this aim, and especially in our understanding of the geochemical and geophysical stratigraphy of pockmarked sediments in different bathymetric settings. Once all analyses are complete this data will be published in high-quality peer-reviewed Open Access journals. There is considerable interest already in this project from marine environmental consultants, marine planning agencies and from the offshore industry working in Scottish waters.

8. Appendices

8.1. Appendix 1: Table showing types of analysis undertaken on selected SA1019S cores.

Core	Section	Location	Length	X-Ray	MSC L-S	MSC L-ICS	MSC L-XYZ	ITRAX	PSA/CN
SA1019S - GC006	A	Stornoway	0.77	X	X	X	X	X	
	B	Stornoway	1.44	X	X	X	X		
SA1019 - GC008	A	Stornoway	0.68	X	X	X	X	X	
	B	Stornoway	1.5	X	X	X	X		
SA1019S - GC011	A	Stornoway	0.66	X					
	B	Stornoway	1.5	X					
SA1019S - GC012	B	N. Minch	1.5	X					
SA1019S - GC014	A	N. Minch	0.89	X	X	X	X		
	B	N. Minch	1.42	X	X	X	X		
SA1019S - GC015	A	N. Minch	0.9	X	X	X	X		
	B	N. Minch	1.43	X	X	X	X		
SA1019S - GC018	A	Loch. Eishart	0.89	X	X	X	X		

	B	Loch. Eishart	1.43	X	X	X	X		
SA101 9S – GC019	A	Loch. Eishart	0.4	X	X	X	X		
	B	Loch. Eishart	1.44	X	X	X	X		
SA101 9S – GC020	A	Loch Eishart	0.41	X	X	X	X		
	B	Loch Eishart	1.42	X	X	X	X		
SA101 9S – GC021	A	East Eigg	0.8	X	X	X	X	X	X
	B	East Eigg	1.4	X	X	X	X	X	X
SA101 9S – GC022	A	East Eigg	0.8		X	X	X		
	B	East Eigg	1.4	X	X	X	X		
SA101 9S – GC023	A	East Eigg	0.37	X	X	X	X	X	X
	B	East Eigg	1.5	X	X	X	X	X	X
SA101 9S – GC024	A	Summer Isles	0.9	X					
	B	Summer Isles	1.5	X					
SA101 9S – GC027	A	N. Sea	0.79	X	X	X	X	X	X
	B	N. Sea	1.45	X	X	X	X	X	X

